POLITECNICO DI TORINO

Corso di Laurea Magistrale in Ingegneria Biomedica

Tesi di Laurea Magistrale

Development of a bioresorbable fixation system for small bone segments

Relatore
Prof. Cristina Bignardi

Candidata
Lorenza Di Gialluca

Correlatore
Prof. Giuseppe Perale

Anno Accademico 2017/2018

Index

Figure Index

Table Index

Equation Index

Preface

This master thesis in biomedical engineering by Ms. Lorenza Di Gialluca is part of a wider multidisciplinary research project coordinated by Industrie Biomediche Insubri SA, *a.k.a.* IBI, a Swiss med-tech company manufacturing orthobiological medical devices.

IBI is continuously improving its product portfolio, running both internal R&D activities and acquiring also strategically complementing IPR assets. IBI, indeed, has recently purchased a patent bundle on an innovative bioresorbable osteosynthesis device with high angular stability.
Indeed, this thesis entitled "Development of a bioresorbable fixation system for small bone segments" is part of the wider study aiming at assessing proof of concept of this piece of innovation.

Here, Lorenza was confronted, and accomplished, with the development of this innovative device, from scratch to a highly satisfactory working prototype.
In the spirit of offering an industrial perspective and given the overall complexity of the task to be addressed in a relatively short timeframe, Eleonora was teamed with a chemical engineering master student, Eleonora Cignoli, from Politecnico di Milano and with Gabriela Hortelan, a master student in industrial engineering from the University of San Paulo, Brasil.

This master thesis work is, hence, the successful result of 9 months of work by a multicompetence team, to which Lorenza provided an essential contribution. Indeed, the supervision and guidance were provided by the team from IBI, namely product and process engineer Dr. Alberto Cingolani, with the precious cooperation of Dr. Tommaso Casalini from SUPSI, Prof. Tomaso Villa and Ing. Fabio Zambon from the LABS, Politecnico di Milano, Prof. Filippo Rossi from the Physical-chemistry Lab, Politecnico di Milano, Dr. Marco Binelli, Antoine Klaue and Stefano Caimi from ETH Zurich and Prof. Dr. Kaj Klaue from the Moncucco Hospital, Lugano, all being scientifically coordinated by myself.

Giuseppe Perale

Prof. Dr. Giuseppe Perale, PhD
Exec. VicePresidente
Industrie Biomediche Insubri SA
Switzerland

Mezzovico-Vira, 22.11.2018

Sommario

I dispositivi convenzionali di fissazione per la chirurgia ortopedica (ad esempio i fili di Kirschner) potrebbero essere sostituiti da soluzioni meno invasive e sistemi riassorbili realizzati, ad esempio, con materiali biodegradabili.

Ovviamente, questi dispositivi sono in contatto con il corpo e devono, pertanto, soddisfare specifici requisiti: essere non tossici, biocompatibili e con adeguate proprietà biomeccaniche e fisiche.

Tra i possibili materiali, sicuramente i polimeri, tra cui l'acido polilattico, offrono una valida alternativa in quanto sono biodegradabili, bioriassorbibili e non tossici per il corpo. Affinché tale soluzione possa prevalere sui sistemi già esistenti, sono necessari ulteriori progressi e sviluppi al fine di superare le limitazioni meccaniche da cui sono affetti i polimeri. Quest'ultime, difatti, si verificano non solo in situ, ma anche nel momento in cui il dispositivo di fissazione viene impiantato all'interno dell'osso umano. Per tali motivi, l'ottimizzazione svolta in questo lavoro di tesi si è concentrata su due principali aspetti: il primo, ovviamente, riguarda la composizione del polimero, in quanto essa influenza le proprietà meccaniche del dispositivo, sia durante l'impianto, sia durante il tempo di guarigione, essendo soggetta a degrado. Il secondo parametro, invece, riguarda la forma del pin e, di conseguenza, la sua abilità di agire come un vero e proprio sistema di fissazione e di rispondere ai carichi assiali e tangenziali.

Allo stato dell'arte quindi, un pin, ottimizzato secondo i parametri citati, potrebbe essere una soluzione estremamente favorevole per lo sviluppo di un approccio meno invasivo in chirurgia ortopedica.

Lo scopo di questo progetto è quello di identificare un'adeguata geometria del dispositivo e un'ottima composizione del polimero, assumendo 6-8 settimane di degrado.

Il degrado chimico e il comportamento meccanico sono stati sviluppati in un modello creato tramite il software COMSOL Multiphysics: il degrado del polimero sarà simulato attraverso un modello matematico basato su leggi di conservazione che permettono di valutare la cinetica del fenomeno. Una volta stabilita la combinazione ottima tra i due parametri citati, il pin con le opportune specifiche sarà prodotto per injection molding da una compagnia in Svizzera, sterilizzato tramite raggi β e testato su teste di femore. Inoltre, il pin scelto sarà

confrontato con i dispositivi già disponibili sul mercato dopo essere stato sottoposto ad una completa caratterizzazione chimica (GPC) e ad un'analisi delle perfomance.

Abstract

Bioresorbable pins represent, nowadays, a valid alternative to conventional methods for fixations of small bones in orthopaedics surgeries (i.e., Kirschner wires). As they have the need to get in contact with the body, they are generally made out of materials that meet specific requirements, such as being nontoxic, biocompatible and having adequate biomechanical properties and physical structure, which means that they have to support adequate mechanical strength and to be designed in a specific geometry that allows surface-specific reactions promoting degradation when put within the body [2]. In this sense, biodegradable polymers (e.g., polylactic acid) represent a valid and versatile solution, as they exhibit at once most of the aforementioned characteristics. On the other hand, the mechanical limitations of the involved polymers, not only once in place, but also when properly installed into the patient's bone, can still represent an issue and slow down this solution in the overcoming of the traditional ones.

Two major directions can be identified for optimization: the first one is surely the composition of the polymer, as this affects the initial mechanical properties at installation and their evolution through degradation over time. The second is instead the actual shape of the pin and, as a consequence, its ability to properly act as a fixation mean and its response to axial and tangential loads over time.

As a matter of fact, an optimized pin would be extremely beneficial in the development of a less invasive approach to orthopaedical surgeries, as this would avoid a second intervention for the removal of the fixation tools.

Starting from four commercially available biodegradable polymers and aiming at identifying an optimal shape for the cross section of the pin and an optimal composition of the polymer, assuming 6-8 weeks degradation, a model for both the degradation and mechanical behaviours of the pin have been developed in COMSOL Multiphysics. Specifically, the polymer degradation has been simulated through a mathematical model considering that the degradation occurs mostly through hydrolysis, whereas the mechanical model has been developed thanks to FEM analysis, by properly loading the tested device. Once the final best-case has been established, pins having the desired specification have been produced via injection moulding, treated with β-sterilization (25-30 kGy irradiation) and finally tested in human femoral head for laboratory use. Moreover, the optimized pin has been compared

with the devices already available on the market, after being subjected to a chemical characterization and performance analysis.

Chapter I

1. Introduction

A bone fracture (FRX) is a medical condition in which there is a partial or complete break in the continuity of the bone. In severe cases, the bone may be broken into several pieces [4].

A FRX may be the result of high force impact or stress, or a minimal trauma injury in medical conditions that weaken the bones, such as osteoporosis, osteopenia, bone cancer, or osteogenesis imperfecta. In these cases, the fracture is then properly termed a pathologic fracture [5].

In general, fractures are treated with a conservative approach that provides immobilization by means of a plaster bandage.

However, in some circumstances it is necessary to stabilize the skeletal segments using mechanical devices, as Kirschner wire or bioresorbable pins, applied as a result of surgery: this is the case of osteosynthesis.

1.1 Osteosynthesis

Osteosynthesis is defined as a method of therapy of bone fractures that involves the execution of a surgical operation and the installation of devices to hold together two distinct skeletal segments. In general, this approach, when possible, enables to avoid prolonged immobilization with the plaster.

The fixation of fractures by osteosynthesis is usually classified in:

- **Internal**: when the elements of stabilization are totally implanted inside the body. In particular, internal fixation (pins, Kirschner wires, screws, plates or bioresorbable devices) indicates any method of holding together the fragments of a fractured bone without the use of devices external to the skin. In some instances, the device is removed at a later operation (e.g., Kirschner wires), but it may remain in the body permanently or even be reabsorbed (e.g., bioresorbable devices).

- **External**: when most of the implant is external to the organism, e.g., external fixators of Ilizarov, Hoffman etc. External fixation is a technique in which individual bone fragments are held in place by percutaneous wires or pins attached to an external frame. It is used for fractures associated with severe soft-tissue injury or contamination, to minimize the surgical trauma and, for example, in cases of open fractures, to allow observation and treatment of the overlying soft tissues.
- **Elastic or flexible**: a fixation device is defined as elastic if it allows a movement between fragments under functional load, i.e., the fragments move relative to each other when a load is applied through the fracture site. The healing of a fracture with elastic fixation typically occurs with the formation of bone callus, i.e., a soft collar formed at the broken ends of the bones, that joins the bone fragments and proceeds in 4 steps: inflammation, soft callus, hard callus and remodelling.
- **Rigid**: when no movement is allowed. The rigid fixation reduces the fracture and holds it together as if it were an intact bone. In fact, when a rigid support is placed, the motility of the fracture is reduced, and a minimum displacement occurs under functional load. Absolute stability decreases the deformation at the fracture site to a point that allows direct healing without visible callus.

Osteosynthesis is applied when the choice of the conservative method can't guarantee a satisfying result, when the fracture is complicated by an injury that requires a rapid surgical intervention and when conventional plasters should be large enough to limit the patient's life quality.

In particular, the advantages of osteosynthesis approach are:

- **Rapid healing**: as already mentioned, in general, there are four stages of bone healing. With osteosynthesis, in particular by using a rigid fixation device, the second one, which would involve the formation of a fracture callus, could be avoid, since the mechanical device determines a direct and complete contact between bone fragments. This reduces the time required for bone healing.
- **Stabilization of the fractured bone segments**, in order to guide and help the healing process, to restore the anatomic conditions and to maintain the vascularization of soft tissues and bone.

- **Early mobilization**, since sometimes the conventional plasters would require a too prolonged immobilization, causing the degeneration of patient's conditions.
- **Restoration of full functionality**: both for upper and lower limbs, osteosynthesis treatment guarantees an earlier patient's self-sufficiency, with respect to the use of plasters.

Therefore, osteosynthesis is a valid alternative procedure with respect to the conventional one and it presents some important advantages, mostly from the patient's point of view.

1.2 Small Bone Fractures and Fixation Systems

Osteosynthesis can be used for the healing of different bones and the most frequent applications involve the fractures of small bones.

Small bones refer to those bones that have the characteristic of being wider than long. Their shape is roughly cuboid or scaphoid with a thin layer of compact bone surrounding the spongy bone in the inner part, thus, they don't contain bone marrow. Their main function is to provide support and stability to small movements but also in the absence of movement. Examples of short bones are the bones found in the carpus, which means the bones located in the hand, and the tarsal bones, which are located in the foot.

These bones, like all the others human bones, can be subjected to fractures. In particular, a hand fracture is a break in one of the bones in the hand. This includes the small bones of the fingers (phalanges) and the longer ones within the palm (metacarpals). On the other hand, the weight-bearing bones of the foot are especially vulnerable to stress fractures, i.e., a small crack in a bone, or severe bruising within a bone, because of the repetitive forces they must absorb during normal activities.

Concerning the fixation systems for small bone fractures, one of the most frequently implied technique is the use of metallic osteosynthesis material (Kirschner wires) leading to good clinical results by stable fixation of the bony fragments. However, the surgical removal of the metallic implants after fracture healing is required, also because of the deficiency of load transmission during the process of bone healing, due to stress protection by the rigid metallic osteosynthesis plates and some possible disadvantages of long-lasting metallic fixation as inflammative reactions of the surrounding tissues or allergic reactions, caused by corrosion.

In *Figure 1.1*, an example of a phalanx fracture with Kirschner wires as fixation system is reported:

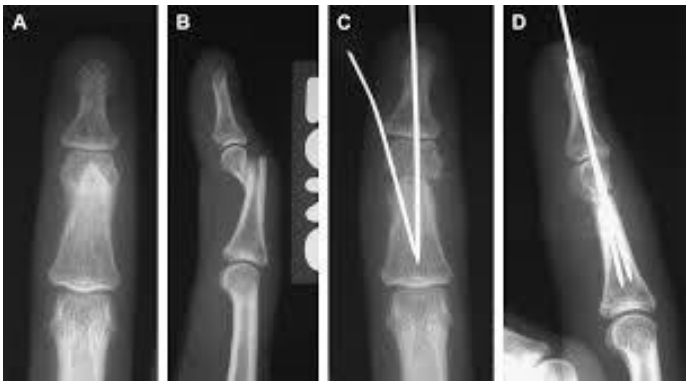

Figure 1.1: Examples of phalanx fracture treated by Kirschner wires

Another existing technique is the use of biodegradable devices, which prevent an atrophy of bone just as the second operative procedure for the removal of the metallic implants. They have been developed mostly as modifications of different poly-α-hydroxy acids, which are less stiff than the metallic implants and are completely resorbed after a definite period.

1.3 Kirschner Wires

Most fractures in small bones heal up well by themselves given time and appropriate support and exercises. In the case the bones are very badly out of position after a fracture, the finger or other bone elements may not work so well if not hold in place. Kirschner wire fixation is one option that may be considered in such circumstances [Site 1].
Kirschner wire (or K wire) (*Figure 1.2*) was invented by Martin Kirschner in 1909. It has a great role in management of orthopaedic trauma and correction of deformities. Kirschner wire is also known as K pin.
Kirschner wires are sterilized, sharpened, smooth stainless-steel pins available in different diameters and lengths.

They are used both in surgical and conservative management of fractures. In surgery they are either used to hold the fracture fragments temporarily before definitive implant is put or are used as for definitive treatment or fractures too [Site 2].

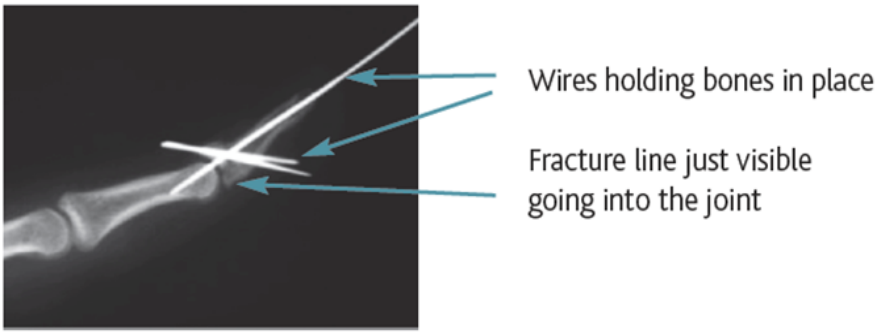

Figure 1.2: K-wires in a phalanx

K-wire surgical techniques are typically less invasive than various other procedures, including plates and screws, for treating bone fractures. Kirschner wires are often driven into the bone through the skin (percutaneous pin fixation) using a power or hand drill [Site 3].

The advantages with the use of these wires include the ability to remove pins easily once healing is adequate, the low cost and the fact that they are typically easy to apply in a percutaneous fashion, limiting soft tissue damage. The application requires minimal soft tissue disruption, thus preserving soft tissue and periosteal stability [7].
However, there are several disadvantages, as the need for additional immobilization during the early healing process and infections. In particular, the major issues occur because of:

- **Swelling, stiffness and scar pain**: local swelling around the surgical site can persist for several months, the fingers are characterized by many layers of tissue that normally glide smoothly over each other during motion, but can become stuck down after an injury and an operation. This will make the finger stiff and poorly mobile. Early exercises to regain normal gliding between the tissue layers is important but, with K-wire fixation, it cannot start until the wires are removed, usually 4 weeks after the surgery. Occasionally patients are troubled by more swelling and stiffness than average;
- **Infection**: minor infections around K wires as they exit the skin are fairly common, occurring in up to 10% of patients. Occasionally a significant infection around a K wire will mean that it has to be removed early;
- **Nerve Damage**: the nerves most at risk with these operations are the small skin branches supplying sensation around the K wire. If fixation has been very difficult, the nerves supplying the tip of the finger can be damaged. Often this is just bruising

around the nerve which will recover, but rarely numbness in the fingertip will persist after this sort of injury;

- **Metalwork problems**: K wires used in hand fracture fixation are strong enough to support fracture fragments but not to resist bending and straightening of the finger. Sudden extra loads on the finger, particularly if the splint has been removed for some reason, can result in the wires breaking inside the finger or falling out. This can mean that more surgery is required;
- **Loss of bony position**: K wires used in hand fracture fixation are supporting the bony fragments, not rigidly fixing them. Sudden extra loads on the finger, particularly if the splint has been removed for some reason, can result in the bone fragments moving out of position. This can mean that more surgery is required;
- **Failure of bone healing**: this is a rare complication for most hand fractures but does occasionally occur. If the bones do not heal up securely further surgery may be required.

Another issue is that, after four weeks from the installation of the wire, the patient has surely to undergo an operation for the removal of the wire. This is done with pliers and it is usually uncomfortable. Then, a check x-ray will usually be taken after the wires have been removed to look at the position of the bony fragments.

Due to all these reasons, new osteosynthesis devices have been found, such as bioresorbable polymeric pins.

1.4 Bioresorbable Polymeric Pins

Usually, tissues have sufficient healing or regeneration capacity and need only the temporary presence of a biomaterial to support, augment, or replace tissues or to guide their regrowth. For example, bioabsorbable (biodegradable or resorbable) polymeric materials are absorbed by the body and then disappear when, after healing, the device is no longer needed. Biodegradable polymers are applicable to those medical devices in which tissue repair or remodelling is the goal (e.g., artificial skin, cartilage repair, peripheral nerve repair), but not where long-term material stability is required (e.g., artificial heart, kidney, liver).

A material can be defined as bioresorbable when its degradation is mediated, at least, partly from a biological system.

Medical applications of resorbable implants were reviewed with special emphasis on orthopaedic polymeric implants.

The mechanical properties and degradation time of a bioresorbable device can be tailored to a specific application by adjusting the molecular weight, crystallinity, and hydrophilicity of the polymer. For example, compositions with higher hydrophilic and amorphous structures and a lower molecular weight resorb faster, yet they often sacrifice mechanical strength. Conversely, higher crystallinity and molecular weight improve mechanical properties and decrease resorption rates.

Degradation involves polymer long chains that are reduced into segments that can be absorbed by cells. In the human body, degradation follows two phases:

1. Fission of long chains occurs because of hydrolysis, enzymatic attack, or both.
2. Segments are dissolved in extracellular fluids by phagocytosis or via metabolism.

Therefore, the main advantage of biodegradable polymers could be that the products of degradation are not toxic or eliminated from the body by a natural metabolic pathway with minimal side effects [2].

Bioresorbable polymers belonging to the aliphatic polyester family currently represent the most attractive group of polymers that meet the various medical and physical demands for safe clinical applications.

This is mainly due to their high level of biocompatibility, defined by the degradation product, acceptable degradation rates, and versatility regarding physical and chemical properties [8].

As mentioned in the Biocompatibility Manifesto [9], the biocompatibility, i.e., the ability of a material to locally trigger and guide non-fibrotic wound healing, reconstruction and tissue integration, is directly related to the biotolerability, i.e., the ability of a material to reside in the body for long periods of time with only low degrees of inflammatory reaction.

1.4.1 Type of Bioresorbable Polymers

As previously state, in general the polymers employed in biomedical applications belong to aliphatic polyesters since they degrade *in situ* through hydrolysis.

Degradation products are metabolized by the human body itself.

These polymers have a chemical structure characterized by the presence of ester groups along the chains. They are classified according to their production process:

- Naturally occurring polyesters (e.g. shellac, a resin, is a mixture of monoesters and polyesters (secreted by female lac bug), with a backbone mainly consisting of aleuritic acid, terpenic acids, and minor fatty acids)
- Microbial polyesters (e.g. polyhydroxyalkanoates (PHAs) comprise a large class of polyesters that are produced by bacterial fermentation of sugar and lipid to store carbon and energy)
- Condensation polyesters
- Polyesters from ring-opening polymerization

Overall, certainly the most attractive classes of polymer in biomedical application is represented by polylactic acid (PLA) and its copolymers with polycaprolactone (PCL). Nevertheless, the latter is also used alone.

In general, there are two enantiomeric forms of pure PLA, poly-L-lactide (PLLA) and poly-D-lactide (PDLA), with opposite configurational structures. They are obtained by the ring opening-polymerization method.
PLLA is an aliphatic polyester with a crystalline structure, good biodegradability and biocompatibility, reasonably good mechanical properties, and processability in forming fibres. Various factors affect its degradation rate once inserted in the patient body, such as molecular weight, enantiomeric composition of the polymer, size and shape of the implant, environmental features, processing methods, and sterilization. Of the two enantiomeric forms, PLLA degrades the slowest. It is generally considered that simple hydrolysis is the main degradation mechanism for PLLA.
PDLA is amorphous, resulting in a weaker and more rapidly degrading material.
Actually, polymerization of racemic mixture of L- and D-lactide leads to the synthesis of poly-(D,L-lactide) (PDLLA). PDLLA is used for the preparation of bioabsorbable sutures, controlled drug release systems, stents, stent coatings, and tissue engineering scaffolds. PDLLA is a glassy, amorphous polymer that degrades by bulk hydrolysis in vivo [11].
PDLLA has a Tg of approximately 55°C and it is a rigid material. Its Young's modulus and stress at break values are close to 3.5 GPa and 65 MPa, respectively.

On the other hand, pure PCL is very flexible among the synthetic biodegradable polymers, and it is easy to process. Its major applications reside in controlled drug delivery systems and in implants for orthopaedics surgery. PCL has a low glass transition temperature (approximately -60 °C), a low melting point (60°C), and a high thermal stability.

Because of its low glass transition temperature, the PCL amorphous phase displays high molecular mobility at body temperature. Moreover, its significant degree of crystallinity, substantial hydrophobicity and high molecular weight ensure long in vivo degradation time, which occurs by hydrolysis, as for other aliphatic polyesters.

The complete breakdown of the polymer could occur within 2 years, depending on the degree of crystallinity. PCL is highly compatible with osteoblasts; hence, it may be suitable for long-term implant applications. As mentioned before, it is very common to adopt PCL in combination with other biopolymers.

As a copolymer, it is worth to mention poly(L-lactide-co-ε-caprolactone) (PLACL) obtained by the ring-opening polymerization of L-lactide (cyclic dimer of L-lactic acid) and ε-caprolactone as monomers.

Copolymerization of lactide with ε-caprolactone can be an appropriate method for the control of mechanical properties, shape-memory behaviour, degradation rate and controlled drug-release properties [6].

The glass transition temperature depends on the feed composition, i.e., on the ratio between L-lactide and ε-caprolactone monomers fed. For example, the Tg of poly(L-lactide-co-ε-caprolactone) characterized by a feed ratio equal to 70/30 is about 15°C.

Fernándeza J. et al. [6] reported that tuning the copolymer composition affects the elastic modulus of the final polymer, which can be reduced from 1343.1 MPa with a PLA/PCL ratio of 90/10 to about 12 MPa when moving to 70/30. The elastomeric character of the copolymers also increases with PCL content and consequently also the strain recovery. These results demonstrate that mechanical properties of PLACL can be tuned by both adjusting composition during synthesis and a well-controlled thermal process during manufacturing.

1.4.2 Polymer Mechanical Properties

Mechanical properties of a material are basic parameters, which reflect its structure and function.

The structural behaviour of a material is determined by conducting mechanical tests on specimens subjected to loading conditions. The material behaviour of a specimen is not influenced by its geometry, but reflects the intrinsic properties of the material itself.
There are basically three types of force: tensile, compressive and shear, which are determined by the direction and effect of the forces acting on the body.
Within this elastic range, the deformation induced by the forces is linearly proportional to the magnitude and direction of the applied force, a relationship known as Hooke's law (*Equation 1.1*):

$$\sigma = E\epsilon$$

Equation 1.1: Hooke's law

- Strain is a dimensionless measure of relative deformation or percentage change in length. When a load is applied axially to a bar or rod of uniform cross-section, the proportional change in length is $\Delta l / l_0$, called normal strain and denoted by ε;

- Stress is defined as the force per unit area and may be classified as tensile, compressive or shear depending upon how the load is applied. Normal axial stresses (σ) can be either tensile or compressive. Shear stresses, denoted by τ, occur when equal and opposite forces have different lines of action which tend to alter the shape of the object without changing its volume.
  Stress has units of pascals (1 Pa = $1Nm^{-2}$).
  The physiological stress levels for bone are generally in megapascal range and it is in accordance with the load applicated in the simulation of mechanical model;

- For axial loading the slope of the stress–strain curve within the elastic region is called the modulus of elasticity, or Young's modulus, E (expressed in Pascals, Nm^{-2}).
  Balanced axial forces applied to a prismatic bar not only produce an axial strain but also give rise to a lateral or transverse strain (ε_l) with a consequent change in cross-sectional area. The ratio of the lateral strain to the axial strain is quantified by another material constant known as Poisson's ratio (ν) of the material. For an isotropic (i.e., when the material has the same properties in all directions) linear elastic material, relationships among the elastic constants can be expressed as (*Equation 1.2*):

$$E = 3K(1 - 2\nu)$$
$$E = 2G(1 + \nu)$$

Equation 1.2: Relationship between Poisson's ratio and Young's modulus

Where E is Young's modulus, G is the shear modulus which characterizes the relationship between shear stress and shear strain and K is the bulk modulus defined as the modulus of volume expansion.

The relationship between the load applied to a structure and the resulting deformation is called a load-deformation curve. Where possible, it is generally preferable to convert loads into stresses, and deformations into strains, and thereby replot the relationship as a stress–strain curve. The advantage is that the stress–strain curve gives information directly relating to the intrinsic material properties of the specimen, and is independent of the specimen size and geometry.

The stress–strain curve (*Figure 1.3*) for all materials is typically divided into two regions, the elastic and plastic ones, respectively, which are divided by the yield point. In the first region, the behaviour is linearly elastic. The second phase is known as the plastic region where an increase in strain results in small or even no increase of the stress.

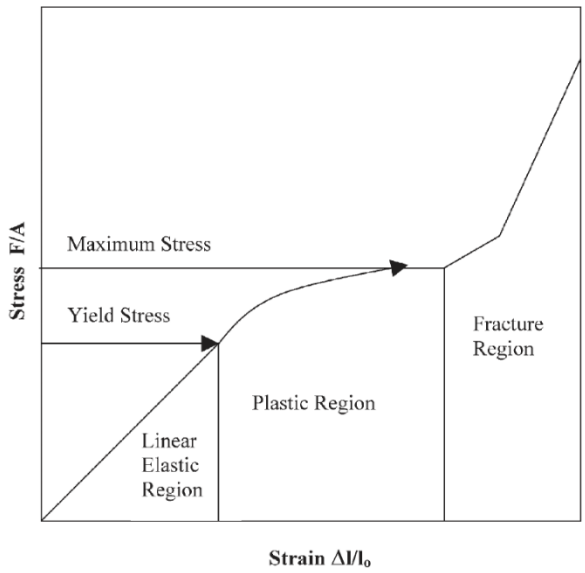

Figure 1.3: Schematic diagram of a typical stress-strain curve. The linear, plastic and fracture region are shown. Note that stress is computed as the applied force F divided by the cross-sectional area (A) and the strain is computed as the deformation (Δl) divided by the original length l_o

The point/region where the deformation changes from being elastic to at least partially plastic is the yield point. Although material reaching this point may still have far to go before it actually breaks, it is permanently damaged to some extent once it enters the plastic region. The amount of post yield strain that occurs in a material before fracture is a measure of the ductility of the material. A material showing a large post-yield strain is referred to as ductile, whereas a material showing little post-yield strain is described as brittle.

Mechanical failure can be defined as the degradation of a material property beyond its elastic limits or loss of material continuity. The maximum stress the material can sustain is called the ultimate strength, and the breaking strength is the stress at which the material actually breaks catastrophically.
Fatigue is the damage due to repetitive stresses below the ultimate stress. Fatigue is a slow progressive process, as opposed to an acute catastrophic process which results when the ultimate strength of a material is surpassed.
The area under the stress–strain curve is a measure of the amount of energy needed to cause a fracture. This property is called energy absorption or toughness of material and is an important property from a mechanics point of view.

Bioresorbable polymers have different mechanical behaviours. In *Figure 1.4,* typical tensile curves for polymeric materials with a brittle or ductile behaviour are reported:

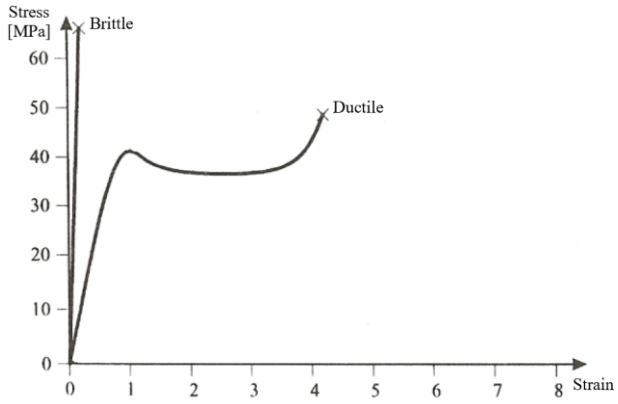

Figure 1.4: Typical tensile curves for polymeric materials with a brittle or ductile behavior

In the case of brittle material, the only linear stroke is observed, followed by break.
In the case of ductile material, the curve is characterized by three different zones: a linear stroke, corresponding to little strains, in which the strain can be recovered after the removal of the load; an area in which the material undergoes significant plastic deformations (yielding); a final breaking zone.

1.4.3 Insertion Procedure of Bioresorbable Pins

The following surgical technique exemplifies the basic procedure during implantation of a biodegradable pin.
In the considered example, during the insertion of a bioresorbable pin into a finger, the affected joint is opened and prepared for fusion. The articular surfaces (proximal and distal) are sawn flat considering the desired end position (*Figure 1.5*):

Figure 1.5: Section and joint preparation

The proximal and distal articular surfaces are drilled with a drill of 2 mm of diameter: in this way, a bore is generated in the cancellous bone (*Figure 1.6, Figure 1.7*).

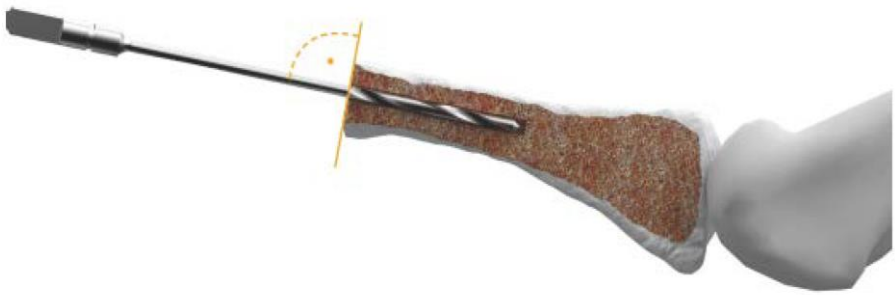

Figure 1.6: Proximal bore

Figure 1.7: Distal bore

In most of the cases, an insertion pen is used in aid. The pin is inserted from the front of the pen. For the length of the pin, the insertion pen is set to the appropriate length. The scale outside the pen serves this purpose (*Figure 1.8*).

Figure 1.8: Insertion of the pin into the insertion pen

To facilitate the insertion of the implant into the bone, the resorbable implant can be moistened with sterile saline solution.

The tip of the pin should protrude slightly out of the instrument, so that when placing the insertion pen on the hole, the exact positioning is reached. The pin is inserted into the drill hole by lightly tapping the back of the insertion pen. The depth can be read on the lateral scale on the insertion pen. The pin should not be exposed to excessive stress during insertion (*Figure 1.9*).

Figure 1.9: Insertion of the pin at the beginning of the phalanx

The length of the remaining pin can be shortened to the desired length with a side cutter. The distal phalanx is manually pushed over the distal end of the pin with a slow, steady pressure until both bone segments are flush with each other (*Figure 1.10*).

Figure 1.10: Pushing of the distal phalanx over the distal end of the pin

During implantation, no bending or torque may be applied to the pin.
Finally, the wound is stitched up and the surgeon determines the period of time necessary for healing (*Figure 1.11*).

Figure 1.11: Wound closure

1.4.4 Polymer Degradation

As described in *Casalini et al.* [10], aliphatic polyester degradation in vivo firstly occurs due to the hydrolysis mechanism: water penetrates into the matrix and breaks ester bonds; the resulting oligomers can diffuse in and out of the matrix and, since degradation is enhanced in acid environments, they act as a catalyst for the hydrolysis reaction because of their carboxyl groups.

Polymer hydrophilicity/hydrophobicity and crystallinity determine the water uptake and thus hydrolysis dynamics: hydrophilic and amorphous materials can retain a greater amount of water and thus are subjected to a faster degradation. Water uptake is also influenced by molecular weight: the initial amount of adsorbed water decreases as the molecular weight of undegraded device increases.

On one hand, if the characteristic time of water penetration into the matrix is lower than the depolymerization one, then homogeneous or bulk degradation takes place since the entire matrix is subjected to hydrolysis reaction. In contrast, if ester bonds are hydrolysed faster than water diffusion, heterogeneous or surface degradation occurs: only the surface is subjected to degradation, while the bulk remains intact. Currently, it is widely accepted that the degradation mechanism also depends on device geometry.

Polymer degradation occurs also due to mechanical loads. In fact, since the pin is subjected to a stress distribution, in the regions where the loads are higher there is a faster degradation with respect to the parts where the loads are lower. As a matter of fact, mechanical loads accelerate the degradation and therefore it is necessary to pay attention in the region subjected to the stress distribution, where high values of stress are reached.

The aforementioned mechanical loads are due to forces applied both during implantation and in situ during the healing of the bone.

In order to evaluate the chemical degradation as a function of mechanical load, it has been important to link the degradation constant to the stress distribution.

1.4.5 Geometry

In general, a bioresorbable pin needs to have a shape that allows on one hand a good mechanical stability, especially on the edges of the pin, and on the other hand, proper degradation behaviour in the first sixty days in order to avoid the degeneration of the cross section into a circle: this would cause the no-respect of one of the most important

requirements of a fixation system, i.e., biomechanical stability. In this case, in fact, the two bone fragments linked by the fixation device would rotate one with the other because subjected to a physiological torsional load. In this sense, a proper geometry needs to be designed in order to guarantee the biomechanical stability of the two bone fragments, even if subjected to the aforementioned load.

1.4.6 Manufacturing Process

Bioabsorbable polymers can be injection moulded with extremely small features and thin sections. However, this process requires special dedicated moulding equipment since many of these devices have small intricate 3D structures. The material can also be extremely sensitive to temperature; therefore, temperature control is a critical factor: bioresorbable polymers need to be processed at the lowest temperature possible. If the material is exposed to elevated temperatures, this can quickly result in monomer formation and alter the mechanical properties.

Due to both the sensitive nature and high cost of bioabsorbable polymers, it is essential to have dedicated processes and equipment in place that are developed specifically for injection moulding of small complex bioabsorbable parts. [Site 7]

In general, the injection moulding process to manufacture a finished plastic is composed by the following steps:

- The prepared thermoplastic is poured into the hopper;
- The material funnels down into the screw which is heated to melt the plastic;
- The barrel is heated at staged temperatures along its length to allow the material to solidify and to move along the screw;
- The screw rotates and this moves the material forward with the pressure and speed determined to fill the cavity efficiently;
- When the material exits the nozzle at the end of the barrel it is injected into the feed channels of the mould tool;
- The feed channels allow this material to flow into the open cavity of the mould tool which forms the shape of the finished product;
- The mould tool is held at a constant temperature to allow ease of material flow and to also draw out the heat from the product after injection, so, the material sets off to a solid form;

- After a predetermined cooling time the mould tool is opened when the moving platen carrying the ejection half is retracted;
- The mould tool opens with the product held in the ejection half of the tool;
- The ejection system then moves forward to release the product from the mould tool;
- The product is gathered in the collection box after the cycle is complete or the parts can be picked from the tool as required.

After the moulded parts are produced, they will be removed from the machine area [Site 11].

In *Figure 1.12*, a schematic representation of the injection moulding machine is reported:

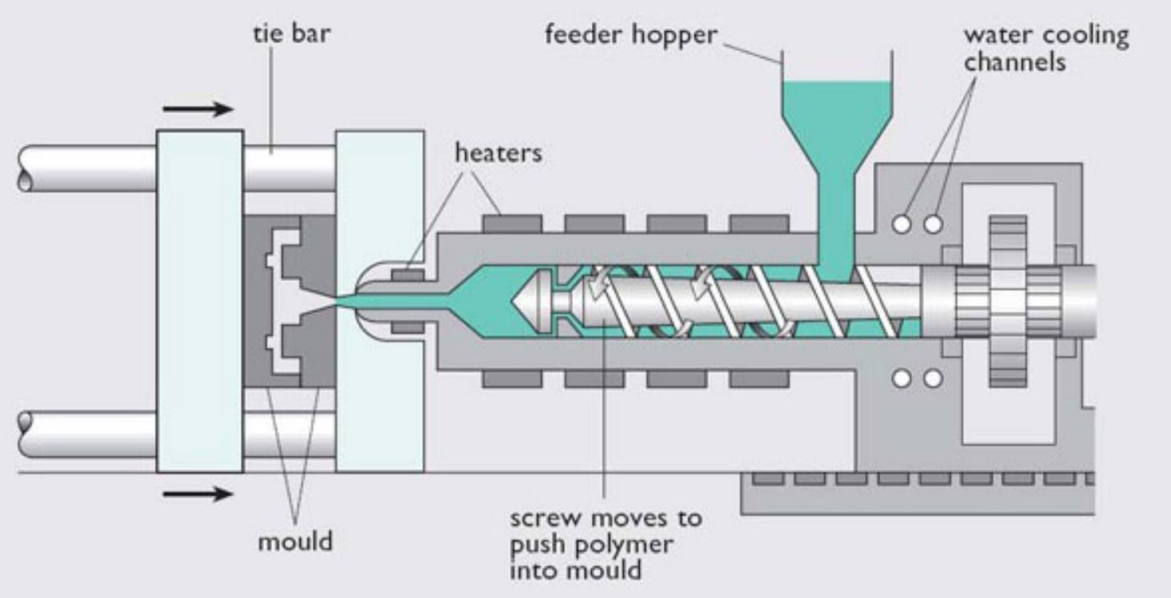

Figure 1.12: Schematic representation of the injection moulding machine

1.4.7 Sterilization Method

Sterilization of a medical device is often referred to as terminal, because it occurs on the fully finished, already packed and ready to be sold product.

Sterilization of a product is properly intended to remove all the living microorganisms contained in or adhering to it and, in particular for medical devices, it requires a specific protocol which must ensure full sterilization and limited damage on the product. In fact, it would be impossible to analytically test again each individual device as it would mean removing the packaging and indirectly invalidating the previous sterilization.

Therefore, both the number and resistance of microorganisms in the environment in which the treatment is performed and the necessity to limit the interference with the initial desired characteristics of the final product must be taken into consideration as sterilization conditions [19]

Sterilization with electron beams (β-sterilization) has been a widespread process for decontamination of medical products, laboratory articles, packaging materials for the pharmaceutical and food industry and other applications for more than 30 years.
The major benefits of the process are:

- Electron beam sterilization is a practically "cold" process especially well-suited for products which do not permit sterilization with heat or steam;
- This sterilization process doesn't require toxic and environmentally harmful ethylene oxide for the treatment;
- The products are released parametrically and are available immediately after the treatment without quarantine or degassing times;
- Unlike sterilization with gamma rays of cobalt 60, only current is used for the treatment, making the process energy-efficient and environmentally friendly;
- The energy requirement is significantly lower than for heat or x-ray sterilization processes. [Site 9]

Due to the precision of the high energy irradiation dose, it is possible to process products in a very short time. The accelerators used do not cause any activation of the irradiated product or any harm to the environment. The E-beam sterilization process is based on penetrating unsterile products and their packaging with high-energy electrons which are ionizing and therefore have a germicidal effect.
By passing through the "curtain" of electrons, the energy is absorbed by the material. This results into the chemical stimulation of molecules and atoms and the generation of free radicals. [Site 10]
These last species induce breaks in the DNA double helix, preventing replication and enabling sterilization effects. Due to its mechanism of action, it is important to limit the duration of the whole irradiation to the minimum (generally just few minutes), otherwise great damage on the final products, such as polymers embrittlement, oxidative damage, and colour change might occur. Indeed, especially for polymer-based devices, ionizing

radiations exhibit an important side effect that affects their performance, such as a decrease in both number and weight average molecular weight, and modification of the chain distribution and conformation.

The molecular weight decrease is proportional to the radiation dose and the specific trend depends on material composition (which determines the reactions pathways), degree of crystallinity, and sterilization environment.

This phenomenon has an important impact on the final behaviour of devices made of aliphatic polyesters, which in general reflects on the mechanical properties of the finite device.

Finally, radiations also influence the glass transition temperature, melting temperature, and the degree of crystallinity. [19]

1.4.8 Characterization Technique

One of the practical characterization techniques to determine the molecular weight distribution is the Gel Permeation Chromatography, during which the polymer sample injected into the instrument is separated according to its molecular weight on the basis of its size (hydrodynamic radius) once dissolved in solution.

GPC gives data about:

- Molecular weight (Mn, Mw)
- Polydispersity (PD)
- Monomer conversion

Although polymer molecules can be described as long chains of monomers linked together, they don't exist like that in solution. Once they have been dissolved, the molecules coil up on themselves to form a coil conformation, which resembles a ball of string. Therefore, although they are chains, when they are analysed by GPC, they behave like tiny spheres, with dimension dependent on the molecular weight (*Figure 1.13*):

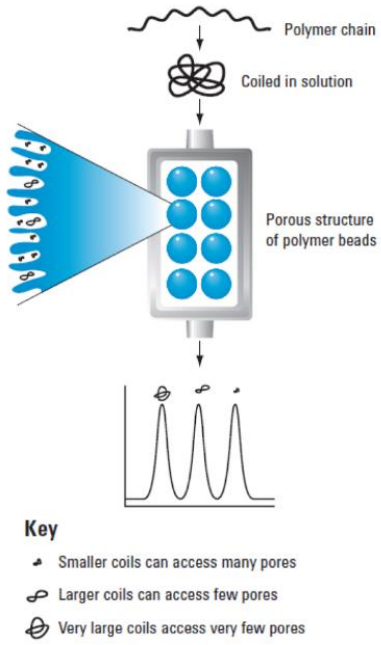

Figure 1.13: Schematic representation of the GPC principles

In *Figure 1.14*, the GPC set up is reported:

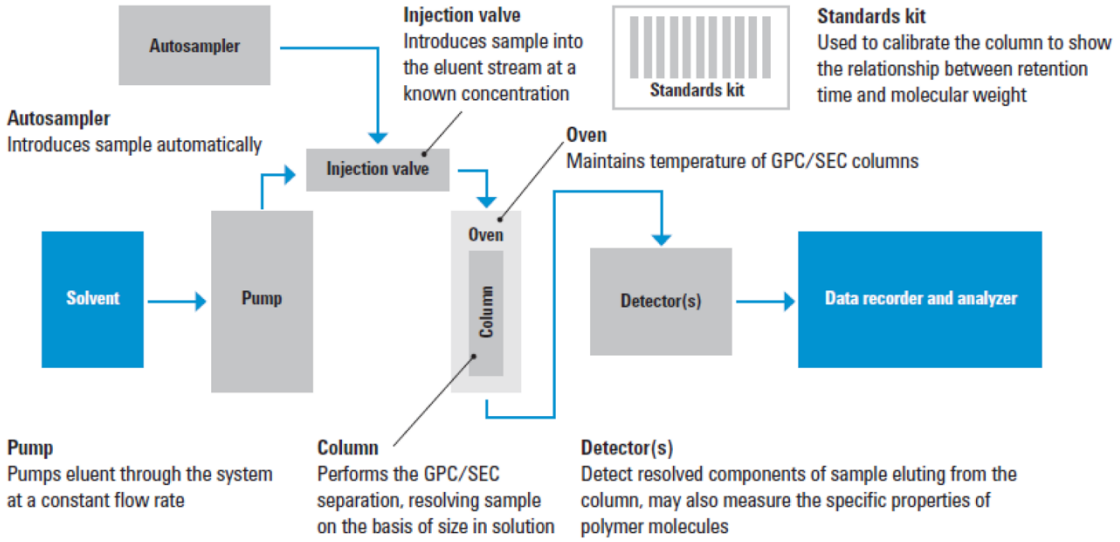

Figure 1.14: GPC set up

The detector signal is then converted into a chromatogram, that is a function of the intensity, which is proportional to the amount of polymer and the retention time which is related to the molecular weight. In this sense, a calibration curve is required in order to be able to obtain

the molecular weight distribution. Calibration curve can be performed through the analysis of a reference polymer with known molecular weight and polydispersity. By knowing the reference polymer characteristics, it is possible to correlate the retention time with the molecular weight.

1.5 Current State of Art of Biodegradable Pins

In *Table 1.1*, some competitors with their pins already commercially available are listed: all the devices are available in different diameters and length, and they have a similar surgical technique for the implantation.

Competitors	***Cross Section and Composition***	***Description***
INION [Site 4]	 Red areas indicate the corners of Inion FreedomPin™ hexagonal shaft shape that lock the pin into the pilot hole by slight deformation within insertion. FreedomPin™ is made of a proprietary blend of L-lactide, D,L-lactide and trimethylene carbonate (TMC) which results in a tough material that is easy to handle and biodegrades completely and which is intended for internal fixation during the repair of bones and joints.	 The Inion FreedomPin™ is a strong and versatile resorbable pin to use in even more challenging orthopaedic fixations. With a unique manufacturing method and angular shaft shape design the Inion FreedomPin™ offers many clear benefits over the traditional round shaped pin implants. It is, for example, over three times stronger than recent generation pins, it is available in four different diameters (1.5 mm, 2.0 mm, 2.7 mm and 3.2 mm) for wider range of applications and it can be cut to desired length during the operation. The Inion FreedomPin™ products are indicated for maintenance of alignment and fixation of bone fractures, osteotomies, arthrodesis or bone grafts in the presence of appropriate additional immobilization (e.g. rigid fixation implants, cast, brace).

[Site 4]	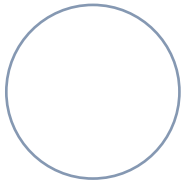 Inion OTPS™ Pin has a circular cross section and it is a biodegradable product made of a proprietary blend of L-lactide, D,L-lactide and trimethylene carbonate (TMC) which results in a tough material that is easy to handle and biodegrades completely and which is intended for internal fixation during the repair of bones and joints.	 Inion OTPS™ Pins have optimized handling properties, strength and degradation characteristics that support a more natural healing process. The Inion OTPS™ Pins retain their strength while bone healing occurs and then gradually lose their strength between 18 and 36 weeks to progressively load the bone. Complete mass loss will occur within 2-4 years. The Inion OTPS™ Pins degrade by hydrolysis and over a period of time are metabolized through natural processes in the body into carbon dioxide and water which are then exhaled and excreted.
[Site 5]	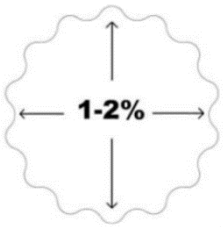 Material memory effect: dimensional changes in human body conditions, i.e., diameter will increase and length will decrease 1-2% compared to the initial dimensions. ActivaPin™ is made of PLGA and it biodegrades in the body safely and in a controlled manner within approximately two years, eliminating the need for implant removal surgery. Implant is supplied γ-sterilized.	 Bioretec's ActivaPin™ is ideal for fixation of fractures and osteotomies in upper and lower extremities. Self-Locking SL™ technology and grooved surface design enable pins to stay in place with improved rotational stability. ActivaPin™ is available in diameters 1.5, 2.0, 2.7 and 3.2 mm and lengths 20 – 70 mm. Bending modulus is close to the value of cortical bone, contrary to metals. ActivaPin™ maintains its intended function for at least 8 weeks.

acumed [Site 6]	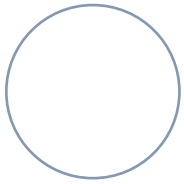 The Biotrak Pin offers surgeons a headed fixation solution with a multifaceted fin design intended to facilitate fixation and compression and protect against rotational forces.	 The Biotrak resorbable fixation system is designed to provide fixation for small bones and bone fragments in the upper and lower extremities, including fractures, fusions, and osteotomies. Biotrak fixation devices are made of 100% poly L-lactic acid (PLLA), allowing the implant to resorb over five years as the bone heals.
CONMED [Site 12]	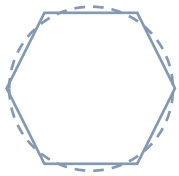 SmartPin implants have a hexagonal cross section and they are made of PLLA, in order to manufacture an absorbable device.	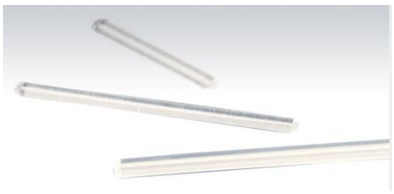 The implants provide non-load bearing immobilization of cancellous bone fragments and no stress shielding. The 1.5 mm Bone Fixation Kit provides surgeons with a simple, safe and resorbable solution for bone fixation, delivering good patient comfort. SmartPin eliminates the need for implant removal. The implants are available individually packed and sterile in a wide range of sizes and lengths.

WRIGHT FOCUSED EXCELLENCE	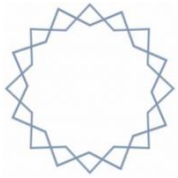 The RFS™ (Resorbable Fixation System) Pin System has a hexadecagonal cross section. It is made of oriented bioresorbable polymer poly(L-lactic/co-glycolic acid PLGA copolymer 85L/15G).	 These polymers have a long history of safe medical use and degrade in vivo by hydrolysis into an alpha hydroxyl acid that is metabolized by the body.

Table 1.1: Competitors

Even if all of these devices are available on the market, they show some disadvantages, among which the main important are:

- The shape of the cross section is not the optimal one because it loses stability in short time after pin implantation: the shape tends to become circular, mostly due to hydrolysis degradation;
- The composition of the pin: even if they are made of bioresorbable polymers, they have a too long reabsorption time, due to both nature and composition, i.e., a too high molecular weight, of the polymer. As a consequence, the pin remains in situ for a too long unnecessary time.

1.6 Aim of the Work

In this work, the focus has been posed on the development of a new pin able to overcome the general limitation of the ones already available on the market, that is, preserving its mechanical properties and function unaltered for at least 60 days, still being able to naturally fade away in appropriate time upon implantation.

First of all, an optimal composition and molecular weight are required in order to guarantee the right degradation time, also in correlation with mechanical stability. In general, the weight average molecular weight of the pin after 8 weeks of implantation has to be above 45 kDa, Therefore, this parameters on the raw polymer have been assessed with the help of a mathematical degradation model. Four commercially available and biocompatible polymers, belonging to aliphatic polyester family, have been selected and tested: two Poly(D,L-lactides) and two Poly(L-lactides-co-ε-caprolactone), both at high and low initial molecular weight, respectively.

At the same time, a new shape of the bone fixation system has been investigated in order to guarantee a proper mechanical stability. In fact, during and after the implantation, the pin is subjected to mechanical stresses due to both surgery and healing process. These have been considered through a suitable mechanical model which allowed to understand the mechanical stress distribution along the geometry of the device. In this sense, the attention has been mostly focused on the cross section of the pin because, as already mentioned, one of the requirements is that it must not degenerate into a circle, causing the loss of the contact and the torsion between the two fractured bone extremities. Thus, three geometries, whose cross sections are all characterized by an internal circle but differ for the shape of the edges, have been considered: the first one with four more squared edges (1), the second one with four more circular edges (2) and the third one with four more sharp edges (3).
Within the edges, the degradation will be more considerable because the loads are greater in these areas than in the rest of the cross section. This has been verified through a model which couples degradation with mechanical stresses.

The final outcome is an optimized bioresorbable pin for bone fixation with proper shape, (geometry 3) and composition (200 kDa Mw Poly(D,L-lactide)). Moreover, sample with

these specifications have been produced by injection moulding, sterilized with β-sterilization and finally ex vivo tested in human femoral heads for lab scale fixation experiments.

Chapter II

2. Materials and Methods

2.1 Materials

The following four bioresorbable polymers with different initial molecular weights belonging to the aliphatic polyester family have been compared with those commercially available and considered. The characteristics of the selected polymers together with the suppliers of those commercially available are reported in *Table 2.1:*

#POLYMER	POLYMER NAME	SUPPLIER	INITIAL MW	INITIAL MN	PD
Polymer 1	Poly(L)-lactide-co-ε-caprolactone	CORBION	183 kDa	114.4 kDa	1.6
Polymer 2	Poly(L)-lactide-co-ε-caprolactone	EVONIK	80 kDa	65 kDa	1.23
Polymer 3	Poly(DL)-lactice Acid	CORBION	76 kDa	40 kDa	1.9
Polymer 4	Poly(DL)-lactice Acid	CORBION	200 kDa	140 kDa	1.4

Table 2.1: Characteristics of the selected polymers. Mw and Mn are the weight and number average molecular weight, respectively, and PD is the polydispersity

The product data sheets of each tested polymer are reported in *Appendix A*.

Tetrahydrofuran (THF) (Sigma Aldrich, Steinheim, Germany) has been used as supplied.

2.2 Processing and Analytics

2.2.1 Injection Moulding

SAMAPLAST AG, a plastic processing company in St. Margrethen (Switzerland), has been contacted for injection moulding for both dog bone samples and the final optimized pins. The injection mould machine characteristics are:

- Microprocessor controlled
- 150 – 3500 kN locking force
- Product with a weight from 0.01 to 1000 grams [Site 8]

2.2.2 Sterilization Method

LEONI, a global provider of products, solutions and services for energy and data management in the automotive sector, healthcare and other industries in Däniken, (Switzerland), has been contacted for β-sterilization of both dog bone samples and the final optimized pins.

2.2.3 Gel Permeation Chromatography

Weight-average (Mw) and number-average molecular weight (Mn) values and molecular weight distributions (Mw/Mn) values of the polymers pre and after β-sterilization were evaluated using a Jasco LC-2000Plus gel permeation chromatograph (GPC) equipped with a refractive index detector RI-2031Plus (Jasco, Oklahoma City, OK, USA) using 3 Agilent (Santa Clara, CA, USA) PLgel columns, 5 $*10^{-6}$ m particle size, 300*7.5 mm (Mw range: $5*10^{2}$ to $17*10^{5}$ $g*mol^{-1}$). THF was chosen as eluent at a flow rate of 0.5 $mL*min^{-1}$ at 35 °C. The GPC samples were injected using a Jasco AS-2055Plus autosampler. The instrument was calibrated using polystyrene standards from 580 to 3,250,000 Da (Polymer Laboratories, Church Stretton, UK).

This analysis has been run at Politecnico di Milano, Dipartimento di Chimica, Materiali e Ingegneria Chimica “Giulio Natta”.

2.2.4 Tensile Test

Tensile test, although relatively simple to be run, is one of the most accurate methods for measuring polymer properties. For accurate results, specimens should have a reduced and uniform cross-sectional area over the central length, widening out at the ends where the specimen will be gripped; in theory, the applied tensile force is distributed uniformly over the cross-sectional area within the central region. This is the reason why dog bone samples have been used, when possible, for tensile tests (*Figure 2.1*). In other cases, directly the formed pins have instead been implied.

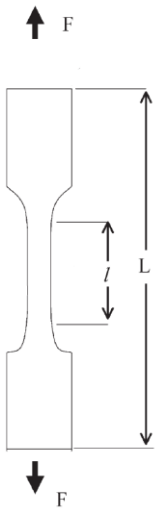

Figure 2.1: Schematic representation of a dog bone sample with applied forces

In order to analyse the selected polymers, tensile tests have been run at "Department of Materials" at ETH, in Zurich, with Shimadzu AGS-X machine having the following characteristics:

- Load cell options ranging from 1 N to 300 kN
- Table top test frames at 10 kN
- Integrated operation panel
- Trapezium X universal testing software [Site 13]

Dog bone samples made of Poly(L)-lactide-co-ε-caprolactone (*Polymer 1*) and pins made of Poly(D,L-lactide) (*Polymer 4*) have been injection moulded for this purpose, part of them have been sterilized and then they have been tested.

In particular, three different batches of dog bones samples not sterilized yet made of Polymer 1, three different batches of sterilized dog bones samples made of Polymer 1, three formed pins not sterilized yet made of Polymer 4 and three formed and sterilized pins made of Polymer 4 have been tested. Results have been used to determine Young's modulus and the maxima strain and stress at break.

In *Figure 2.2,* dog bone samples made of Polymer 1 are represented:

Figure 2.2: Dog bone samples

In *Figure 2.3*, one of the formed pins made of Polymer 4 is represented:

Figure 2.3: One of the formed pins implied in tensile tests

In *Figure 2.4*, the sample behaviour during the tensile test is shown:

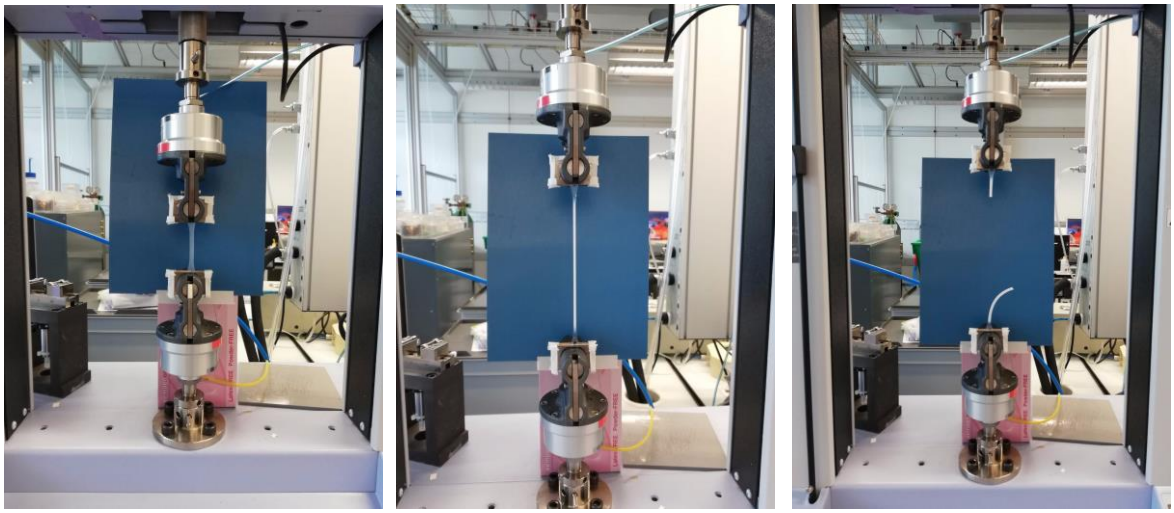

Figure 2.4: Sample behaviour during the tensile test

2.2.5 Torsion and Bending Test

The aim of a torsion test is to determine the behavior exhibited by a material when twisted or under torsional forces as a result of applied torques.

Torsion test twists a sample to a specified degree, with a specified force, or until the material fails in torsion. A twisting force is applied to the tested sample by fixing one end and applying a torque to the other end so that the sample is rotated about its axis [Site 14].

Formed pins (*Figure 2.3*) made of Poly(D,L)-lactide (*Polymer 4*) have been injection moulded and sterilized for this purpose.

In order to run this test, it has been necessary to implant the pins inside blocks of Sawbone of about 40 x 60 x 20 mm. Sawbone is a biomechanical test material made of rigid polyurethane foam and used as an alternative to cadaver bone for testing orthopaedic implants, instruments and instrumentation.

In *Figure 2.5* the samples preparation for the test is shown:

Figure 2.5: Samples preparation

Bending test allows for the determination of materials ductility, bend strength, fracture strength and resistance to fracture, in order to determine whether a material will fail under pressure.

A three-point bending tests deform the sample at the midpoint causing a concave surface without the occurrence of fracture. The test sample is loaded in such a way to create the concave surface at the midpoint with a specified radius of curvature according to the standard in relation to which the test is performed [Site 14].

In contrast, a four-point bending test provide the addition of a fourth bearing which brings a much larger portion of the pin to the maximum stress.

Formed pins (*Figure 2.3*) made of Poly(D,L)-lactide (*Polymer 4*) have been injection moulded and sterilized for this purpose, and then examined with both types of bending tests.

In order to analyse the selected polymer, both torsion and four-points bending tests have been run at "Laboratory of Biological Structure Mechanics" at Politecnico di Milano, with a MTS 858 Bionix servohydraulic testing machine (S/N 1014952, MTS, Minneapolis, MN). The MTS testing machine has been equipped by an axial-torsional hydraulic actuator, with 25 kN axial capacity and 250 Nm torsional capacity, a ±100 mm range LVDT displacement transducer and a ±140° range ADT angular transducer mounted on the actuator. The load applied to the test sample has been measured by a MTS axial/torsional load cell (model

662.20D-05, S/N 1007099, ± 25 kN maximum axial load, ± 250 Nm maximum torsional load). The machine has been driven by Test Star 790.01 digital controller.

Three-points bending tests have been run at "Department of Materials" at ETH, in Zurich, with Shimadzu AGS-X machine having the following characteristics:

- Load cell options ranging from 1 N to 300 kN
- Table top test frames at 10 kN
- Integrated operation panel
- Trapezium X universal testing software [Site 13]

In *Figure 2.6* and *2.7*, torsion and bending test procedures are shown, respectively:

Figure 2.6: Torsion test procedure

In particular, four sterilized pins have been tested. Results have been used to determine the maximum shear modulus and the maxima shear stress and strain.

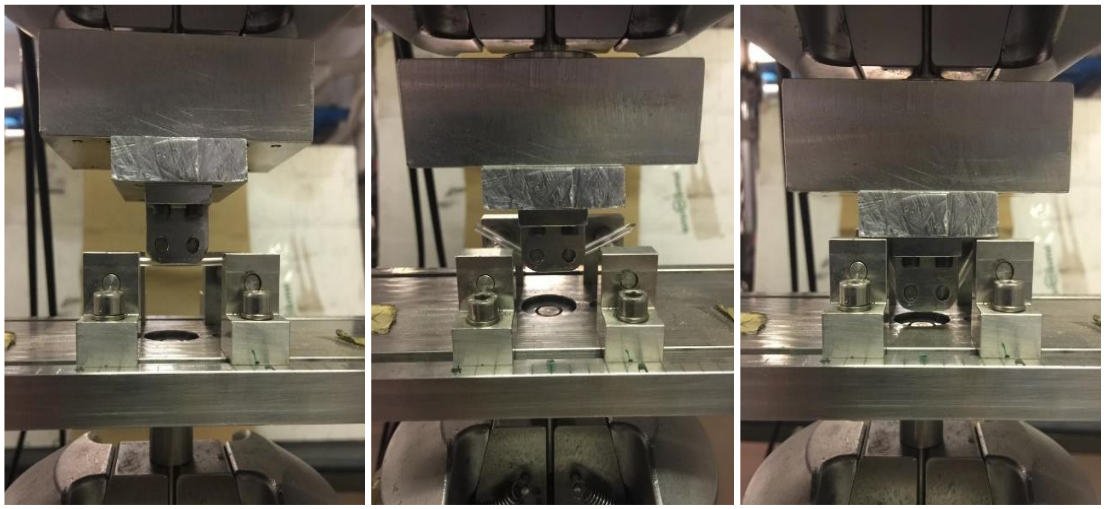

Figure 2.7: Bending test procedure

In particular, three injected and sterilized pins have been implied for four-points bending test, while three injected and not sterilized yet pins and three injected and sterilized pins have been used as samples for three-points bending test. Results have been used to determine the maximum bending modulus and the maxima stress and strain.

2.2.6 Implantation Test

The qualitative analysis on the injected pins with composition and shape finally selected as optimal have been run on human femoral head at “Clinica Luganese Moncucco” (Lugano, Switzerland), with the help of PD Dr. med. Kaj Klaue.

The following instruments have been selected for this purpose:

A. Orthopedic drill;
B. Four bone drill bits which differs in diameter (2 mm, 2.5 mm, 3.2 mm and 3.5 mm);
C. 300 g orthopedic bone hammer;
D. Orthopedic impactor;
E. Oscillating saw equipment;
F. 2.5 mm & 3.5 mm tap sleeve;
G. Surgical clamp;
H. Human femoral head;
I. Bioresorbable optimized pins.

Chapter III

3. Model Development

3.1 Optimization strategy

The reason behind the selection of the four initial polymers is related to the necessity to find a commercially available polymer which, at the same time, guarantees the respect of the imposed requirements, i.e., a final weight average molecular weight above 45 kDa after 60 days of degradation. This, in fact, is the necessary condition in order to be able to respect another important requirement, i.e., the mechanical properties stability.

The reason behind the selection of the three initial geometries is related on one hand to the need to guarantee the mechanical stability during the bone healing and on the other hand to orthopaedic conditions.

It is important to underline that the model outcomes will allow to derive a proper polymer/geometry combination.

In *Figure 3.1*, the flow chart of the optimization strategy is reported:

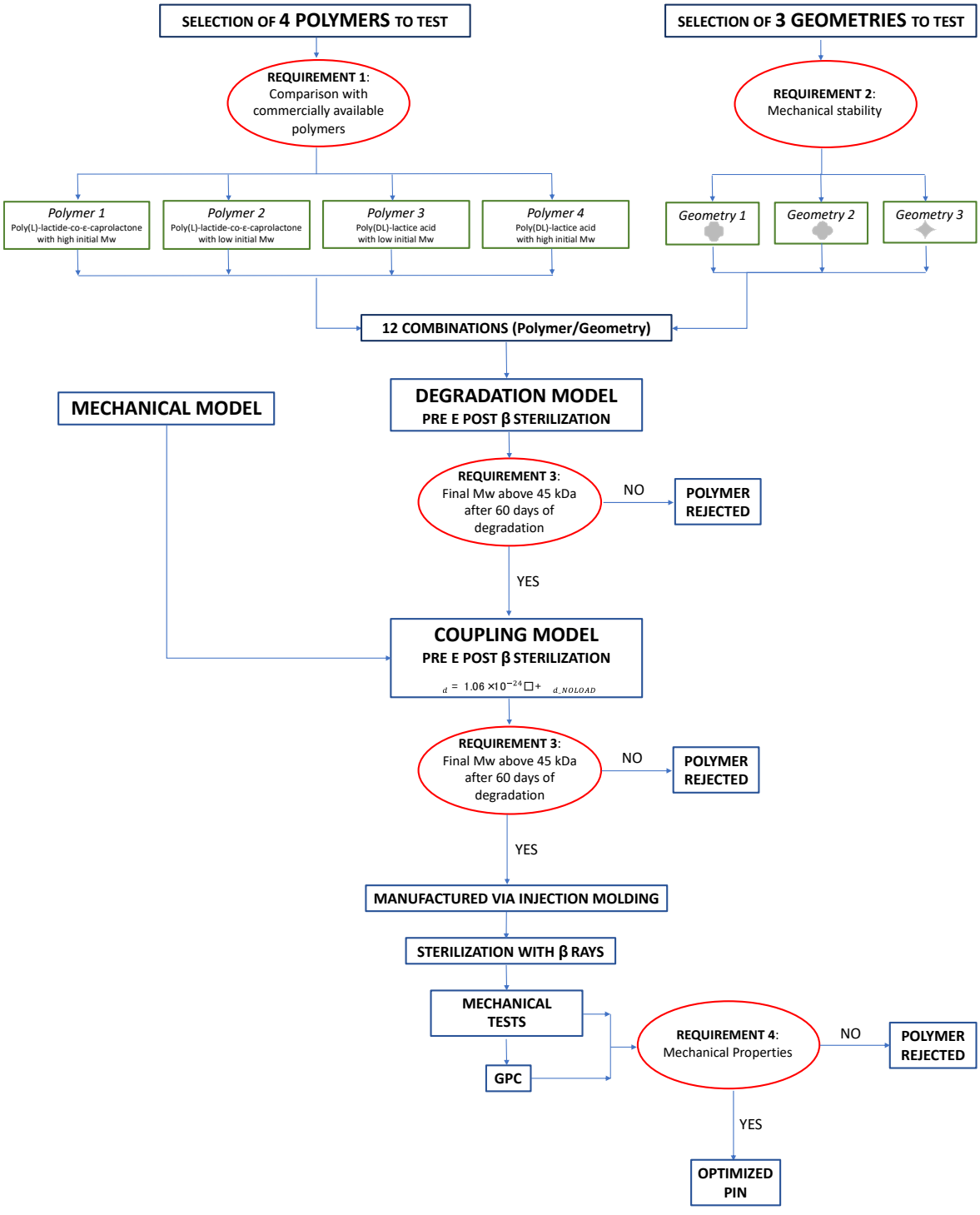

Figure 3.1: Flow chart of the optimization strategy

3.2 Degradation Model

Upon implantation, each one of the selected polymers presents the feature of being completely reabsorbed by the body. In this sense, the degradation of the pin has been modelled by selecting a proper mathematical degradation model.

In this work, the method of choice is the model described in *Casalini et al.* [10]. Polymer degradation occurs due to the hydrolysis mechanism: water penetrates into the matrix and breaks ester bonds, which constitute the polymer backbone. The resulting oligomers can diffuse in and out of the matrix and act as a catalyst for the hydrolysis reaction because of their carboxyl groups, as degradation is enhanced in acid environments.

The dynamics of both water diffusion and hydrolysis regulate the degradation mechanism. Diffusion coefficients can be related to monomer concentration and molecular weight in order to describe the device hydrolysis-diffusivity interplay.

Degradation phenomena are described through mass conservation equations, by means of population balances, which allow a detailed treatment of chain hydrolysis and explicitly consider the autocatalytic effect, assuming a degradation rate proportional to the concentration of acidic moieties. Mass balances also consider diffusion phenomena (assumed as Fickian) since the resulting oligomers can diffuse through the matrix and their local concentration determines the hydrolysis increase due to autocatalytic effects.

Polymer degradation, due to acid-catalysed hydrolysis mechanism, is described according to the following kinetic scheme:

$$P_{n+m} + W + H^+ \rightarrow P_n + P_m + H^+$$

Equation 3.1: Polymer Degradation Kinetic Scheme

According to kinetic *Equation 3.1*, a water molecule (W) breaks one long chain (P_{n+m}) in two smaller ones (P_n, P_m); among the degradation products, only water and oligomers up to nonamers diffuse inside the matrix, whereas longer chains are assumed to be non-diffusing. The model also relies on the following assumptions: isothermal system (thus no energy balance is required), degradation constant independent on the chain length (a widely accepted approximation in the polymer reaction engineering field), constant volume

(reasonable for bulk eroding polymers, as the ones used in this work) and hydrolysis rate also proportional to [COOH] concentration. (*Equation 3.2*):

$$r_n = k_d C_w P_n [COOH] = k_d C_w P_n \sum_{n=1}^{\infty} P_n$$

Equation 3.2: Hydrolysis rate expression

These assumptions allow writing mass conservation equations for the monomer (*Equation 3.3*), the diffusing oligomers (with a chain length comprised between 2 and 9, *Equation 3.4*), the polymeric chains (with a number of monomeric units equal or higher than 10, *Equation 3.5*) and water (*Equation 3.6*), respectively:

$$\frac{\partial C_M}{\partial t} = \nabla(D_M \nabla C_M) + 2k_d C_W \sum_{j=2}^{\infty} C_j \sum_{j=1}^{\infty} C_j$$

Equation 3.3: Monomer mass conservation equation

$$\frac{\partial C_n}{\partial t} = \nabla(D_n \nabla C_n) + 2k_d C_W \sum_{j=n+1}^{\infty} C_j \sum_{j=1}^{\infty} C_j - (n-1) k_d C_W C_n \sum_{j=1}^{\infty} C_j \quad 2 \leq n \leq 9$$

Equation 3.4: Mass conservation equation of the diffusing oligomers with a chain length comprised between 2 and 9

$$\frac{\partial C_n}{\partial t} = 2k_d C_W \sum_{j=n+1}^{\infty} C_j \sum_{j=1}^{\infty} C_j - (n-1) k_d C_W C_n \sum_{j=1}^{\infty} C_j \quad n > 9$$

Equation 3.5: Mass conservation equation of the polymeric chains with a number of monomeric units equal or higher than 10

$$\frac{\partial C_W}{\partial t} = \nabla(D_W \nabla C_W) - k_d C_W \sum_{j=1}^{\infty} (j-1) C_j \sum_{j=1}^{\infty} C_j$$

Equation 3.6: Water mass conservation equation

where C_M, C_n, and C_w are the molar concentrations of monomer, polymeric chains of length n, and water, respectively; D_M, D_n, and D_w are diffusion coefficients for monomer, diffusing

oligomers, and water, respectively and k_d is the degradation kinetic constant. The model assumes that diffusion follows Fickian behaviour; diffusion coefficients are included into the derivative operator since they depend on molecular weight, which varies along the characteristic degradation length as hydrolysis takes place. Since the degrading polymer chains may consist of up to 10^4–10^5 units and it would be necessary to solve a quite large number of differential equations, a way to reduce the complexity of the problem is to apply the method of moments. The generic *k*th order statistical moment is defined as follows (*Equation 3.7*):

$$\mu_k = \sum_{n=1}^{\infty} n^k \, C_n$$

Equation 3.7: Generic kth order statistical moment

Partial differential equations describing time evolution of statistical moments can be obtained as follows, after some computations (*Equation 3.8*):

$$\frac{\partial \mu_k}{\partial t} = \sum_{n=1}^{\infty} n^k \frac{\partial C_n}{\partial t}$$

$$\sum_{n=1}^{\infty} \sum_{j=n+1}^{\infty} C_n = \mu_1 - \mu_0$$

$$\sum_{n=1}^{\infty} n \sum_{j=n+1}^{\infty} C_n = \frac{\mu_2}{2} - \frac{\mu_1}{2}$$

$$\sum_{n=1}^{\infty} n^2 \sum_{j=n+1}^{\infty} C_n = \frac{\mu_3}{3} - \frac{\mu_2}{2} + \frac{\mu_1}{6}$$

Equation 3.8: Partial differential equations describing time evolution of statistical moments

A closure equation can express the third order statistical moment (*Equation 3.9*):

$$\mu_3 = \frac{\mu_2}{\mu_0 \mu_1}(2\mu_0\mu_2 - \mu_1^2)$$

Equation 3.9: Third order statistical moment

Monomer, oligomers and water mass balances can be, thus, reformulated in terms of statistical moments (*Equation 3.10*):

$$\frac{\partial C_M}{\partial t} = \nabla(D_M \nabla C_M) + 2k_d C_W(\mu_0 - C_M)\mu_0$$

$$\frac{\partial C_n}{\partial t} = \nabla(D_n \nabla C_n) + 2k_d C_W\left(\mu_0 - \sum_{j=1}^{n} C_j\right)\mu_0 - (n-1)k_d C_W C_n \mu_0 \quad 2 \le n \le 9$$

$$\frac{\partial C_W}{\partial t} = \nabla(D_W \nabla C_W) - k_d C_W(\mu_1 - \mu_0)\mu_0$$

Equation 3.10: Monomer, oligomers and water mass balances in terms of statistical moments

Three partial differential equations describing the time evolution of statistical moments of order zero, one and two can be obtained by applying the definition of *k*th order moment (*Equation 3.11*):

$$\frac{\partial \mu_0}{\partial t} = \sum_{j=1}^{9} \nabla\left(D_j \nabla C_j\right) + k_d C_W(\mu_1 - \mu_0)\mu_0$$

$$\frac{\partial \mu_1}{\partial t} = \sum_{j=1}^{9} \nabla\left(D_j \nabla C_j\right)$$

$$\frac{\partial \mu_2}{\partial t} = \sum_{j=1}^{9} \nabla\left(D_j \nabla C_j\right) + \frac{k_d C_W \mu_0}{3}\left(\mu_1 - 2\frac{\mu_2^2}{\mu_1} + \frac{\mu_2 \mu_1}{\mu_0}\right)$$

Equation 3.11: Three partial differential equations describing the time evolution of statistical moments

The large number of differential equations (10^4–10^5) needed to describe the concentration evolution in time of polymeric chains with a chain length equal to or higher than 10 are thus substituted by these three partial differential equations. Although the detail concerning chain length distribution is lost, statistical moments allow computing average properties of interest such as polydispersity and molecular weights, whose spatial and temporal evolution influence the effective diffusion coefficient. Moreover, the moments of the first three orders have a physical meaning: the zeroth order moment is equal to the overall polymer concentration per unit volume, the first order moment represents the overall concentration of monomeric units per unit volume, and the second order moment is related to polymer polydispersity.

Properties of interest can be expressed through statistical moments:

$$\textit{Number Average Molecular Weight: } M_n = \frac{\mu_1}{\mu_0} MW_{mon}$$

$$\textit{Weight Average Molecular Weight: } M_w = \frac{\mu_2}{\mu_1} MW_{mon}$$

$$\textit{Polydispersity: } PD = \frac{\mu_0 \mu_2}{\mu_1^2}$$

where MW_{mon} is the monomeric unit molecular weight.

At the polymeric device/environment interface the mass transfer resistance at the device surface is considered (*Equation 3.12*):

$$-D_i \nabla C_i = k_{C,i}^{ext} C_{b,i} \quad i = water, monomer\ and\ oligomers$$

Equation 3.12: Boundary Condition at the interface

where $C_{b,i}$ is the *i*th species concentration in the bulk phase of surrounding environment and $k_{C,i}^{ext}$ is the *i*th species mass transfer coefficient. Such value is equal to 0 for monomer and oligomers and to 0.055 mol/cm^3 for water. This is consistent with the periodic removal of the surrounding constituted by water.

The mass transfer coefficient is estimated through Sherwood number (*Equation 3.13*):

$$Sh = 2 = \frac{2k_{C,i}^{ext}R}{D_{i,W}}$$

Equation 3.13: Definition of Sherwood number

where $D_{i,w}$ is the diffusion coefficient in water environment, equal to 10^{-6} cm^2/s and 10^{-5} cm^2/s for monomer and water respectively.

Initial conditions for water, monomers and oligomers consider a null concentration since the devices are supposed to be anhydrous and without residual short chains.

Initial conditions for statistical moments are referred to non-degraded polymer and computed as follows (*Equation 3.14*):

$$\mu_0(t=0) = \frac{\rho_{pol}}{M_n(t=0)}$$

$$\mu_1(t=0) = \frac{M_n(t=0)}{MW_{mon}}\mu_0(t=0)$$

$$\mu_2(t=0) = \frac{\mu_1^2(t=0)}{\mu_0(t=0)}PD(t=0)$$

Equation 3.14: Initial conditions for statistical moments

The involved parameters are related to polymer degradation phenomena and transport phenomena inside the polymeric matrix. Because the model is based on first-principles, such quantities have a specific physical meaning (kinetic constants, diffusion coefficients, and so on) and thus can be independently and robustly estimated from experimental data.

The hydrolysis kinetic constant k_D is fitted from experimental data, from time evolution of weight-average molecular weight.

As for diffusion coefficients, the model assumes an expression that takes into account the diffusivity increase as hydrolysis occurs through time and spatial evolution of number average molecular weight M_n (*Equation 3.15*):

$$D_i = D_i^0 \exp\left[2.5\left(1 - \frac{M_n(t,r)}{M_n(t=0)}\right)^{0.5}\right] \quad i \leq 9$$

Equation 3.15: Diffusion coefficient expression

where D_i^0 is the diffusion coefficient of the *i*th oligomer (including monomeric units) before the degradation onset.

This equation is also employed to describe the diffusivity of water. This functional form has been used for all simulation performed.

Model consistency can be verified through mass balances, writing closure equations which represent the fundamental mass conservation. For what concerns polymer degradation, a closure equation can be formulated thanks to the physical meaning of the first order statistical moment, that is, the number of monomeric units for a unit volume. For every time instant *t**, the initial amount of monomeric units must be equal to the sum of the amount at time *t** and the fraction of monomeric units which left the device in the time interval 0 – *t**. This can be expressed as follows (*Equation 3.16*):

$$\mu_1(t=0) \cdot volume = \int_V \mu_1(V, t=t^*)dV + \int_0^{t^*}\int_S -D_M \nabla C_M dS dt$$

Equation 3.16: Closure equation

where *S* is the device external surface. The first integral represents the amount of the overall monomeric units at time *t**, while the second one is the overall monomer loss at time *t**.

The error related to polymer degradation can be defined as follows (*Equation 3.17*):

$$\epsilon_{deg} = \frac{\int_V \mu_1(V, t=t^*)dV + \int_0^{t^*}\int_S -D_M \nabla C_M dS dt - \mu_1(t=0) \cdot volume}{\mu_1(t=0) \cdot volume} \cdot 100$$

Equation 3.17: Error related to polymer degradation

3.2.1 Model validation

A model may be valid for one set of experimental conditions and invalid for another one. A model is considered valid for a set of experimental conditions if the model accuracy is within the range of accuracy required for the model intended purpose. This usually requires identifying the model output variables of interest and specifying the required acceptable range of accuracy for each variable, i.e., the range that the difference between that model variable and the corresponding system variable can have for the model to be valid.
Operational validation is determining whether the simulation model output behaviour has the accuracy required for the model intended purpose over the domain of the model intended applicability. To obtain a high degree of confidence in a simulation model and its results, comparisons between the model and system output behaviours for several different sets of experimental conditions are usually required.

Therefore, in order to validate the model degradation used in this work, the following steps have been considered:

1. Three papers have been selected, each one studying the behaviour of the degradation of a bioresorbable polymeric device with a specific geometry. The degradation models used in these studies are different with respect to that implemented in this thesis.
2. Each literature data set has been used as input data for the degradation model selected for this work.
3. For each bioresorbable polymeric device with a specific geometry a simulation has been run.
4. The output behaviour of the model resulting from the three different simulations has been compared with the output literature data set (in particular, graphical comparison of data).

The devices studied in the selected papers are:

1. Microparticles made of PLGA [10]
2. Rods made of PLLA [8]
3. Film made of PDLLA [13]

All the simulations have been run with COMSOL Multiphysics.

3.2.1.1 First validation

The polymeric microparticle made of PLGA is modelled as a sphere of constant volume with radial variations in concentrations, being subjected to hydrolysis degradation.
The following simulation input data have been considered (*Table 3.1*):

Radius [µm]	7.9
MW_{mon} [Da]	83
M_W [Da]	29310
PD [-]	1.6
k_d [$cm^6/mol^2/s$]	1.386×10^{-3}

Table 3.1: Microparticle parameters for first validation

The microparticle geometry is the following (*Figure 3.2*):

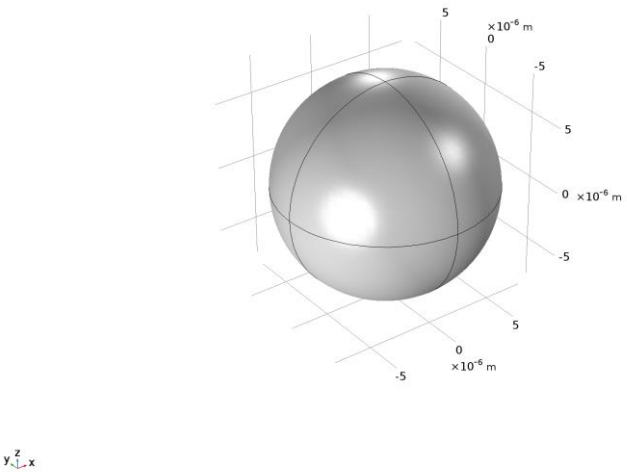

Figure 3.2: Microparticle geometry

The simulation has been run with different mesh size, in order to find the mesh-independent model (*Figure 3.3*):

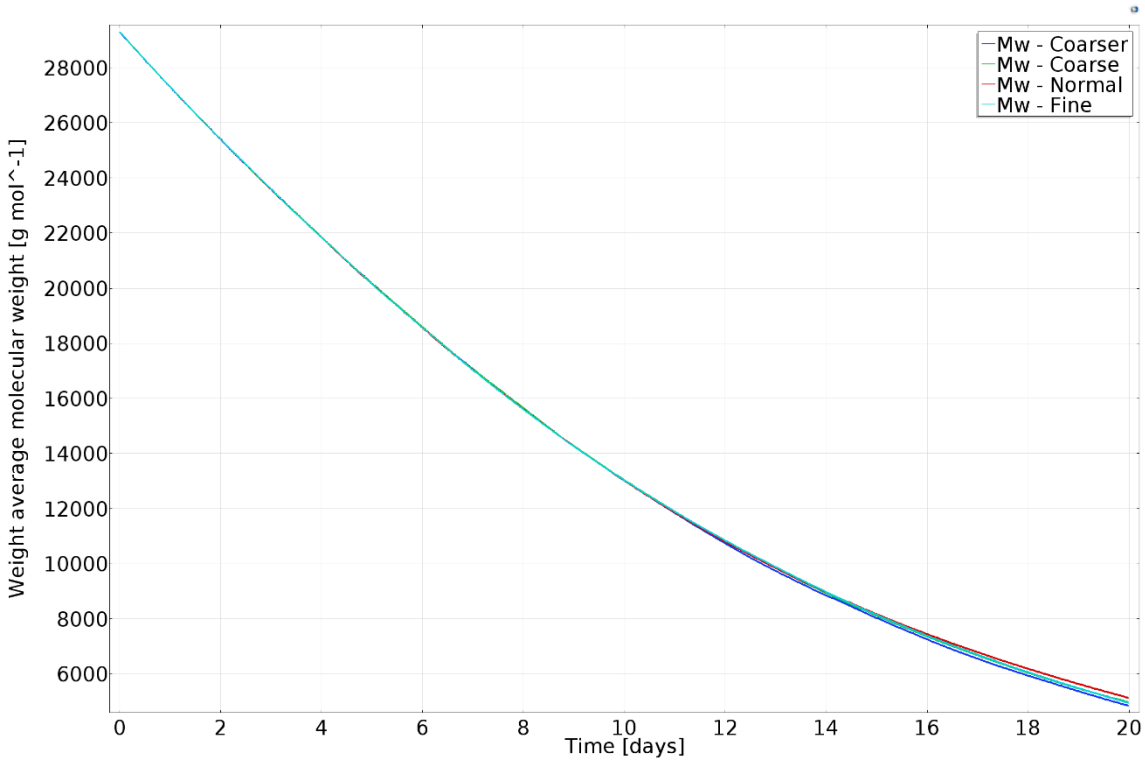

Figure 3.3: Simulation with different meshes

It is possible to notice that the best compromise among all the behaviour is obtained by selecting the Normal mesh (*Figure 3.4*):

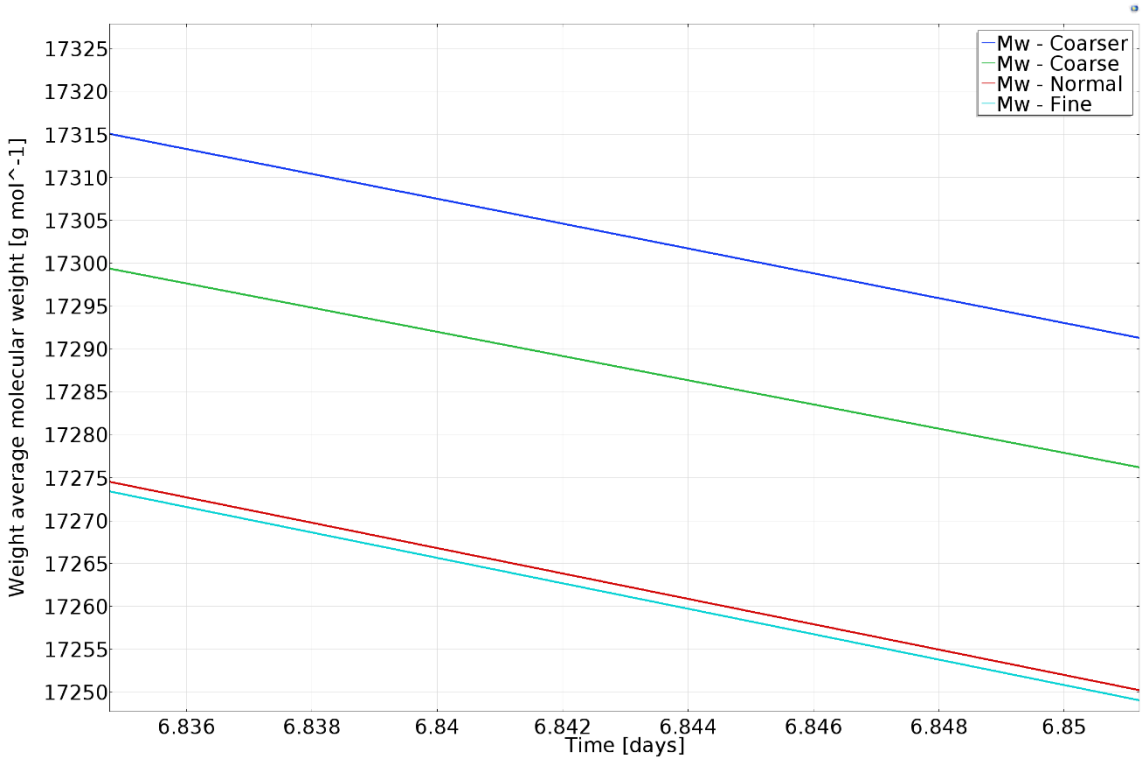

Figure 3.4: Detail of the result trends with the different meshes

The considerations regarding the mesh-independent model have been verified and assumed as valid for the following two validations.

In *Figure 3.5*, the comparison between literature and simulation results is reported:

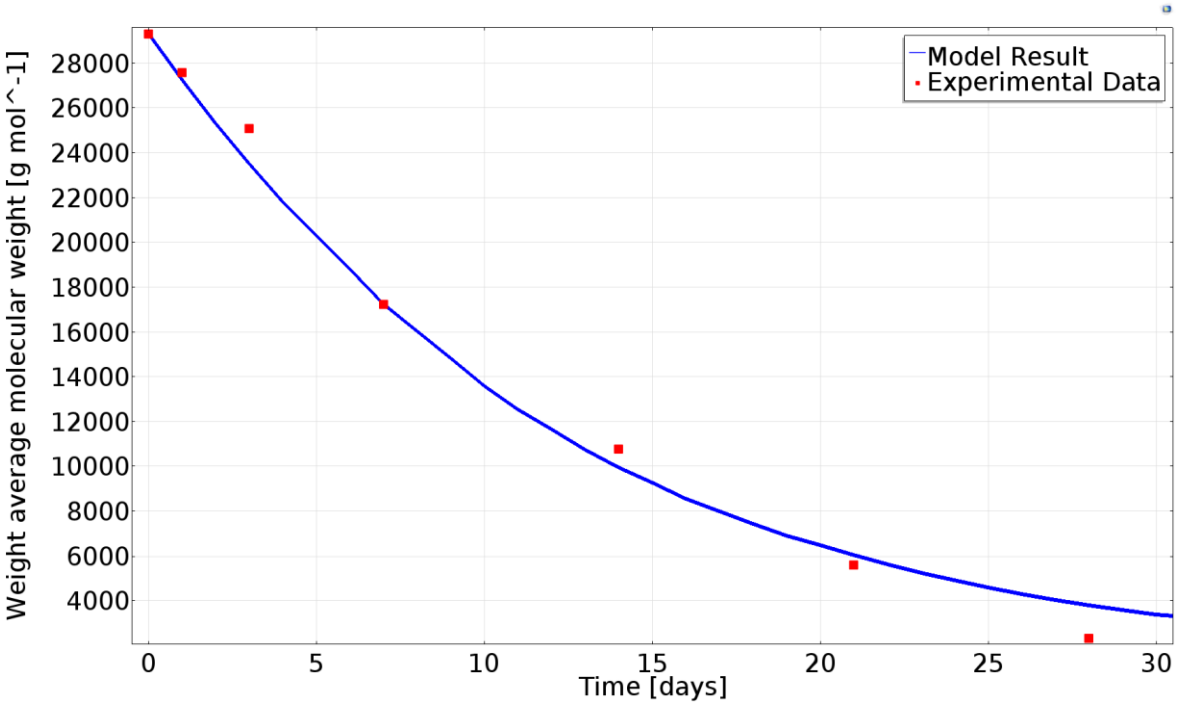

Figure 3.5: Validation result

It can be seen that the trends are similar.

In order to verify the model consistency, the error estimation can be computed through mass balances, writing closure equations which represent the fundamental mass conservation, as previously mentioned.

The error estimation can be localized in the first hours of degradation, since then it settles. The error depends on both the mesh size and the Time Step (TS). Therefore, the simulation has been firstly run by considering half day of degradation, with a Time Step equal to six minutes, testing different meshes (*Figure 3.6*):

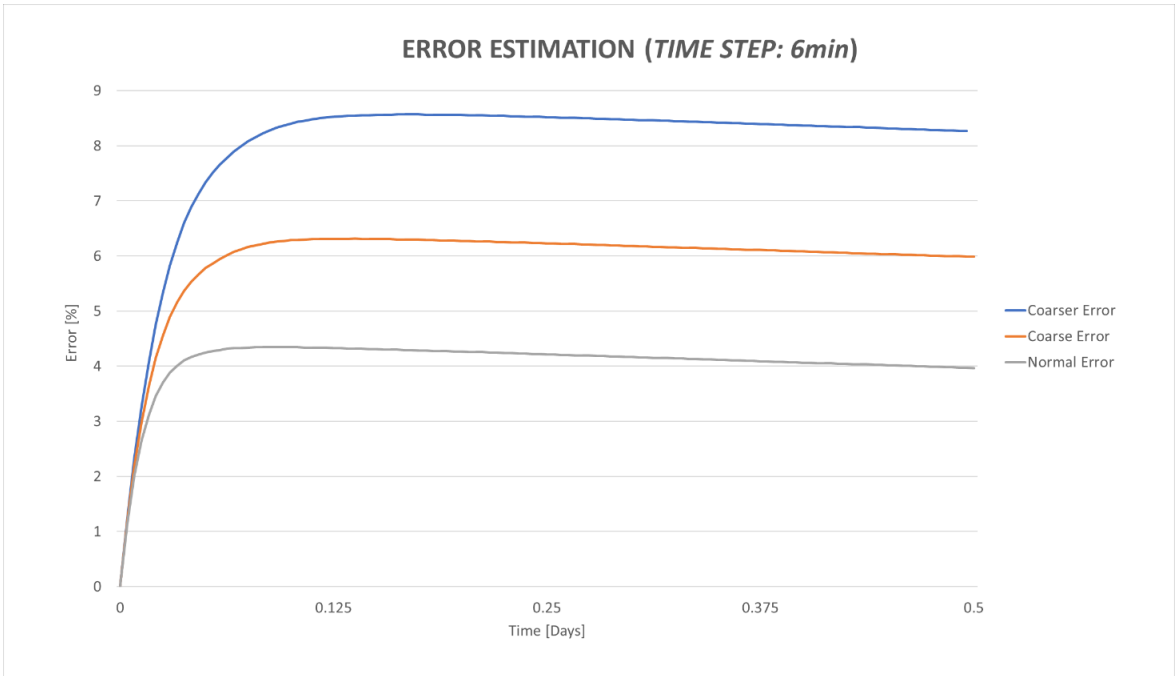

Figure 3.6: Error estimation with a TS equal to 6 min

It is possible to notice that the error really depends on the mesh density: by increasing the mesh density, the error decreases. Furthermore, this validates the use of the Normal mesh in order to have a mesh-independent model.

Then, the dependency on the Time Step can be studied by reducing it. Thus, a second simulation has been run by considering a Time Step equal to one minute (*Figure 3.7*):

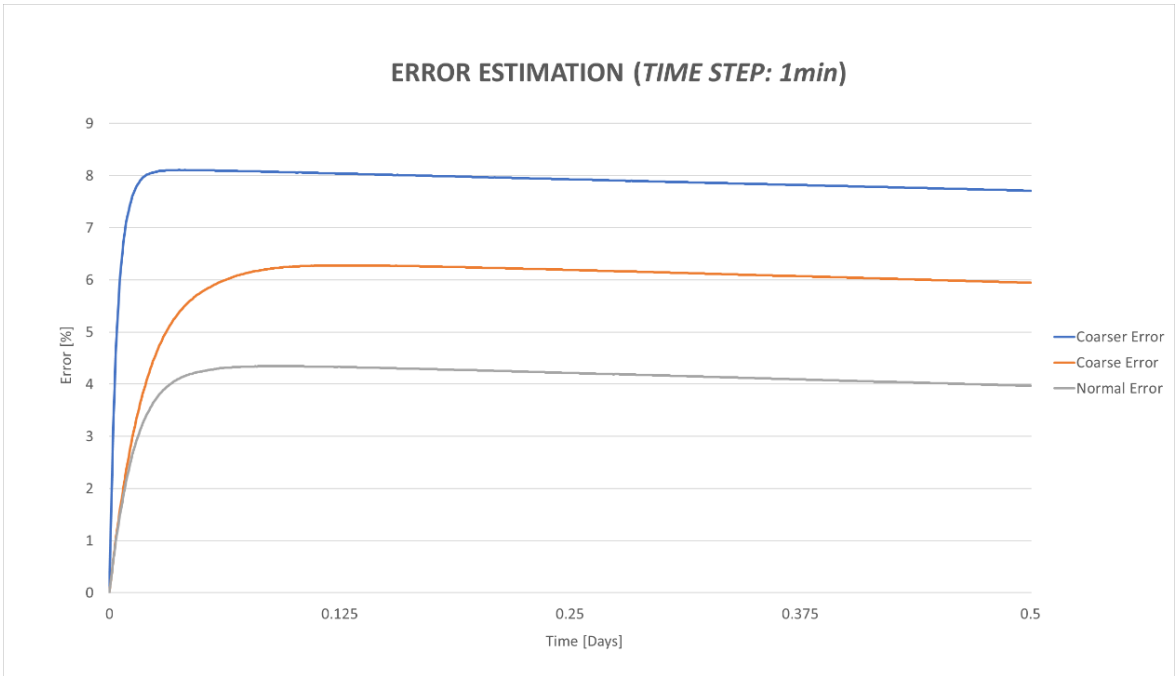

Figure 3.7: Error estimation with a TS equal to 1 min

A further confirmation that the Normal mesh is the best choice can be deduced: by modifying the Time Step, only the Normal mesh trends have a negligible variation.

Finally, both graphs show an artefact in the initial error: this is due to a "print Time Step" in the initial transient.

All these considerations allow to validate the model and they have been assumed as valid for the following two validations.

3.2.1.2 Second validation

The PLLA rod is characterized by a thickness equal to 0.8 mm, a diameter equal to 2 mm and a length of 30 mm.

The following simulation input data have been considered (*Table 3.2*):

Radius [mm]	1
Length [mm]	30
MW_{mon} [Da]	90.1
M_W [Da]	399000
PD [-]	2.57
k_d [$cm^6/mol^2/s$]	7.27×10^{-5}

Table 3.2: Rod parameters for second validation

The rod geometry is the following (*Figure 3.8*):

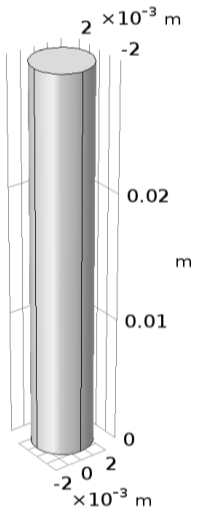

Figure 3.8: Rod geometry

In *Figure 3.9*, the comparison between literature and simulation results is represented:

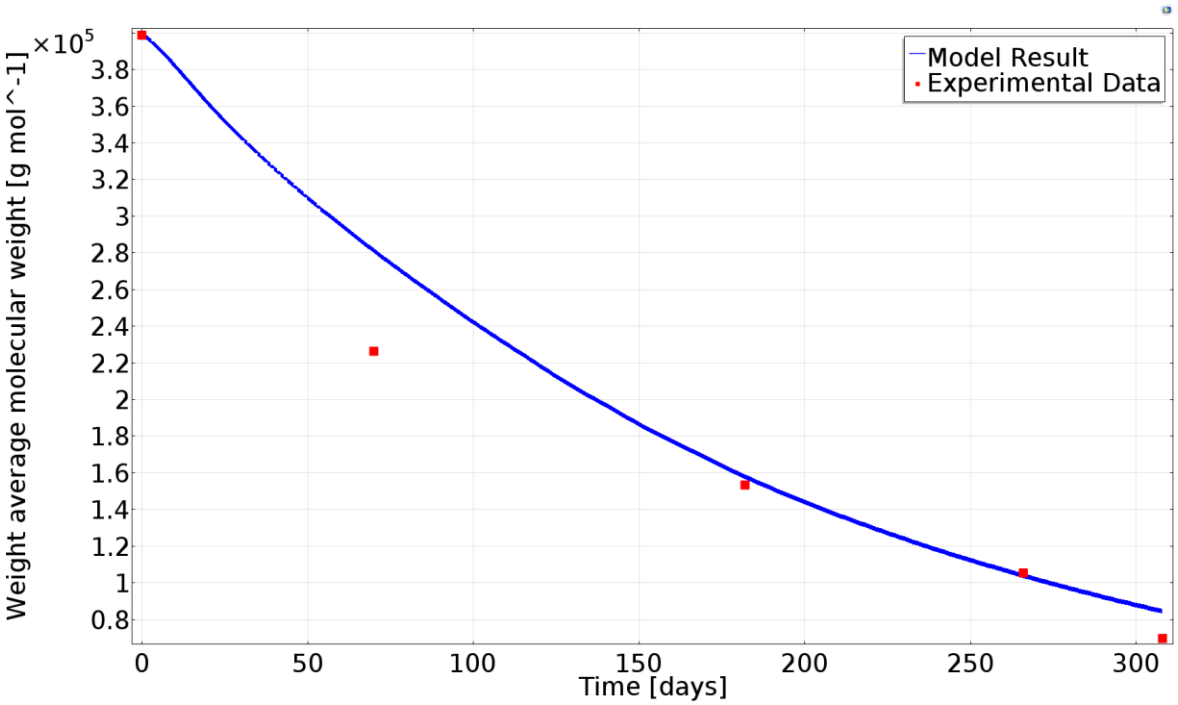

Figure 3.9: Validation result

It is noticeable that the trends are similar.

In conclusion the chemical model used in this project is validated.

3.2.1.3 Third Validation

The mechanism of degradation of 15 x 10 x 0.3 mm PDLLA film has been investigated.

The following simulation input data have been considered (*Table 3.3*):

Width [mm]	10
Length [mm]	15
Thickness [mm]	0.3
MW_{mon} [Da]	90.1
M_W [Da]	67000
PD [-]	2
k_d [$cm^6/mol^2/s$]	1.34×10^{-4}

Table 3.3: Film parameters for third validation

The film geometry is the following (*Figure 3.10*):

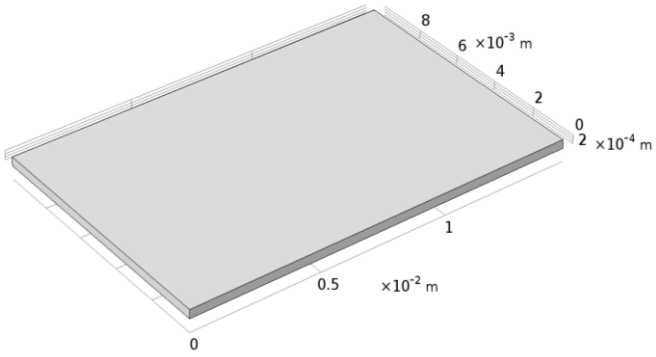

Figure 3.10: Film geometry

In *Figure 3.11*, the comparison between literature and simulation results is possible:

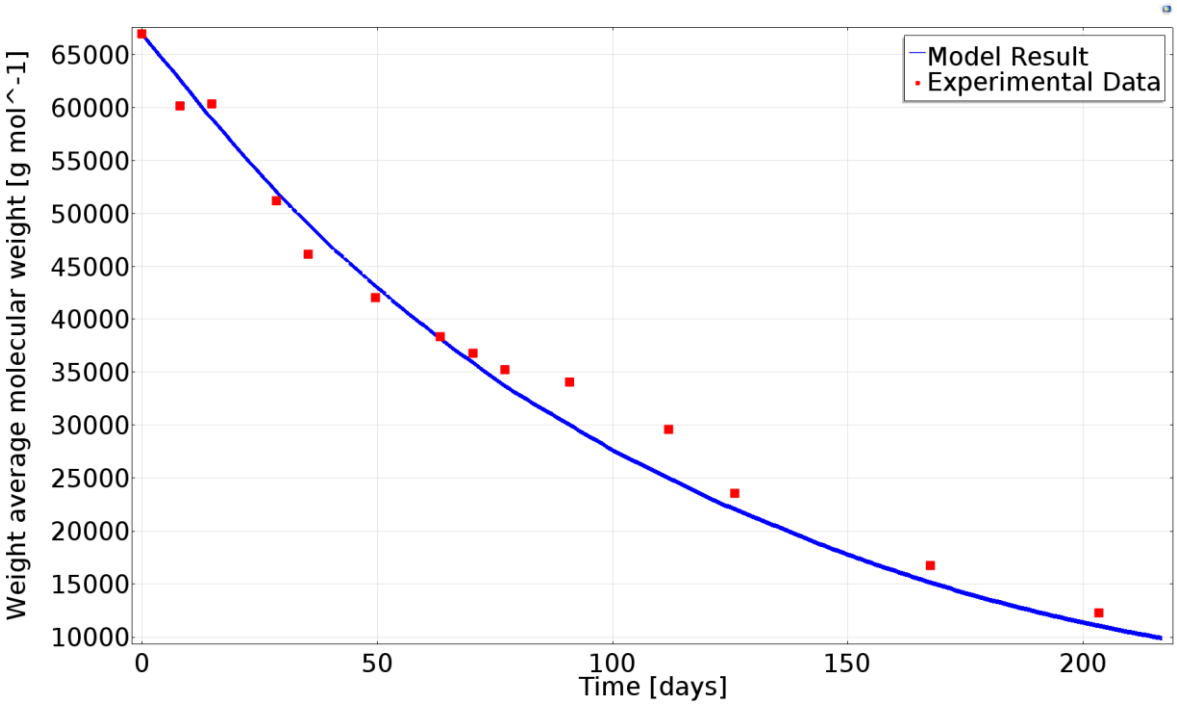

Figure 3.11: Validation result

It is noticeable that the trends are similar.

In conclusion the chemical model used in this project is validated.

3.2.2 Degradation Constant Extrapolation

In order to able to design an optimized pin, first of all it has been mandatory to derive the degradation constant for each polymer, with an optimization process.

A literature research in order to find studies describing the degradation of bioresorbable polymers with characteristics and properties similar to those of the polymers selected for this thesis have been necessary.

However, since the degradation constant is not explicitly indicated and, moreover, a different mathematical degradation model is used, the graphical extrapolation of the experimental data set followed by an optimization process based on the degradation model described in *Chapter 3.2.* have been required.

3.2.2.1 Polymer 1: PLACL with high initial molecular weight

S. Dånmark et al. [20] has been selected for what concern the degradation constant derivation of Polymer 1. Here, the behaviour of different polymers is studied; thus, the choice of the polymer with characteristics more similar to Polymer 1 has been necessary. In *Table 3.4*, the comparison between the properties of the polymer finally selected for this study and of Polymer 1 are reported:

	Polymer from Literature	**Polymer 1**
Mw [kDa]	165	183
Mn [kDa]	110	114.4
PD [-]	1.5	1.6

Table 3.4: Polymer from literature and Polymer 1 characteristics

The extrapolation of the experimental data set has been done by focusing on *Figure C.1* reported in Appendix C.

By implementing the experimental data set on COMSOL Multiphysics and selecting the Optimization tool, it has been found that the degradation constant value for Polymer 1 is:

$$k_D = 5.0254 \times 10^{-16} \frac{cm^6}{mol^2\, s}$$

In *Figure 3.12*, the optimization result is shown:

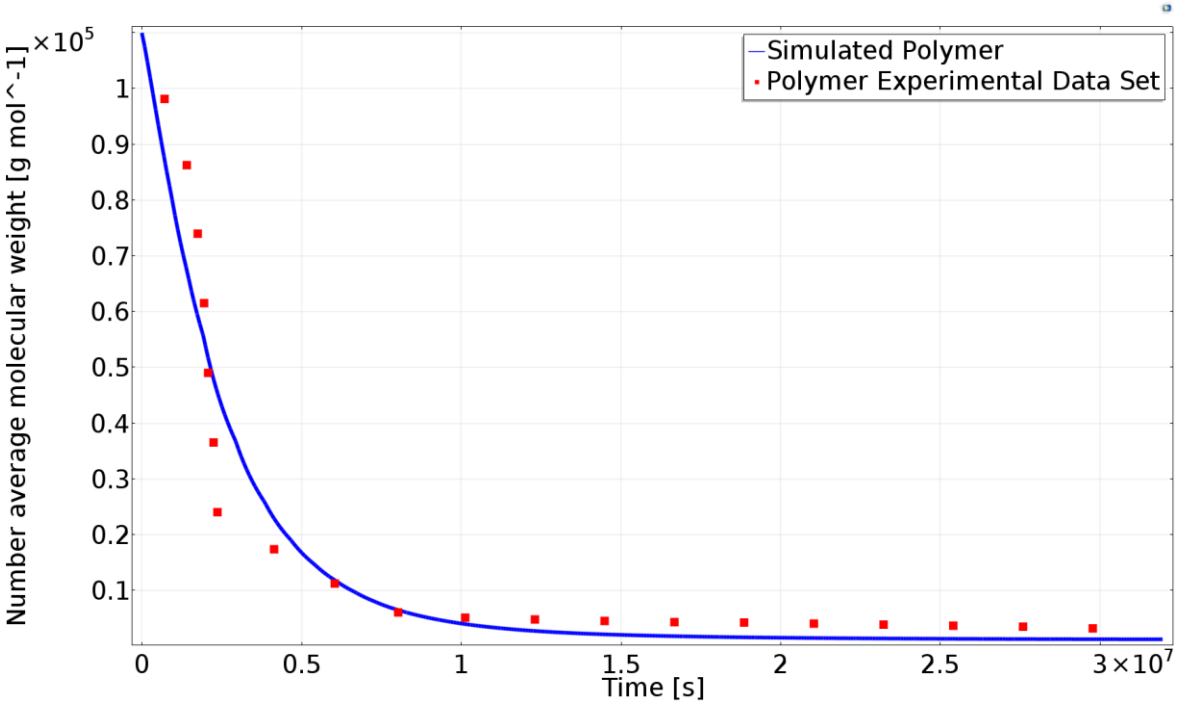

Figure 3.12: Optimization result - Polymer 1

It is possible to notice that the optimization results, obtained by applying the degradation model described in *Chapter 3.2.*, fit quite well the literature experimental data.

3.2.2.2 Polymer 2: PLACL with low initial molecular weight

S. Dånmark et al. [20] has been selected for what concern the degradation constant derivation of Polymer 2. Here, the behaviour of different polymers is studied; thus, the choice of the polymer with characteristics more similar to Polymer 2 has been necessary. In *Table 3.5*, the comparison between the properties of the polymer finally selected for this study and of Polymer 2 are reported:

	Polymer from Literature	**Polymer 2**
Mw [kDa]	105	80
Mn [kDa]	52.5	65
PD	2	1.23

Table 3.5: Polymer from literature and Polymer 2 characteristics

The extrapolation of the experimental data set has been done by focusing on *Figure C.1* reported in Appendix C.

By implementing the experimental data set on COMSOL Multiphysics and selecting the Optimization tool, it has been found that the degradation constant value for Polymer 2 is:

$$k_D = 5.4121 \times 10^{-16} \frac{cm^6}{mol^2\, s}$$

In *Figure 3.13*, the optimization result is shown:

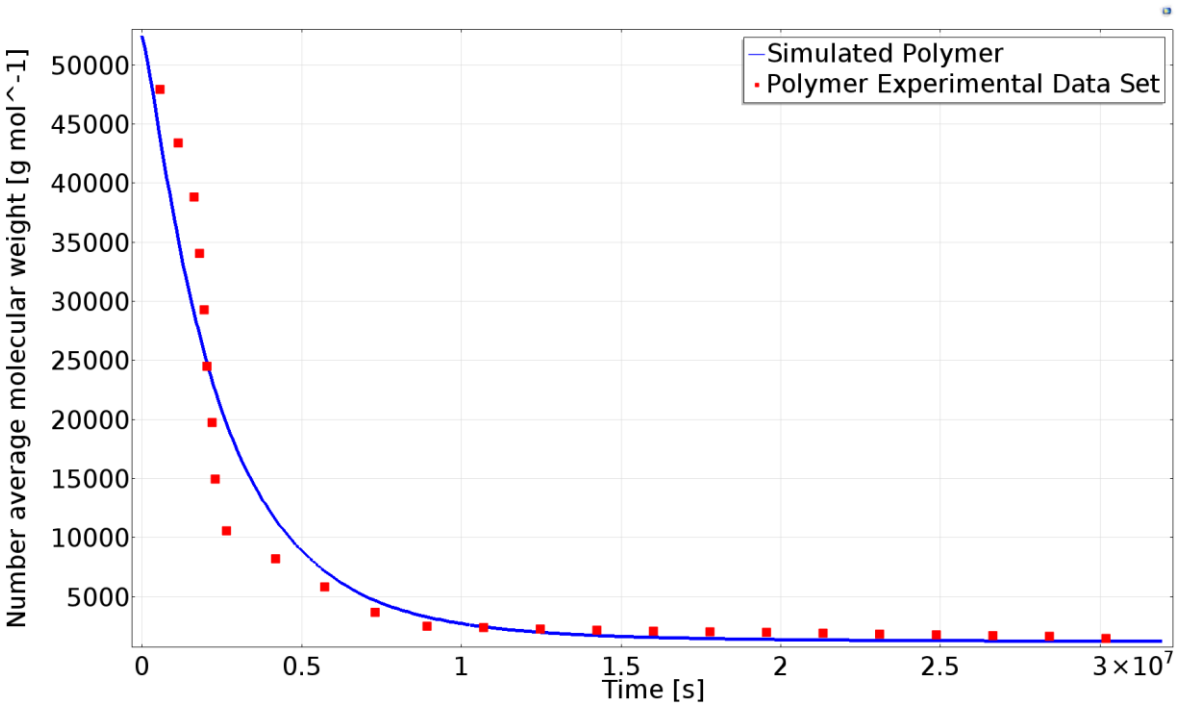

Figure 3.13: Optimization result - Polymer 2

It is possible to notice that the optimization results, obtained by applying the degradation model described in *Chapter 3.2.*, fit quite well the literature experimental data.

3.2.2.3 *Polymer 3*: PDLLA with low initial molecular weight

I. Grizzi et al. [13] has been selected for what concern the degradation constant derivation of Polymer 3.

In *Table 3.6*, the comparison between the characteristics of the polymer selected from literature for this study and of Polymer 3 are reported:

	Polymer from Literature	Polymer 3
Mw [kDa]	94	77
Mn [kDa]	49.5	40
PD	1.9	1.9

Table 3.6: Polymer from literature and Polymer 3 characteristics

The extrapolation of the experimental data set has been done by focusing on *Figure C.2* reported in Appendix C.

By implementing the experimental data set on COMSOL Multiphysics and selecting the Optimization tool, it has been found that the degradation constant value for Polymer 3 is:

$$k_D = 1.5918 \times 10^{-16} \frac{cm^6}{mol^2\, s}$$

In *Figure 3.14*, the optimization result is shown:

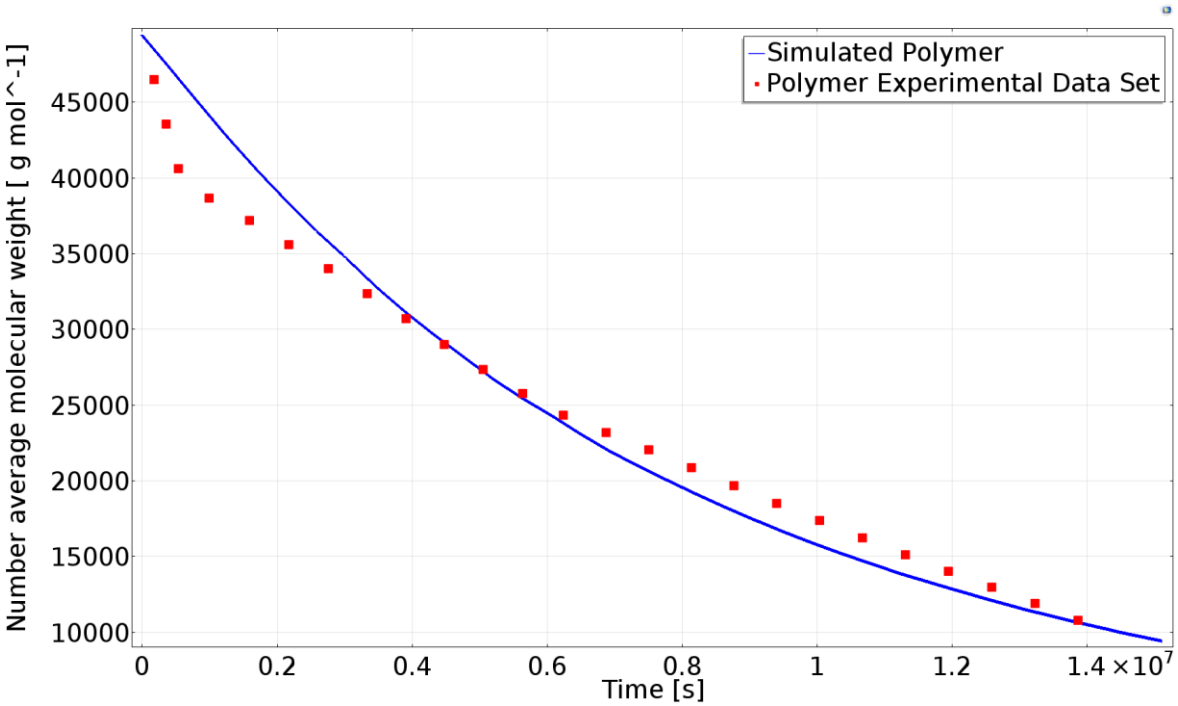

Figure 3.14: Optimization result - Polymer 3

It is possible to notice that the optimization results, obtained by using the degradation model described in *Chapter 3.2.*, fit quite well the literature experimental data.

3.2.2.4 *Polymer 4*: PDLLA with high initial molecular weight

Yu-Bo Fab et al. [17] has been selected for what concern the degradation constant derivation of Polymer 4.

As reported in *Table 3.7*, the characteristics of the polymer selected from literature for this study and the comparison with the characteristics of Polymer 4 are the following:

	Polymer from Literature	**Polymer 4**
Mw [kDa]	200	200
Mn [kDa]	125	142
PD	1.6	1.4

Table 3.7: Polymer from literature and Polymer 4 characteristics

The extrapolation of the experimental data set has been done by focusing on *Figure C.3* reported in Appendix C.

By implementing the experimental data set on COMSOL Multiphysics and selecting the Optimization tool, it has been found that the degradation constant value for Polymer 4 is:

$$k_D = 1.4219 \times 10^{-16} \frac{cm^6}{mol^2\, s}$$

In *Figure 3.15*, the optimization result is showed:

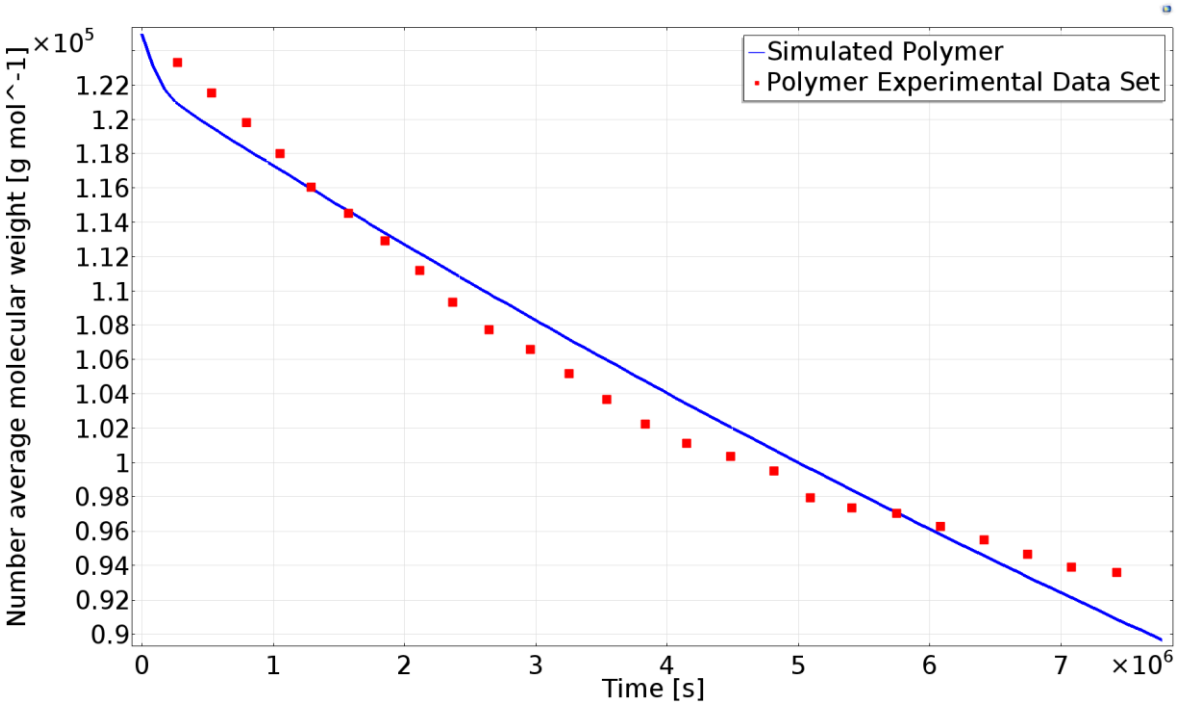

Figure 3.15: Optimization result - Polymer 4

It is possible to notice that the optimization results, obtained by using the model degradation described in *Chapter 3.2.*, fit quite well the literature experimental data.

In this case, the optimization curve is more linear than those of the previous simulations because the degradation time set by the selected paper is about 50% less than the degradation time set by those considered for the previous simulations.

3.3 Geometry

By comparing the geometries of the devices already available on the market with their problems and by taking into account the published patents, the attention of this work has been focused onto three different geometries, reported in *Figure 3.16*, *3.17* and *3.18*, all having a length of 5 cm and an internal radius of 2 cm for orthopaedic reasons [21]:

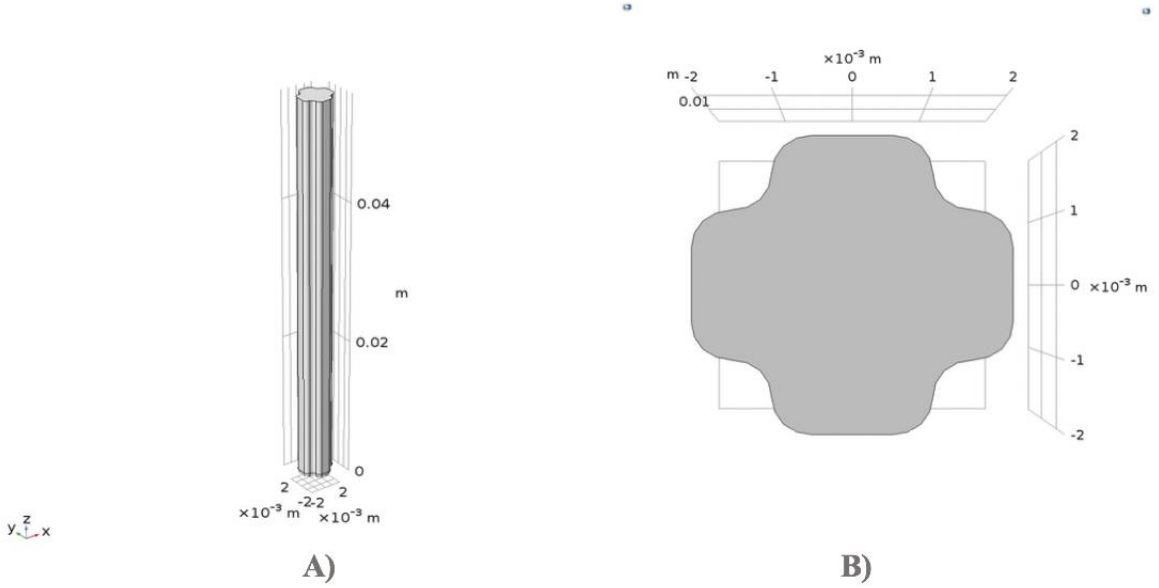

Figure 3.16: A) Geometry 1 and B) its cross section

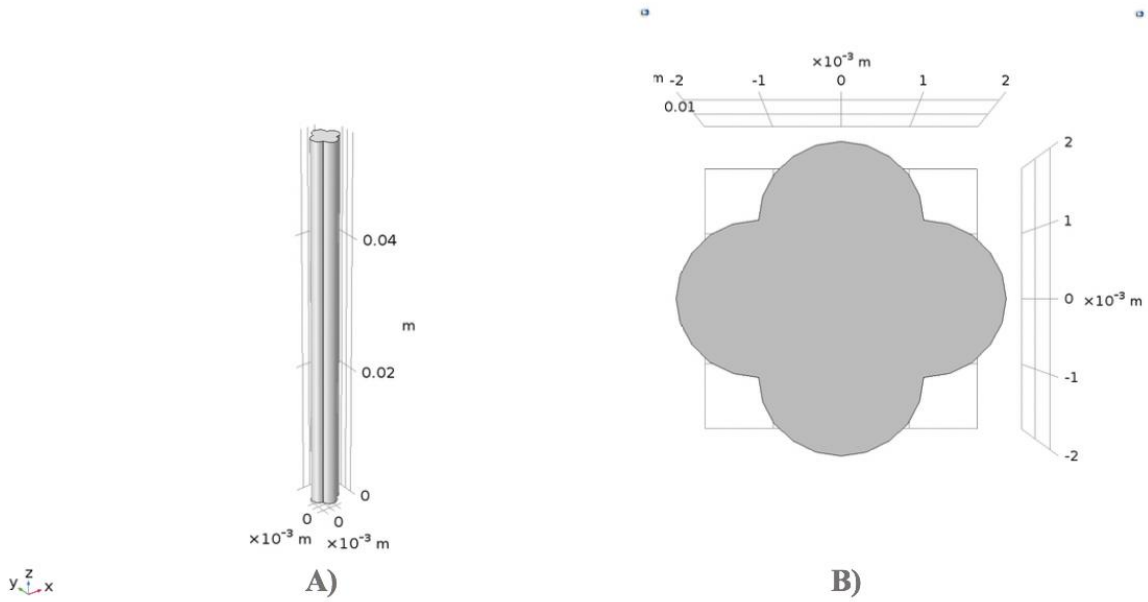

Figure 3.17: A) Geometry 2 and B) its cross section

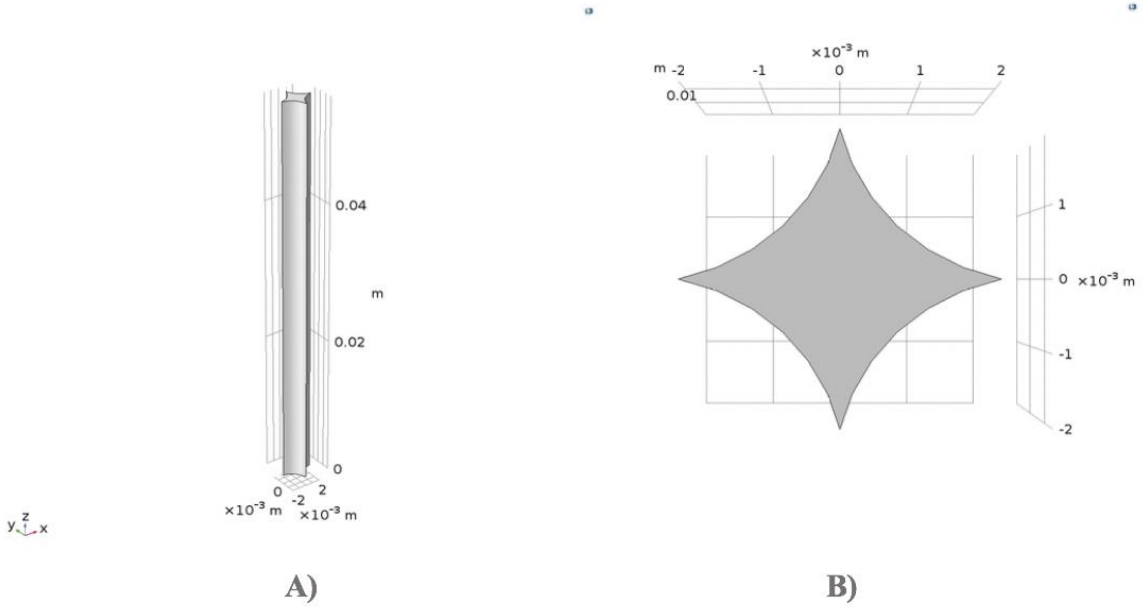

Figure 3.18: A) Geometry 3 and B) its cross section

3.4 Mechanical Model

Once the polymeric device is implanted into the body, it bears the loads from internal or external, and the complicated load conditions are various around the implanted polymer. The influence of mechanical load should not be omitted when controlling the appropriate degradation rate for polymer fixation [17].

The purpose of this study is to examine how the load affects the hydrolytic degradation of the selected polymers.

Therefore, a literature study has been done in order to find possible physiological force and pressure acting on the human bone. As *Chen-Yuan Chung* [18] reports, for a patient weighing 800 N, an equivalent pressure of 2.5 MPa can be applied to an end surface of the bone, while the other end is fixed. In order to mimic the in vivo loading conditions, a torque of 1 Nm is applied to the fractured bone, in addition to the pressure; the study is based on a simplified 3D finite element (FE) model of a bone-implant system and its representation is reported in *Figure 3.19*:

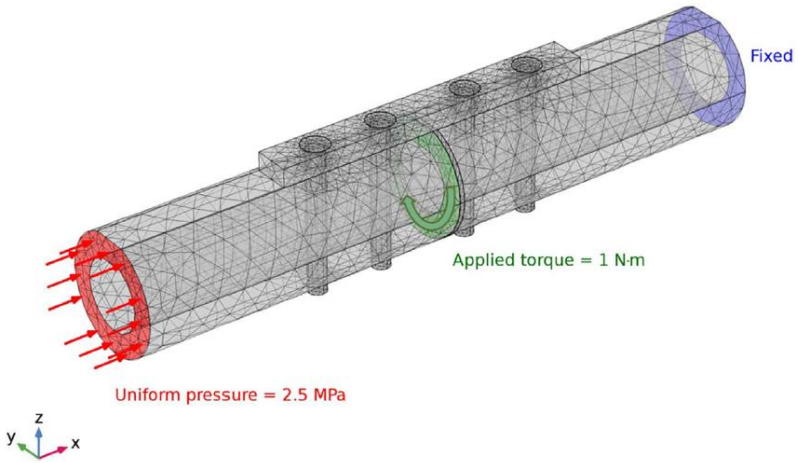

Figure 3.19: Representation of the applied loads

The simulations for each geometry have been run by applying the same aforementioned both pressure and torque and by considering only half of the pin, since a fracture divides the bone in two parts and the pin is used to connect them. Therefore, during the implantation, the two extremities of the pin are placed into the two part of the fractured bone, respectively. The representation of applied loads on the three different geometries tested in this thesis is reported in *Figure 3.20*:

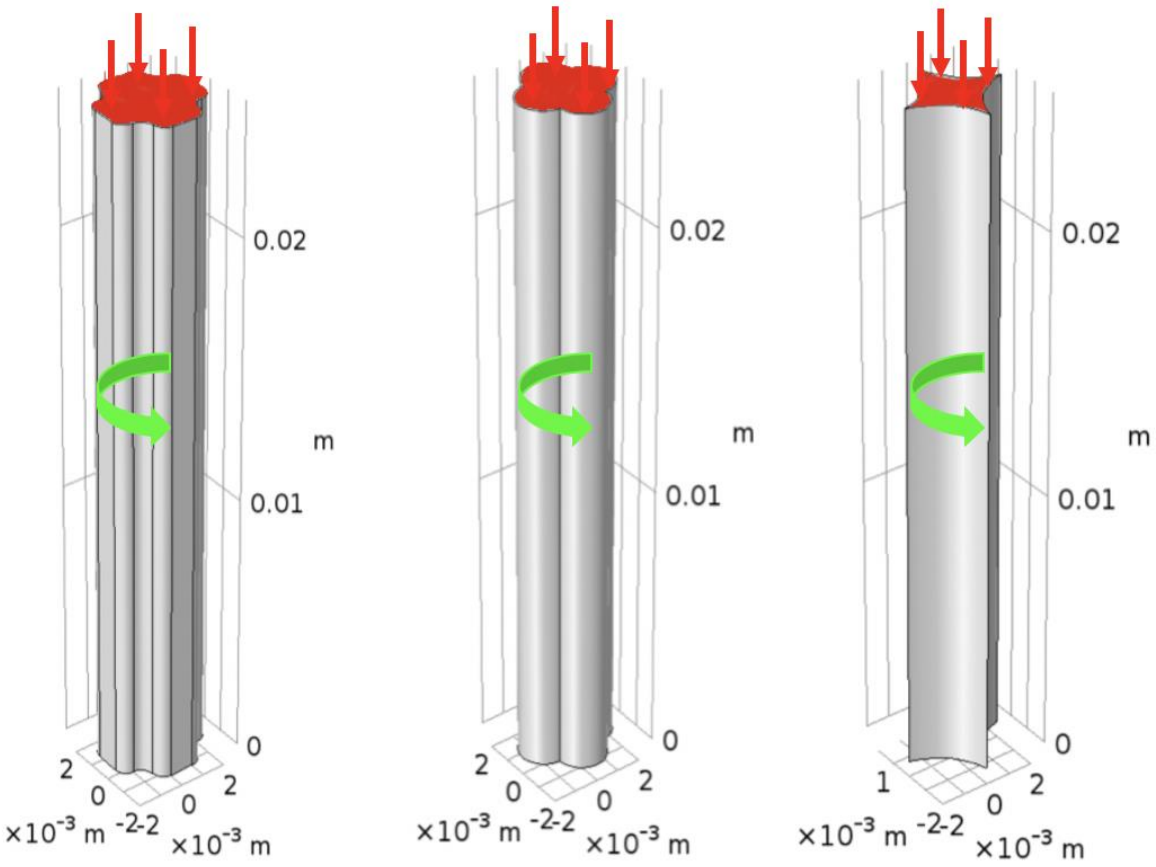

Figure 3.20: Mechanical model

3.5 Coupled model

In order to evaluate the degradation of the pin in 60 days affected by both hydrolysis and loads, it has been necessary to find a way to correlate these two phenomena.

As discussed in *Yu-Bo Fan et al.* [17], by applying an increasing load, the molecular weight progressively decreases by a factor of about 20-25%, thus a linear correlation between the degradation constant and Von Mises stress has been considered as valid to represent the link between the two degradation and mechanical models.

In order to obtain the final linear law, the evaluation of the degradation constants has been necessary. First of all, from the *Yu-Bo Fan et al.* [17], the extrapolation of two experimental data sets, regarding the same polymer, has been done: one set refers to the unload polymer and the other to the load one (*Figure 3.21*):

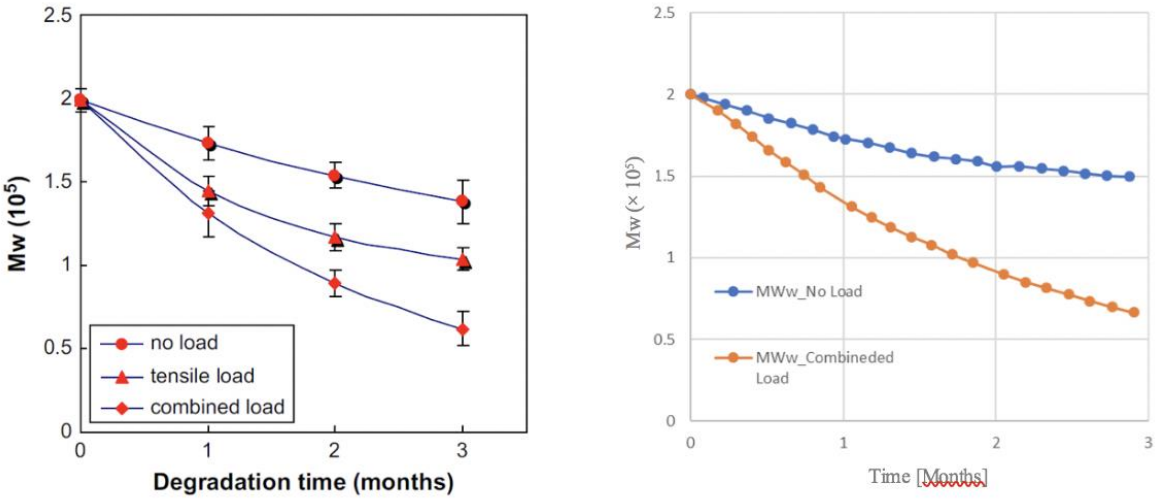

Figure 3.21: Experimental data set for degradation constant evaluation: on the left the original graph from [17] and on the right the extrapolated one

Secondly, the experimental data have been fitted with the model degradation described in *Chapter 3.2* and implemented in COMSOL Multiphysics: the obtained values of degradation constants for each data set are:

$$k_{d\_NOLOAD} = 1.4219 \times 10^{-16}$$
$$k_{d\_LOAD} = 4.0586 \times 10^{-16}$$

From the percentage ratio between the two k_d, the degradation constant increases of 286% by applying the load.

Then, the increase of the 286% has been applied to the value of the degradation constant obtained for Polymer 1, as described in *Paragraph 3.2.2.1*:

$$k_{d\_NOLOAD} = 5.0254 \times 10^{-16}$$
$$k_{d\_LOAD} = 1.93954 \times 10^{-15}$$

Finally, it has been possible to derive the linear law: the idea was to express the previous two degradation constants as a function of Von Mises stress distribution. This was possible because the molecular weight of the polymer studied in *Yu-Bo Fan et al.* [17] is very similar to that of both Polymer 1 and Polymer 4.

The following graph (*Figure 3.22*) represents the derivation of the law:

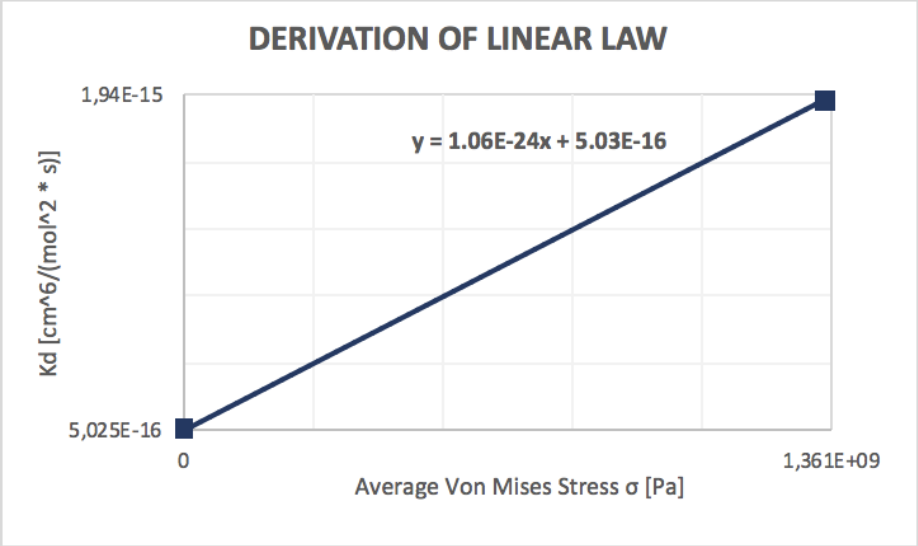

Figure 3.22: Derivation of the Linear law

k_{d_NOLOAD} has been correlated to a Von Mises stress equal to zero, while k_{d_LOAD} has been correlated to an average Von Mises stress value obtained from previous simulation.
The linear law expression is, therefore (*Equation 3.20)*:

$$k_d = 1.06 \times 10^{-24}\,\sigma + k_{d\_NOLOAD}$$

Equation 3.18: Linear Law

The two models have been coupled in COMSOL Multiphysics, dividing the simulation in two steps:

a. Stationary step for the mechanical model, with Solid Mechanics tool
b. Time dependent step for the degradation model, with Coefficient Form PDE tool

From a., Von Mises stress distribution has been obtained in order to be able to evaluate the degradation constant as a function of Von Mises stress distribution and so of the space (*Equation 3.20*).
After that, from b., the degradation model has been simulated by setting a computational time equal to 60 days.

Chapter IV

4. Results and Discussion

In the presented chapter, the results obtained by simulation with COMSOL Multiphysics software are reported.

4.1 Degradation Model Results

4.1.1 Influence of Polymer Composition

The mathematical degradation model has been implemented in COMSOL Multiphysics and simulated by selecting the Coefficient Form PDE tool. In this case, the degradation model has been considered without application of any load.

All the simulations have been run by considering a degradation time equal to 60 days, since the project aim is to identify an optimal shape for the cross section of the pin and an optimal composition of the polymer, assuming 6-8 weeks of degradation and moreover, the pin has to be developed in such a way to maintain its mechanical properties unaltered for the same period. Results for each possible polymer/geometry combination are presented in the following.

PLACL and PDLLA with high initial molecular weight (Polymer 1 and Polymer 4) and the aforementioned characteristics have been the first two polymers which composition behaviours during degradation have been investigated, for each geometry, in pre-sterilization conditions. In this sense, *Figure 4.1* reports the trend of the weight average molecular weight of PLACL and PDLLA with 183 kDa and 200 kDa as initial value of the weight molecular weight, respectively, for each geometry and during 60 days of degradation:

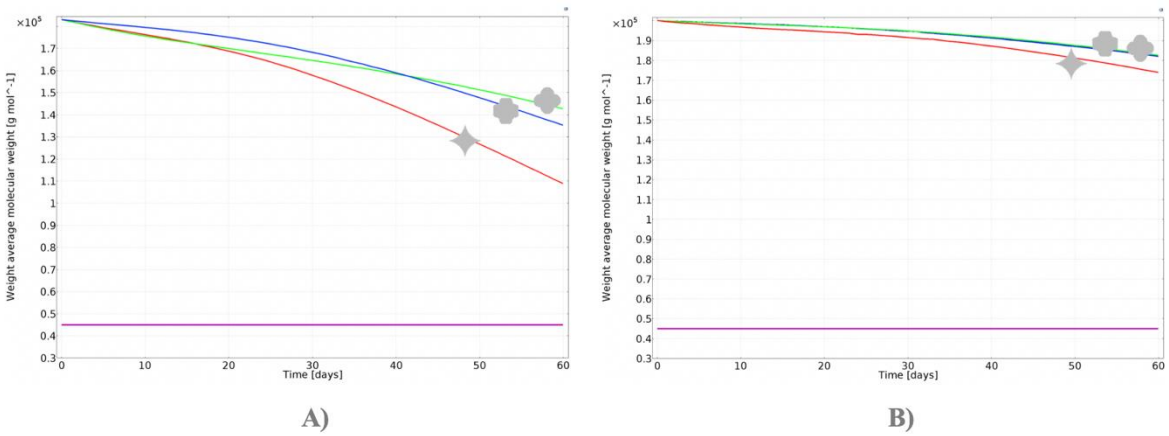

Figure 4.1: Trend of the weight average molecular weight of A) PLACL (initial Mw of 183 kDa) and B) PDLLA (initial Mw of 200 kDa), for each geometry and during 60 days of degradation, in pre-sterilization conditions

First of all, it is possible to notice that in both cases the final value of the weight average molecular weight is above the threshold one, i.e., 45 kDa. In fact, it has been demonstrated [19] that if the weight average molecular weight is above the aforementioned value, the mechanical properties and Young's modulus of the polymer remain constant. For this reason, the value of the weight average molecular weight had to be checked during the degradation time, i.e., 60 days, in order to guarantee that the pin properties are optimal for the bone healing. However, since the polymers have to be subjected to β-sterilization, their initial molecular weight will decrease of about 30% after this treatment [19]; for this reason, simulations that take into account post-sterilization conditions have been run: (*Figure 4.2*):

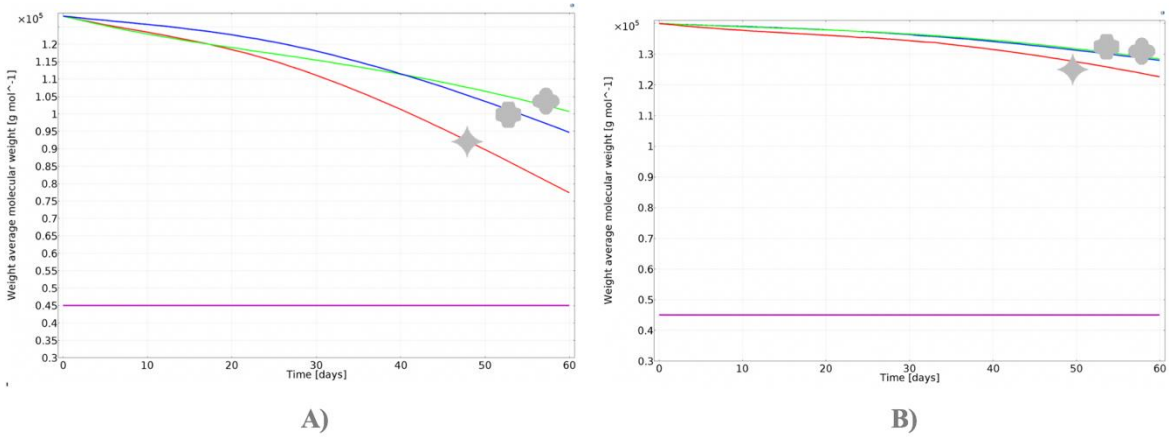

Figure 4.2: Trend of the weight average molecular weight of A) PLACL (initial Mw of 128.1 kDa) and B) PDLLA (initial Mw of 140 kDa), for each geometry and during 60 days of degradation, in post-sterilization conditions

It is possible to notice that in both cases the final value of the weight average molecular weight is above the threshold one, i.e., 45 kDa. Therefore, Polymer 1 and Polymer 4 can be considered as two of the best solutions for the achievement of this thesis purpose.

Another important consideration that can be deduced from *Figure 4.1* is that Geometry 1 and Geometry 2 have a very similar degradation behaviour, which is extremely different for Geometry 3. Specifically, Geometry 1 and Geometry 2 degrades much slower than Geometry 3 because an important component of the selected model degradation is related to the water diffusion. In this sense, the time of water diffusion into the cross sections of both Geometry 1 and Geometry 2 is slower than that into the cross section of Geometry 3, due to the particular shape of the latter. Therefore, since it is known that Geometry 3 is the best shape from an orthopaedic point of view and the requirement that must be satisfied through these simulations is that the value of the weight average molecular weight after 60 days of degradation need to exceed the threshold, i.e., 45 kDa, regarding the two polymers with low initial molecular weight (Polymer 2 and Polymer 3), it has been considered as appropriate to investigate first of all the degradation behaviour related to Geometry 1. *Figure 4.3* reports the trend of the weight average molecular weight of PLACL and PDLLA with 80 kDa and 76 kDa as initial value of the weight molecular weight, respectively, for Geometry 1 and during 60 days of degradation in pre-sterilization conditions:

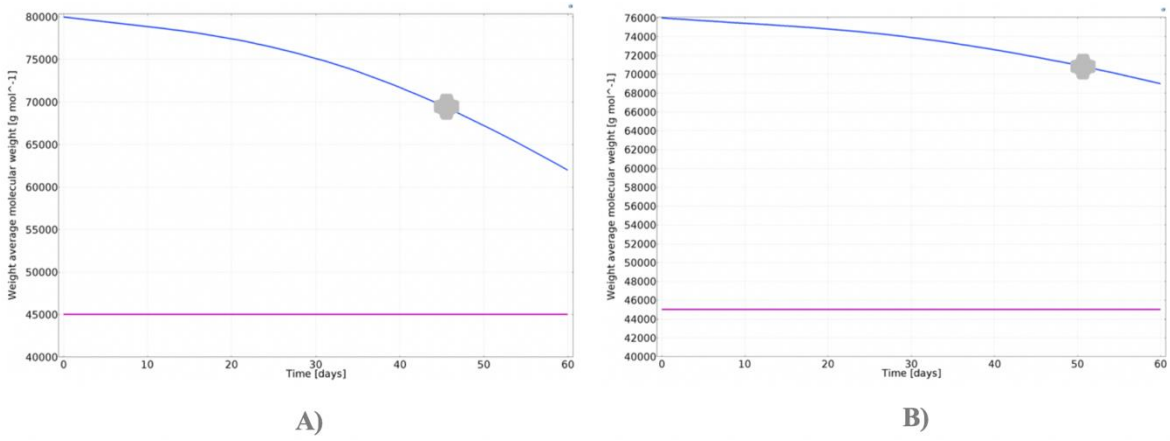

Figure 4.3: Trend of the weight average molecular weight of A) PLACL (initial Mw of 80 kDa) and B) PDLLA (initial Mw of 76 kDa), for Geometry 1 and during 60 days of degradation, in pre-sterilization conditions

It can be notice that the weight average molecular weight values obtained after 60 days of simulation in pre-sterilization conditions for both A) and B) are little higher than the threshold, i.e., 45 kDa. By considering that Geometry 1 is the one which, together with Geometry 2, shows a much slower degradation with respect to Geometry 3 and that these simulations refer to pre-sterilization conditions, it has been considered reasonable to investigate the degradation behaviour of PLACL and PDLLA with low initial molecular weight in post-sterilization conditions, always related to the only Geometry 1.

Figure 4.4 reports the trend of the weight average molecular weight of PLACL and PDLLA with low initial molecular weight in post-sterilization conditions, i.e., with 56 kDa and 53.2 kDa as initial value of the weight molecular weight, respectively, for Geometry 1 and during 60 days of degradation:

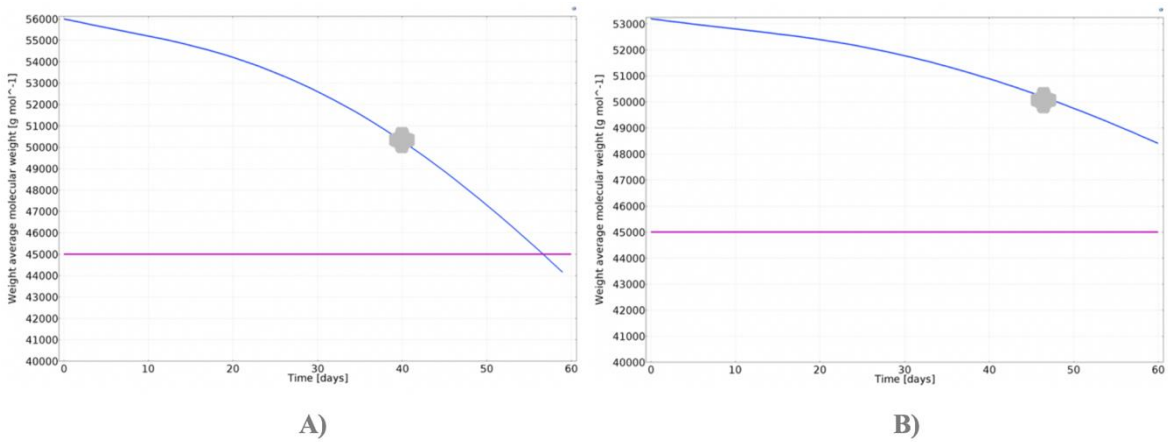

Figure 4.4: Trend of the weight average molecular weight of A) PLACL (initial Mw of 56 kDa) and B) PDLLA (initial Mw of 53.2 kDa), for Geometry 1 and during 60 days of degradation, in post-sterilization conditions

It can be noticed that the weight average molecular weight value obtained after 60 days of simulation in post-sterilization conditions is below the threshold one for A) and too close to 45 kDa for B). This makes both Polymer 2 and Polymer 3 useless for the aim of this thesis, since they can't guarantee the optimal properties of the pin required for the bone healing.

For this reason, Geometry 2 and Geometry 3 have not been tested for both polymers.

4.1.2 Influence of the Geometry

In *Figure 4.5* and *4.6,* the graphs which summarize all the previous considerations related to Geometry 1 are reported, pre and post sterilization respectively:

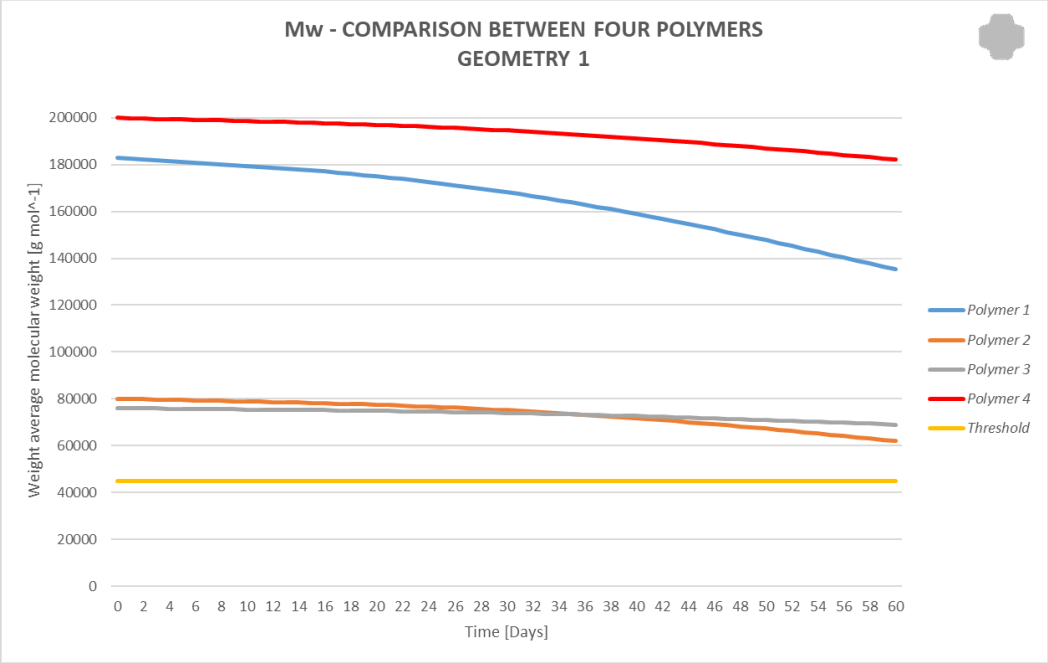

Figure 4.5: Comparison related to Geometry 1, in pre-sterilization conditions

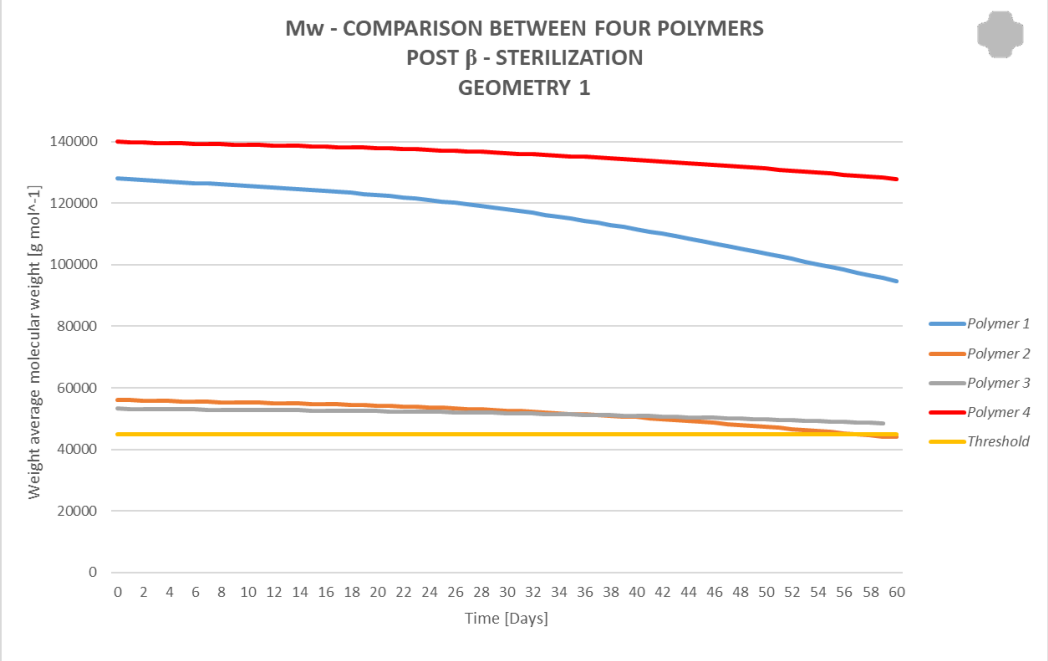

Figure 4.6: Comparison related to Geometry 1, in post-sterilization conditions

The graphs show in a better way what already said: Polymer 2 and Polymer 3 are not good candidates for the development of the optimize pin.

Thus, the following figures will be focused only on Polymer 1 and Polymer 4 behaviour. In particular, in *Figure 4.7* and *4.8* and in *Figure 4.9* and *4.10* the graphs which summarize all the previous considerations related to Geometry 2 and Geometry 3 in pre and post-sterilization conditions, respectively, are reported:

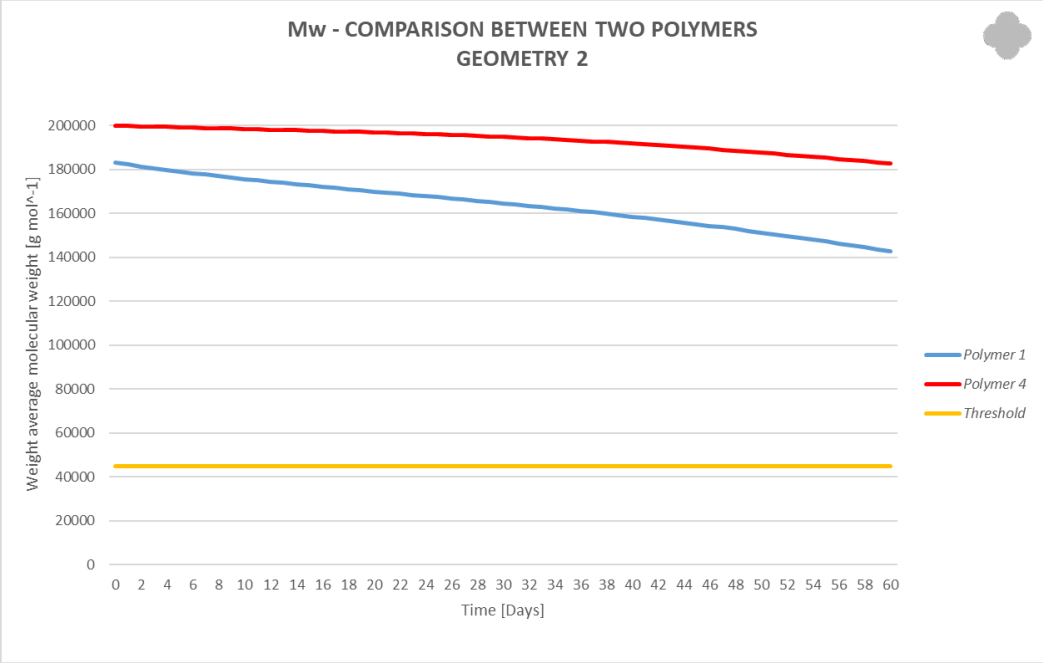

Figure 4.7: Comparison related to Geometry 2, in pre-sterilization conditions

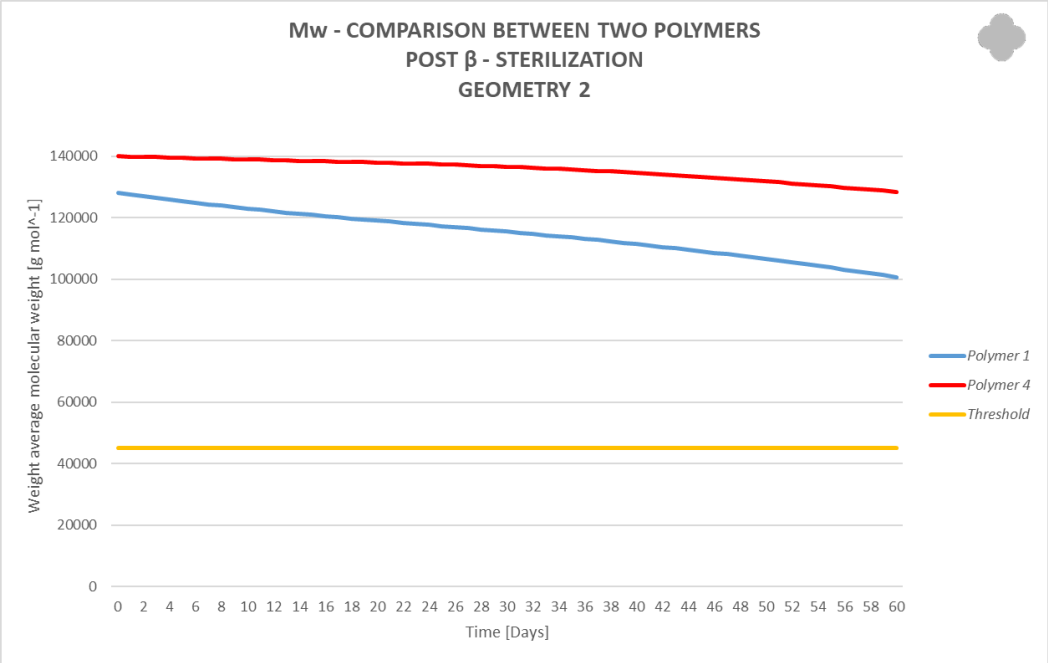

Figure 4.8: Comparison related to Geometry 2, in post-sterilization conditions

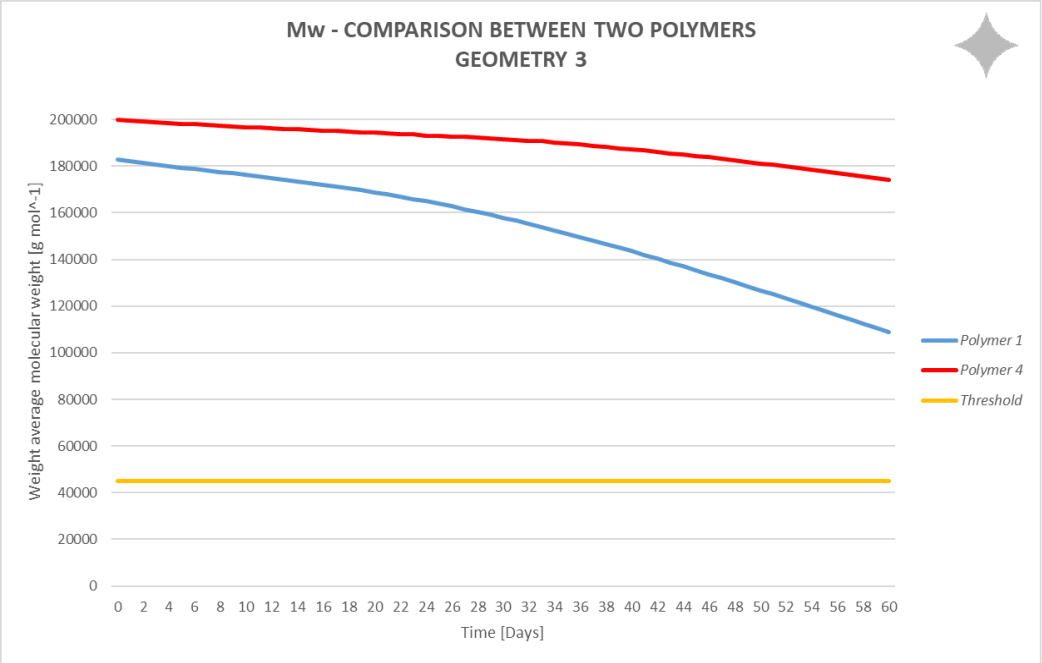

Figure 4.9: Comparison related to Geometry 3, in pre-sterilization conditions

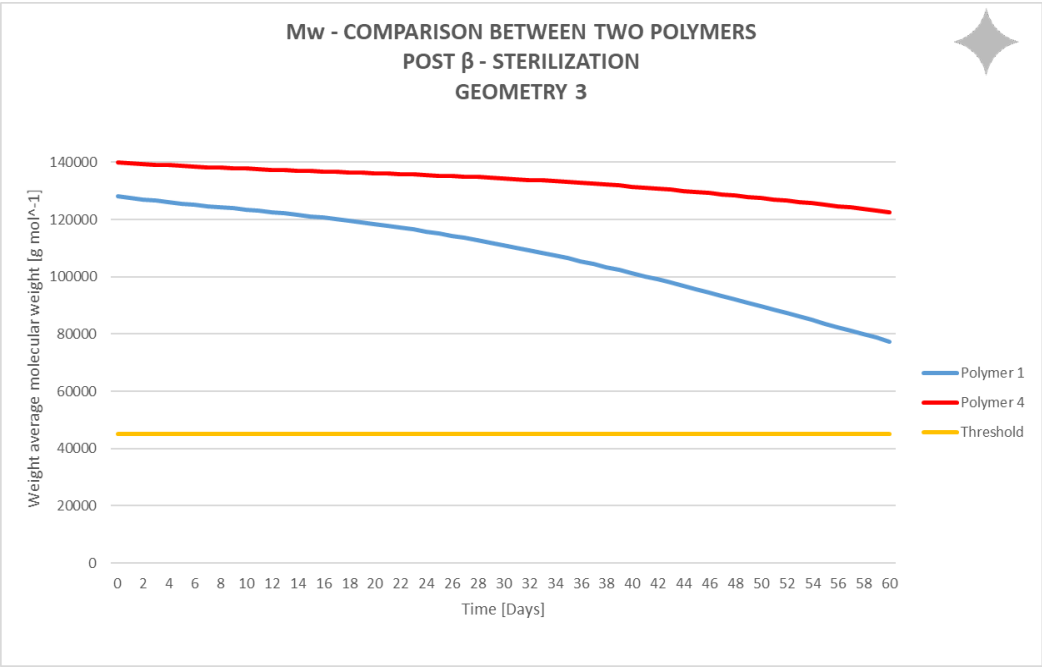

Figure 4.10: Comparison related to Geometry 3, in post-sterilization conditions

To conclude, from the degradation model results, it can be observed that Polymer 1 and Polymer 4 are suitable candidates for the development of the optimized pin. However, these considerations are not sufficient to draw conclusions about the perfect polymer composition

of the bone fixation system. Therefore, results about mechanical model and coupling between degradation and mechanical ones will follow.

Anyway, since from model degradation alone it can be observed that the weight average molecular weight of both Polymer 2 and Polymer 3, after 60 days of degradation, reaches a value too close to the threshold one, the coupling between degradation and mechanical models has been done only for Polymer 1 and Polymer 4.

4.2 Mechanical Model Results

In order to demonstrate the mechanical load influence on the degradation rate of the polymeric fixation, first of all, the evaluation of Von Mises stress distribution has been necessary. The simulations for each geometry have been run by applying a fixed constraint at the basis, a pressure of 2.5 MPa on the top and also a torque of 1 Nm, as explained in *Chapter 3.4*.

Furthermore, only half of the pin has been considered for the simulations of each geometry, since a fracture divides the bone in two parts and the pin is used to connect them. Therefore, during the implantation, the two extremities of the pin are placed into the two part of the fractured bone respectively.

The following results have been obtained by Solid Mechanics tool on COMSOL Multiphysics.

In *Figure 4.11* and *4.12*, Von Mises stress distributions are reported for each geometry:

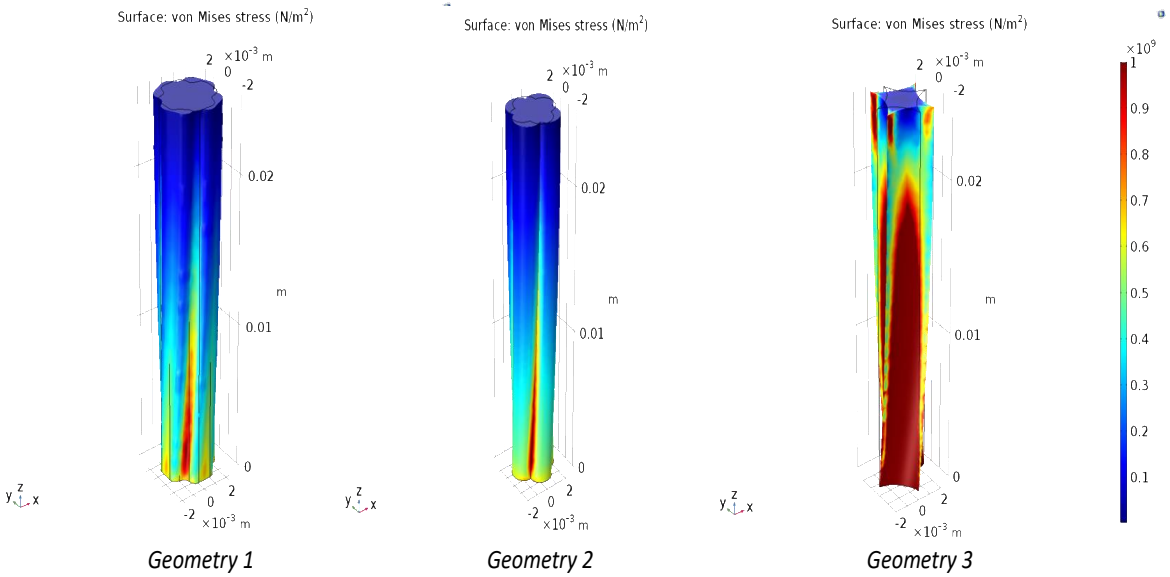

Figure 4.11: Von Mises stress distributions

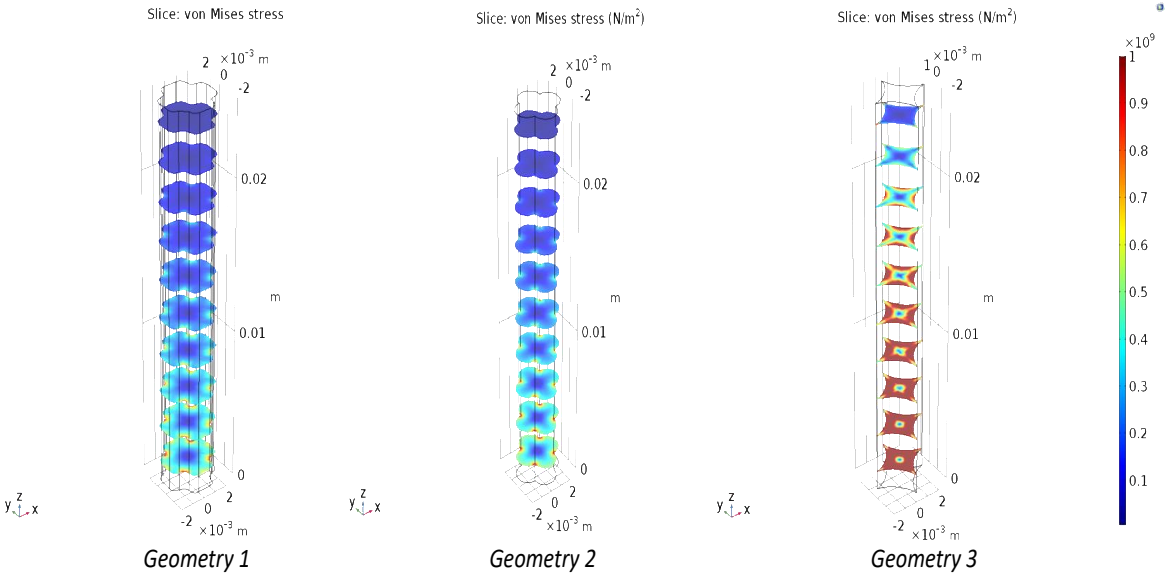

Figure 4.12: Slice representation of Von Mises stress distribution

It can be seen that, since at the basis a fixed constraint has been applied, Von Mises stress distribution is higher in this section than on the top. This behaviour is common to all the geometries and it can be better noticed for Geometry 3.

What is different among the geometries is the stress distribution on the edges: in particular regarding Geometry 3, the edges are important zones of stress concentration since they are sharper than those of the other two geometries.

4.3 Coupled Model Results

As already said, the two models have been coupled in COMSOL Multiphysics, dividing the simulation in two steps.

It is important to underline that the degradation constant will increase with the increase of the stress. This can be better seen from the slice representation of the degradation constant behaviour as a function of the space, as reported in *Figure 4.13* and *4.14*, for all the geometries and Polymer 1 and Polymer 4, respectively:

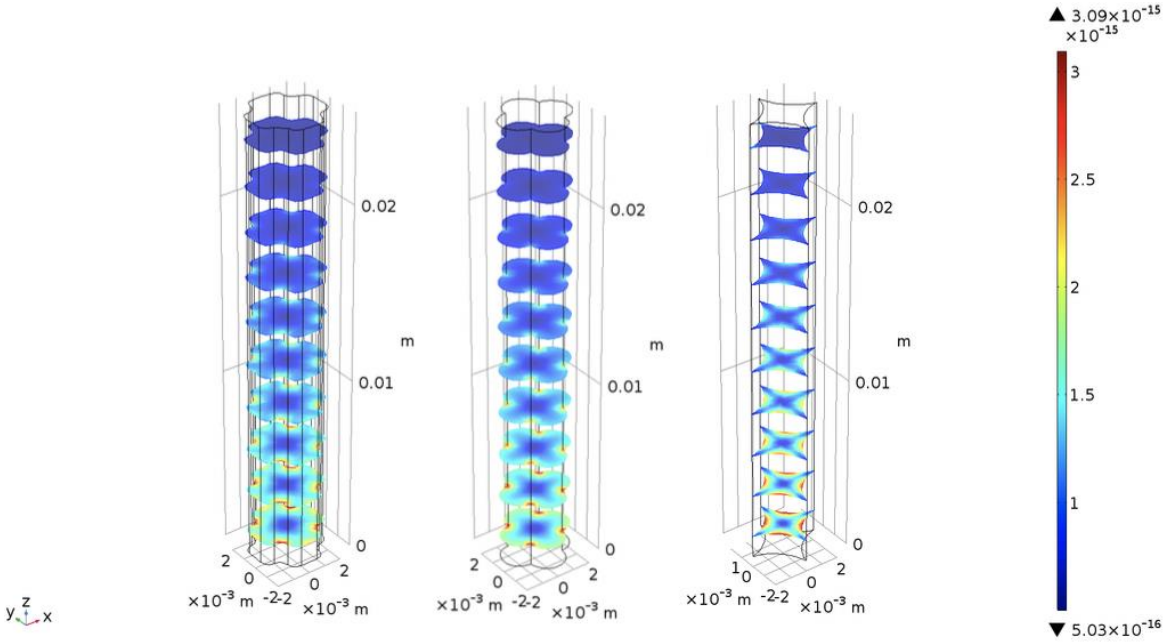

Figure 4.13: Slice representation of Polymer 1 degradation constant behavior for the three geometries

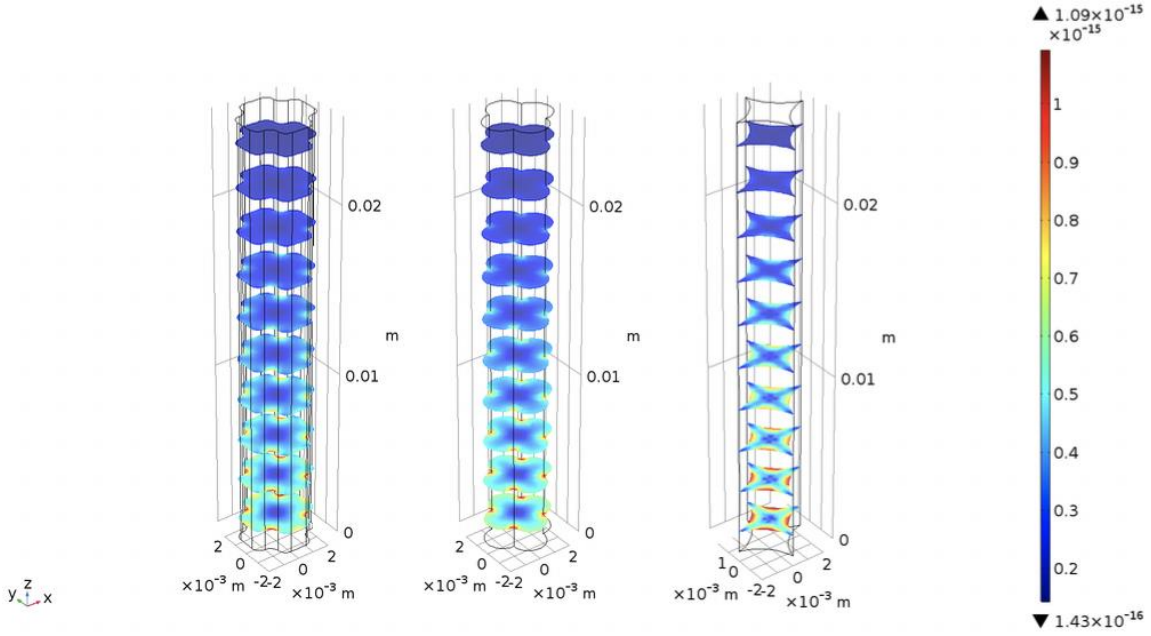

Figure 4.14: Slice representation of Polymer 4 degradation constant behavior for the three geometries

The degradation constant value for both Polymer 1 and Polymer 4 is higher at the basis, since a fixed constraint has been applied on this section, and therefore Von Mises stress distribution is higher than that on the top, as reported in *Chapter 4.2*.

After that, the degradation model has been simulated by setting a computational time equal to 60 days.

4.3.1 *Polymer 1*

In *Figure 4.15* and *4.16*, the comparison among the weight average molecular weight behaviours as a function of the three geometries is reported, in pre and post-sterilization conditions respectively:

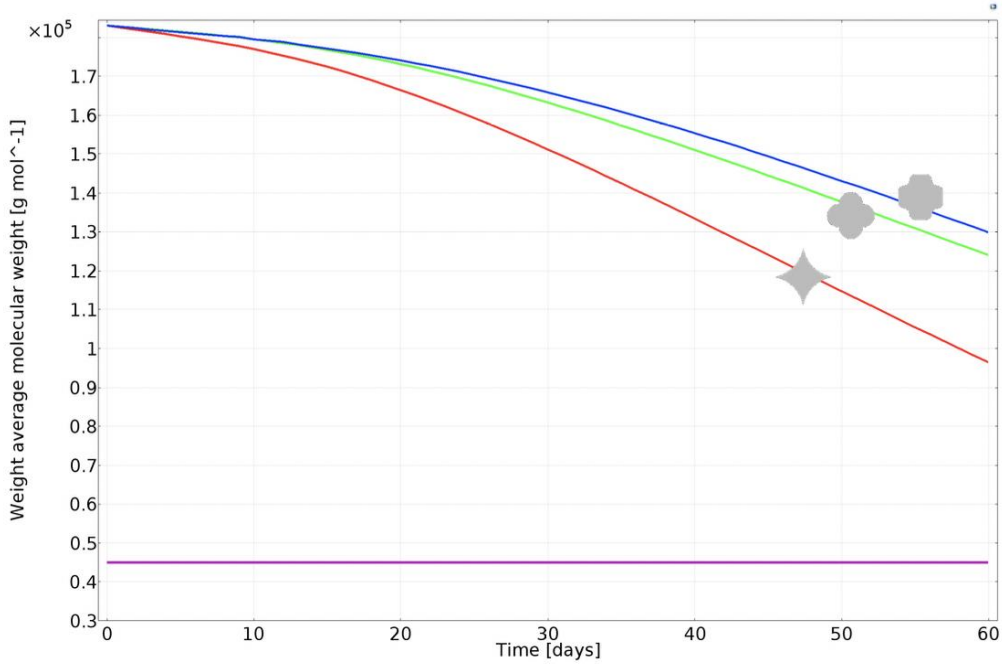

Figure 4.15: Weight-average molecular weight with an initial Mw of 183 kDa

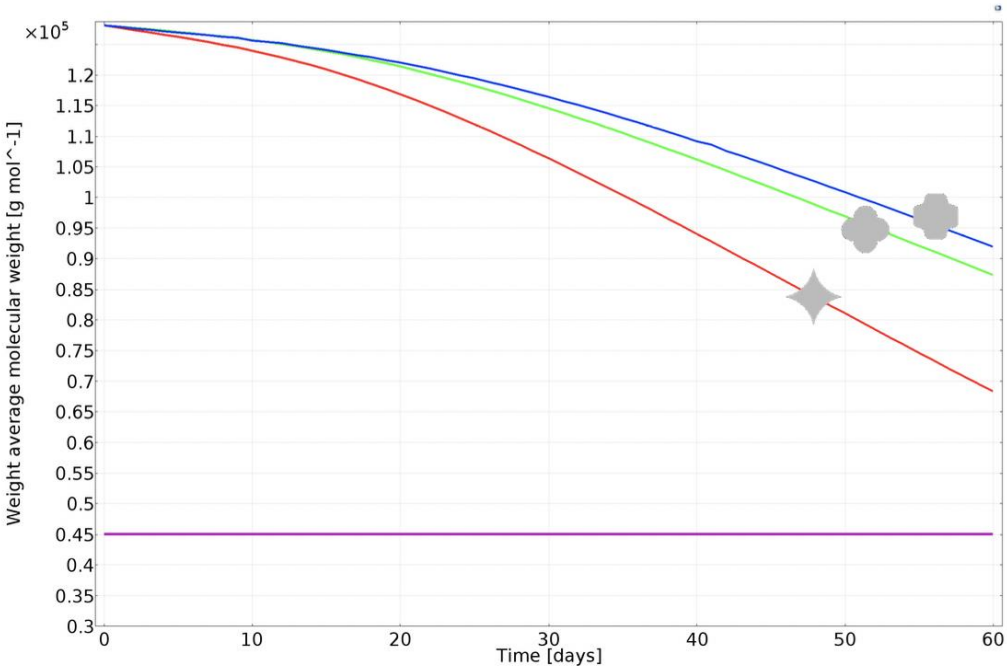

Figure 4.16: Weight average molecular weight with an initial Mw of 128.1 kDa (30% loss)

For the three geometries tested, and in particular after sterilization, the final values of the weight average molecular weight remain above 45 kDa, i.e., the threshold. Therefore, Polymer 1 continues to be one of the best candidates for the achievement of the thesis purpose.
It is important to notice, however, that the final values of the weight average molecular weight after coupling, for all the geometries, both in pre and post-sterilization conditions are smaller than those obtained from the degradation model alone, as reported in *Chapter 4.1*. This consideration shows that the degradation of the polymer is influenced by the mechanical loads, in a not negligible way.

It can be noticed that Geometry 1 and Geometry 2 are similar in terms of weight average molecular weight loss, while Geometry 3 is the one that shows a major decrease of the weight average molecular weight and this could be explained by the particular shape of Geometry 3 and, most of all, of its cross section. Nevertheless, Geometry 3 is the best orthopaedic form and, moreover, its weight average molecular weight value after 60 day of degradation always remains above the threshold value.
In order to represent and better show the real behaviour of the weight molecular weight distribution as a function of the degradation due to both hydrolysis and mechanical loads and of both the geometry cross sections and the height of the pin, i.e., the space, four different heights have been selected, as reported in *Figure 4.17*:

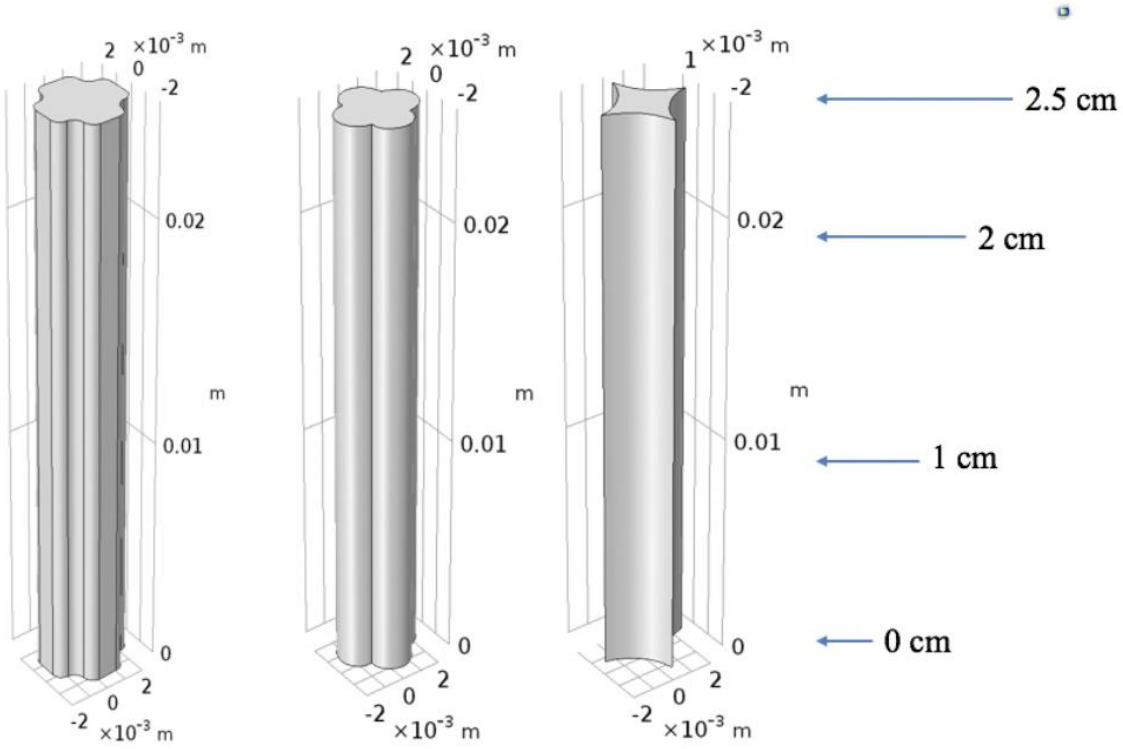

Figure 4.17: Representation of the selected heights

By doing so, the comparison among the weight molecular weight distributions as a function of the three different cross sections at the four different heights and at a degradation time equal to zero, 30 and 60 days, respectively, has been possible.

In *Figure 4.18*, the considered cross sections are represented:

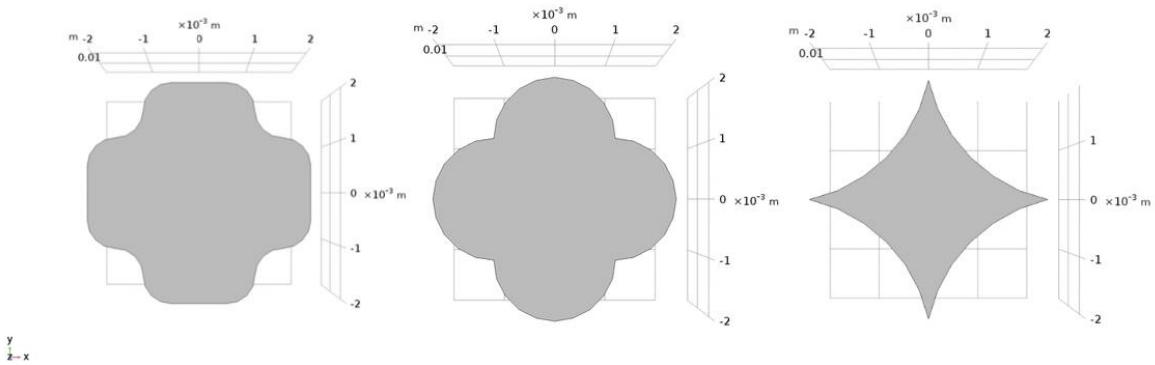

Figure 4.18: Representation of the selected cross section

Figure 4.19, 4.20, 4.21, 4.22, 4.23 and *4.24* show the final result of the behaviour of the weight molecular weight distributions for the three geometries, in pre-sterilization conditions:

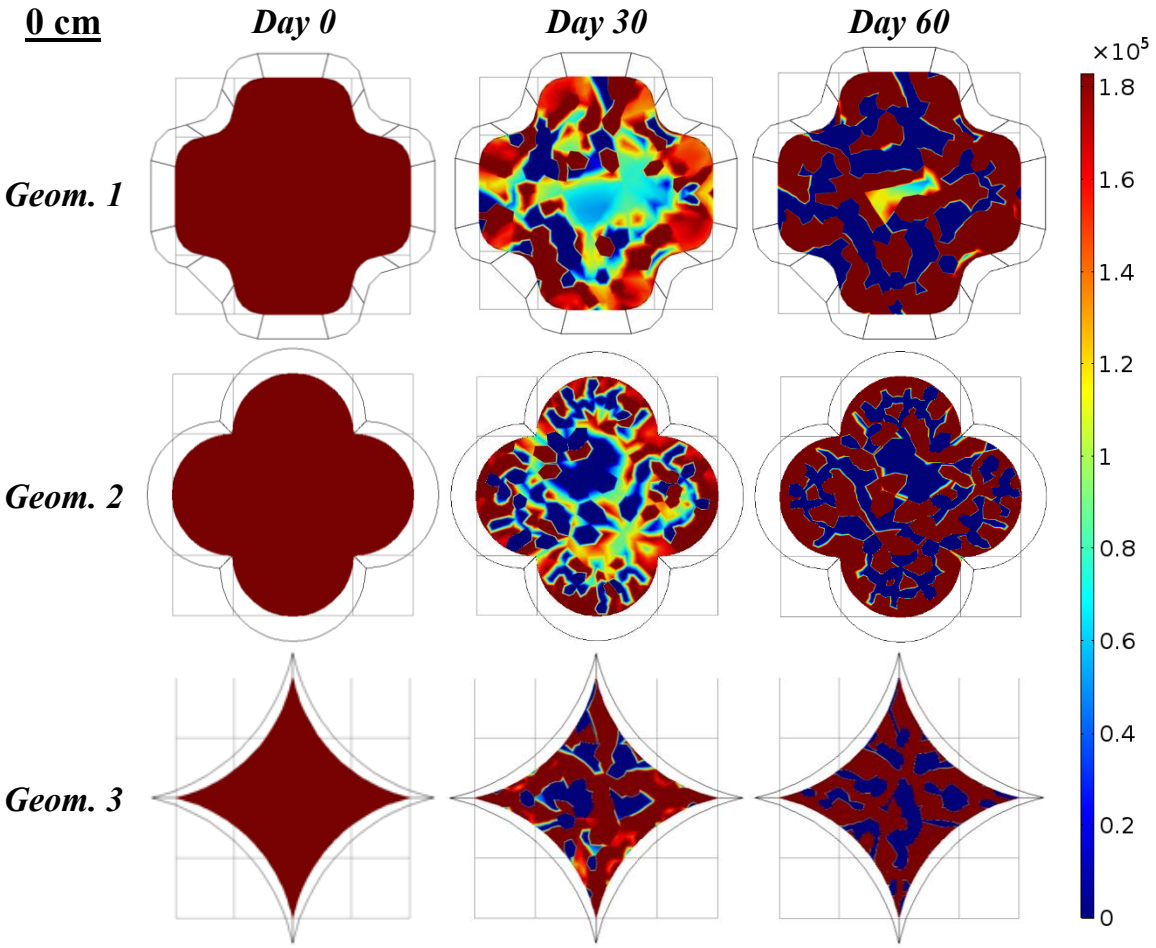

Figure 4.19: Weight molecular weight distribution at the base, as a function of degradation time and geometry, with an initial Mw equal to 183 kDa

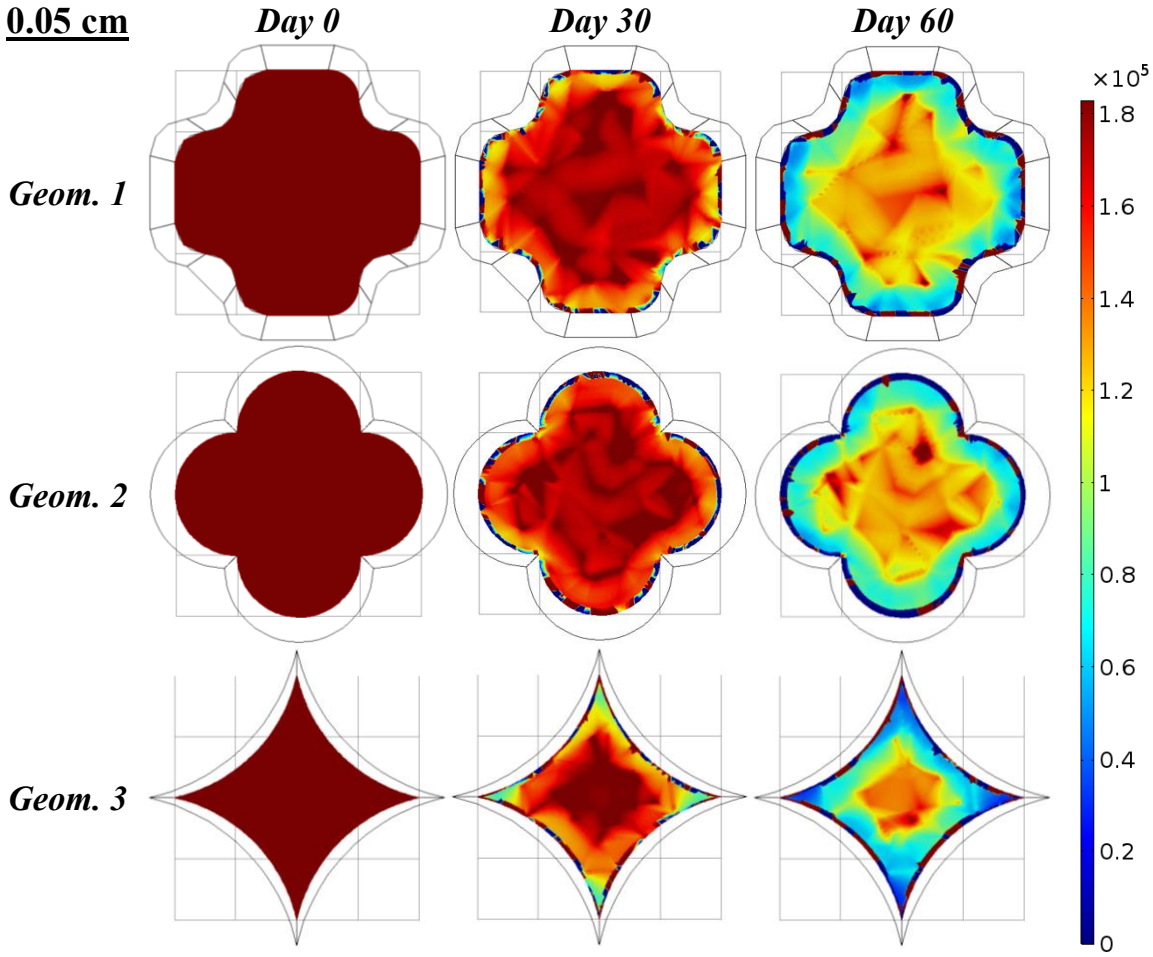

Figure 4.20: Weight molecular weight distribution at 0.05 cm from the base, as a function of degradation time and geometry, with an initial Mw equal to 183 kDa

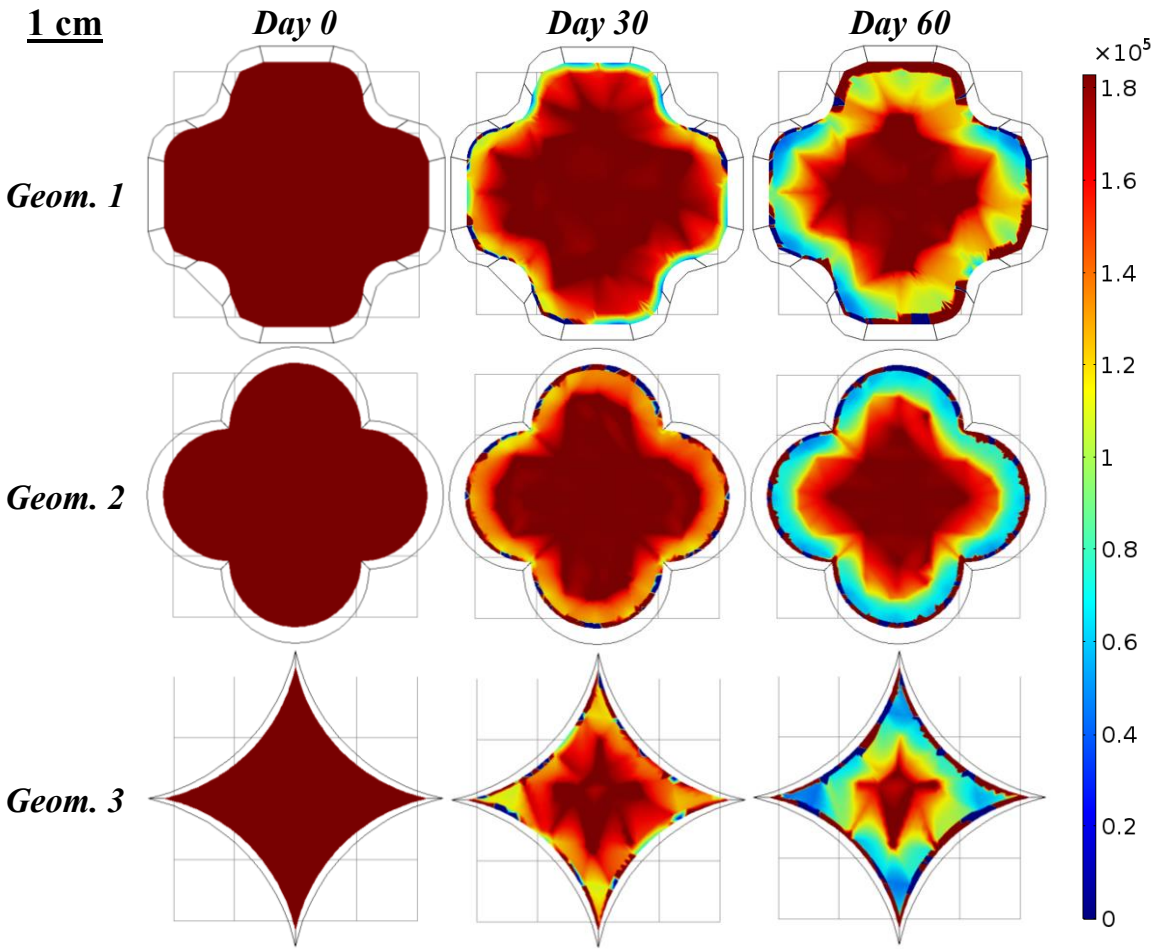

Figure 4.21: Weight molecular weight distribution at 1 cm from the base, as a function of degradation time and geometry, with an initial Mw equal to 183 kDa

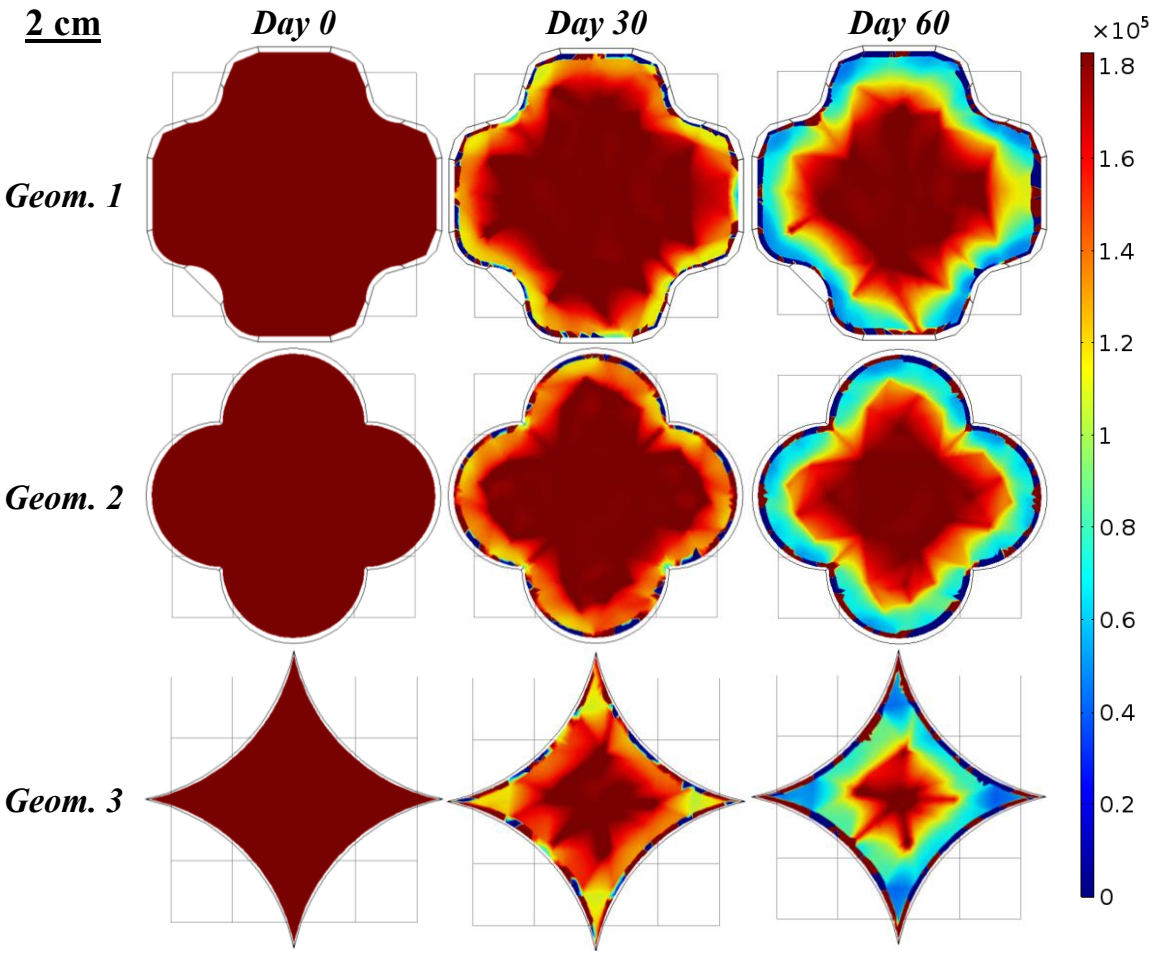

Figure 4.22: Weight olecular weight distribution at 2 cm from the base, as a function of degradation time and geometry, with an initial Mw equal to 183 kDa

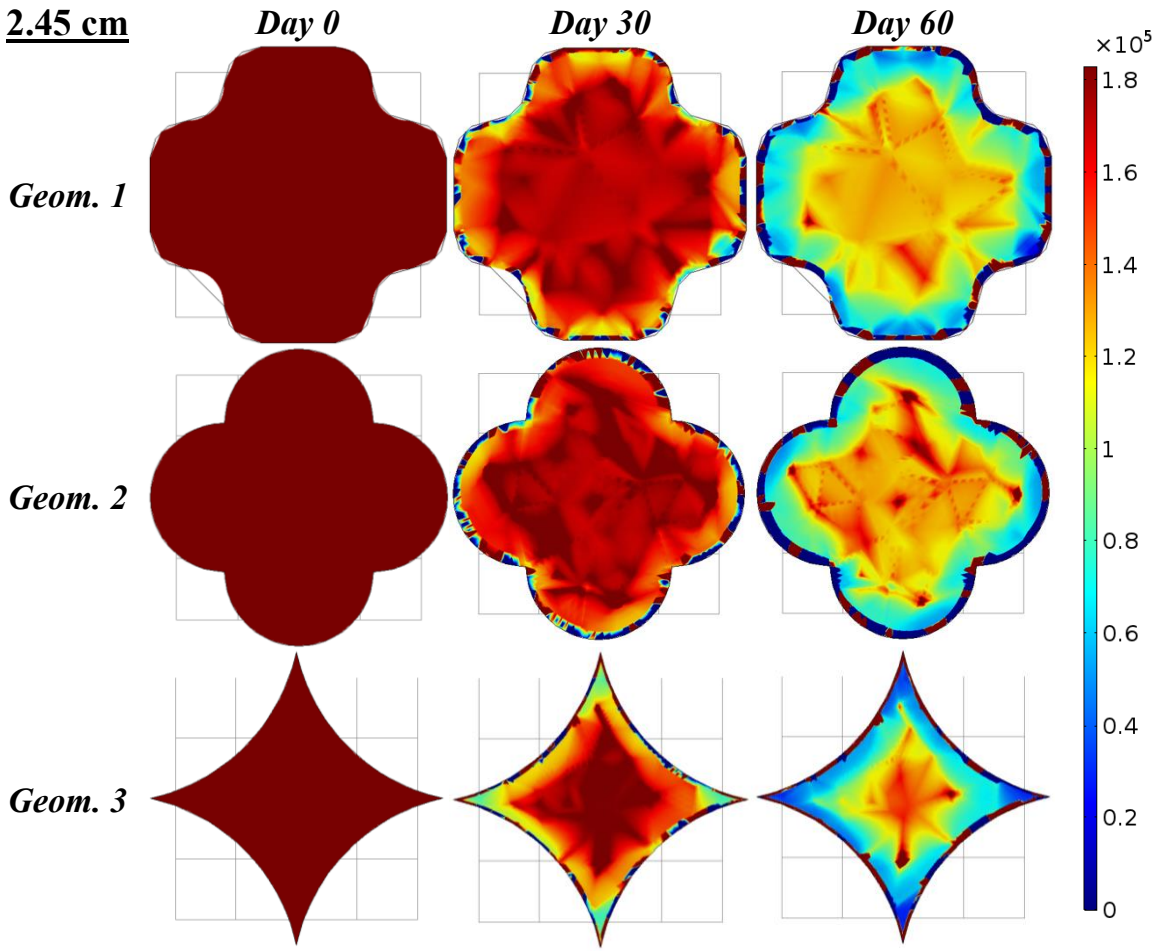

Figure 4.23: Weight molecular weight distribution at 2.45 cm from the base, as a function of degradation time and geometry, with an initial Mw equal to 183 kDa

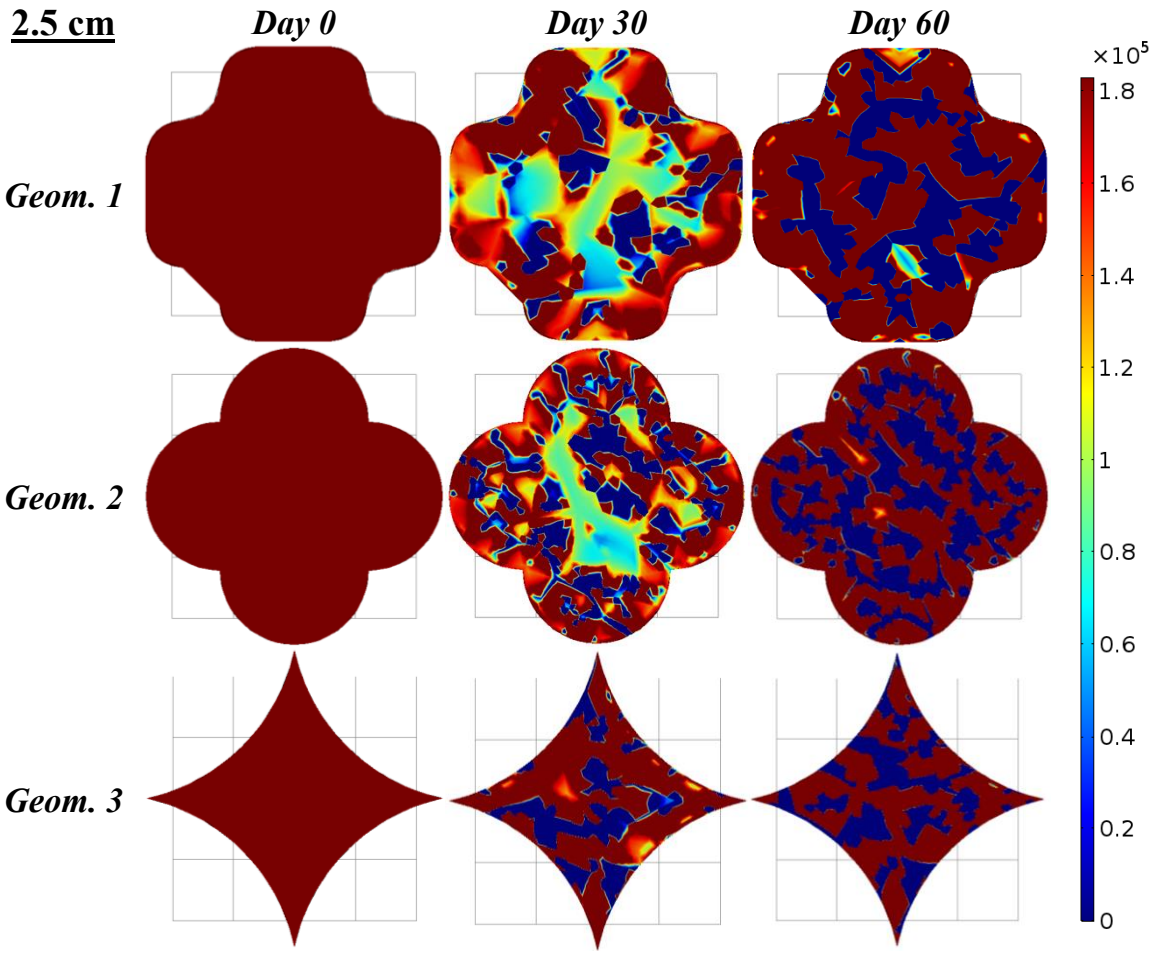

Figure 4.24: Weight molecular weight distribution at 2.5 cm from the base, as a function of degradation time and geometry, with an initial Mw equal to 183 kDa

Figure 4.25, 4.26, 4.27, 4.28, 4.29 and *4.30* show the final result of the behaviour of the weight molecular weight distributions for the three geometries, in post-sterilization conditions:

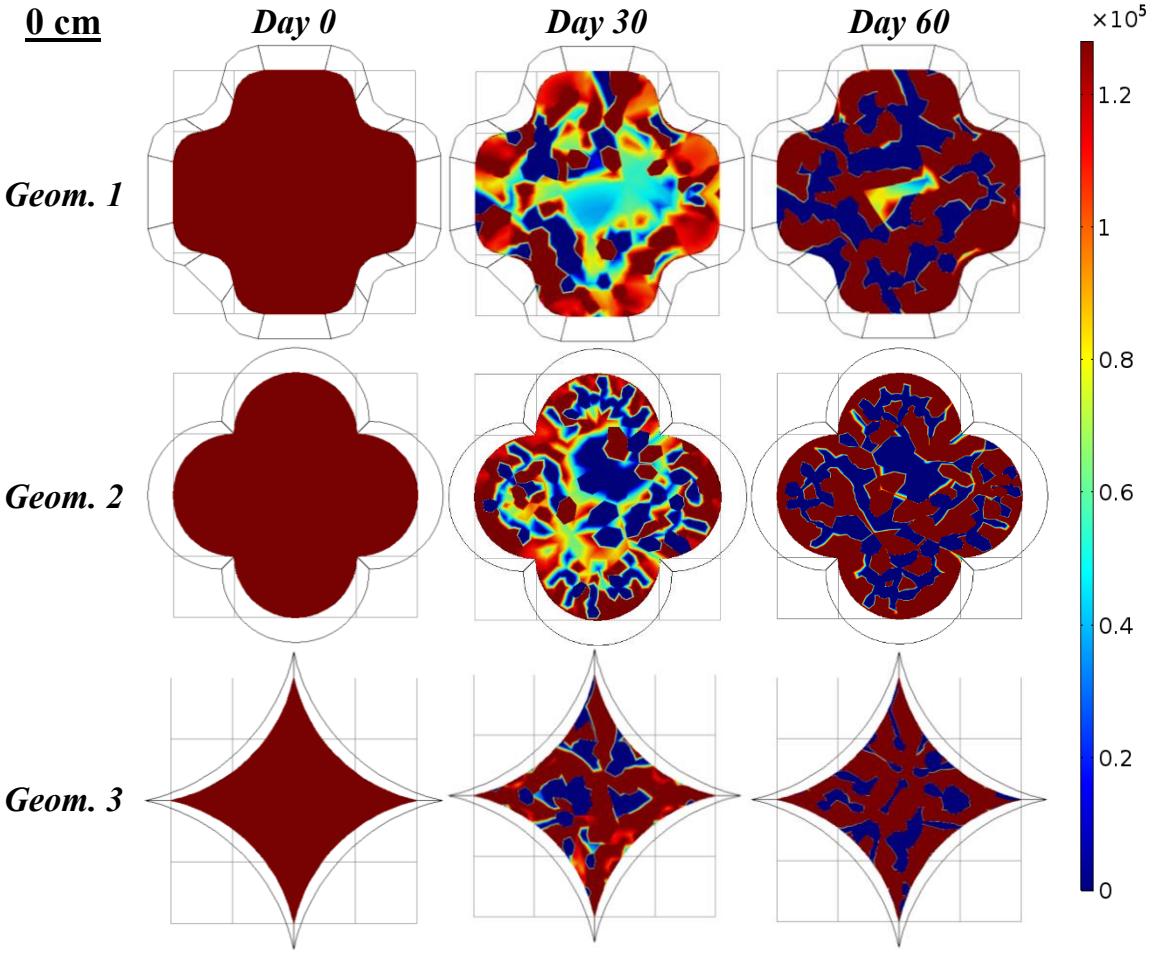

Figure 4.25: Weight molecular weight distribution at the base, as a function of degradation time and geometry, with an initial Mw equal to 128.1 kDa (30% loss)

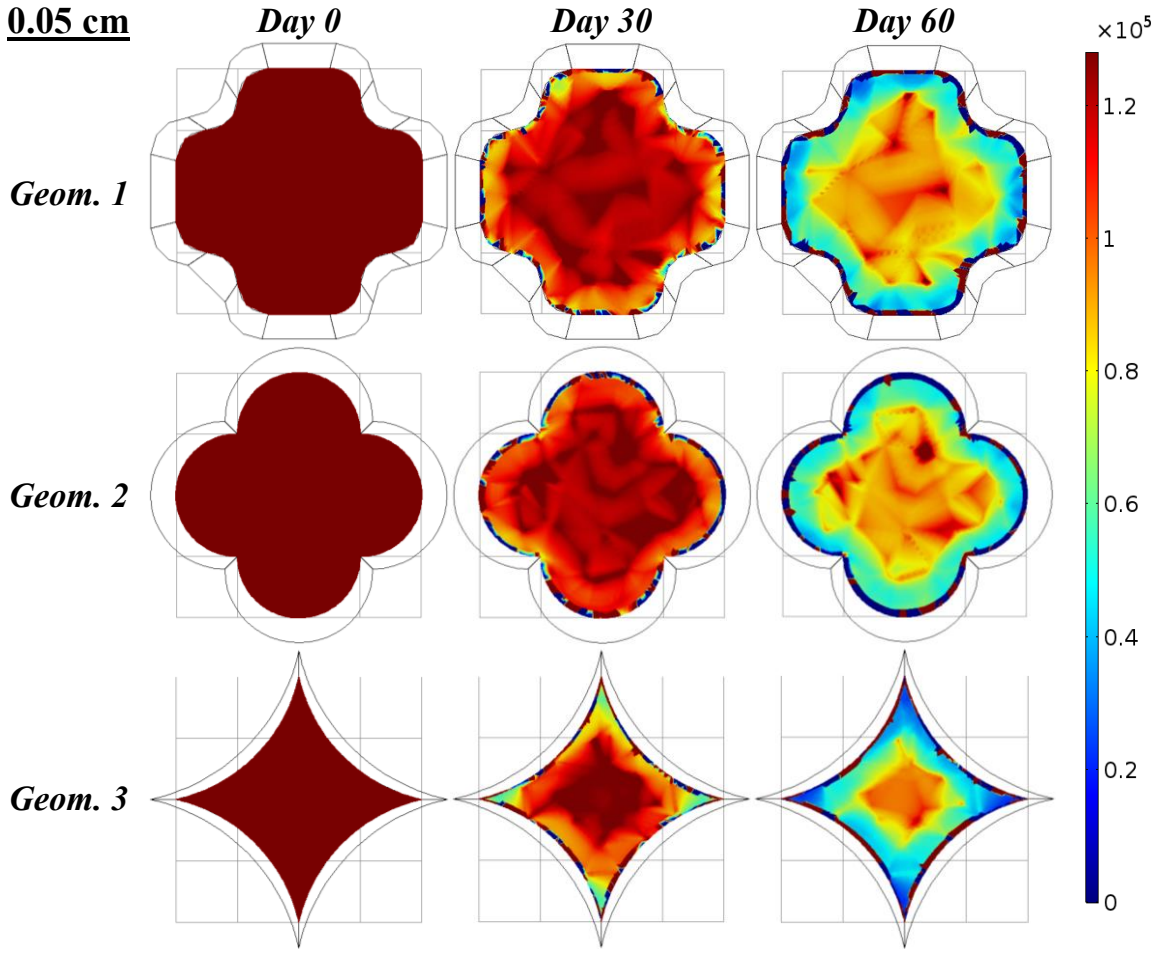

Figure 4.26: Weight molecular weight distribution at 0.05 cm from the base, as a function of degradation time and geometry, with an initial Mw equal to 128.1 kDa (30% loss)

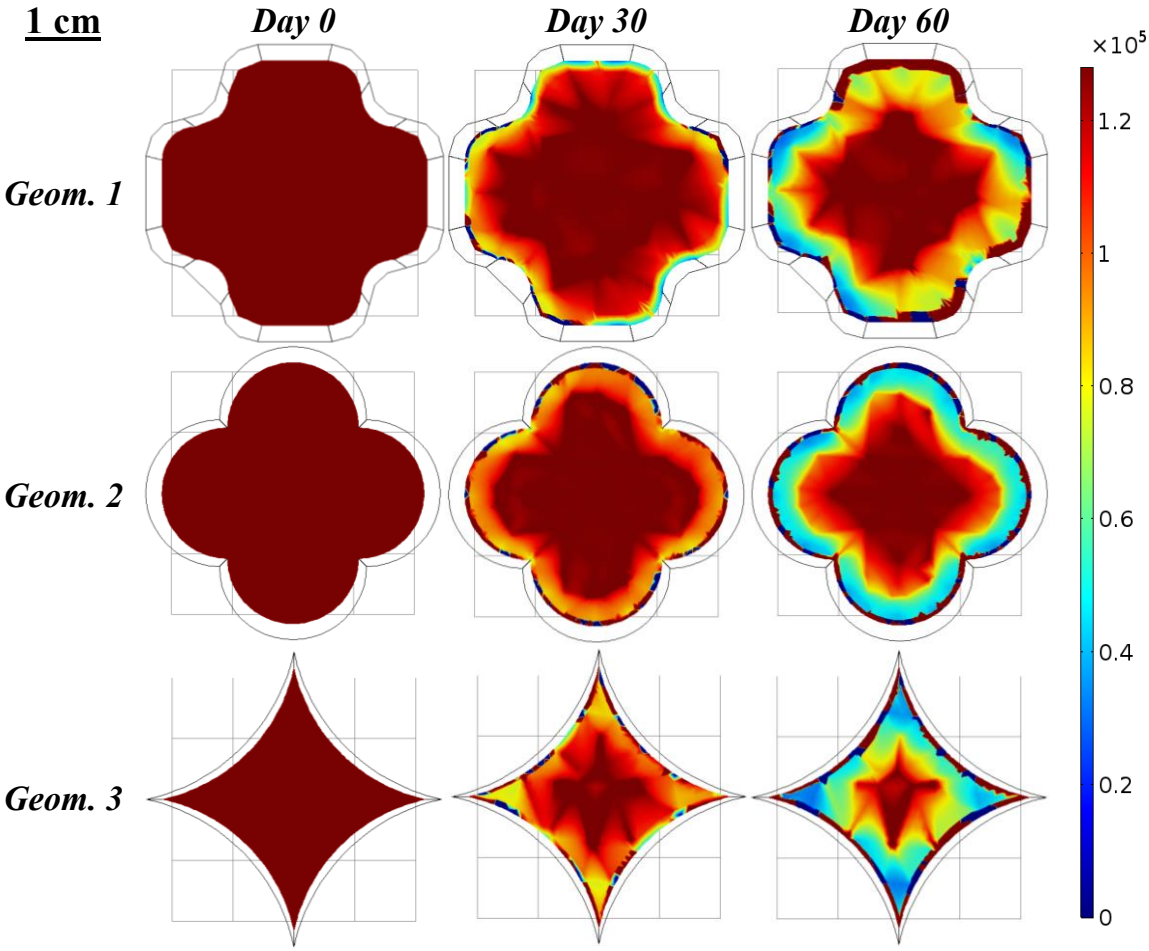

Figure 4.27: Weight molecular weight distribution at 1 cm from the base, as a function of degradation time and geometry, with an initial Mw equal to 128.1 kDa (30% loss)

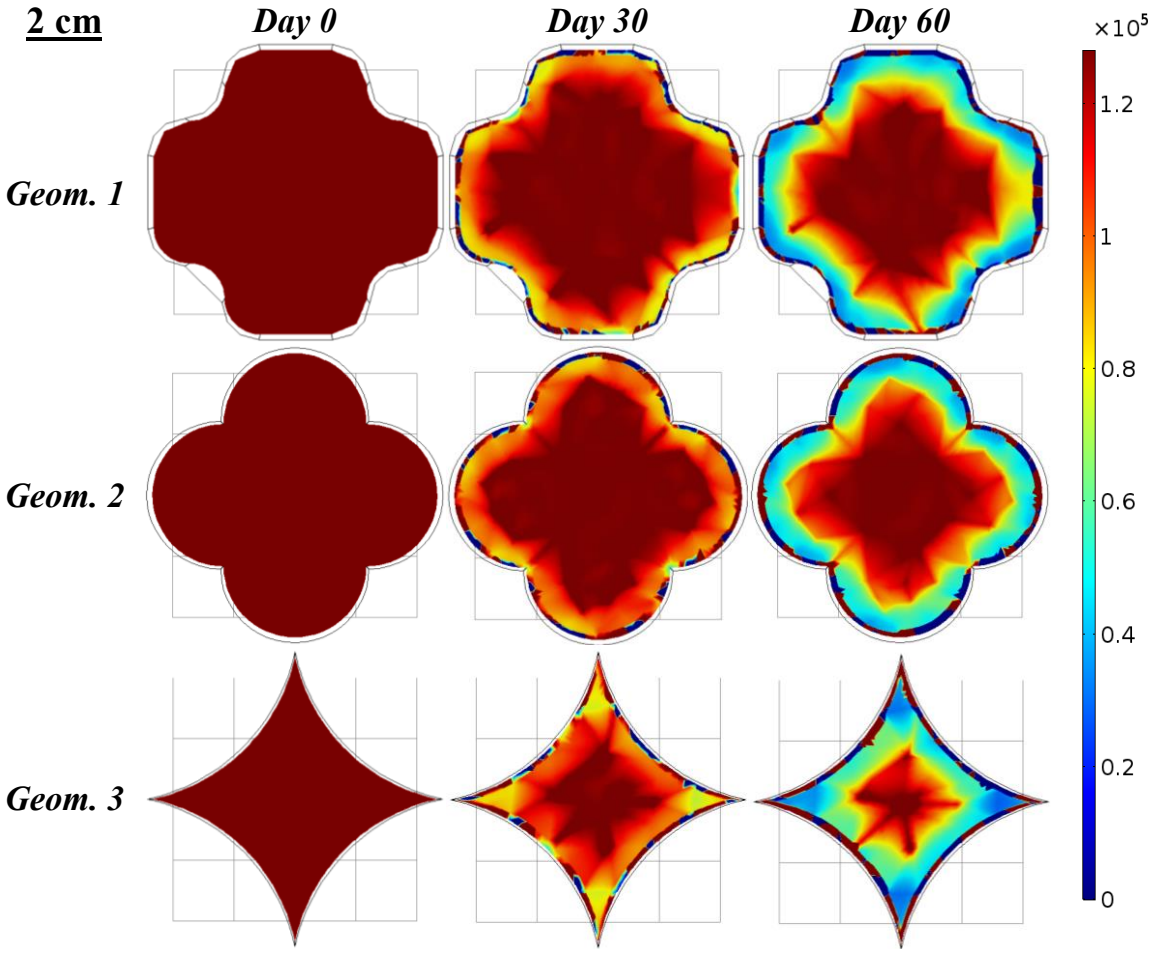

Figure 4.28: Weight molecular weight distribution at 2 cm from the base, as a function of degradation time and geometry, with an initial Mw equal to 128.1 kDa (30% loss)

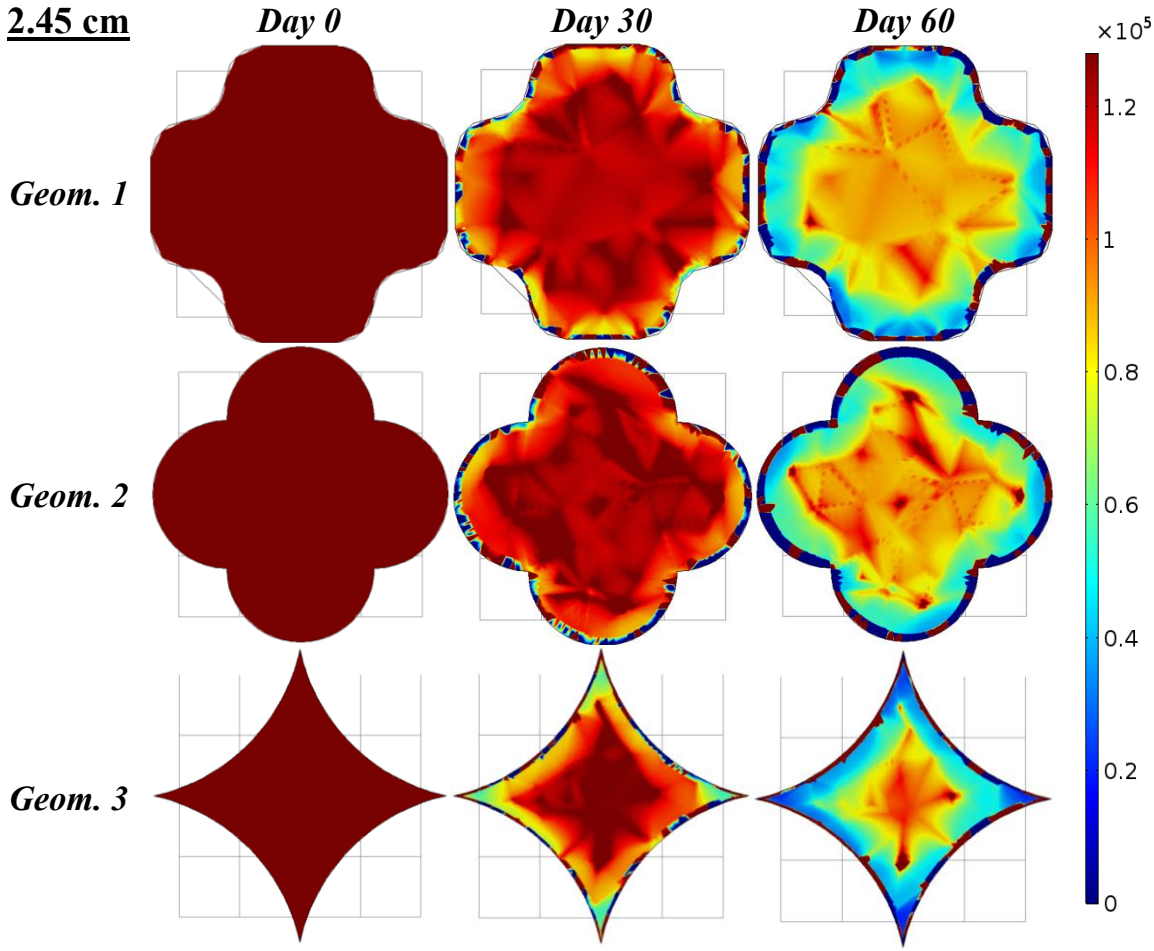

Figure 4.29: Weight molecular weight distribution at 2.45 cm from the base, as a function of degradation time and geometry, with an initial Mw equal to 128.1 kDa (30% loss)

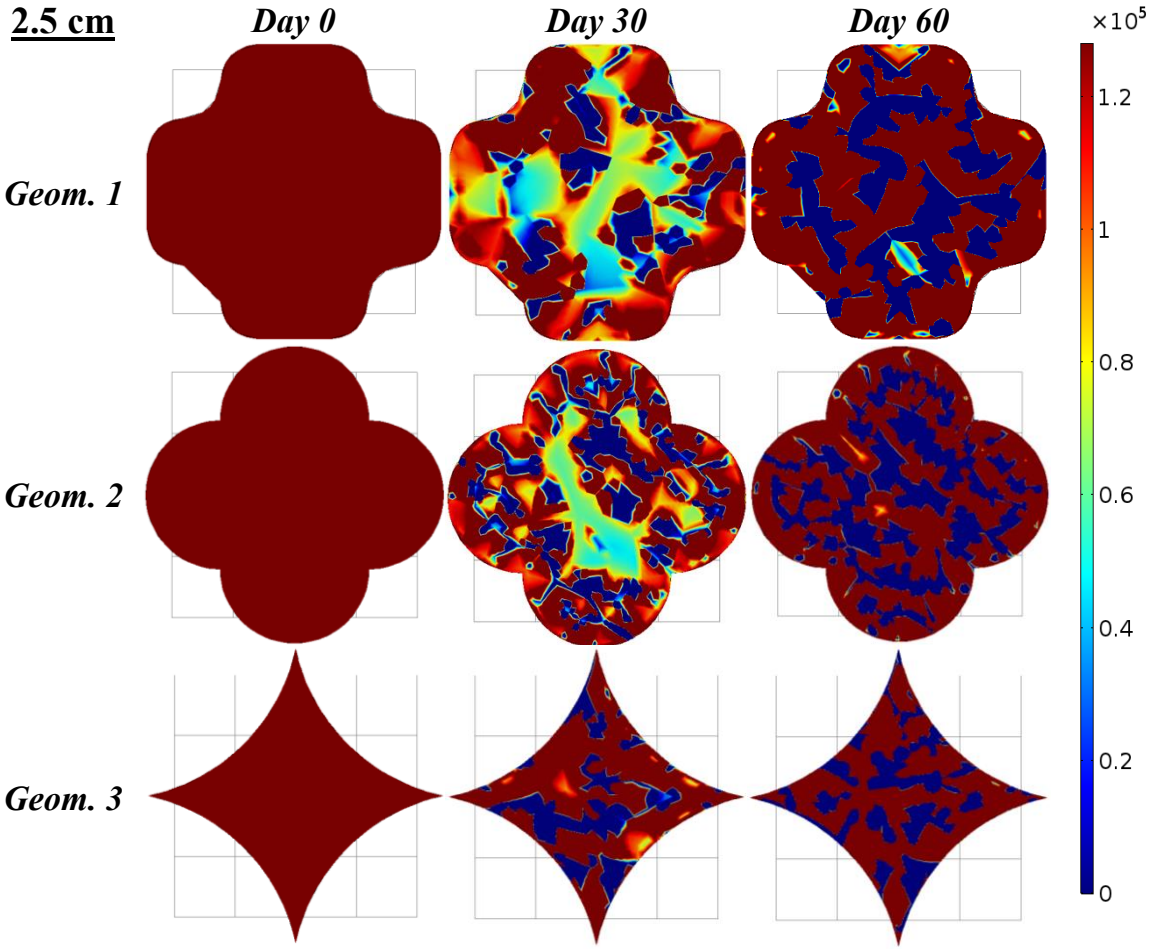

Figure 4.30: Weight molecular weight distribution at 2.5 cm from the base, as a function of degradation time and geometry, with an initial Mw equal to 128.1 kDa (30% loss)

As showed in the previous figures, it has been necessary to introduce two more heights with respect to those aforementioned in *Figure 4.17* for software matters: at the two extremities of the pin, the simulations showed computational problems. Therefore, the two heights immediately near to the top and to the base of the pin have been considered, as reported in *Figure 4.20, 4.26, 4.29* and *4.30*.

From the results obtained and shown in the previous figures, it can be noticed that Poly(L)-lactide-co-ε-caprolactone with high initial molecular weight presents good performances from both chemical degradation and mechanical load point of views.
It has been already observed that, for Polymer 1, the weight average molecular weight value in both pre and post-sterilization conditions and considering 60 days of degradation remains always above 45 kDa, which guarantees a good final result. However, it is important to underline that, as can be observed thanks to the colour scale, the weight molecular weight distribution as a function of the space and the degradation time presents values whom are not all above the threshold one. Obviously, at the base, where the fixed constraint has been applied, the molecular weight loss is higher than that at the top of the pin and, moreover, the molecular weight loss is more pronounced at the edges of the fixation system, since there Von Mises stresses are greater than those presented at the centre of the cross section. Despite this, the loss of the molecular weight is not so high to induce to reject Polymer 1, since, even after 60 days it doesn't bring to a circular cross section, losing stability.
To summarize, in *Figure 4.31* and *4.32* the slice representation of the weight molecular weight distribution for the entire height of the pin is reported, as a function of the different geometries and of the degradation time, in pre and post-sterilization conditions respectively:

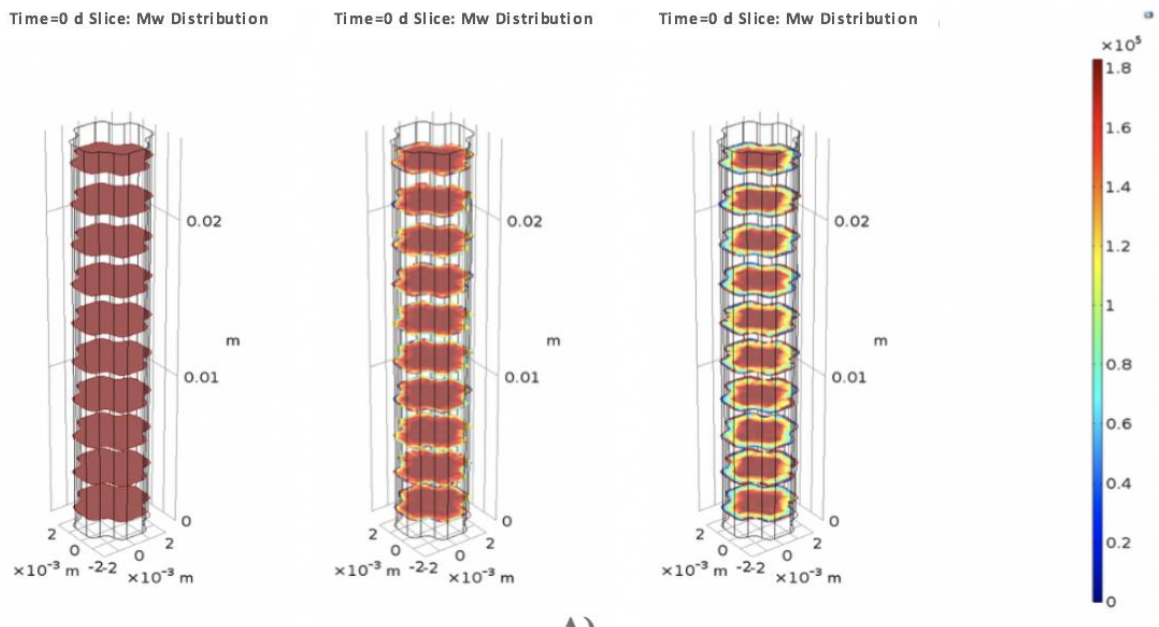
Time=0 d Slice: Mw Distribution
Time=0 d Slice: Mw Distribution
Time=0 d Slice: Mw Distribution
×10⁵
1.8
1.6
1.4
1.2
1
0.8
0.6
0.4
0.2
0
0.02
m
0.01
0
2
0
-2
×10⁻³ m
×10⁻³ m

A)

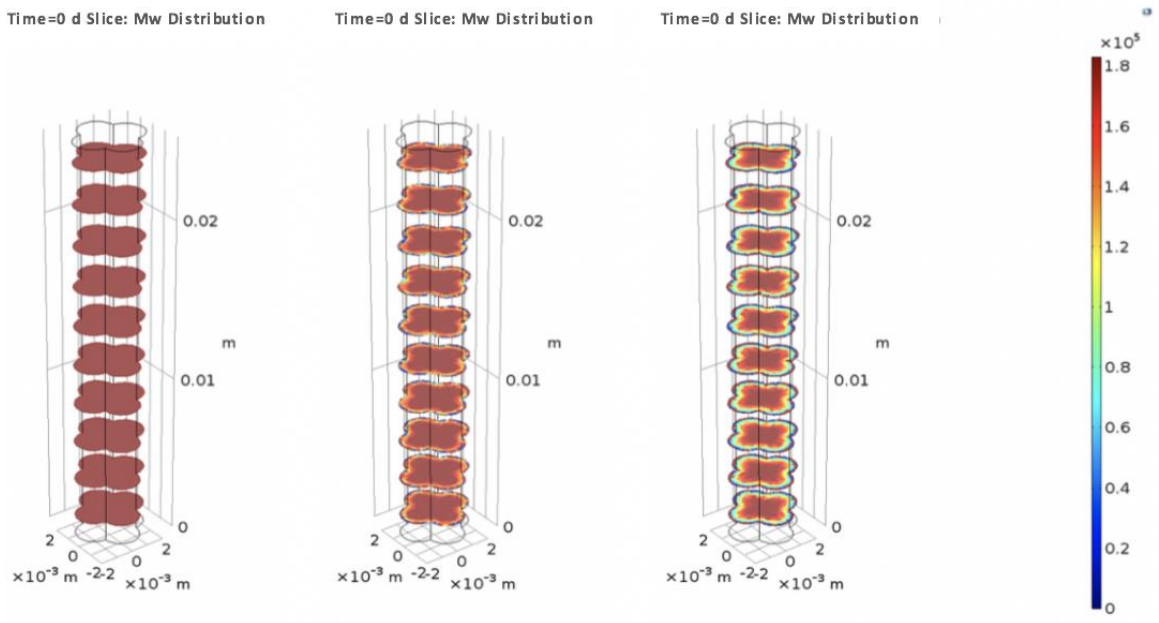
Time=0 d Slice: Mw Distribution
Time=0 d Slice: Mw Distribution
Time=0 d Slice: Mw Distribution
×10⁵
1.8
1.6
1.4
1.2
1
0.8
0.6
0.4
0.2
0
0.02
m
0.01
0
2
0
-2
×10⁻³ m
×10⁻³ m

B)

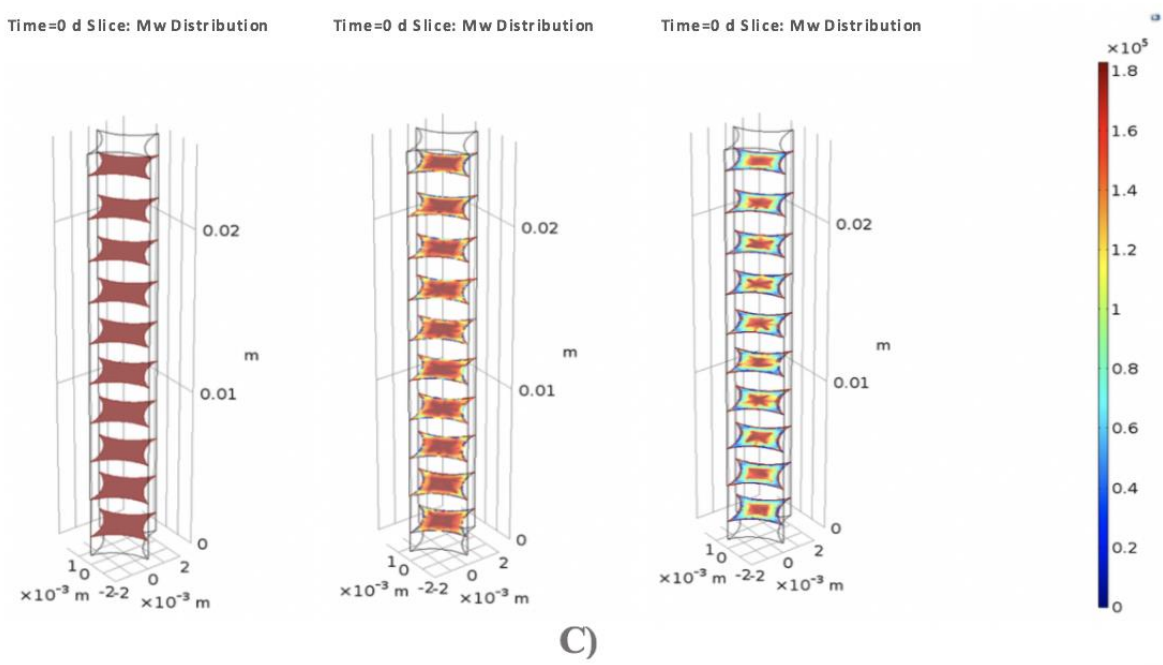

Figure 4.31: Slice representation of the weight molecular weight distribution for A) Geometry 1, B) Geometry 2, C) Geometry 3 with an initial Mw equal to 183 kDa

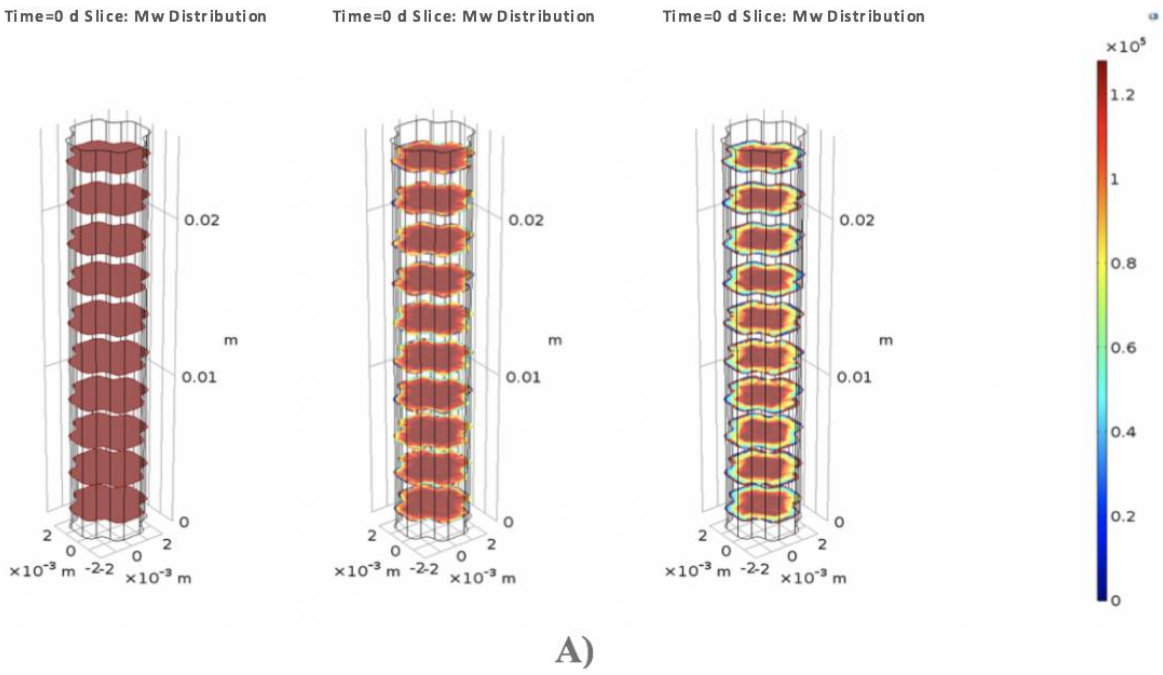

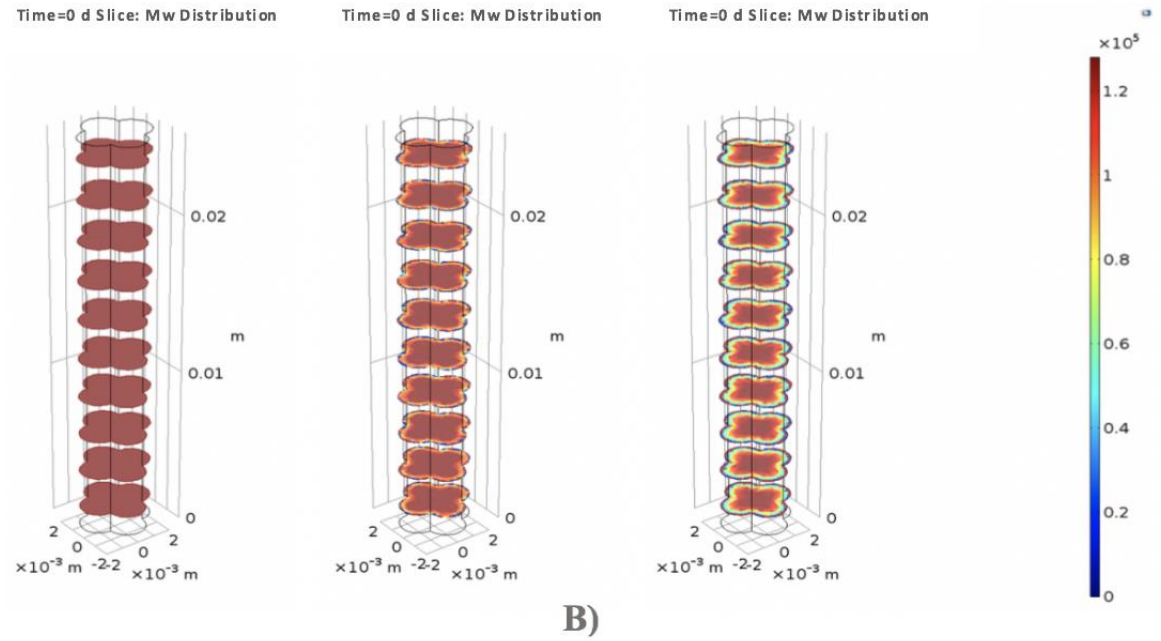

Figure 4.32: Slice representation of the weight molecular weight distribution for A) Geometry 1, B) Geometry 2, C) Geometry 3 with an initial MWw equal to 128.1 kDa (30% loss)

In conclusion, Polymer 1 respects all the aforementioned requirements necessary to develop an optimize bone fixation system.

4.3.2 *Polymer 4*

In *Figure 4.33* and *4.34*, the comparison among the weight average molecular behaviours as a function of the three geometries is reported, in pre and post-sterilization conditions respectively:

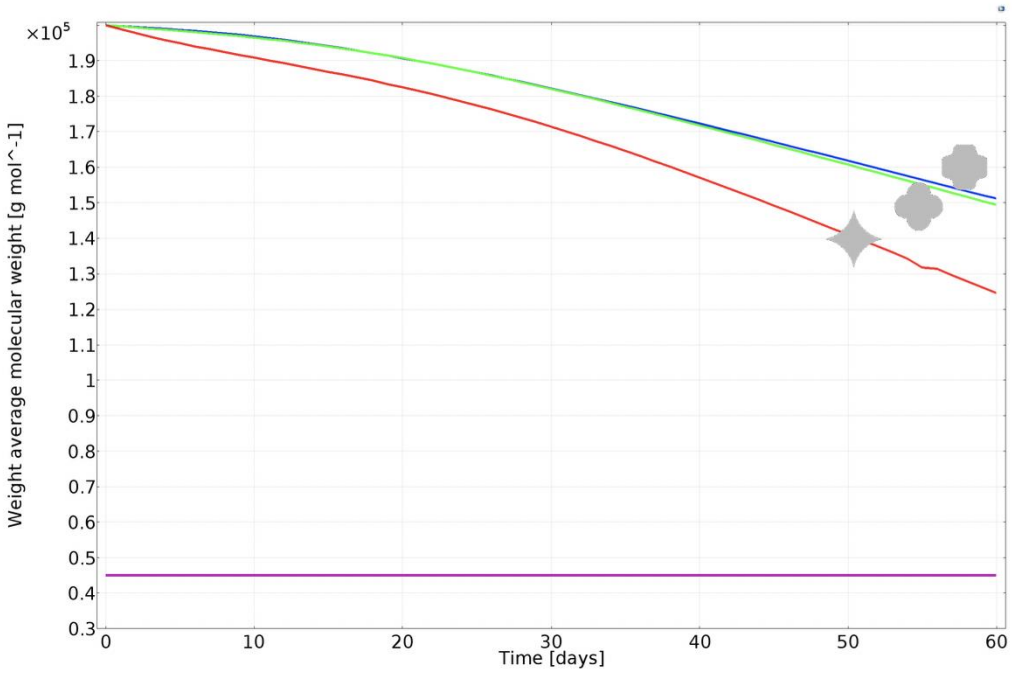

Figure 4.33: Weight-average molecular weight with an initial Mw of 200 kDa

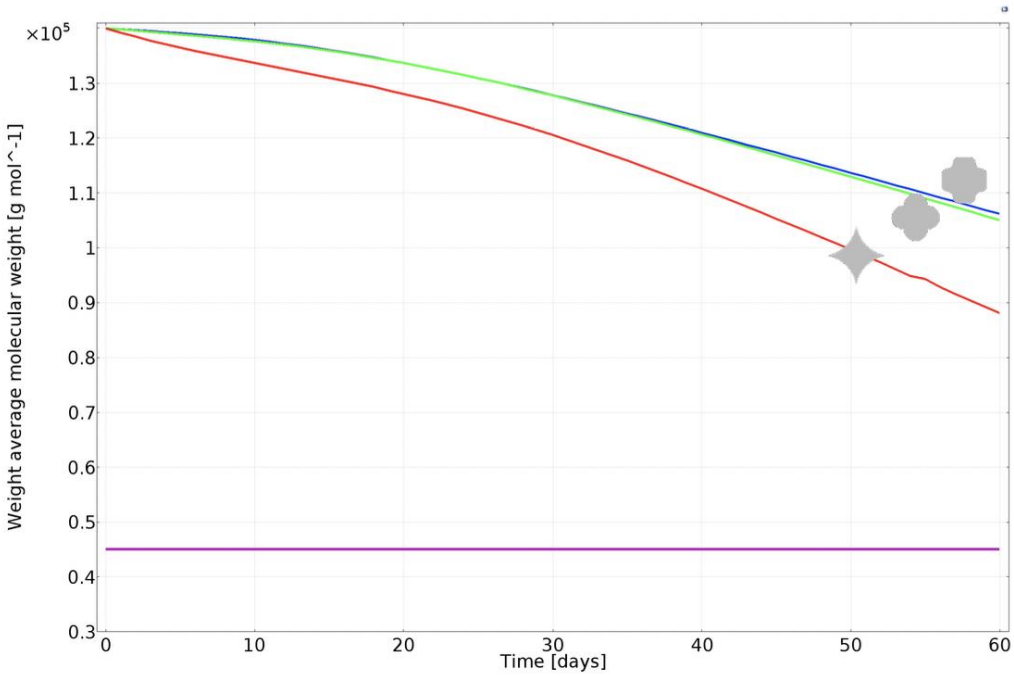

Figure 4.34: Weight average molecular weight with an initial Mw of 140 kDa (30% loss)

For the three geometries tested, and in particular after sterilization, the final values of the weight average molecular weight remain above 45 kDa, i.e., the threshold. Therefore, Polymer 4 continues to be one of the best candidates for the achievement of the thesis purpose.
It is important to notice, however, that the final values of the weight average molecular weight after coupling, for all the geometries, both in pre and post-sterilization conditions are smaller than those obtained from the degradation model alone, as reported in *Chapter 4.1*. This consideration shows that the degradation of the polymer is influenced by the mechanical loads, in a not negligible way.

It can be noticed that Geometry 1 and Geometry 2 are similar in terms of weight average molecular weight loss, while Geometry 3 is the one that shows a major decrease of the weight average molecular weight and this could be explained by the particular shape of Geometry 3 and, most of all, of its cross section. Nevertheless, Geometry 3 is the best orthopaedic form and, moreover, its weight average molecular weight value after 60 day of degradation always remains above the threshold value.

In order to represent and better show the real behaviour of the weight molecular weight distribution as a function of the degradation due to both hydrolysis and mechanical loads and of both the geometry cross sections and the height of the pin, i.e., the space, four different heights have been selected, as reported in *Figure 4.35*:

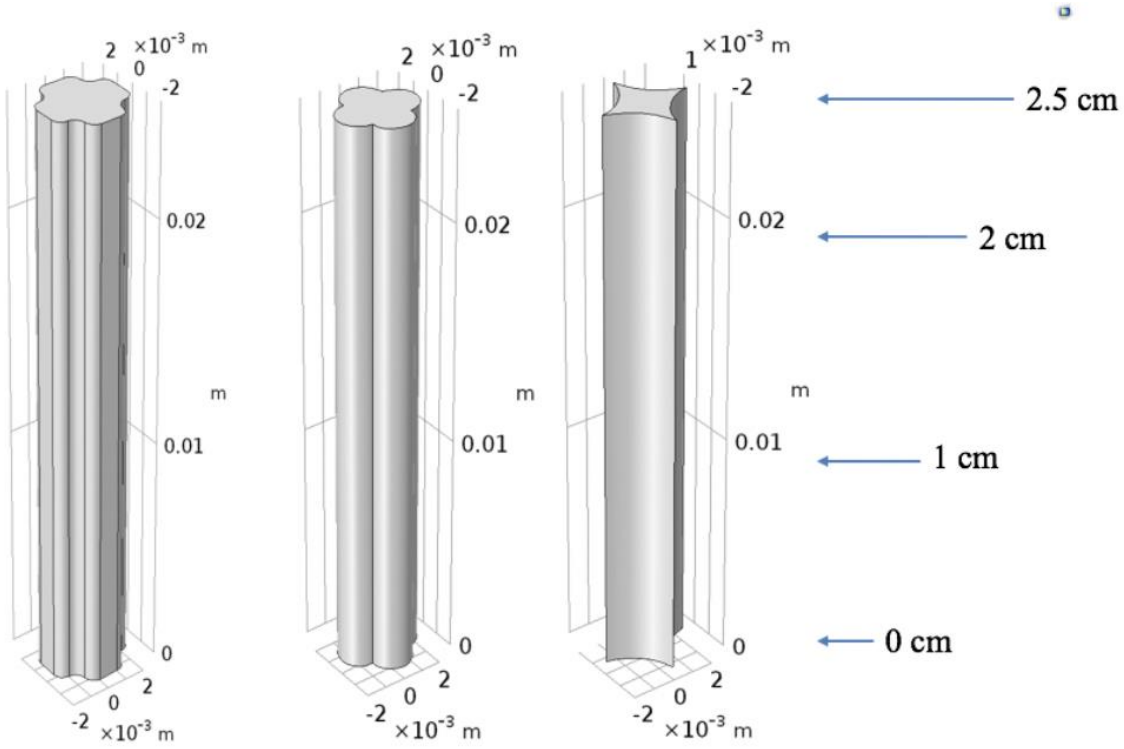

Figure 4.35: Representation of the selected heights

By doing so, the comparison among the weight molecular weight distributions as a function of the three different cross sections at the four different heights and at a degradation time equal to zero, 30 and 60 days respectively has been possible.

In *Figure 4.36*, the considered cross sections are represented:

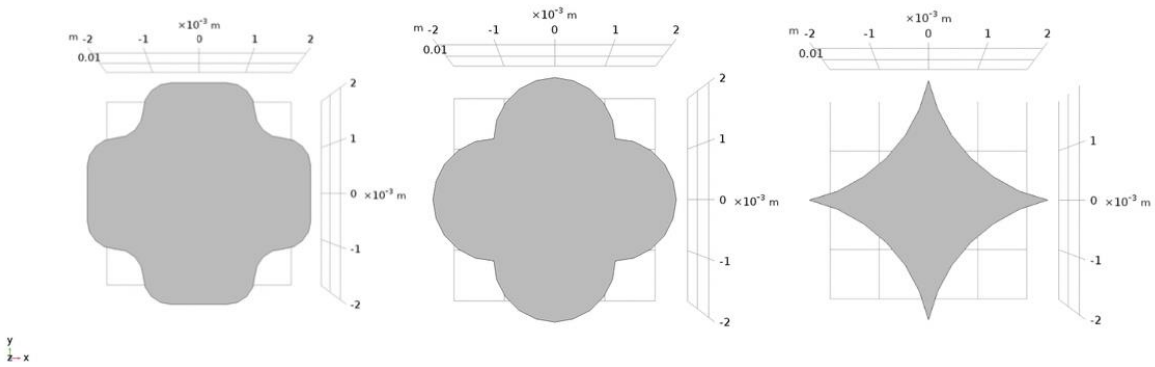

Figure 4.36: Representation of the selected cross section

Figure 4.37, 4.38, 4.39, 4.40, 4.41 and *4.42* show the final result of the behaviour of the weight molecular weight distributions for the three geometries, in pre-sterilization conditions:

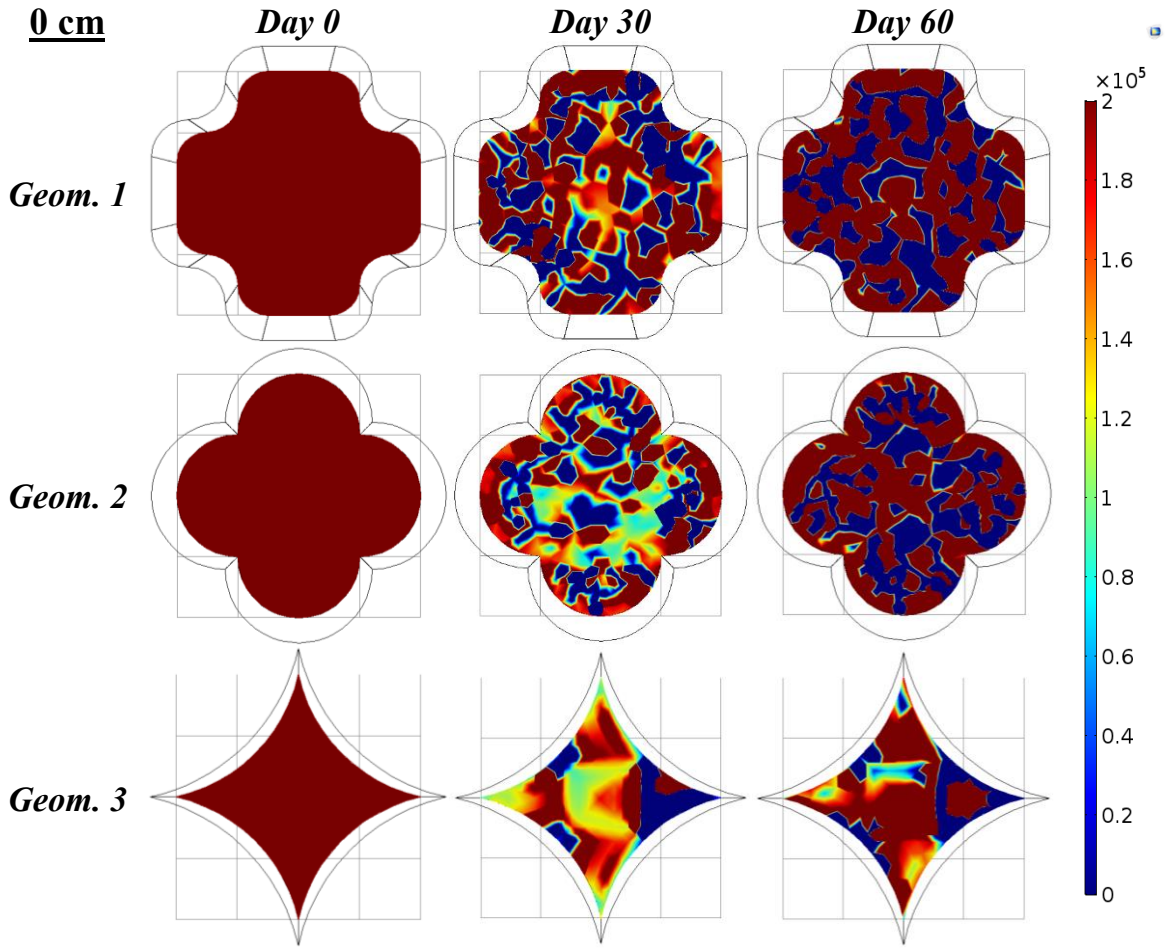

Figure 4.37: Weight molecular weight distribution at the base, as a function of degradation time and geometry, with an initial Mw equal to 200 kDa

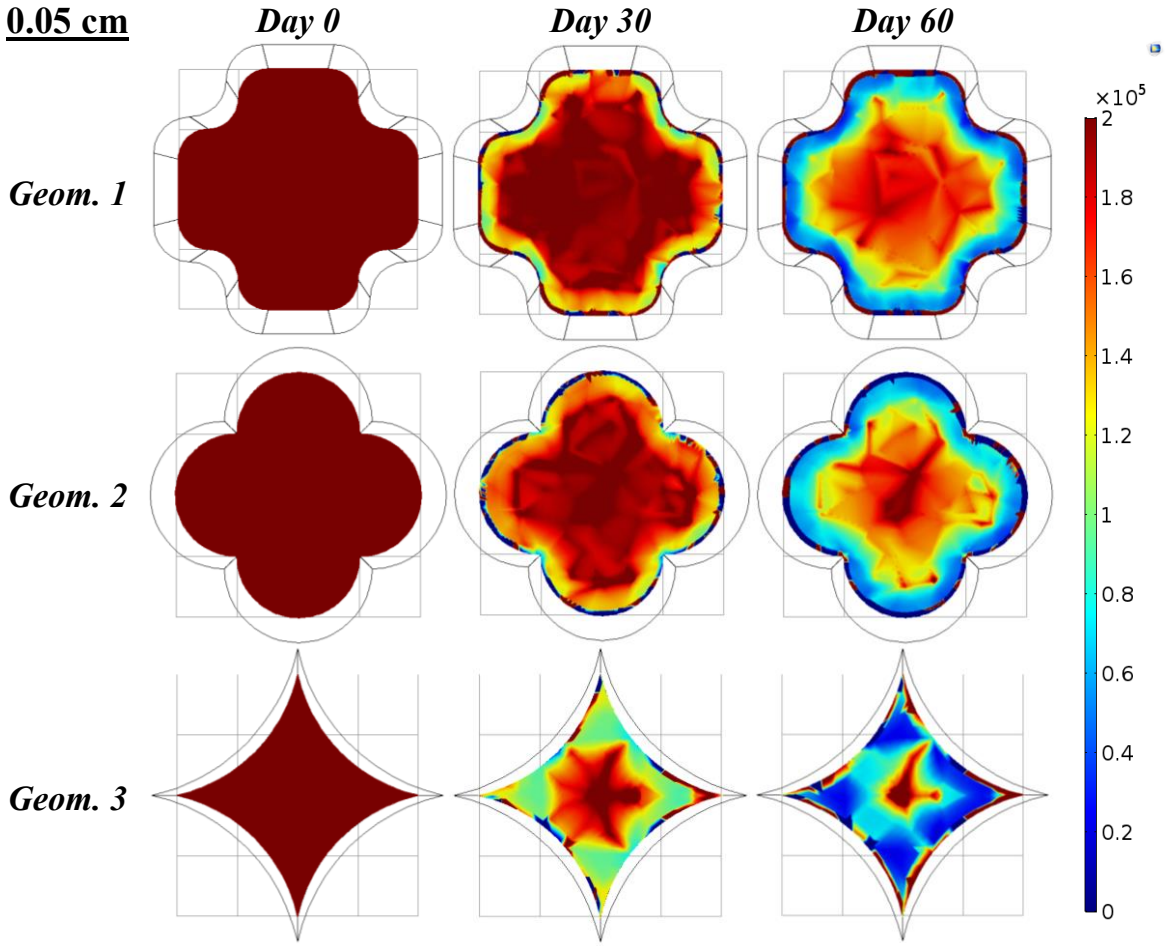

Figure 4.38: Weight molecular weight distribution at 0.05 cm from the base, as a function of degradation time and geometry, with an initial Mw equal to 200 kDa

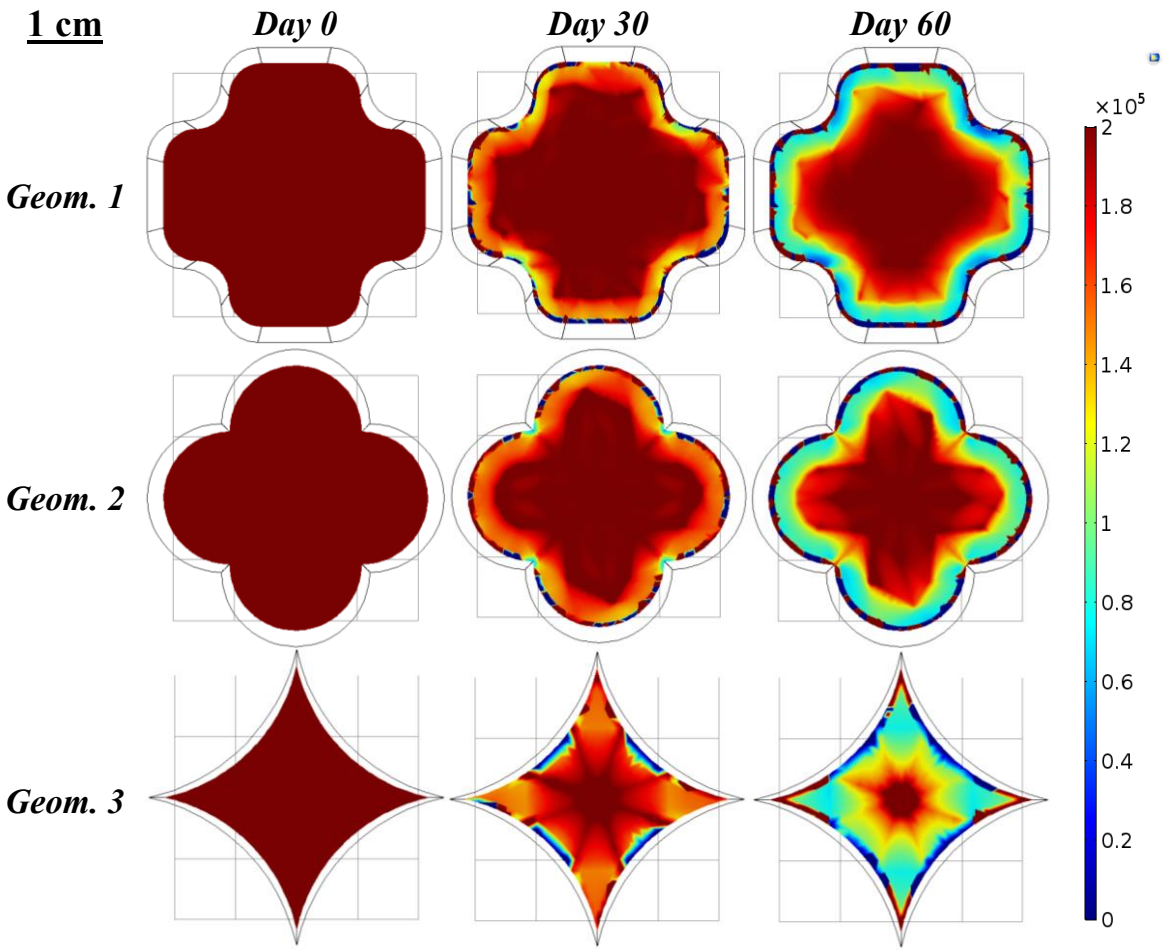

Figure 4.39: Weight molecular weight distribution at 1 cm from the base, as a function of degradation time and geometry, with an initial Mw equal to 200 kDa

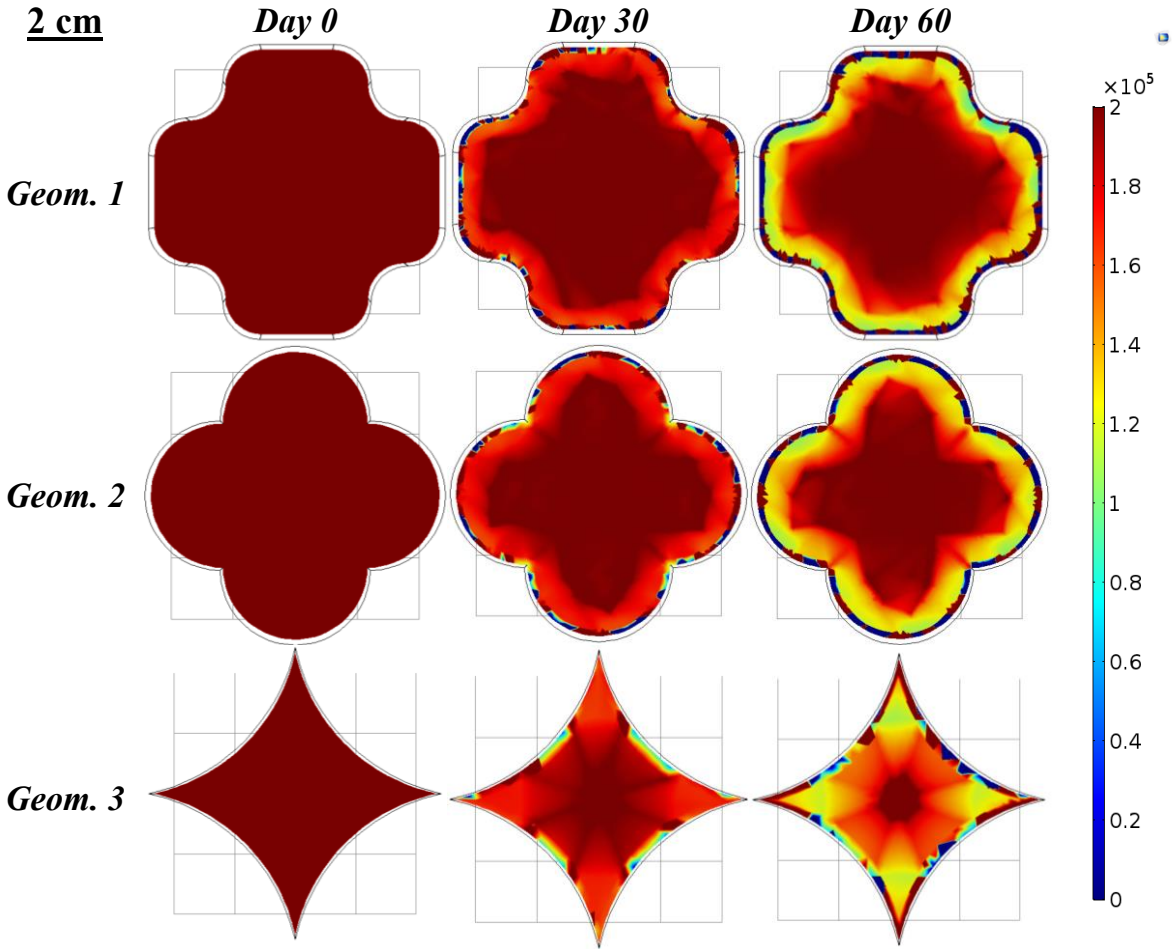

Figure 4.40: Weight molecular weight distribution at 2 cm from the base, as a function of degradation time and geometry, with an initial Mw equal to 200 kDa

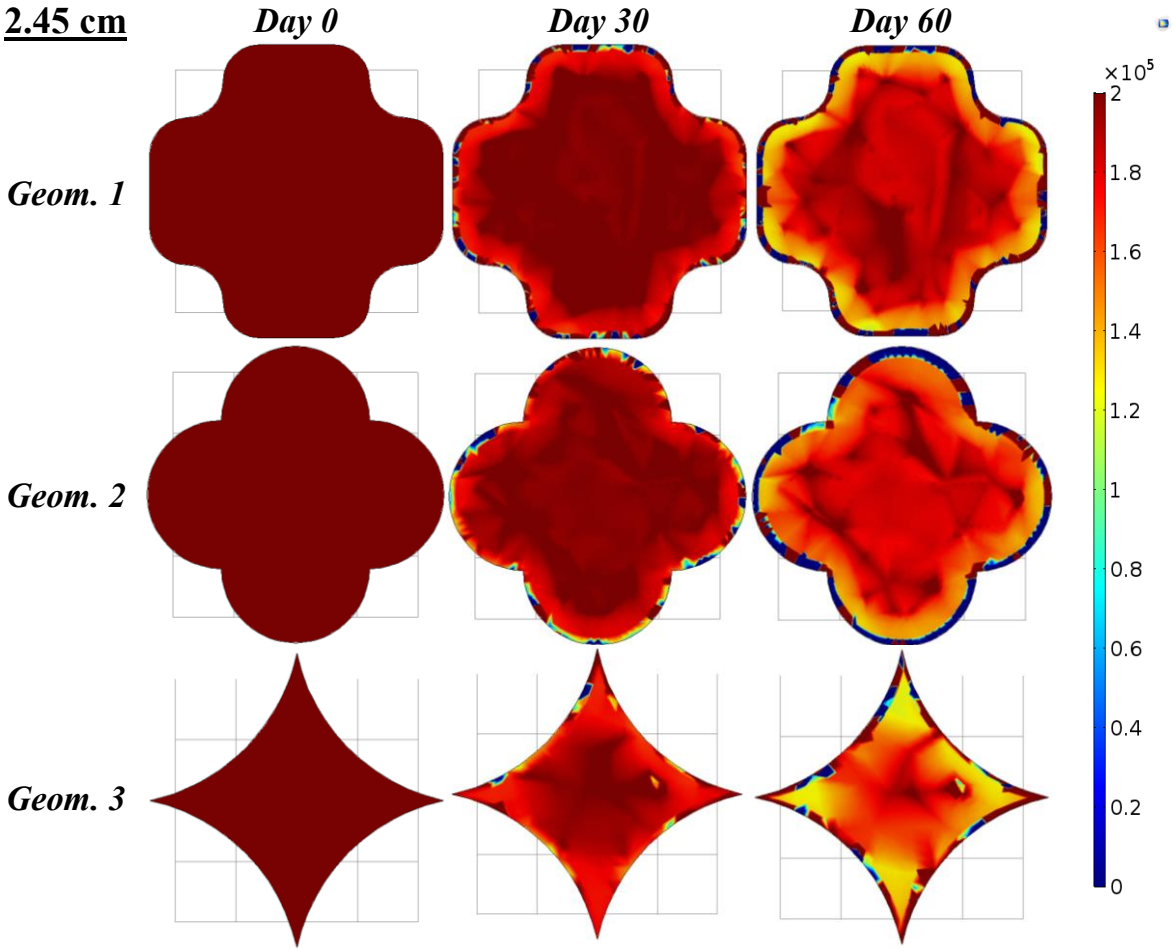

Figure 4.41: Weight molecular weight distribution at 2.45 cm from the base, as a function of degradation time and geometry, with an initial Mw equal to 200 kDa

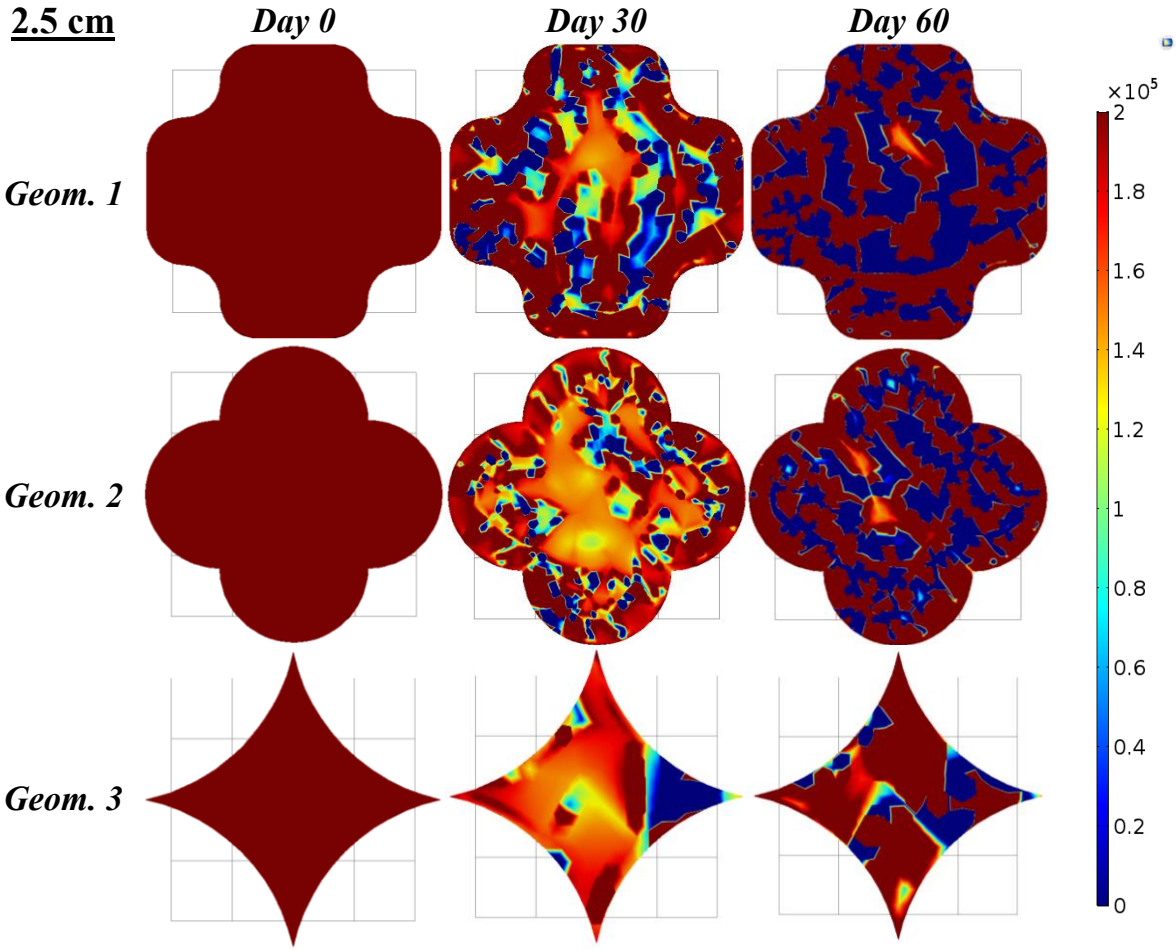

Figure 4.42: Weight molecular weight distribution at 2.5 cm from the base, as a function of degradation time and geometry, with an initial Mw equal to 200 kDa

Figure 4.43, 4.44, 4.45, 4.46, 4.47 and *4.48* show the final result of the behaviour of the weight molecular weight distributions for the three geometries, in post-sterilization conditions:

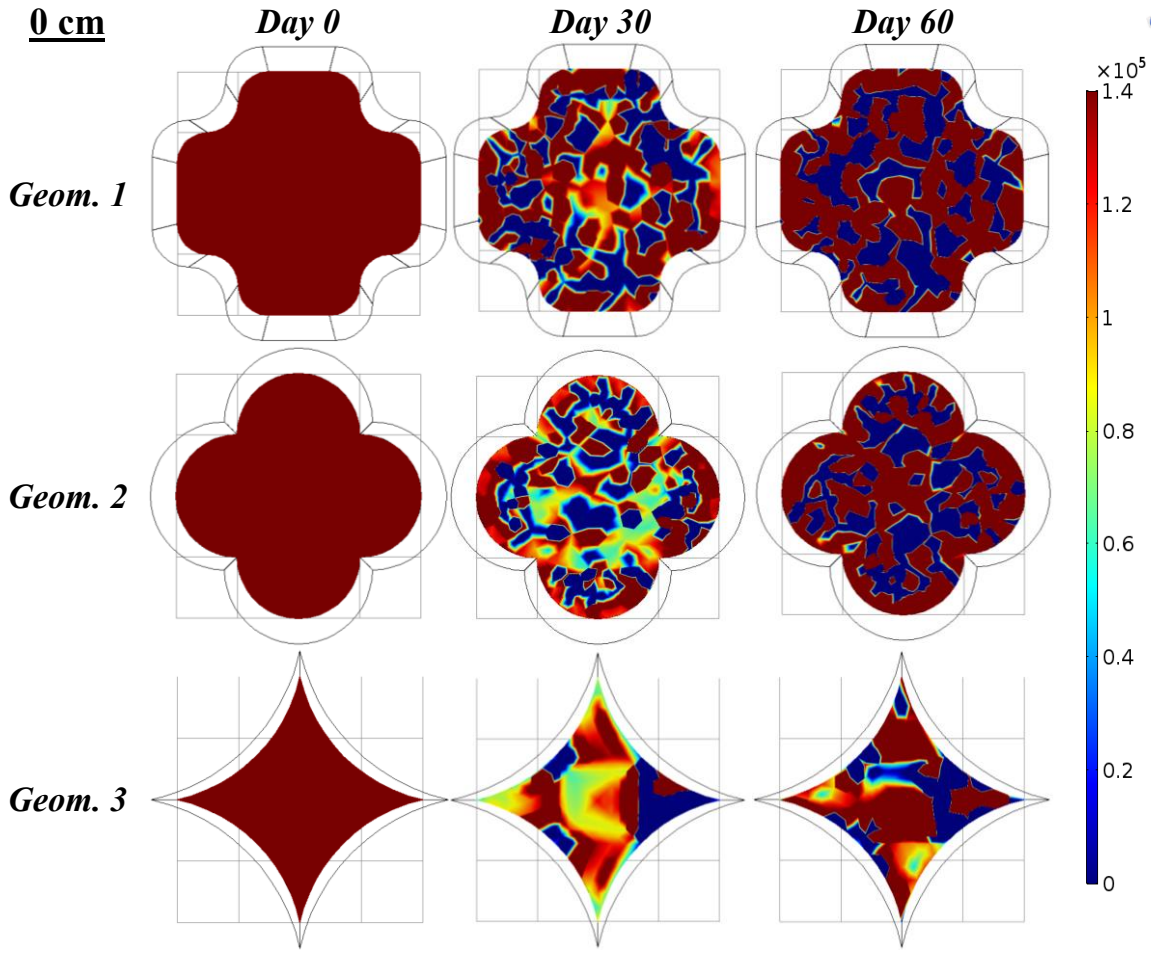

Figure 4.43: Weight molecular weight distribution at the base, as a function of degradation time and geometry, with an initial Mw equal to 140 kDa (30%loss)

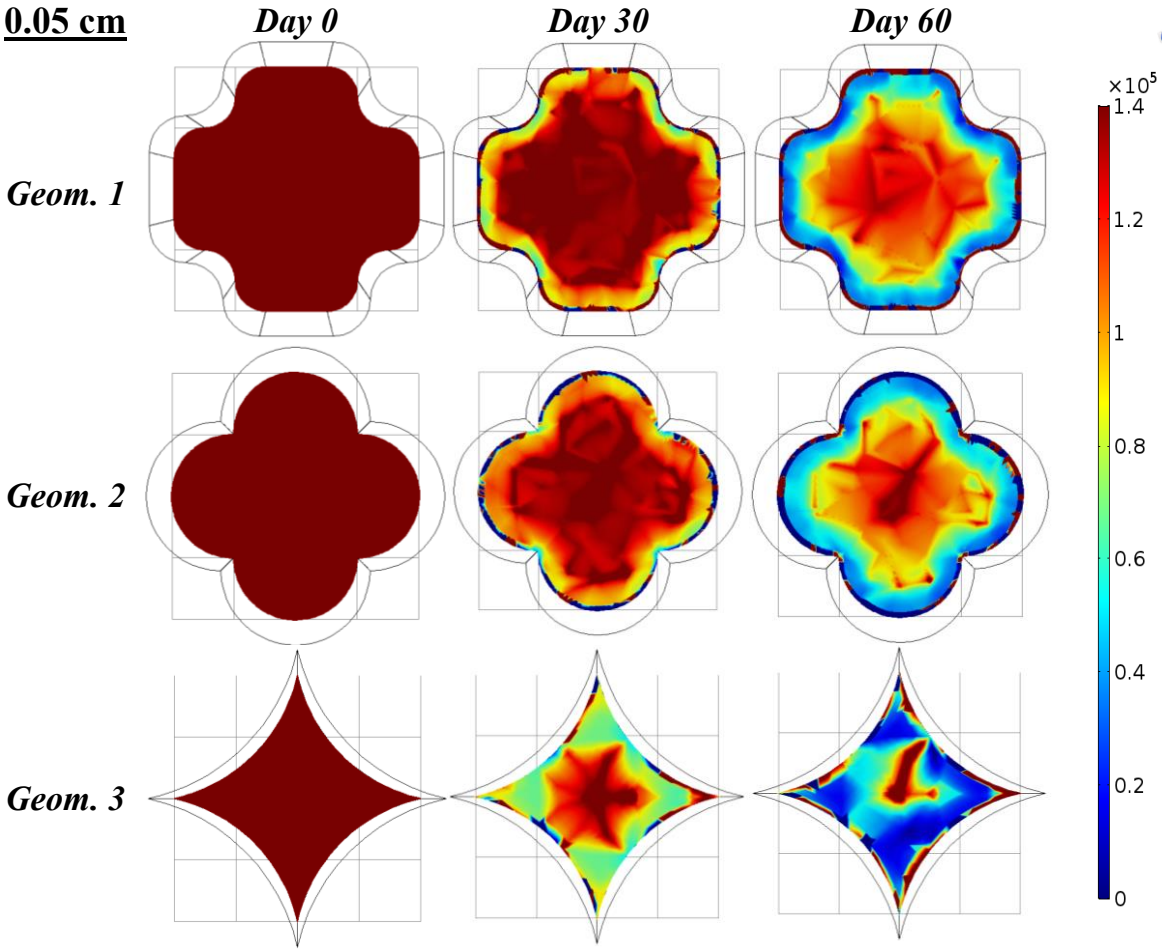

Figure 4.44: Weight molecular weight distribution at 0.05 cm from the base, as a function of degradation time and geometry, with an initial Mw equal to 140 kDa (30%loss)

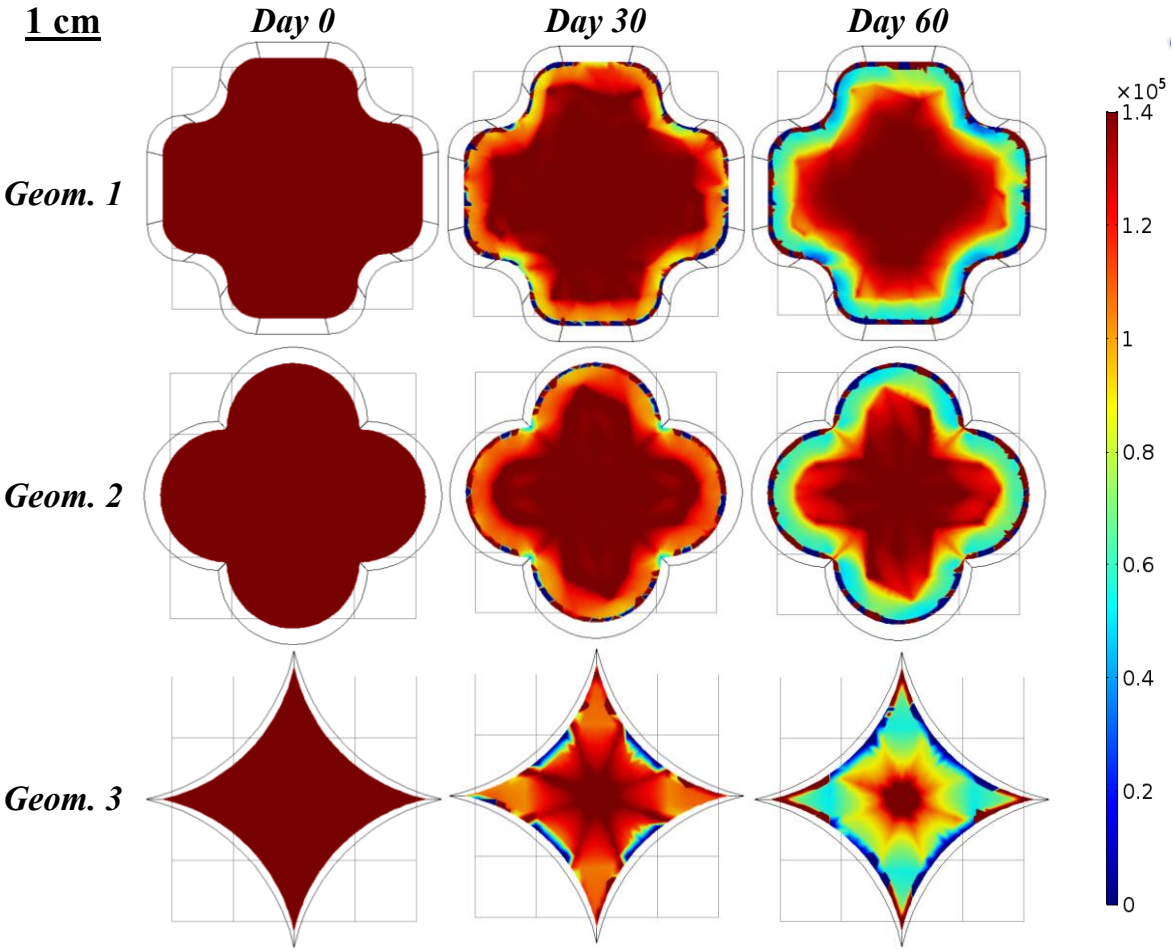

Figure 4.45: Weight molecular weight distribution at 1 cm from the base, as a function of degradation time and geometry, with an initial Mw equal to 140 kDa (30%loss)

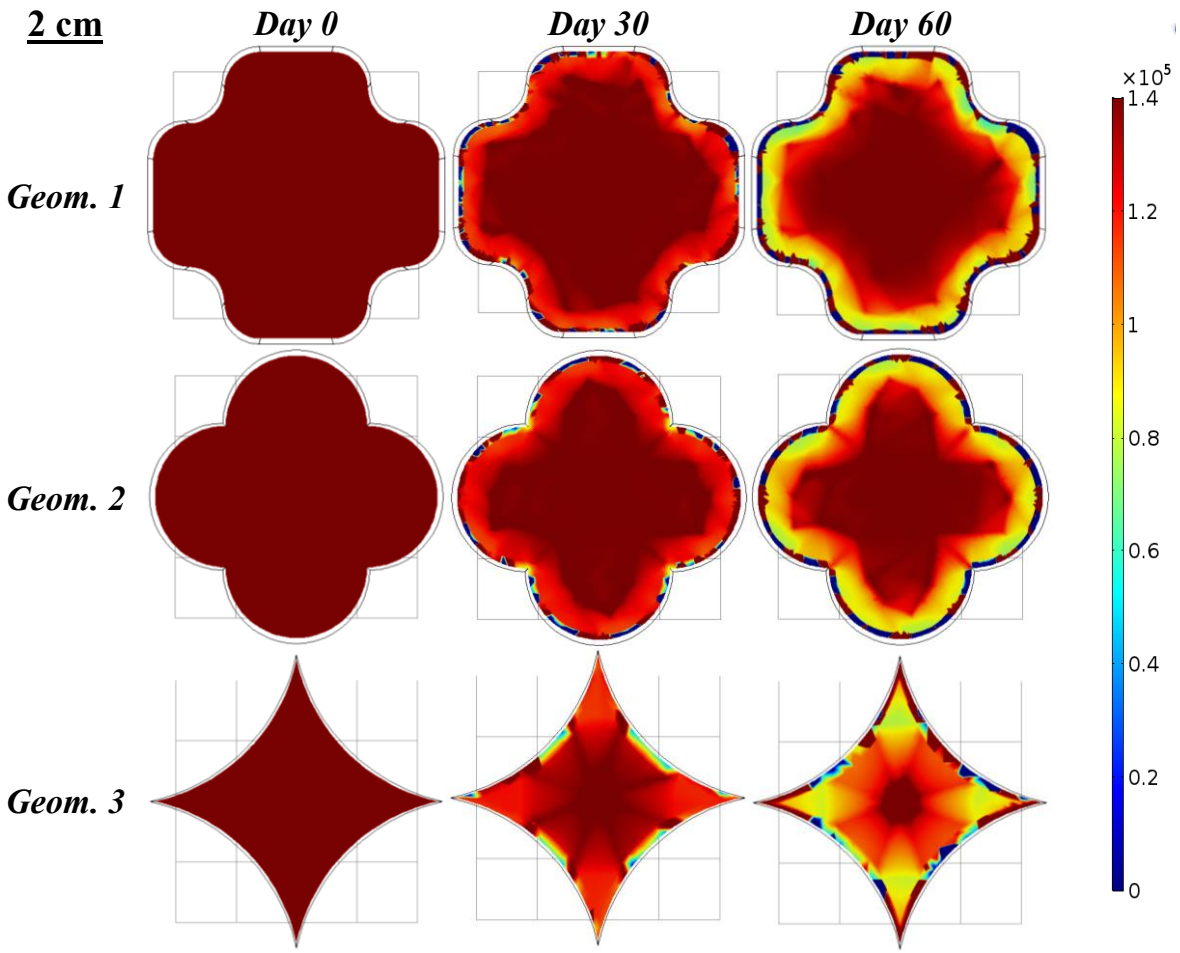

Figure 4.46: Weight molecular weight distribution at 2 cm from the base, as a function of degradation time and geometry, with an initial Mw equal to 140 kDa (30%loss)

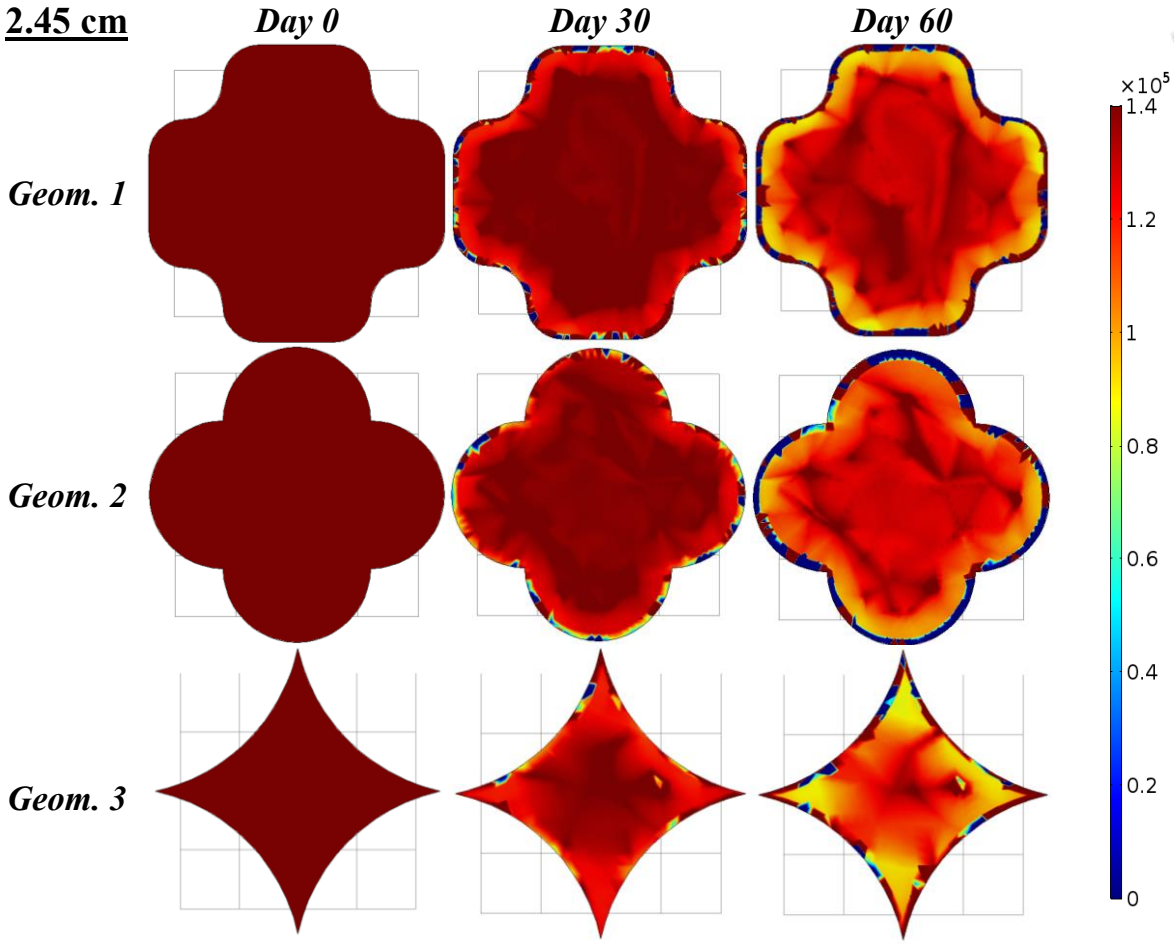

Figure 4.47: Weight molecular weight distribution at 2.45 cm from the base, as a function of degradation time and geometry, with an initial Mw equal to 140 kDa (30%loss)

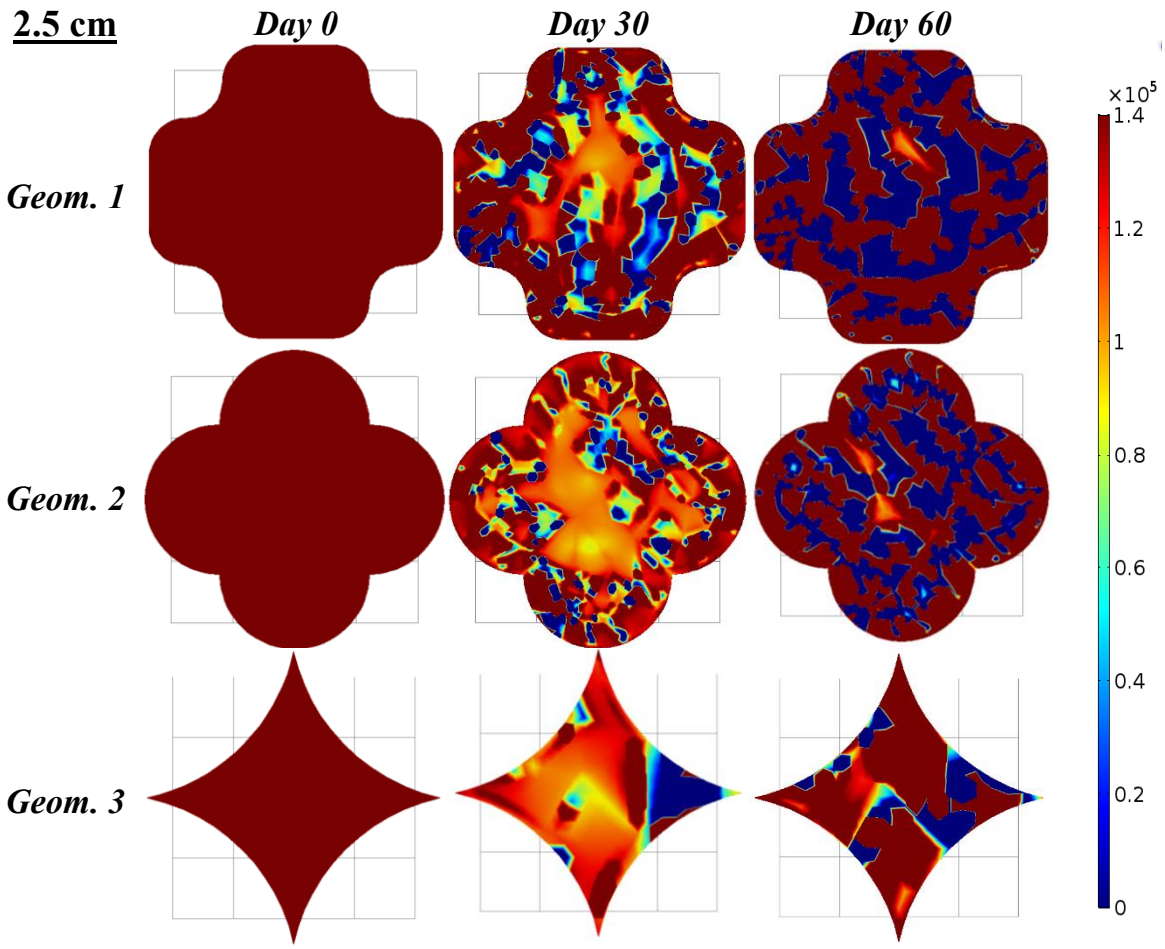

Figure 4.48: Weight molecular weight distribution at 2.5 cm from the base, as a function of degradation time and geometry, with an initial Mw equal to 140 kDa (30%loss)

As shown in the previous figures, it has been necessary to introduce two more heights with respect to those aforementioned in *Figure 4.35* for software matters, as already explain for Polymer 1.

From the results obtained and shown in the previous figures, it can be noticed that Poly(D,L-lactice) acid with high initial molecular weight respects the necessary requirements when subjected to the coupling between chemical degradation and mechanical load effects.
It has been already observed that for Polymer 4 the weight average molecular weight value in both pre and post-sterilization conditions and considering 60 days of degradation, remains always above 45 kDa, which guarantees a good final result. However, it is important to underline that, as can be observed thanks to the colour scale, the weight molecular weight distribution as a function of the space and the degradation time presents values whom are not all above the threshold value. Obviously, at the base, where the fixed constraint has been applied, the molecular weight loss is higher than that at the top of the pin and, moreover, the molecular weight loss is more pronounced at the edges of the fixation system, since there Von Mises stresses are greater than those presented at the centre of the cross section. Despite this, the loss of the molecular weight is not so high to induce to reject Polymer 4, since, even after 60 days it doesn't bring to a circular cross section, losing stability.
To summarize, in *Figure 4.49* and *4.50* the slice representation of the weight molecular weight distribution for the entire height of the pin is reported, as a function of the different geometries and of the degradation time, in pre and post-sterilization conditions respectively:

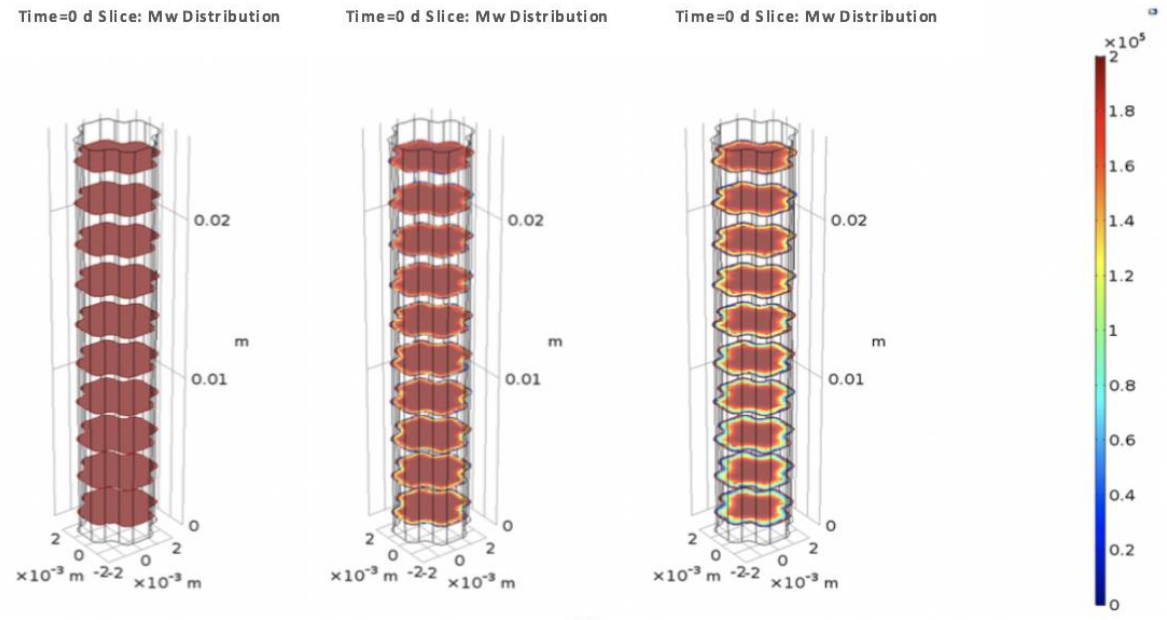
Time=0 d Slice: Mw Distribution
Time=0 d Slice: Mw Distribution
Time=0 d Slice: Mw Distribution
×10⁵
2
1.8
1.6
1.4
1.2
1
0.8
0.6
0.4
0.2
0
0.02
0.01
m
×10⁻³ m
-2-2

A)

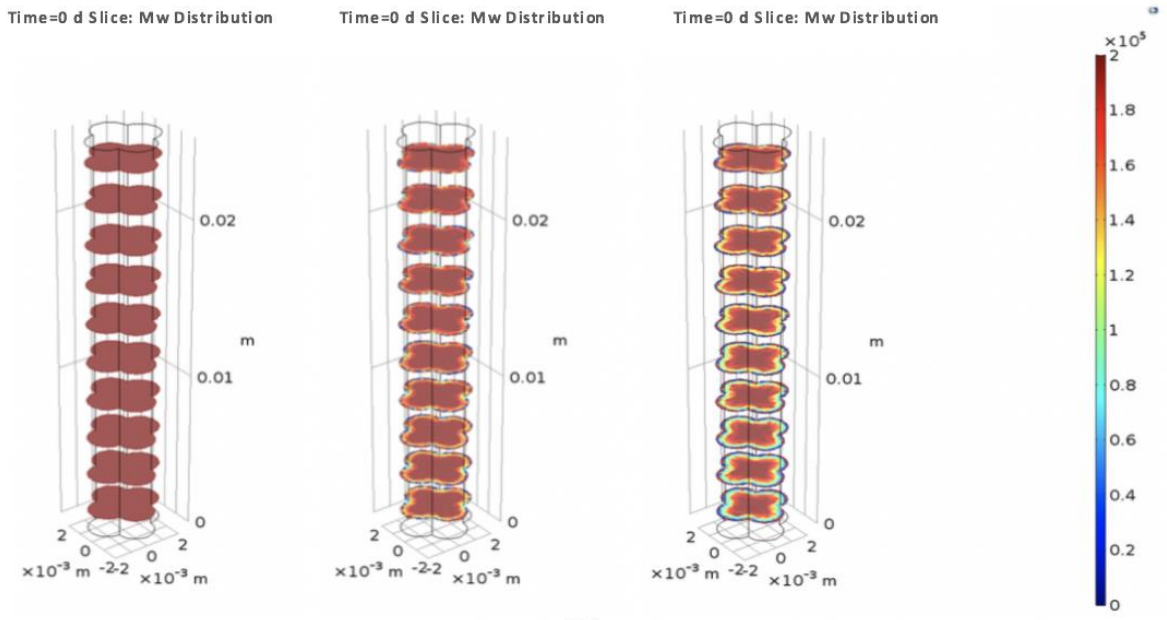
Time=0 d Slice: Mw Distribution
Time=0 d Slice: Mw Distribution
Time=0 d Slice: Mw Distribution
×10⁵
2
1.8
1.6
1.4
1.2
1
0.8
0.6
0.4
0.2
0
0.02
0.01
m
×10⁻³ m
-2-2

B)

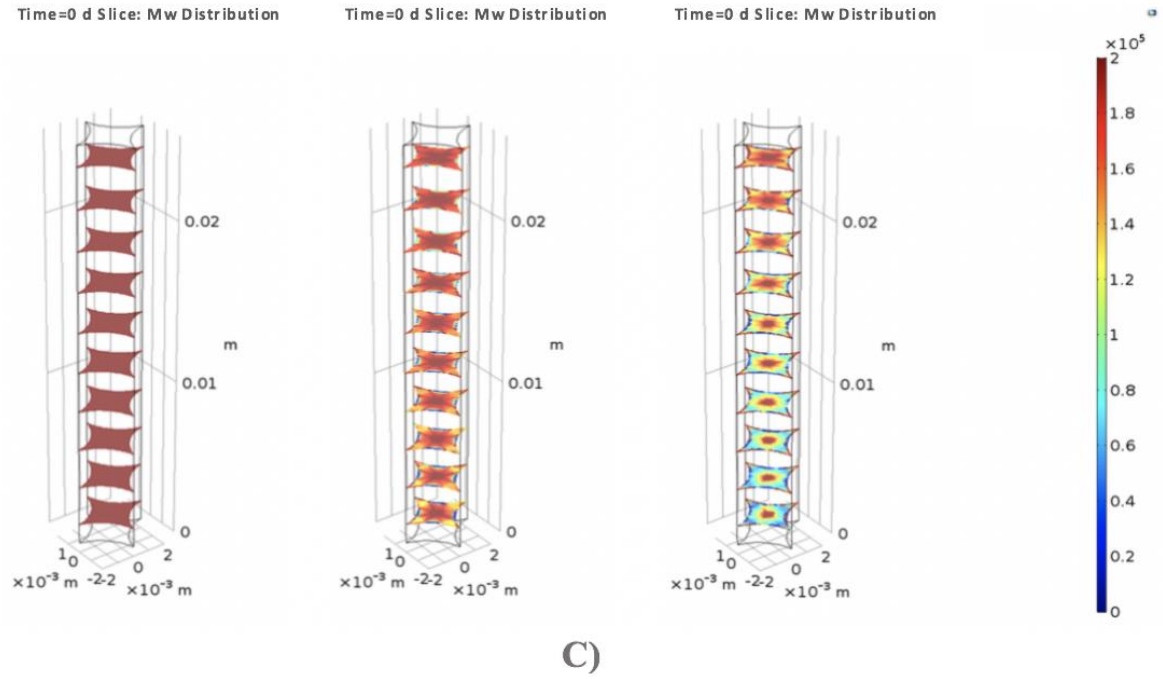

Figure 4.49: Slice representation of the weight molecular weight distribution for A) Geometry 1, B) Geometry 2, C) Geometry 3 with an initial Mw equal to 200 kDa

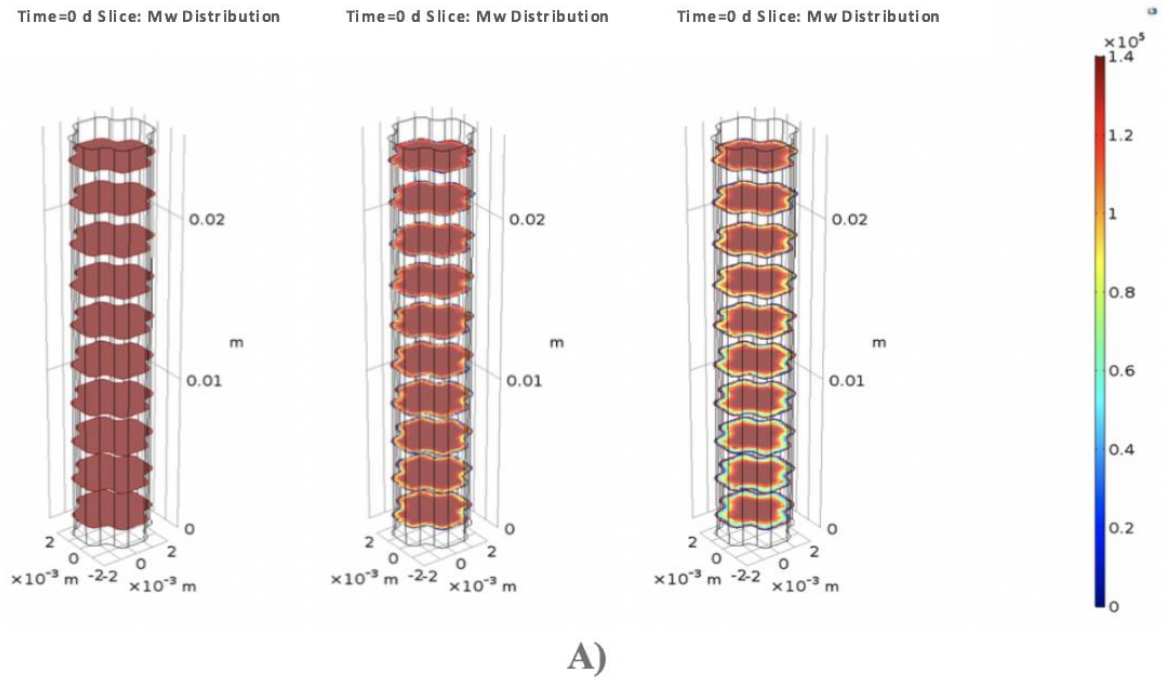

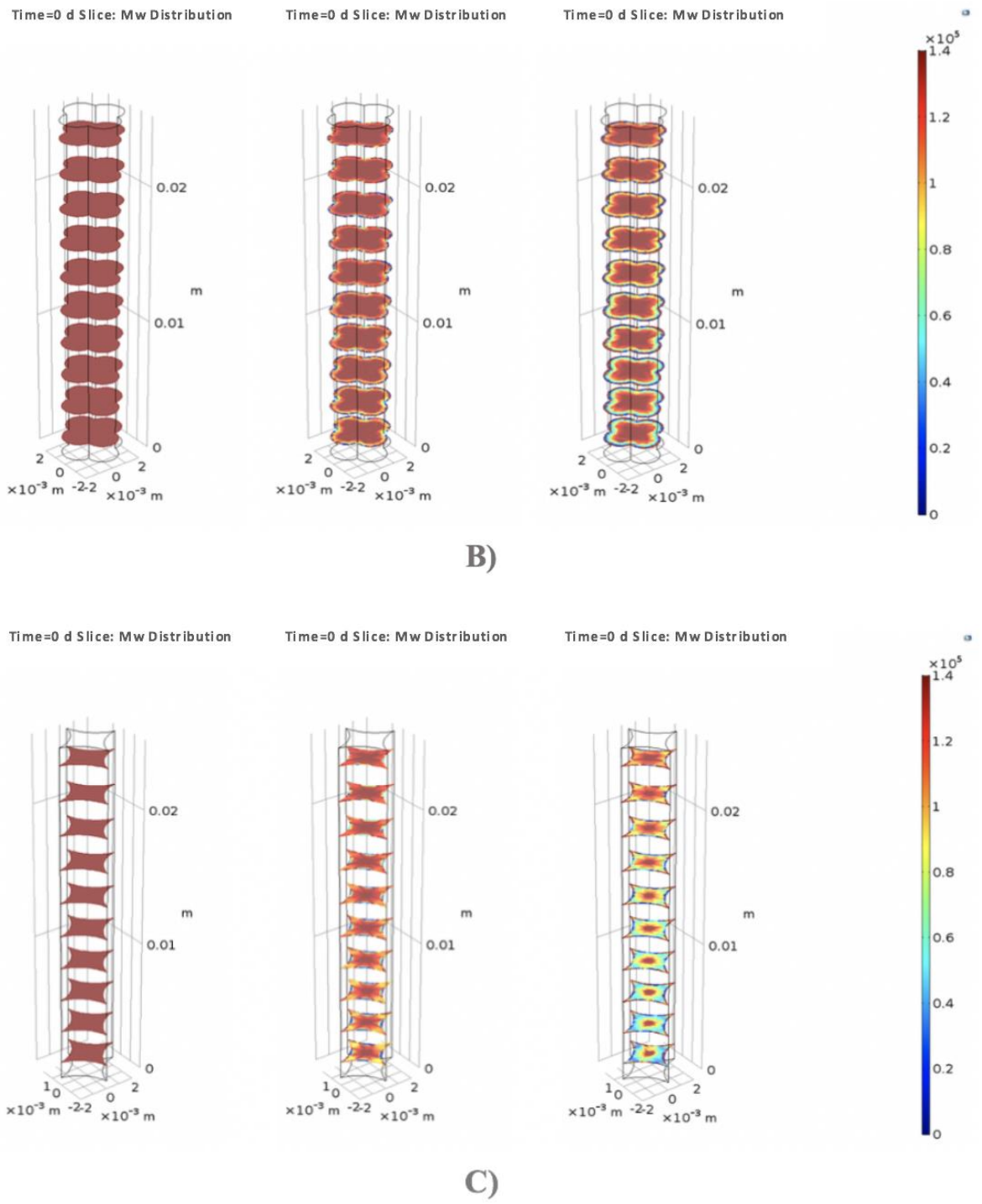

Figure 4.50: Slice representation of the weight molecular weight distribution for A) Geometry 1, B) Geometry 2, C) Geometry 3 with an initial Mw equal to 140 kDa (30% loss)

In conclusion, Polymer 4 respects all the aforementioned requirements necessary to develop an optimize bone fixation system.

4.4 Analytics and Processing Results

As the pristine polymers used for pin formation would have to undergo an inevitable processing and terminal sterilization, it is worth to assess what is the effect of those two aforementioned steps on the polymer initial characteristics, both in terms of composition as well as molecular weight.

4.4.1 *Polymer 1*

All the tests which results are reported in the following have been run by testing dog bone samples made of Polymer 1.

Gel Permeation Chromatography results about weight and number average molecular weight and polydispersity of each injected sample in pre and post-sterilization conditions, respectively, are reported in *Appendix D*.
In *Table 4.3*, the averages on all the batches of the weight and number average molecular weight and polydispersity obtained from GPC are shown, in both pre and post-sterilization conditions:

GPC	Injected Samples	Injected and Sterilized Samples
Average Mw [kDa]	133.6 ± 3.8	119.4 ± 5.3
Average Mn [Da]	86.2 ± 5.7	66.8 ± 3.1
Average PD [-]	1.56 ± 0.09	1.79 ± 0.07

Table 4.1: Averages on all the batches of the Mw, Mn and PD obtained by GPC

The average of the Mw in pre-sterilization conditions is about 27% less than the original Mw of the polymer (183 kDa). This means that injection moulding has a not negligible impact on the molecular weight loss.
The average of the Mw in post-sterilization conditions is about 34% less than the original Mw of the polymer (183 kDa) and about 11% less than the average of the Mw of the non-sterilized sample. As expected, a reduction of the Mw due to the sterilization is seen.

The results obtained by doing tensile tests on each sample of each batch in pre and post-sterilization conditions, respectively, the values of Young's modulus of each sample obtained from the proper linear regression and the averages of Young's modules for each batch in pre and post-sterilization conditions, respectively, the comparison between pre and post-sterilization tensile test results of the samples and the values of both maximum strain and stress at break of each sample of each batch in pre and post-sterilization conditions, respectively are all reported, in *Appendix D.*

In the following, the average values of Young's modulus considering all the batches, in pre and post-sterilization conditions, respectively, are reported (*Table 4.1*):

TENSILE TEST	**Injected Samples**	**Injected and Sterilized Samples**
Average Young's Modulus [MPa]	213 ± 47	280 ± 28

Table 4.2: Average values of Young's modulus considering all the batches, in pre and post-sterilization conditions, respectively

It can be noticed that the two average values of Young's modules for pre and post- sterilized samples are quite similar, as we expected.

In *Table 4.2*, the average values of both maximum strain and stress at break considering all the batches, in pre and post-sterilization conditions, respectively, are reported:

TENSILE TEST	**Injected Samples**	**Injected and Sterilized Samples**
Average Max Strain at Break [-]	2.85 ± 0.21	2.86 ± 0.27
Average Max Stress at Break [MPa]	22.01 ± 0.99	20.65 ± 1.19

Table 4.3: Average values of both maximum strain and stress at break considering all the batches, in pre and post-sterilization conditions, respectively

It can be noticed that the two average strains at break are similar, while the average stress at break of non-sterilized samples is little higher than that of sterilized ones. This is due to the fact that β-sterilization affects the mechanical properties of the samples.

All in all, Polymer 1, though theoretically nice from the model output, resulted to be, in reality, too ductile to be properly used for the development of the optimized pin and therefore is discarded.

4.4.2 *Polymer 4*

After having rejected Polymer 1 as a suitable polymer for the development of the optimized fixation system, all the tests, which results are reported in the following, have been run by testing samples having shape and composition equal to the last combination polymer-geometry left. i.e., Polymer 4-Geometry 3.

In *Table 4.4*, the averages on all the tested injected samples of the weight and number average molecular weight and polydispersity obtained from GPC are shown, for both pre and post-sterilization conditions:

GPC	Injected Samples	Injected and Sterilized Samples
Average Mw [kDa]	150	140
Average Mn [Da]	125	107.7
Average PD [-]	1.2	1.3

Table 4.4: Averages on all the tested injected samples of the Mw, Mn and PD obtained from GPC

The average of the Mw in pre-sterilization conditions is about 36% less than the original Mw of the polymer (235 kDa). This means that injection moulding has a not negligible impact on the molecular weight loss.
The average of the Mw in post-sterilization conditions is about 40% less than the original Mw of the polymer (235 kDa) and about 6.7% less than the average of the Mw of the non-sterilized sample. As expected, a reduction of the Mw due to the sterilization is seen.

The results obtained by doing tensile tests on each injected sample in pre and post-sterilization conditions, respectively, the values of Young's modulus of each injected sample obtained from the proper linear regression and the averages of Young's modules for each injected sample in pre and post-sterilization conditions, respectively, the comparison

between pre and post-sterilization tensile test results of the injected samples and the values of both maximum strain and stress at break of each injected sample in pre and post-sterilization conditions, respectively, are all reported in *Appendix D.*

In the following, the average values of Young's modulus considering all the tested injected pins, in pre and post-sterilization conditions, respectively, are reported (*Table 4.5*):

TENSILE TEST	Injected Samples	Injected and Sterilized Samples
Average Young's Modulus [GPa]	0.91 ± 0.08	1.1 ± 0.1

Table 4.5: Average values of Young's modules considering all the tested injected pins, in pre and post-sterilization conditions, respectively

It can be noticed that the two average values of Young's modules for the injected samples in pre and post-sterilization conditions are quite similar, as we expected.

In *Table 4.6*, the average values of both maximum strain and stress at break by considering all the tested injected samples, in pre and post-sterilization conditions, respectively, are reported:

TENSILE TEST	Injected Samples	Injected and Sterilized Samples
Average Max Strain at Break [-]	0.06 ± 0.02	0.07 ± 0.01
Average Max Stress at Break [MPa]	31.75 ± 6.17	42.79 ± 3.37

Table 4.6: Average values of both maximum strain and stress at break by considering all the tested injected pins, in pre and post-sterilization conditions, respectively

It can be noticed that the two average strains at break are similar, while the average stress at break of the injected samples is smaller than that of injected and sterilized ones. This is due to the fact that β-sterilization affects the mechanical properties of the samples, in particular the behaviour at break. It is important to underline that β-sterilization makes the polymer more rigid than the non-sterilized one.

Polymer 4 results to be less ductile than Polymer 1, which means that the elastic field of the first is wider than that of the latter and this property is important in order to guarantee the maintenance of the mechanical stability required from the optimized pin.

In the light of these considerations, other mechanical tests, i.e., torsion, four-points and three-points bending tests, have been run on injected pins in order to establish if Polymer 4 could be considered as the best candidate for the development of the optimized fixation device.

The results obtained by doing torsion tests on each injected pin in post-sterilization conditions, the values of both maximum shear strain and stress and shear modulus of each injected and sterilized pin obtained from the proper linear regression and the averages of both maximum shear strain and stress and shear modulus in post-sterilization conditions are all reported in *Appendix D.*

In the following, the average values of maximum shear strain and stress and shear modulus by considering all the injected pins in post-sterilization conditions are reported (*Table 4.7*):

TORSION TEST	**Injected and Sterilized Sample**
Average Max Shear Strain [-]	0.043 ± 0.013
Average Max Shear Stress [MPa]	197 ± 129
Average Shear Modulus [GPa]	2.6 ± 0.6

Table 4.7: Average values of maximum shear strain and stress and shear module by considering all the injected pins, in post-sterilization conditions

It can be notice that the average shear modulus is in the order of Giga Pascal. This means that the polymeric pin has a good resistance to the torsion. Therefore, Polymer 4 is suitable in order to realize a proper bone fixation device. To witness this fact, *Figure 4.51* shows how the applied torque has not led to the breakage of the pin: in the device centre, where there is a stress concentration zone, the polymer yield stress has been passed (plastic region) but the polymer point at break has not been reached:

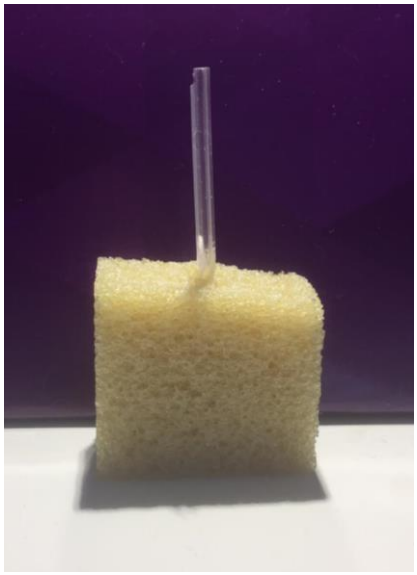

Figure 4.51: Pin after torsion test

The results obtained by doing three-point bending tests on each injected pin, both in pre and post-sterilization conditions, the values of both maximum strain and stress and Young's modulus of each injected pin, both in pre and post-sterilization conditions, obtained from the proper linear regression and the averages of both maximum strain and stress and Young's modulus, both in pre and post-sterilization conditions are all reported in *Appendix D.*

In the following, the average values of maximum strain and stress and Young's modulus considering all the injected pins, in pre and post-sterilization conditions, respectively, are reported (*Table 4.8*):

THREE-POINTS BENDING TEST	**Injected Samples**	**Injected and Sterilized Samples**
Average Max Strain [-]	0.01 ± 0.0006	0.009 ± 6.4E -07
Average Max Stress [MPa]	31.13 ± 2.29	28.62 ± 0.05
Average Young's Modulus [GPa]	3.14 ± 0.03	3.19 ± 0.02

Table 4.8: Average values of maximum strain and stress and Young's modulus considering all the injected samples, in pre and post-sterilization conditions, respectively

It can be notice that the average values of Young's modulus in both conditions are in the order of Giga Pascal: this is a great result for a bone fixation system because it means that the pin has good resistance to bending stress.

Moreover, β-sterilization has a negligible impact on the behaviour of the pin during the bending test. For this reason, the following test, i.e., four-points bending test, has been run by testing only injected and sterilized pins.

The results obtained by doing four-point bending tests on each injected pin in post-sterilization conditions, the values of both maximum strain and stress and Young's modulus of each injected and sterilized sample obtained from the proper linear regression and the averages of both maximum strain and stress and Young's modulus in post-sterilization conditions are all reported in *Appendix D.*
In the following, the average values of maximum strain and stress and Young's modulus, by considering all the injected pins, in post-sterilization conditions are reported (*Table 4.8*):

FOUR-POINTS BENDING TEST	**Injected and Sterilized Pins**
Average Max Strain [-]	0.04 ± 0.003
Average Max Stress [MPa]	1.02 ± 0.28
Average Young's Modulus [MPa]	36.1 ± 0.6

Table 4.9: Average values of maximum strain and stress and Young's modulus by considering all injected and sterilized samples

In this case, the average value of Young's modulus is in the order of Mega Pascal, one order of magnitude less than that obtained from the previous test. This is due to the fact that the four-bending test is characterized by the application of two forces instead of one, as occur in the three-points bending test. As a consequence, the resulting moment during four-points bending is applied in a wider zone than the one of the three-points bending test. Therefore, during the four-points bending test, the samples are more stressed and this results in a decrease of Young's modulus. However, it is difficult to properly compare the results obtained by the two different tests because they have been run with two different load application speeds (2 mm/min for three-points bending test and 12 mm/min for four-points bending test).
Nevertheless, the value of Young's modulus obtained from four-points bending test has to be considered as good in terms of resistance to the bending stress, even because they didn't break during the tests.

Figure 4.52 shows how the applied force has led the polymer to the plastic region but not to at breakage:

Figure 4.52: Pin after bending test

In conclusion, after having evaluating the behaviour of the pins made of Polymer 4 during all the run mechanical tests and analysing the post-processing data, it can be state that the final optimized pin must be characterized by the combination Polymer 4 (poly-(D,L-lactic) acid with a high initial molecular weight) – Geometry 3 (the one with four more sharp edges).

4.5 Ex Vivo Fixation Test on Human Femoral Head on the Optimized Pin

In light of the previously discussed results, pin with Geometry 3 and made of PDLLA (*Polymer 4*) has been identified as the best solution for the development of a bioresorbable fixation device.

Therefore, the injected and sterilized optimized pins have been ex vivo tested on human femoral head at “Clinica Luganese Moncucco” (Lugano, Switzerland), with the help of PD Dr. med. Kaj Klaue.

Firstly, the selection of the proper medical instruments has been necessary. In *Figure 4.53*, the used equipment is reported:

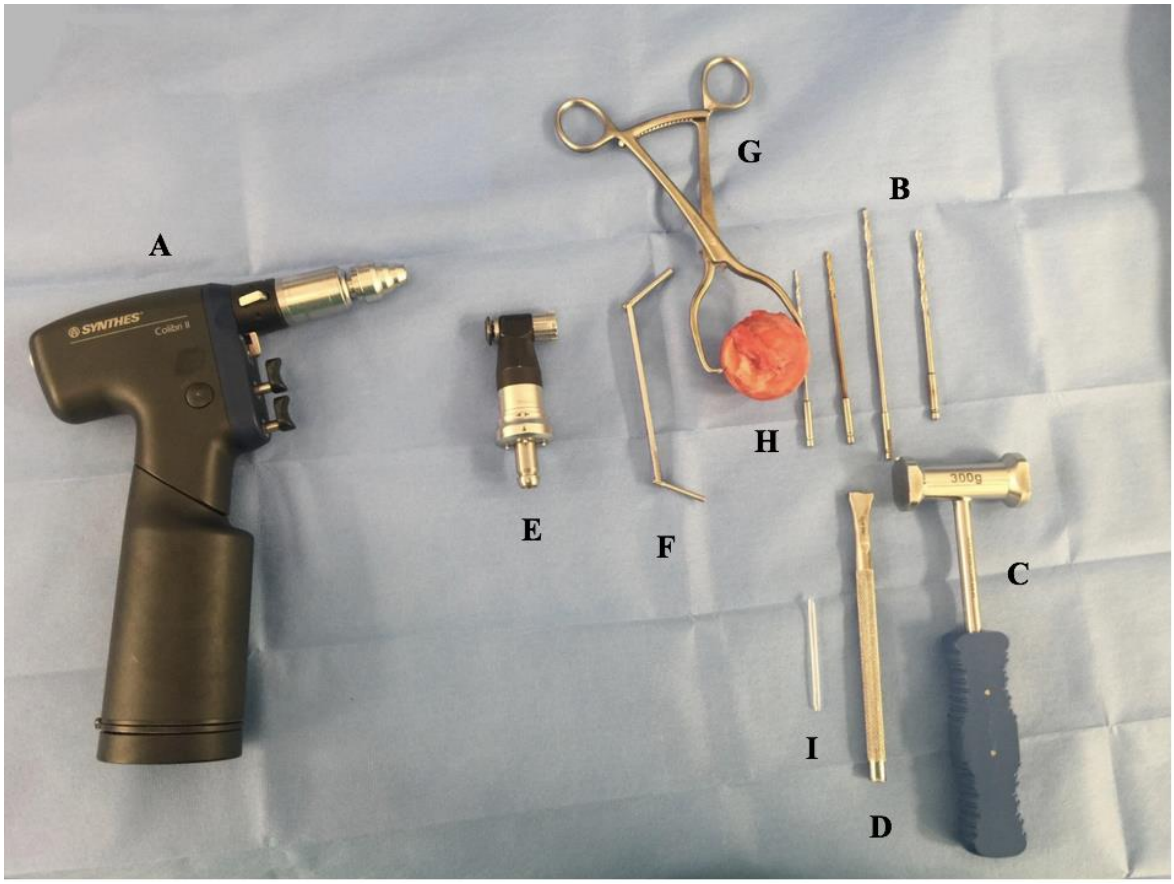

Figure 4.53: Medical instruments selected for ex vivo fixation test on human femoral head

In particular the following instruments have been selected:

A. Orthopedic drill;
B. Four bone drill bits which differs in diameter (2 mm, 2.5 mm, 3.2 mm and 3.5 mm);
C. 300 g orthopedic bone hammer;
D. Orthopedic impactor;
E. Oscillating saw equipment;
F. 2.5 mm & 3.5 mm tap sleeve;
G. Surgical clamp;
H. Human femoral head;
I. Bioresorbable optimized pin.

Secondly, the surgeon proceeded with the human femoral head osteotomy by using a saw blade while stabilizing the bone with the surgical clamp (*Figure 4.54*):

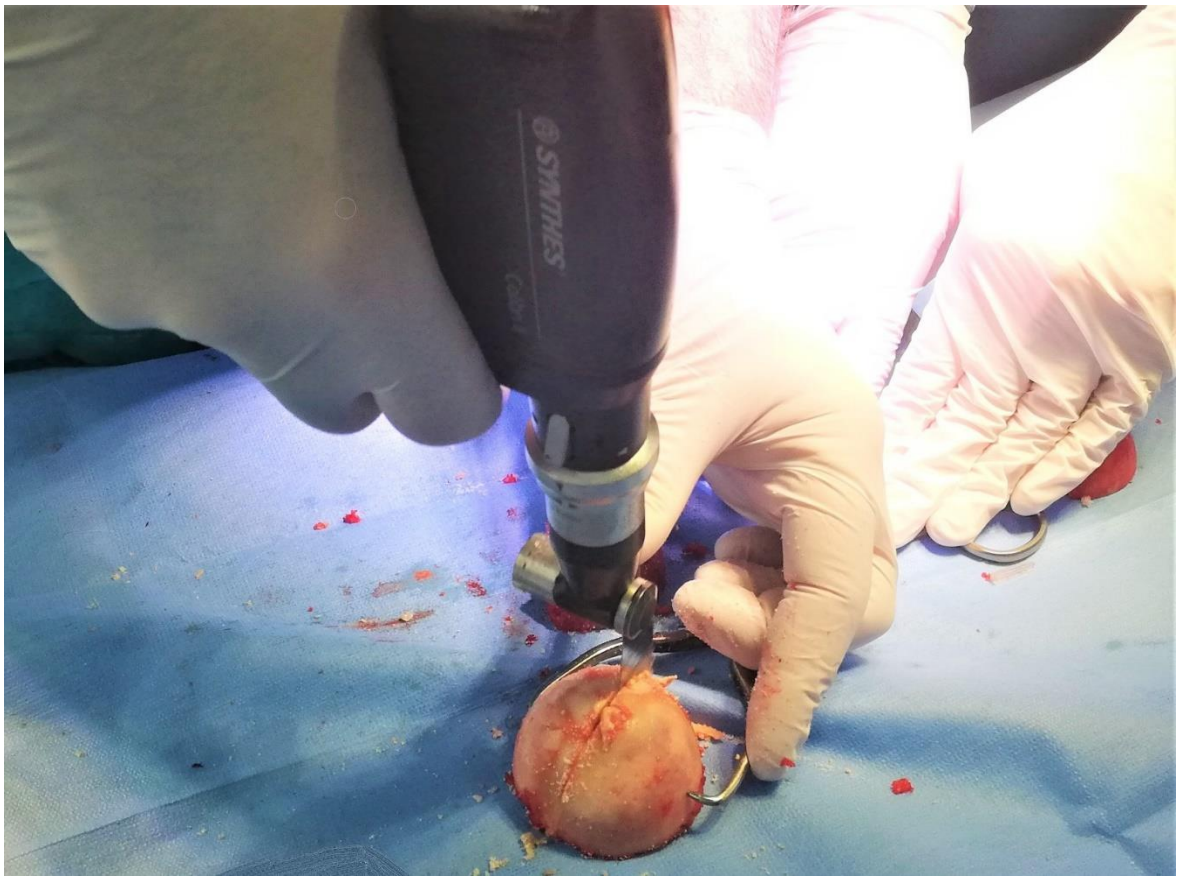

Figure 4.54: Osteotomy

Then, the bone has been holed with the orthopedic drill in order to create the implantation zone: particular attention has been focused on the fact that the hole reaches the other end of the bone relative to the drilling area, by passing through the osteotomy (*Figure 4.55*). For this operation, the surgeon helped himself with the tap sleeve.

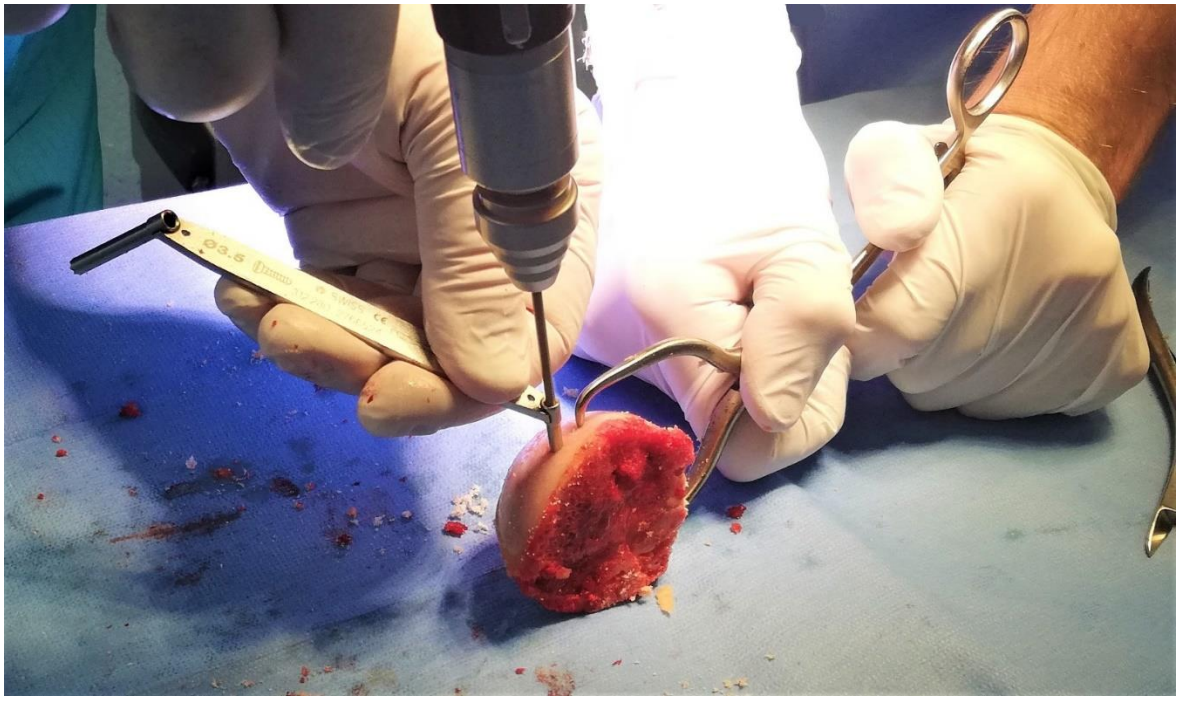

Figure 4.55: Drilling of the human femoral head

At this point, the implantation zone was ready: first, the surgeon placed the pin at the inlet of the hole in order to verify the compatibility of the respective diameters (*Figure 4.56*): after that, with the help of both orthopedic hammer and impactor, he implanted the pin inside the human femoral head (*Figure 4.57*).

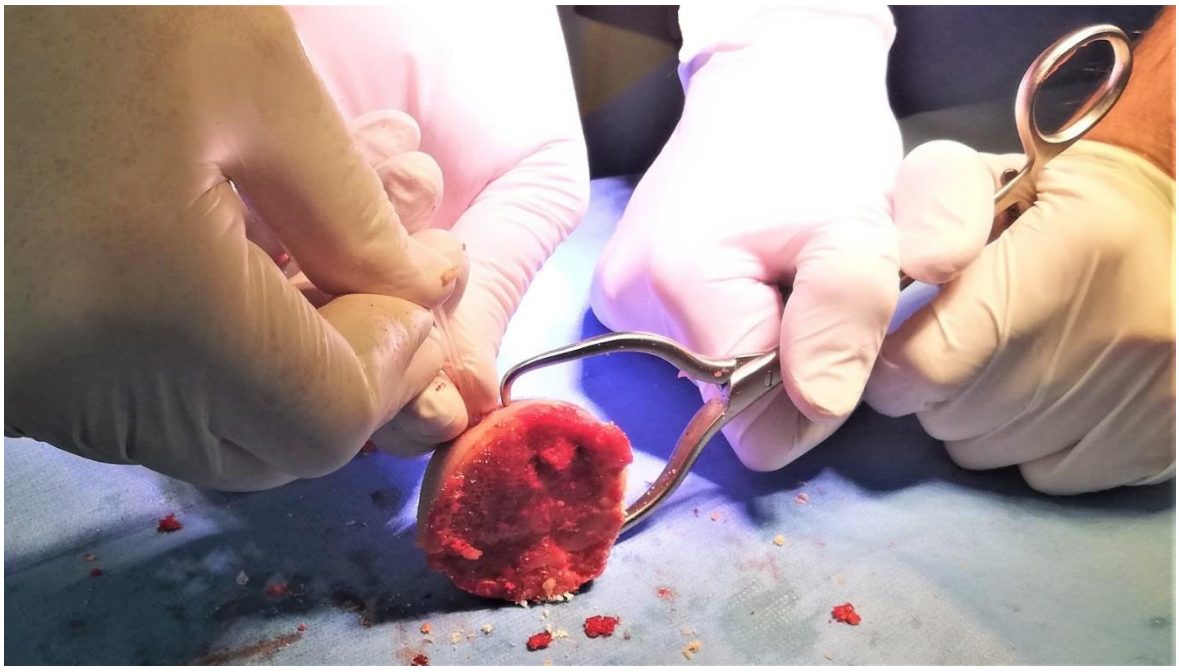

Figure 4.56: Positioning of the pin

Figure 4.57: Implantation of the pin

In *Figure 4.58*, the completely implanted pin is represented:

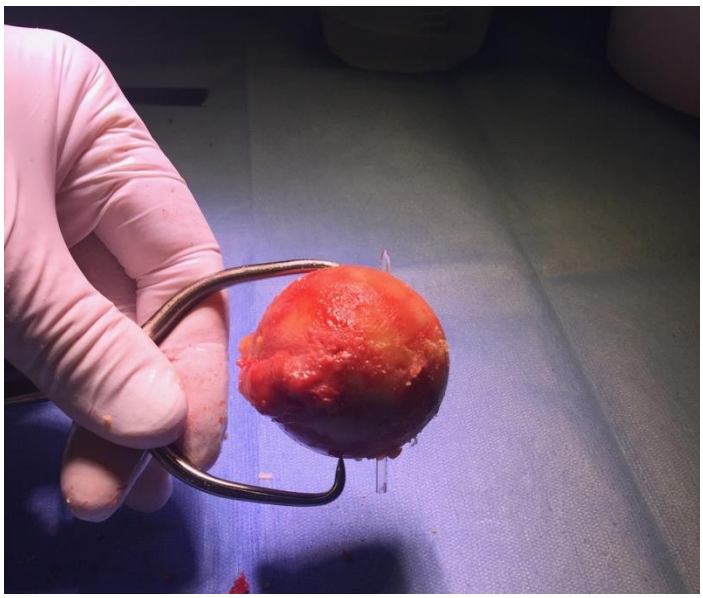

Figure 4.58: Representation of the completely implanted pin

Finally, the stability to the torsion has been verified: the surgeon tried to rotate the two parts of the osteotomized bone in opposite directions.

The aforementioned trial has been repeated with both different human femoral head and the selected drill bits, in order to find the best configuration.
It is possible to affirm that the best configuration is the combination that includes at the beginning the use of 3.5 mm diameter hole for cortical bone and a 2.5 mm diameter hole for cancellous bone. This is due to their different mechanical structure.
With the application of this configuration, the stability to the torsion has been really satisfying from an osteosynthesis method point of view: by applying a torque with the hands, the pin showed a good torsional resistance.
Once implanted and subjected to torsion, the pin has not to lose its shape, in particular concerning its edges, which is necessary to guarantee the proper mechanical stability for the fixation and the bone healing. In order to verify this, a slice of the human femoral head with the implanted pin has been cut. In *Figure 4.59*, the result is reported:

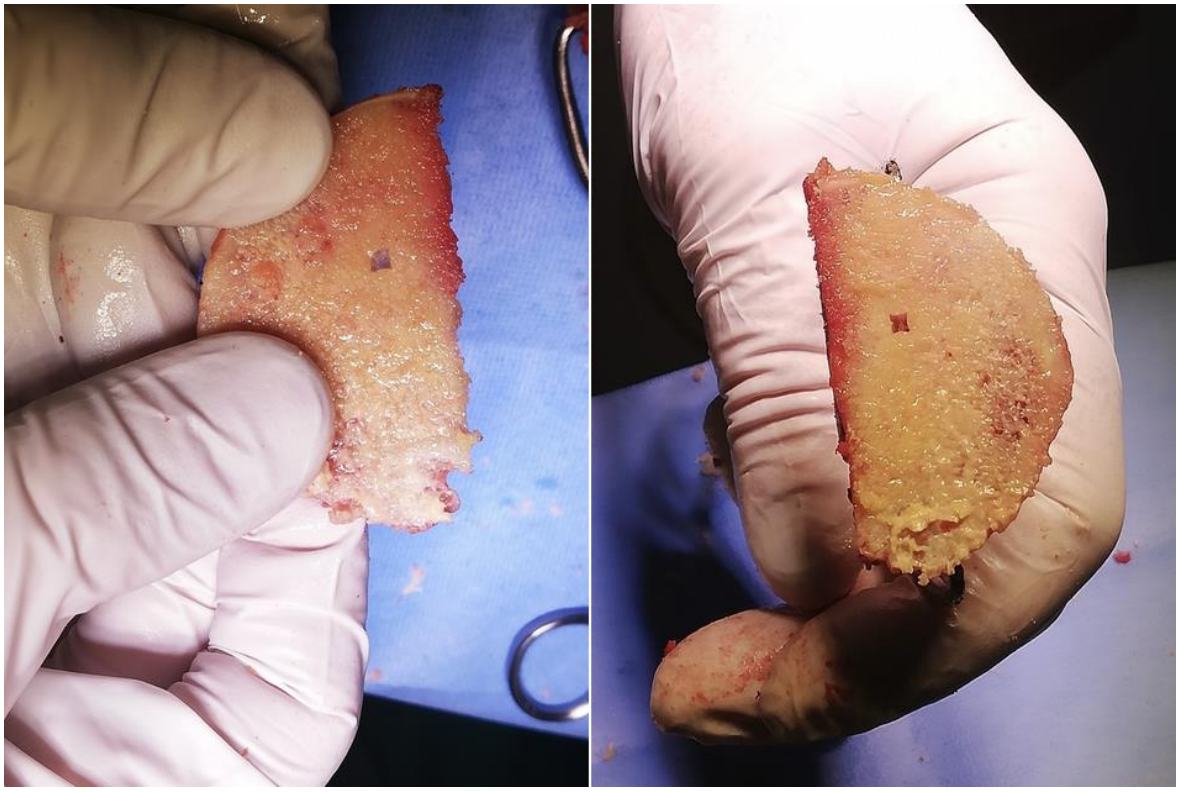

Figure 4.59: Slice of the human femoral head with the implanted pin

It is possible to notice that the shape is perfectly conserved. This means that the implantation impact has not any consequences on the pin which therefore preserves both its integrity and mechanical stability.

4.6 Final Design Specification of the Pin

After the overall simulation and mechanical tests, the final proposed design of the pin is discussed in the following. In particular, in *Table 4.10*, the characteristics of the chosen polymer, provided by the supplier, are reported:

Polymer Type	PURASORB® PDL (Poly- DL-lactide)
Inherent Viscosity [dl/g]	1.4
Residual Monomer [%]	3.0
Molecular Weight Mw [kDa]	235
PD [-]	1.6

Table 4.10: Technical data of the chosen polymer

In *Figure 4.60* and *4.61*, the final shape and relative cross section of the optimized pin, respectively, are reported:

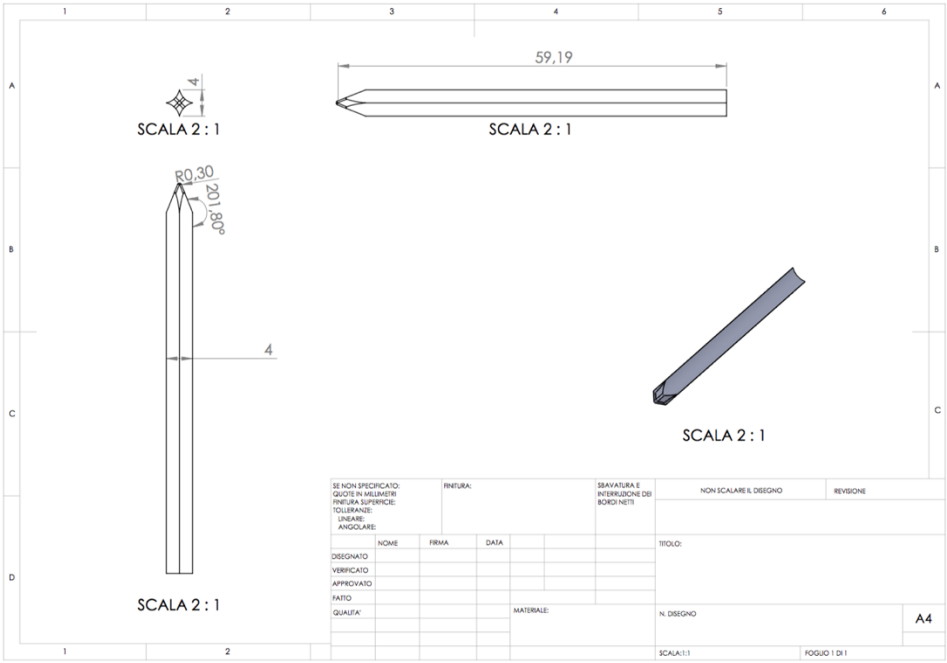

Figure 4.60: CAD of the final optimized pin

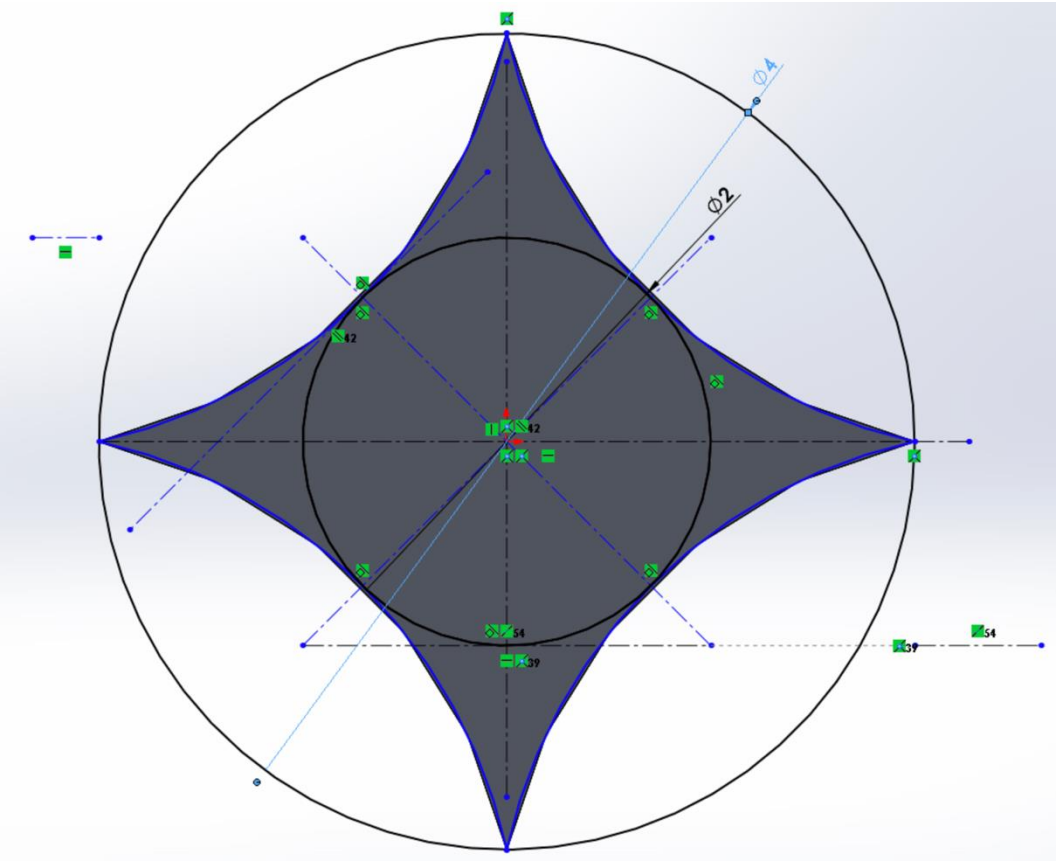

Figure 4.61: Cross section of the final optimized pin

In *Figure 4.62*, the final designed, developed and produced bioresorbable fixation system for small bone segments is represented:

Figure 4.62: Final designed, developed and produced bioresorbable

Chapter 5

5. Conclusion

The aim of this thesis work was the development of a new bioresorbable pin, as fixation system for small bone segments, with an optimal shape and polymer composition, assuming 6-8 weeks of degradation, able to withstand the applied load upon implantation (even after sterilization) and overcome the general limitation of the ones already available on the market.

In this sense, starting from four commercially available biodegradable polymers and three defined shapes, a mathematical model has been developed and applied to identify the best possible combination. Specifically, the polymer degradation has been simulated through a mathematical model considering that the degradation occurs mostly through hydrolysis, whereas the mechanical model has been developed thanks to FEM analysis, by properly loading the tested device. Out of the simulation, two possible combination, namely Polymer 4 and Geometry 3 and Polymer 1 and Geometry 3 resulted to properly fulfil the design specification.

Furthermore, the two aforementioned polymers have also been tested from a mechanical point of view. In this sense, Polymer 1 resulted to be too ductile and was excluded for further development. On the other hand, Polymer 4 nicely showed appropriate mechanical characteristics and pin produced out of it showed excellent response in to stretching, bending and twisting. Finally, these pins have been implanted into ex vivo human's femurs head. Once implanted and subjected to torsion, they kept their shape and in particular the edges which are necessary to guarantee the proper mechanical stability for the fixation and the bone healing.

In conclusion, after the quantitative analysis with mechanical tests and the qualitative one with the ex vivo fixation test on human femoral head, it is possible to affirm that the designed and developed pin (Polymer 4 and Geometry 3) is suitable to be considered as a good

bioresorbable fixation system for small bone segments, in alternative to both K-wires and the pins already available on the market.

References

Bibliography

1. Giuseppe Perale, Tommaso Casalini, Valentina Barri, Michele Müller, Simone Maccagnan, Maurizio Masi (2010), "Lidocaine release from polycaprolactone threads", *Journal of Applied Polymer Science*
2. Giuseppe Perale, Jöns Hilborn (2017), "Bioresorbable Polymers for Biomedical Applications. From Fundamental to Translational Medicine"
3. Wolfgang Heidemann, Stephanie Jeschkeit, Kurt Ruffieux, JuK rgen Hartmut Fischer, Mathias Wagner, G. KruK ger, Erich Wintermantel, Klaus Louis Gerlach (2001), "Degradation of poly(D,L)lactide implants with or without addition of calciumphosphates in vivo", *Biomaterials*
4. Katherine, Abel (2013), "Official CPC Certification Study Guide. American Medical Association"
5. Witmer, Daniel K.; Marshall, Silas T.; Browner, Bruce D. (2016), "Sabiston Textbook of Surgery (20th ed.)"
6. Jorge Fernándeza, Agustin Etxeberriab, Jose-Ramon Sarasua (2012), "Synthesis, structure and properties of poly(L-lactide-co-ε-caprolactone) statistical copolymers", *Journal of the Mechanical Behaviour of Biomedical Materials*
7. Julie E. Adams, Thomas Miller, Marco Rizzo, "The Biomechanics of Fixation Techniques for Hand Fractures"
8. N.A.Weir, F.J. Buchanan, J.F. Orr, G.R. Dickson (2004), "Degradation of poly-L-lactide. Part 1: in vitro and in vivo physiological temperature degradation",
9. Buddy D. Ratner (2011), "The biocompatibility manifesto: biocompatibility for the Twenty- first century", *Journal of Cardiovasc. Trans. Res.*
10. Tommaso Casalini, Filippo Rossi, Stefano Lazzari, Giuseppe Perale, Maurizio Masi (2014), "Mathematical Modeling of PLGA Microparticles: From polymer degradation to drug release", *Molecular Pharmaceutics*
11. Michael Niaounakis (2015), "Biopolymers: Application and Trends", *Elsevier Publishing*
12. Robert G. Sargent (2011), "Verification and validation of simulation models", *Proceedings of the 2011 Winter Simulation Conference*

13. I.Grizzi, H. Garreau, S. Li, M. Vert (1995), "Hydrolytic degradation of devices based on poly (DL-lactic acid) size- dependence", *Biomaterials*
14. C.M. Langton, C.F. Njeh (2003), "The physical measurement of bone", *Institute of Physics Publishing Bristol and Philadelphia*
15. Mohammad S. Ghiasi, Jason Chen, Ashkan Vaziri, Edward K. Rodriguez, Ara Nazarian (2017), "Bone fracture healing in mechanobiological modeling: A review of principles and methods", *Bone Reports*
16. B. Izzawati, R. Daud, M. Afendi, M.S. Abdul Majid, N.A. M. Zain, Y. Bajuri (2017), "Stress analysis of implant- bone fixation at different fracture angle", *Journal of Physics*
17. Yu-Bo Fab, Ping Li, Li Zeng, Xue-Jin Huang (2008), "Effects of mechanical load on the degradation of poly(D,L – lactic acid) foam", *Polymer Degradation and Stability 93*
18. Chen-Yuan Chung (2018), "A simplified application (APP) for the parametric design of screw-plate fixation of bone fractures", *Journal of the Mechanical Behavior of Biomedical Materials*
19. Alberto Cingolani, Tommaso Casalini, Stefano Caimi, Antoine Klaue, Mattia Sponchioni, Filippo Rossi, Giuseppe Perale (2018), "A Methodologic Approach for the Selection of Bio-Resorbable Polymers in the Development of Medical Devices: The Case of Poly(L-lactide-co-"-caprolactone)", *Polymers*
20. S. Dånmark, A. Finne-Wistrand, K. Schander, M.Hakkarainen, K. Arvidson, K. Mustafa, A.-C. Albertsson (2011), "In vitro and in vivo degradation profile of aliphatic polyesters subjected to electron beam sterilization", *Acta Biomaterialia*
21. K. Klaue, Osteosinthesys Device, EP 1 890 620 B1

Sitography

1. http://sussexhandsurgery.co.uk/downloads/surgery/hand/K%20wire%20fixation%20of%20hand%20fractures.pdf
2. http://boneandspine.com/kirschner-wire-or-k-wire/
3. http://www.customkwiremanufacturer.com/
4. https://www.inion.com/Products/orthopaedics/Inion_FreedomSystem/en_GB/inion_freedompin/
5. http://www.bioretec.com/products/ActivaPin-and-ActivaNail/
6. http://www.acumed.net
7. https://www.medicaldesignbriefs.com/component/content/article/mdb/features/16812
8. https://www.samaplast.ch/en/the-company/about-us/
9. https://d3gx8i893xzz0e.cloudfront.net/fileadmin/transportation/publications/data_sheets/sterilisation__technical_report.pdf?1450780119
10. https://www.medica.de/vis-content/event-medcom2017.COMPAMED/exh medcom2017.2543194/COMPAMED-2017-Herotron-E-Beam-Service-GmbH-Paper medcom2017.2543194-ArbKIiqSSNyFRInYfwDRjg.pdf
11. https://www.pentagonplastics.co.uk/injection-moulding-process/
12. http://www.conmed.com/en/products/orthopedics/foot-and-ankle/fixation/smartpin
13. https://www.ssi.shimadzu.com/products/universal-tensile-testing/ags-x.html
14. https://www.testresources.net

Appendix A

A. Polymer Characteristics

1. *Polymer 1* and *Polymer 3*

Product data sheet

PURASORB® PLC 7015

Rev. No. 4 / April 2010

Description	PURASORB PLC 7015 is a GMP grade copolymer of L-lactide and ε-caprolactone in a 70/30 molar ratio and with an inherent viscosity midpoint of 1.5 dl/g. It is supplied in the form of white to light tan granules. PURASORB PLC 7015 is primarily used for medical device applications and is suitable for all commonly used polymer processing techniques.		
Specification	**Test**	**Method**	**Specification**
	Appearance	visual	white to light tan granules
	Identification	FTIR	conforms to reference
	L-lactide content	HNMR	67 - 73 mol%
	Caprolactone content	HNMR	33 - 27 mol%
	Inherent viscosity	$CHCl_3$, 25°C, 0.1 g/dl	1.2 - 1.8 dl/g
	Residual monomer	GC	max. 0.5 wt. %
	For each batch a certificate of analysis is provided, showing the analytical data determined in our quality control laboratory. Additional analytical data can be made available upon request.		
Physical-chemical properties	Molecular formula	$(C_6H_8O_4{*}C_6H_{10}O_2)_n$	
	Chemical name	(3S-cis)-3,6-dimethyl-1,4-dioxane-2,5-dione, polymer with 2-oxepanone	
	CAS Registry number	65408-67-5	
Packaging	PURASORB PLC 7015 can be supplied in 1 or 5 kg packages. Normal packaging consists of an inner bag of clean room grade PE and an outer bag of aluminum coated polyester-PE laminate. The packed product is shipped in an additional bag of PE and in PE containers for added protection.		
Storage & Handling	When stored in the original packaging at low temperatures (-15°C), PURASORB PLC 7015 keeps its initial properties for at least three years. Allow the material to reach room temperature before opening the packaging. After opening the original packaging PURASORB PLC 7015 is best stored in an inert atmosphere and at low temperatures (-15°C).		

INHERENT VISCOSITY AND MOLECULAIR WEIGHT CORRELATIONS

Graphical presentation

The relation between IV and M_w is shown graphically for a number of selected PURASORB polymers in Figure 1.

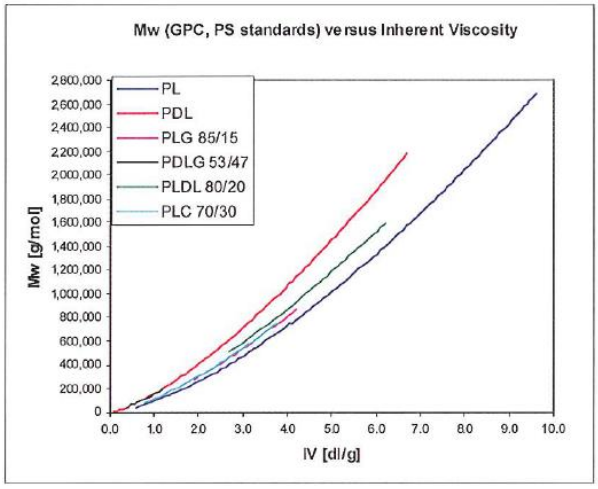

Figure 1: Graphical presentation of relation between IV and Mw for selected PURASORB polymers

Data tables

The relation between IV and M_w for selected PURASORB polymers is also given in Table 2 to 7.

Tabel 2: IV and M_w data for PURASORB PL

IV [dl/g]	M_w [g/mol]	IV [dl/g]	M_w [g/mol]	IV [dl/g]	M_w [g/mol]
0.6	43,000	3.8	674,000	7.0	1,675,000
0.8	66,000	4.0	727,000	7.2	1,746,000
1.0	92,000	4.2	782,000	7.4	1,819,000
1.2	121,000	4.4	838,000	7.6	1,893,000
1.4	152,000	4.6	896,000	7.8	1,968,000
1.6	185,000	4.8	954,000	8.0	2,044,000
1.8	221,000	5.0	1,014,000	8.2	2,120,000
2.0	259,000	5.2	1,075,000	8.4	2,198,000
2.2	298,000	5.4	1,137,000	8.6	2,276,000
2.4	339,000	5.6	1,201,000	8.8	2,356,000
2.6	383,000	5.8	1,265,000	9.0	2,436,000
2.8	427,000	6.0	1,331,000	9.2	2,517,000
3.0	473,000	6.2	1,397,000	9.4	2,599,000
3.2	521,000	6.4	1,465,000	9.6	2,682,000
3.4	571,000	6.6	1,534,000		
3.6	621,000	6.8	1,604,000		

INHERENT VISCOSITY AND MOLECULAIR WEIGHT CORRELATIONS

Tabel 3: IV and M_w data for PURASORB PDL

Polymer 3

IV [dl/g]	M_w [g/mol]	IV [dl/g]	M_w [g/mol]	IV [dl/g]	M_w [g/mol]
0.2	17,000	2.4	523,000	4.6	1,292,000
~~0.4~~	~~43,000~~	2.6	585,000	4.8	1,371,000
0.6	76,000	2.8	648,000	5.0	1,451,000
0.8	114,000	3.0	714,000	5.2	1,532,000
1.0	155,000	3.2	781,000	5.4	1,615,000
1.2	200,000	3.4	849,000	5.6	1,698,000
1.4	248,000	3.6	919,000	5.8	1,783,000
1.6	298,000	3.8	991,000	6.0	1,869,000
1.8	351,000	4.0	1,064,000	6.2	1,956,000
2.0	406,000	4.2	1,139,000	6.4	2,045,000
2.2	464,000	4.4	1,215,000	6.6	2,134,000

Tabel 4: IV and M_w data for PURASORB PLG 85

IV [dl/g]	M_w [g/mol]	IV [dl/g]	M_w [g/mol]	IV [dl/g]	M_w [g/mol]
1.9	276,000	2.7	458,000	3.5	668,000
2.0	297,000	2.8	483,000	3.6	695,000
2.1	319,000	2.9	508,000	3.7	724,000
2.2	341,000	3.0	534,000	3.8	752,000
2.3	363,000	3.1	560,000	3.9	781,000
2.4	387,000	3.2	586,000	4.0	810,000
2.5	410,000	3.3	613,000	4.1	839,000
2.6	434,000	3.4	640,000	4.2	869,000

Tabel 5: IV and M_w data for PURASORB PDLG 50

IV [dl/g]	M_w [g/mol]	IV [dl/g]	M_w [g/mol]
0.2	17,000	0.8	113,000
0.3	30,000	0.9	133,000
0.4	44,000	1.0	153,000
0.5	59,000	1.1	174,000
0.6	76,000	1.2	196,000
0.7	94,000		

INHERENT VISCOSITY AND MOLECULAIR WEIGHT CORRELATIONS

Tabel 6: IV and M_w data for PURASORB PLDL 80

IV [dl/g]	M_w [g/mol]	IV [dl/g]	M_w [g/mol]	IV [dl/g]	M_w [g/mol]
2.7	507,000	3.9	841,000	5.1	1,217,000
2.8	533,000	4.0	871,000	5.2	1,250,000
2.9	559,000	4.1	901,000	5.3	1,284,000
3.0	586,000	4.2	932,000	5.4	1,317,000
3.1	613,000	4.3	962,000	5.5	1,351,000
3.2	641,000	4.4	993,000	5.6	1,385,000
3.3	668,000	4.5	1,025,000	5.7	1,419,000
3.4	696,000	4.6	1,056,000	5.8	1,453,000
3.5	725,000	4.7	1,088,000	5.9	1,488,000
3.6	753,000	4.8	1,120,000	6.0	1,523,000
3.7	782,000	4.9	1,152,000	6.1	1,558,000
3.8	812,000	5.0	1,185,000	6.2	1,593,000

Tabel 7: IV and M_w data for PURASORB PLC 70

IV [dl/g]	M_w [g/mol]	IV [dl/g]	M_w [g/mol]	IV [dl/g]	M_w [g/mol]
0.8	83,000	1.9	282,000	3.0	539,000
0.9	98,000	2.0	304,000	3.1	564,000
1.0	114,000	2.1	325,000	3.2	590,000
1.1	130,000	2.2	347,000	3.3	617,000
1.2	147,000	2.3	370,000	3.4	643,000
1.3	165,000	2.4	393,000	3.5	670,000
1.4	183,000	2.5	416,000	3.6	697,000
1.5	202,000	2.6	440,000	3.7	725,000
1.6	221,000	2.7	464,000	3.8	753,000
1.7	241,000	2.8	489,000		
1.8	261,000	2.9	514,000		

Polymer 1

2. *Polymer 2*

Resomer®
An Evonik product.

Technical Information

RESOMER® LC 703 S

Specification

CAS number	65408-67-5
Chemical name	Poly(L-lactide-co-ε-caprolactone)

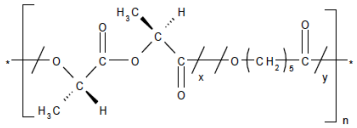

-[($C_6H_8O_4$)$_x$($C_6H_{10}O_2$)$_y$]$_n$-

Description:	white to off-white granulate or flakes
Odour:	nearly odourless
Identity:	NMR-spectrum conforms to reference
Polymer composition:	67:33 to 73:27 molar ratio L-lactide : ε-caprolactone
Inherent viscosity:	1.3 - 1.8 dl/g (0.1 % in chloroform, 25 °C)
Residual monomer:	max. 1 % L-lactide max. 1 % ε-caprolactone
Residual solvent:	max. 890 ppm toluene
Water:	max. 0.5 %
Tin:	max. 60 ppm
Heavy metals:	max. 10 ppm
Sulphated ash:	max. 0.1 %

3. *Polymer 4*

Technical data are reported by the producer and summarized in *Table A. 1*:

Polymer Type	PURASORB® PDL (Poly- DL-lactide)
Inherent Viscosity [dl/g]	1.4
Residual Monomer [%]	3.0
Molecular Weight Mw [kDa]	235
PD [-]	1.6

Table A. 1: Polymer 4 technical data

Appendix B

B. Original Graphs for Validations

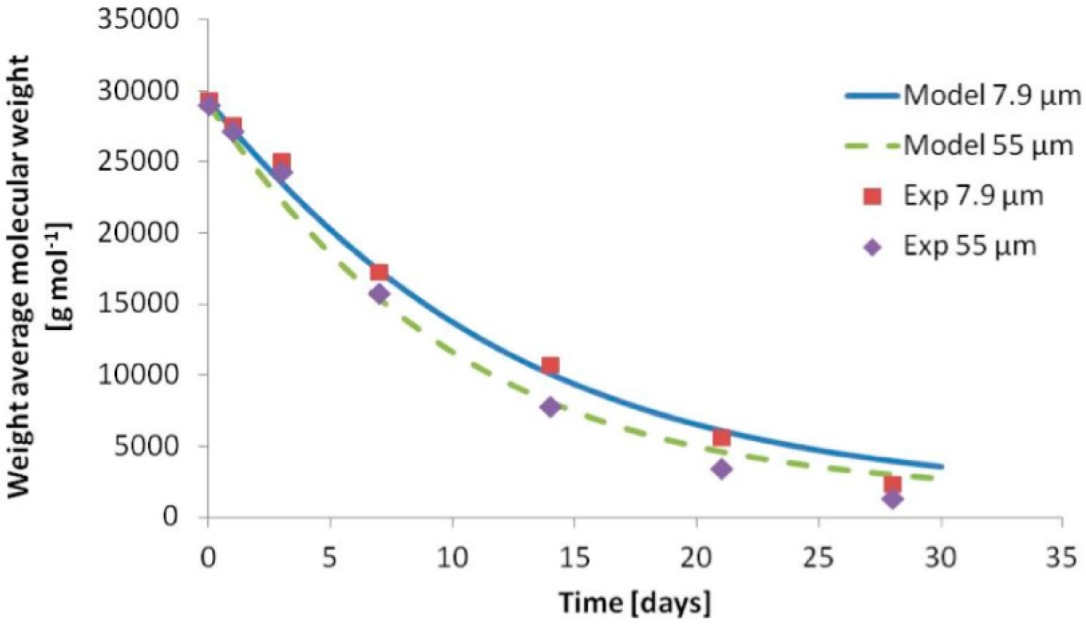

Figure B. 1: Original graph from [10] for first validation

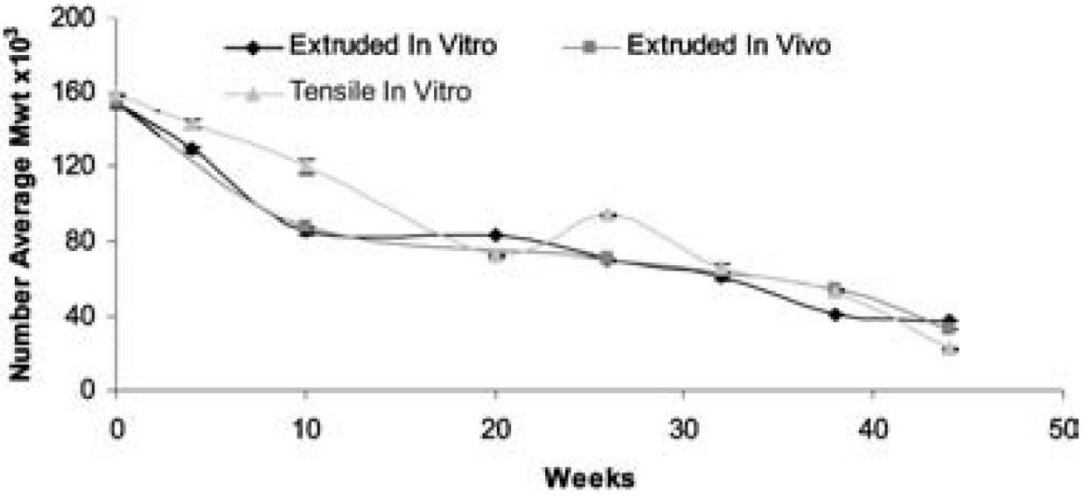

Figure B. 2: Original graph from [8] for second validation

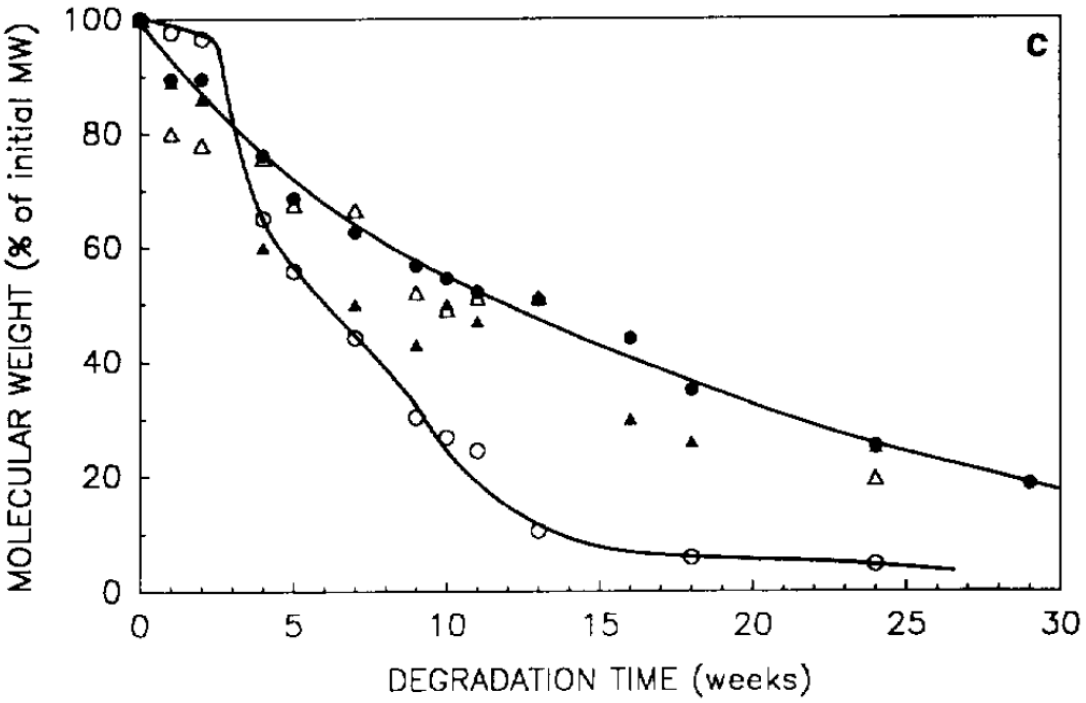

Figure B. 3: Original graph from [13] for third validation

Appendix C

C. Original graphs for the Derivation of the Degradation Constants

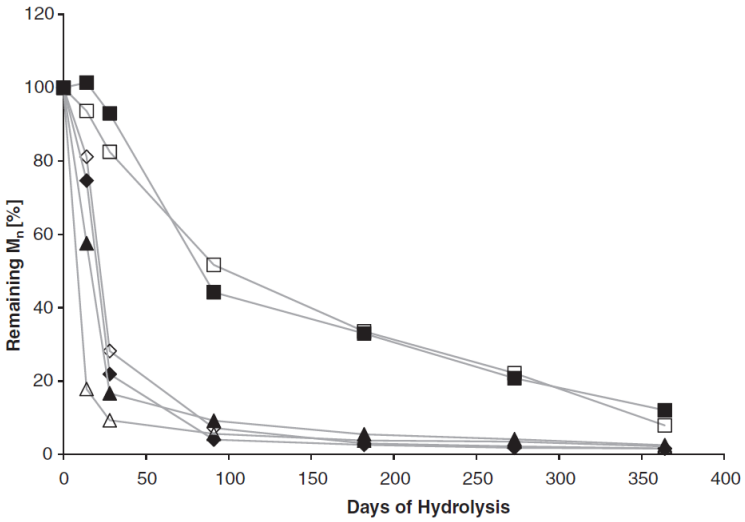

Figure C. 1: Original graph from [20] for the derivation of the degradation constants of Polymer 1and 2 (◆)

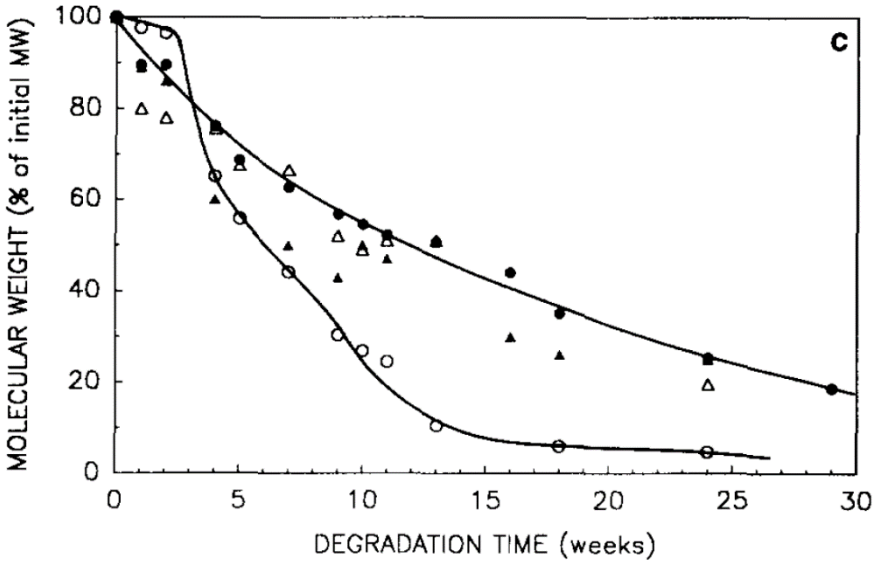

Figure C. 2: Original graph from [13] for the derivation of the degradation constant of Polymer 3 (△)

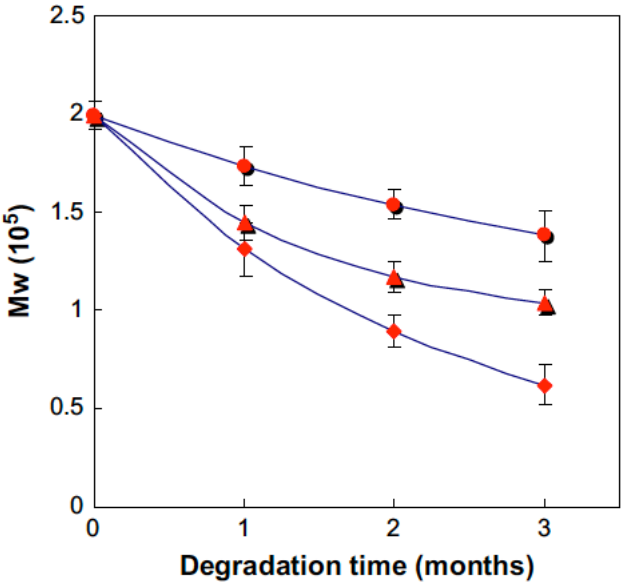

Figure C. 3: Original graph from [17] for the derivation of the degradation constant of Polymer 4 (●)

Appendix D

D. Chemical and Mechanical Characterization of *Polymer 1* and *Polymer 4*

1. *Polymer 1*

1.1 GPC Results

1.1.1 Pure Polymer

In *Table D. 1*, the Gel Permeation Chromatography results about weight and number average molecular weight (Mw and Mn, respectively) and polydispersity (PD) of pure polymer are reported:

	Mw [kDa]	Mn [kDa]	PD [-]
Pure Polymer	173	124	1.4

Table D. 1: Pure polymer characteristics

1.1.2 Injected Samples

In *Table D. 2*, the Gel Permeation Chromatography results about weight and number average molecular weight (Mw and Mn, respectively) and polydispersity (PD) of the injected samples included in all the batches, in pre-sterilization conditions, are reported:

Injected Sample	**Mw [Da]**	**Mn [Da]**	**PD**
2_6	124538	75078	1.6588
2_7	136380	89554	1.5229
2_8	133108	87375	1.5234
7.9_1	136343	91458	1.4908
7.9_3	135163	93059	1.4524
7.9_4	130865	95185	1.3749
7.9_5	132532	84027	1.5773
7.9_6	130766	79846	1.6377
7.9_7	137042	86225	1.5893
10_5	132325	85109	1.5548
10_6	138042	85355	1.6173
10_7	136309	81927	1.6638
Average	**133617.8 ± 3780.9**	**86183.2 ± 5696.9**	**1,5553 ± 0.0874**

Table D. 2: Average values of Mw, Mn and PD of all the injected samples in pre-sterilization conditions

1.1.3 Injected and Sterilized Samples

In *Table D. 3*, the Gel Permeation Chromatography results about weight and number average molecular weight (Mw and Mn, respectively) and polydispersity (PD) of the injected samples included in all the batches, in post-sterilization conditions are reported:

Injected and Sterilized Sample	**Mw [Da]**	**Mn [Da]**	**PD**
S2_1	109281	65565	1.6668
S2_2	117427	64891	1.8096
S2_3	113202	66868	1.6929
S2_4	111983	63113	1.7743
S2_5	118122	67595	1.7475
S2_6	127370	64753	1.967
S2_7	114903	65126	1.7643
S2_8	111035	60613	1.8319
s7.9_1	120502	66985	1.7989
s7.9_2	120383	66339	1.8147
s7.9_4	115893	66295	1.7481
s7.9_5	124351	70477	1.7644
s7.9_6	118031	65014	1.8155
s7.9_7	121077	63331	1.9118
s7.9_8	118054	67418	1.7511
s10_1	124979	71881	1.7387
s10_2	122625	68182	1.7985
s10_3	121351	67428	1.7997
s10_4	124640	74221	1.6793
s10_5	125308	70637	1.774
s10_6	126306	66704	1.8935
Average	**119372.52 ± 5275.21**	**66830.29 ± 3100.03**	**1.7877 ± 0.0731**

Table D. 3: Average values of Mw, Mn and PD of all the injected samples in post-sterilization conditions

1.2 Tensile Test Results

1.2.1 Injected Samples

Batch #2

In *Figure D. 1*, the plots of the strain-stress curves and of the linear regressions for the evaluation of Young's modules for all the tested dog bone samples included in Batch #2 are reported:

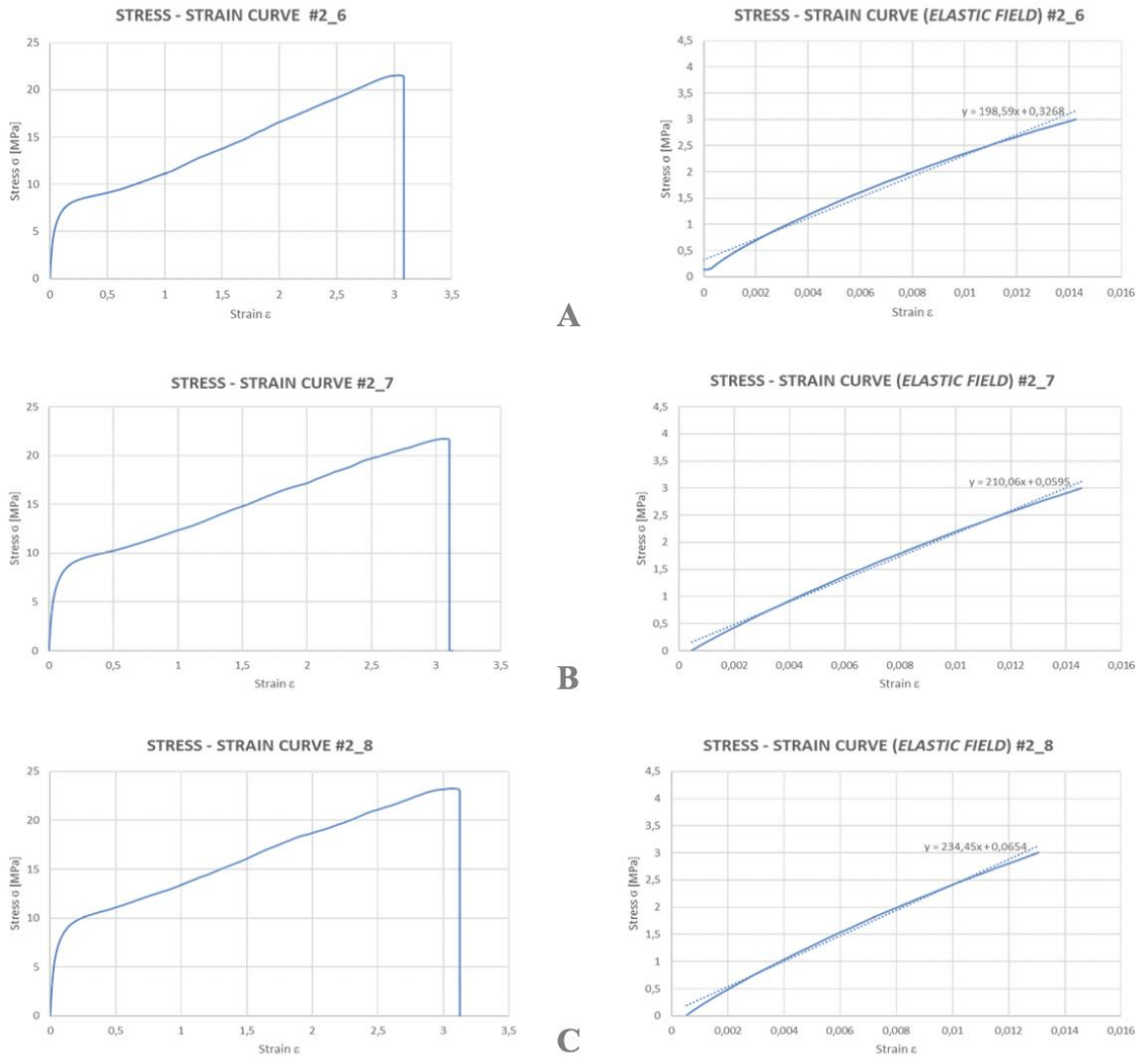

Figure D. 1: Strain–stress curves and linear regressions for the evaluation of Young's modulus for all the tested samples (A, B and C) included in Batch #2

Batch #7.9

In *Figure D. 2*, the plots of the strain-stress curves and of the linear regressions for the evaluation of Young's modules for all the tested dog bone samples included in Batch #7.9 are reported:

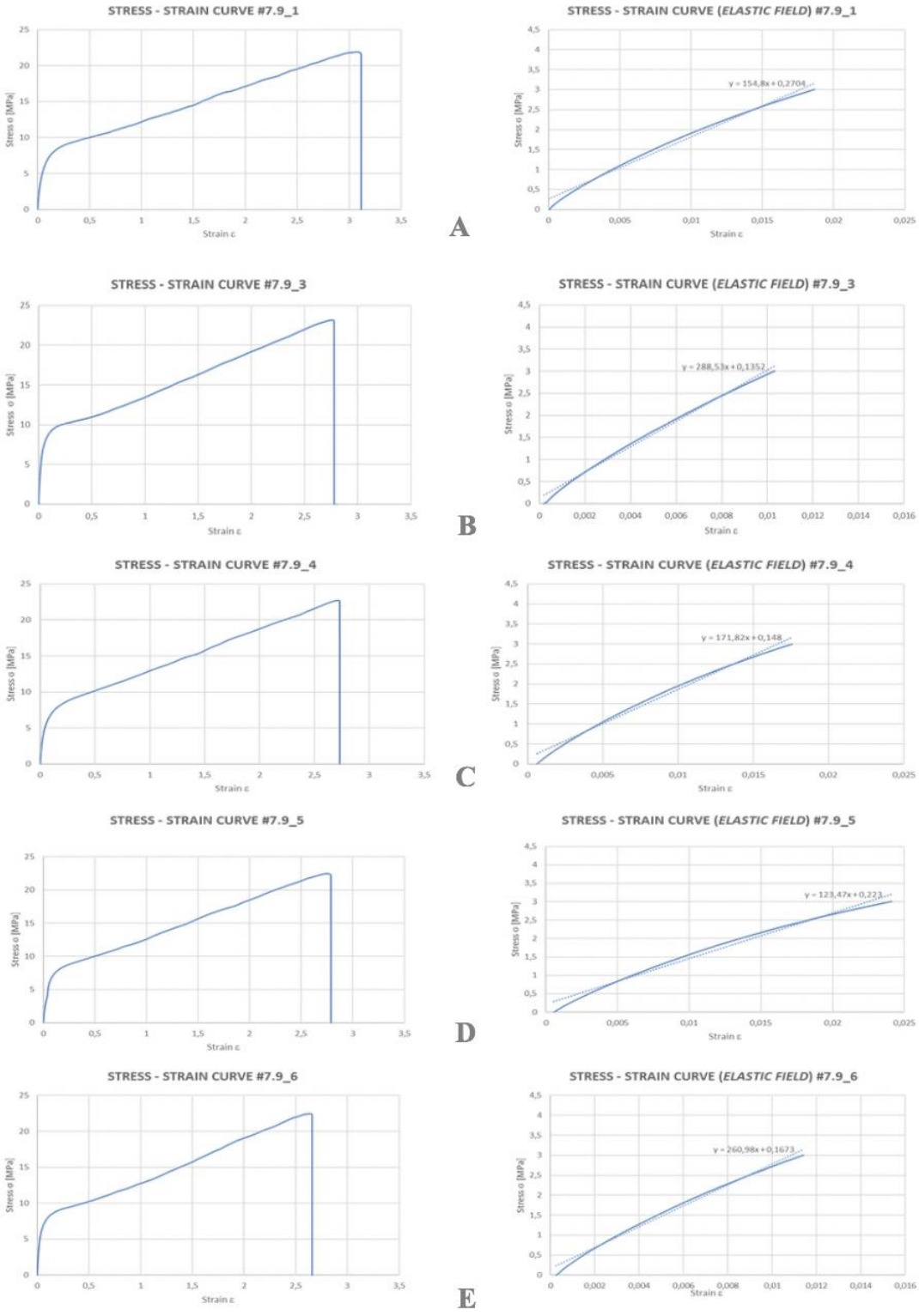

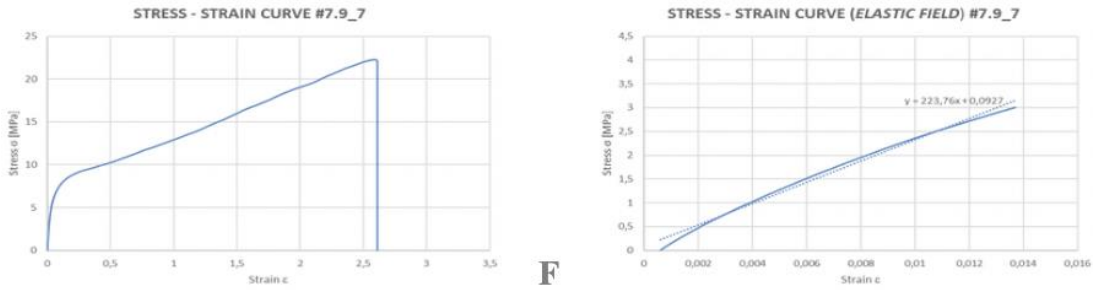

Figure D. 2: Strain – stress curves and linear regressions for the evaluation of Young's modules for all the tested samples (from A to F) included in Batch #7.9

Batch #10

In *Figure D. 3*, the plots of the strain-stress curves and of the linear regressions for the evaluation of Young's modules for all the tested samples included in Batch #10 are reported:

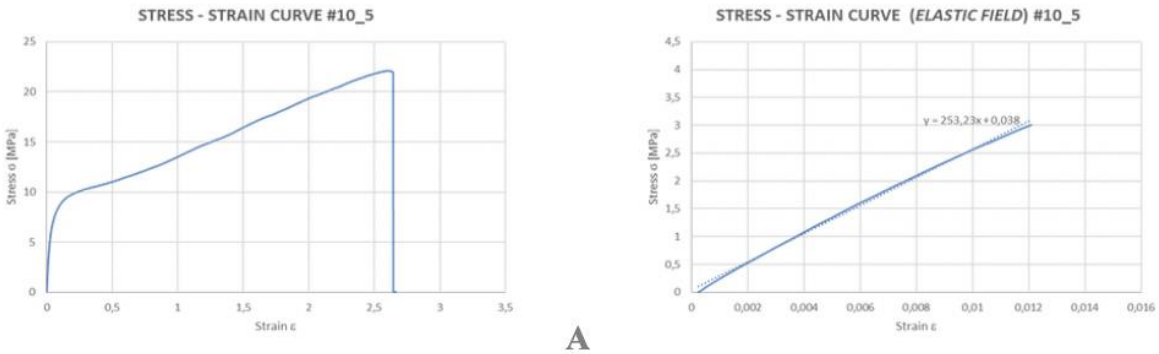

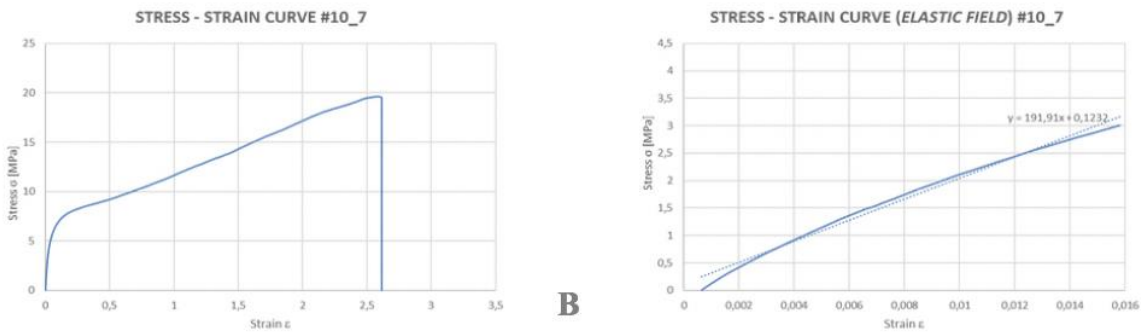

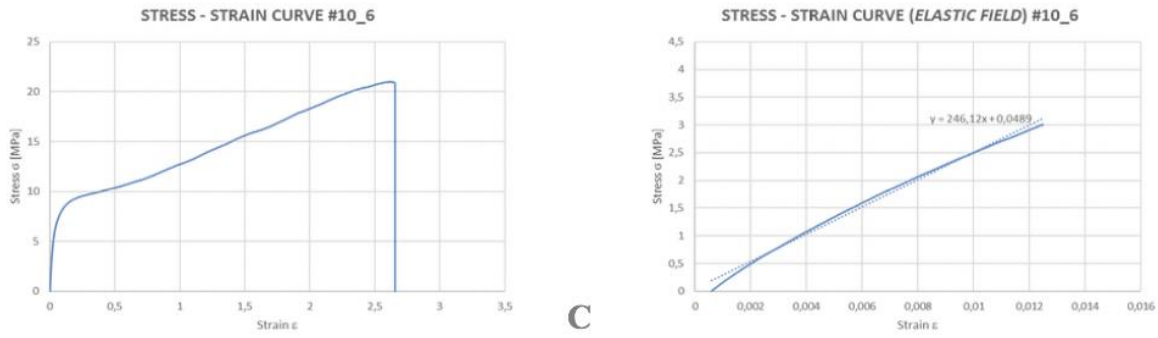

Figure D. 3: Strain- stress curves and linear regressions for the evaluation of Young's modules for all the tested samples (from A, B and C) included in Batch #10

1.2.2 Injected and Sterilized Samples

Batch #s2

In *Figure D. 4*, the plots of the strain-stress curves and of the linear regressions for the evaluation of Young's modules for all the tested dog bone samples included in Batch #s2 are reported:

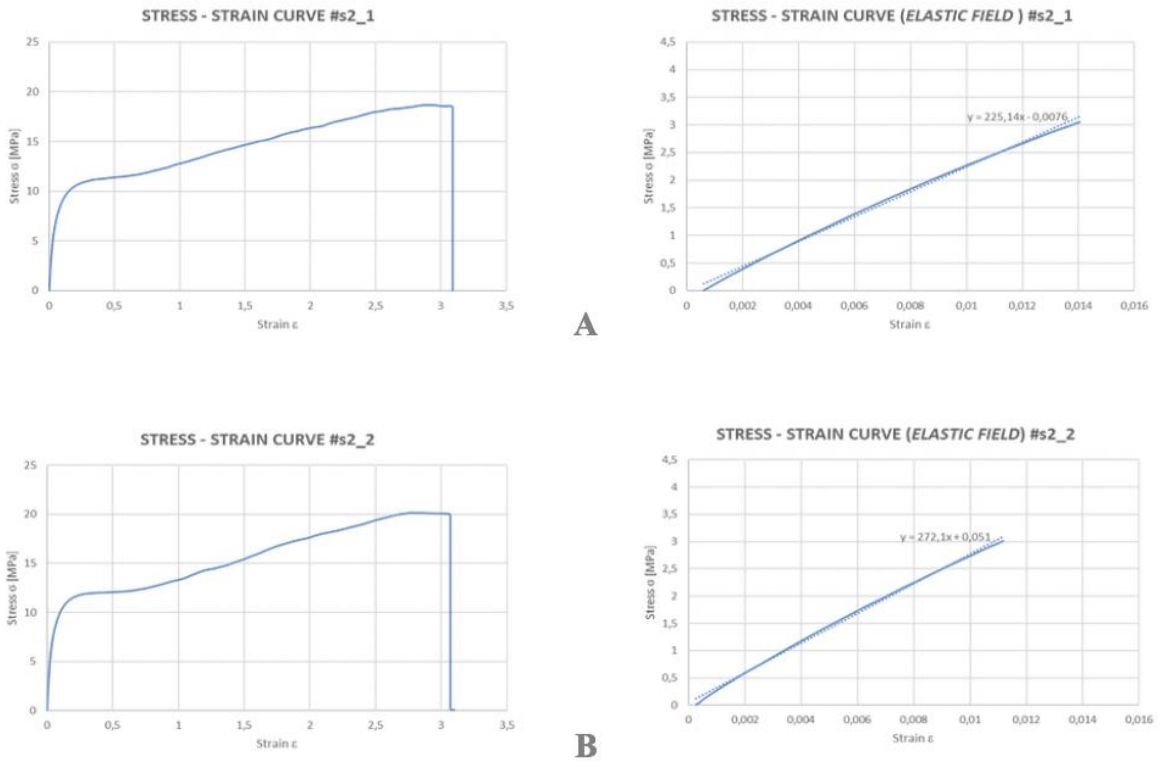

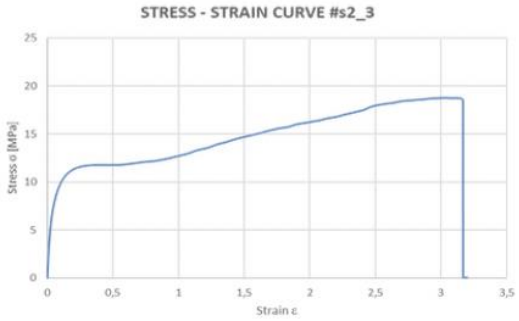
STRESS - STRAIN CURVE #s2_3
Stress σ [MPa]
Strain ε

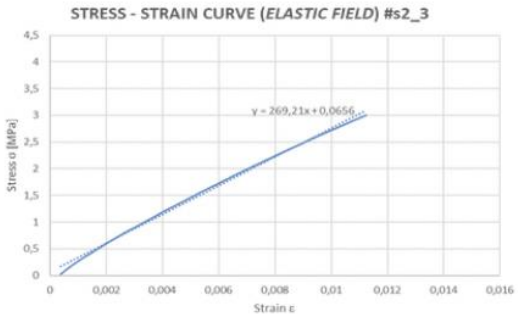
STRESS - STRAIN CURVE (ELASTIC FIELD) #s2_3
y = 269,21x + 0,0656
Stress σ [MPa]
Strain ε

C

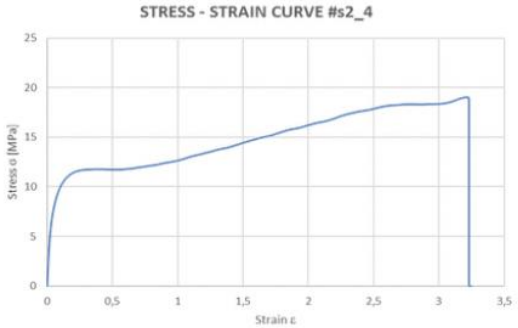
STRESS - STRAIN CURVE #s2_4
Stress σ [MPa]
Strain ε

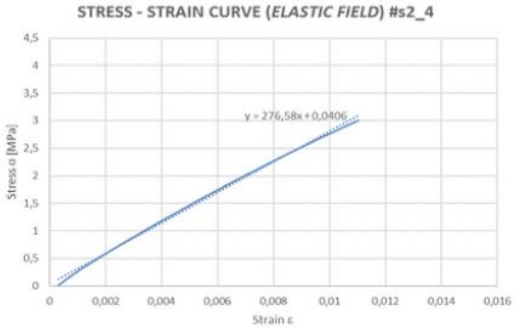
STRESS - STRAIN CURVE (ELASTIC FIELD) #s2_4
y = 276,58x + 0,0406
Stress σ [MPa]
Strain ε

D

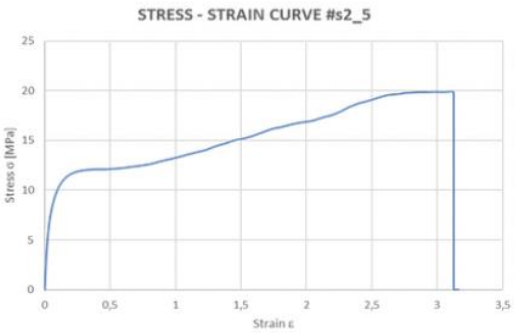
STRESS - STRAIN CURVE #s2_5
Stress σ [MPa]
Strain ε

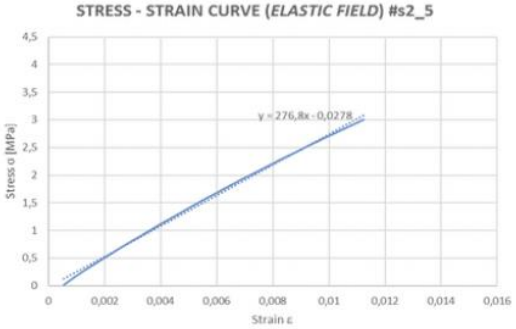
STRESS - STRAIN CURVE (ELASTIC FIELD) #s2_5
y = 276,8x - 0,0278
Stress σ [MPa]
Strain ε

E

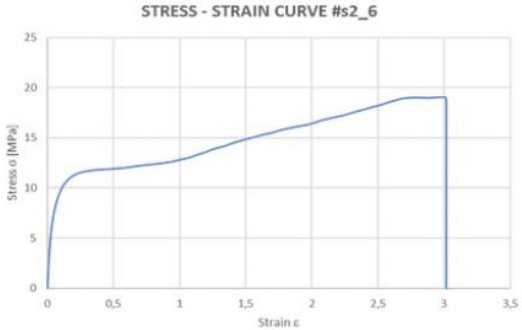
STRESS - STRAIN CURVE #s2_6
Stress σ [MPa]
Strain ε

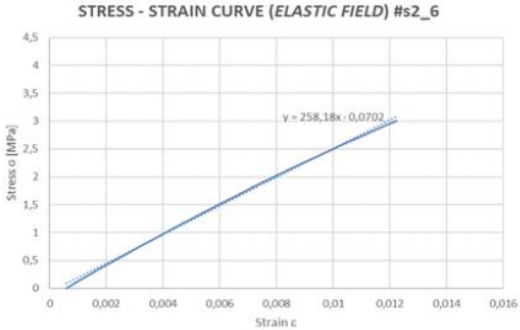
STRESS - STRAIN CURVE (ELASTIC FIELD) #s2_6
y = 258,18x - 0,0702
Stress σ [MPa]
Strain ε

F

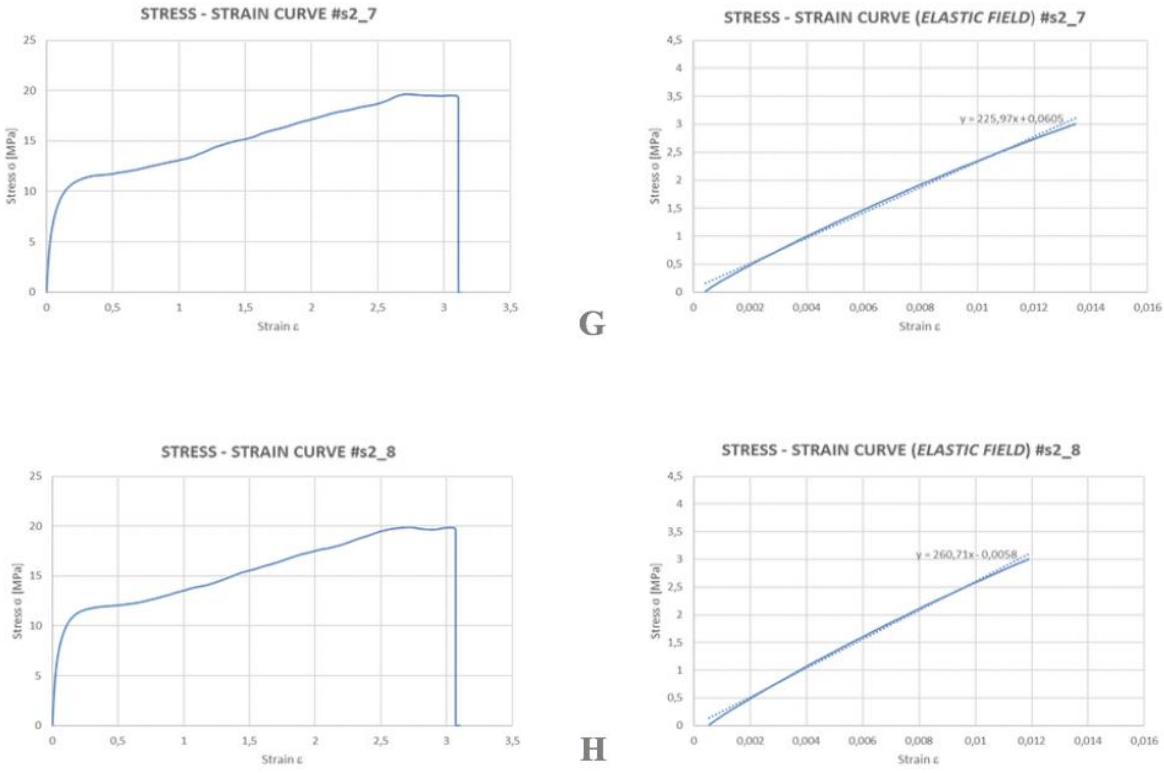

Figure D. 4: Strain- stress curves and linear regressions for the evaluation of Young's modules for all the tested samples (from A to H) included in Batch #s2

Batch #s7.9

In *Figure D. 5*, the plots of the strain-stress curves and of the linear regressions for the evaluation of Young's modules for all the tested dog bone samples included in Batch #s7.9 are reported:

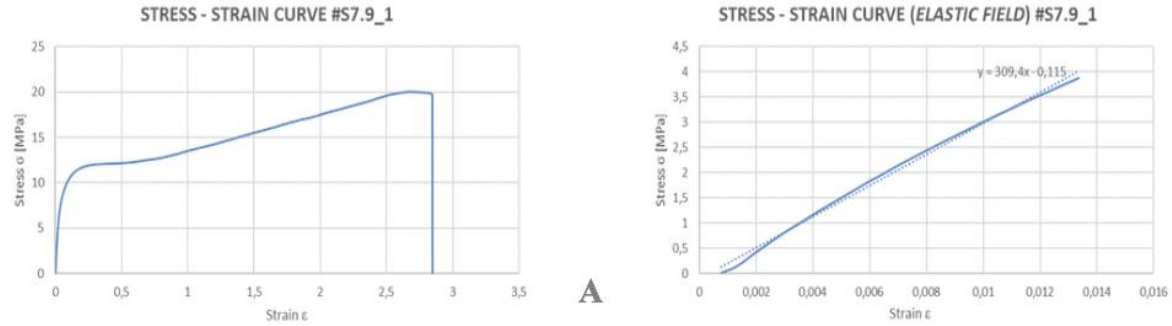

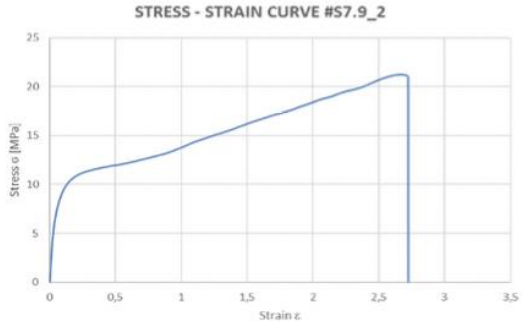
STRESS - STRAIN CURVE #S7.9_2
Stress σ [MPa]
Strain ε

B

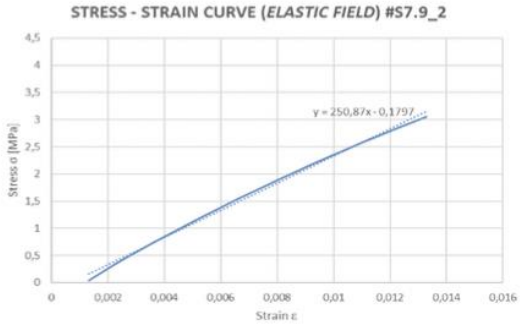
STRESS - STRAIN CURVE (ELASTIC FIELD) #S7.9_2
y = 250,87x - 0,1797
Stress σ [MPa]
Strain ε

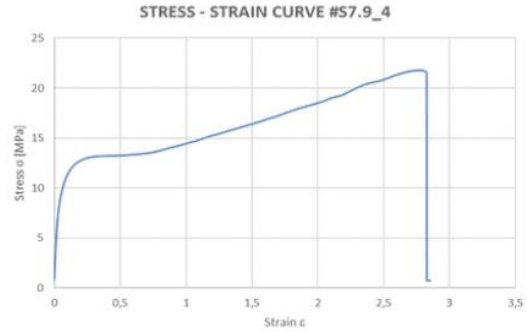
STRESS - STRAIN CURVE #S7.9_4
Stress σ [MPa]
Strain ε

C

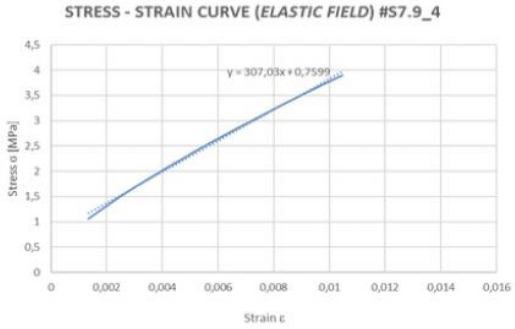
STRESS - STRAIN CURVE (ELASTIC FIELD) #S7.9_4
y = 307,03x + 0,7599
Stress σ [MPa]
Strain ε

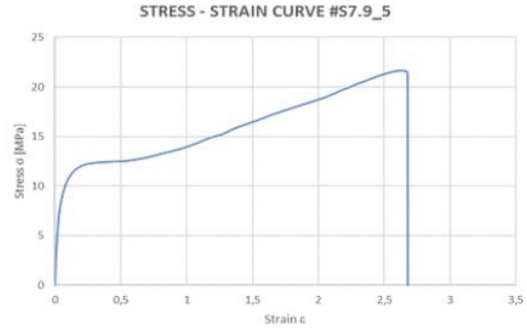
STRESS - STRAIN CURVE #S7.9_5
Stress σ [MPa]
Strain ε

D

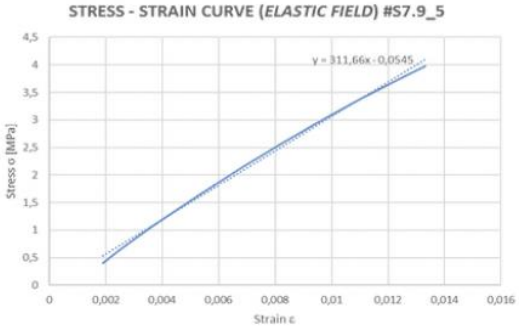
STRESS - STRAIN CURVE (ELASTIC FIELD) #S7.9_5
y = 311,66x - 0,0545
Stress σ [MPa]
Strain ε

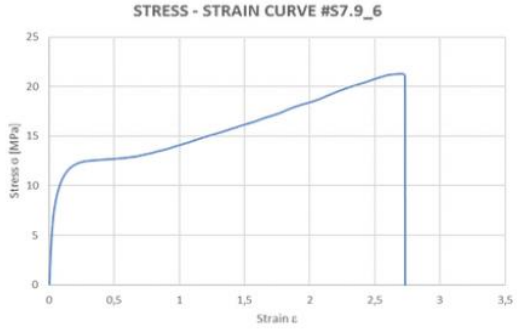
STRESS - STRAIN CURVE #S7.9_6
Stress σ [MPa]
Strain ε

E

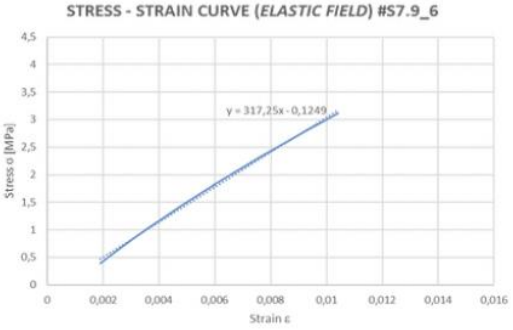
STRESS - STRAIN CURVE (ELASTIC FIELD) #S7.9_6
y = 317,25x - 0,1249
Stress σ [MPa]
Strain ε

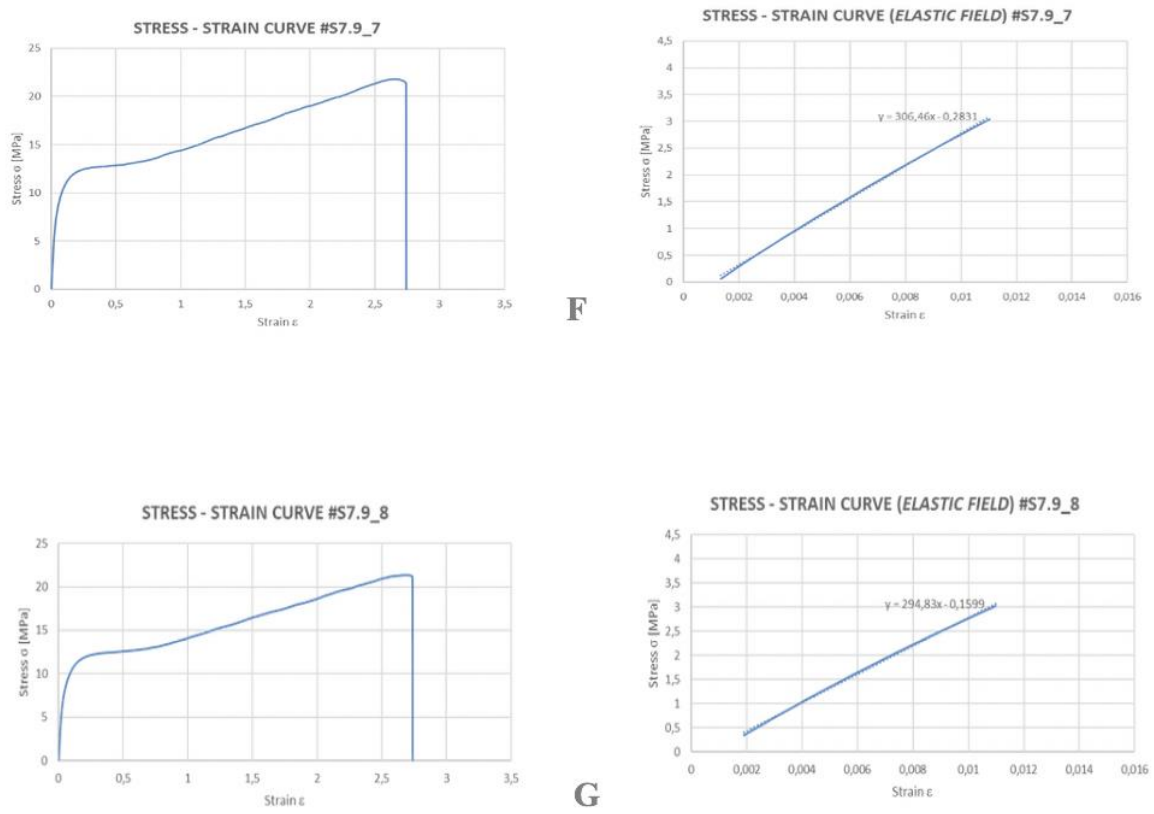

Figure D. 5: Strain-stress curves and linear regressions for the evaluation of Young's modules for all the tested samples (from A to G) included in Batch #s7.9

Batch #s10

In *Figure D. 6*, the plots of the strain – stress curves and of the linear regressions for the evaluation of Young's modules for all the tested samples included in Batch #s10 are reported:

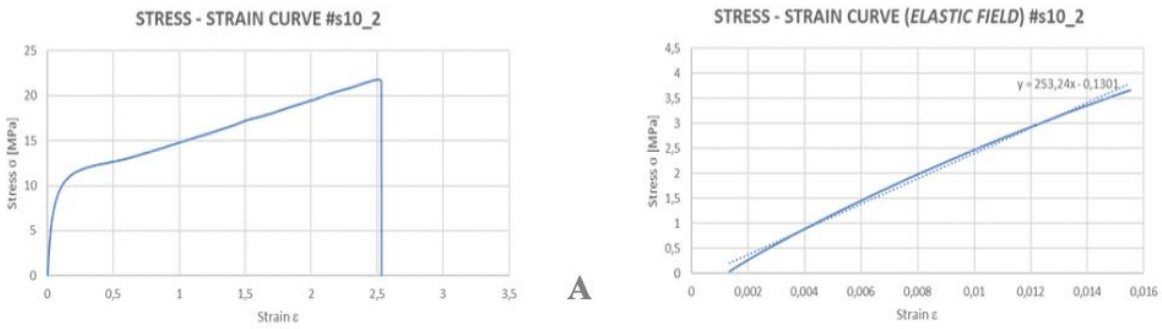

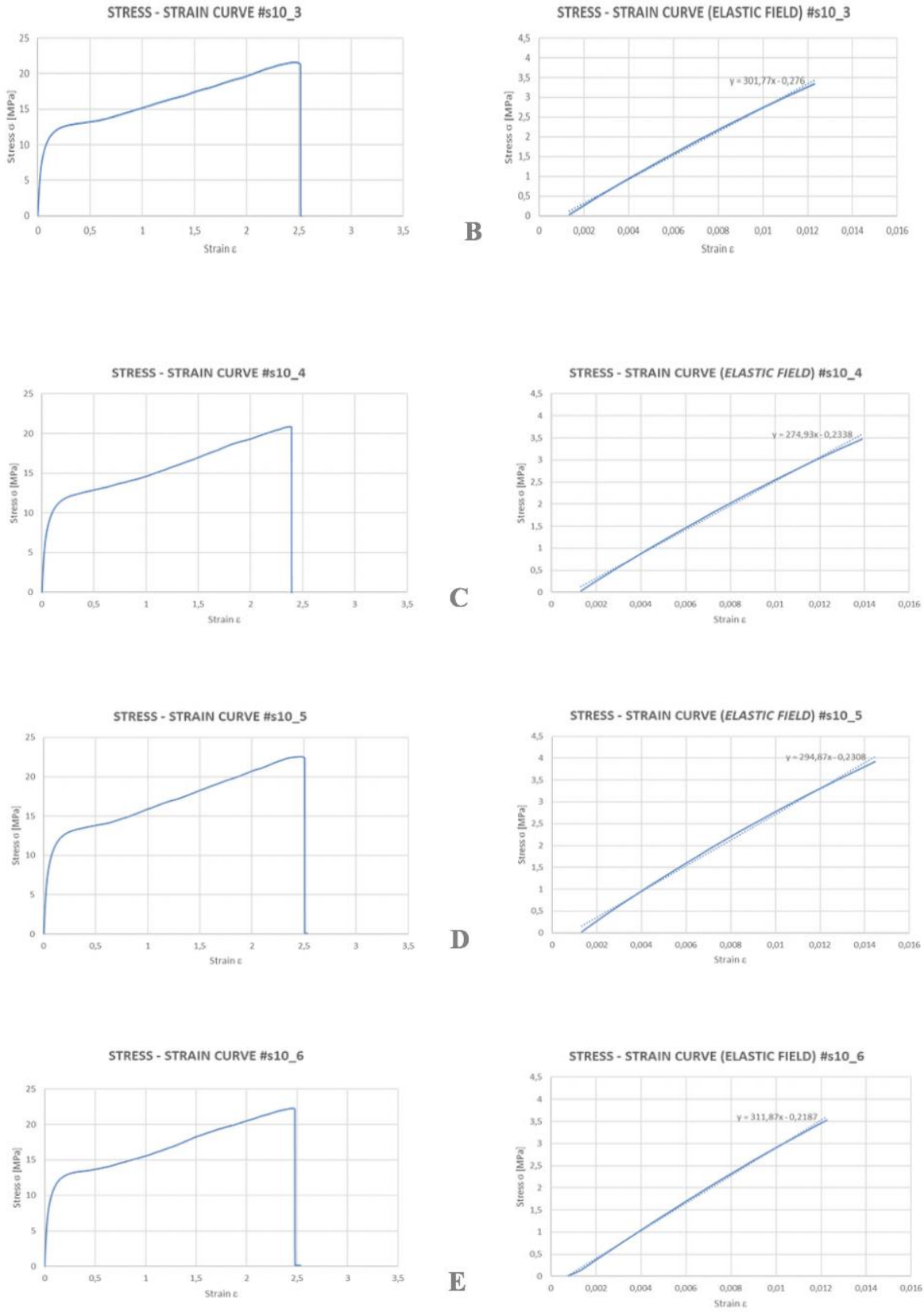

Figure D. 6: Strain-stress curves and linear regressions for the evaluation of Young's modules for all the tested samples (from A to E) included in Batch #s10

1.2.3 Comparison Between Tensile Test Results in Pre and Post-Sterilization conditions of the Injected Samples

In *Figure D. 7*, the comparison between pre and post-sterilization conditions of both tensile test results and linear regressions is reported:

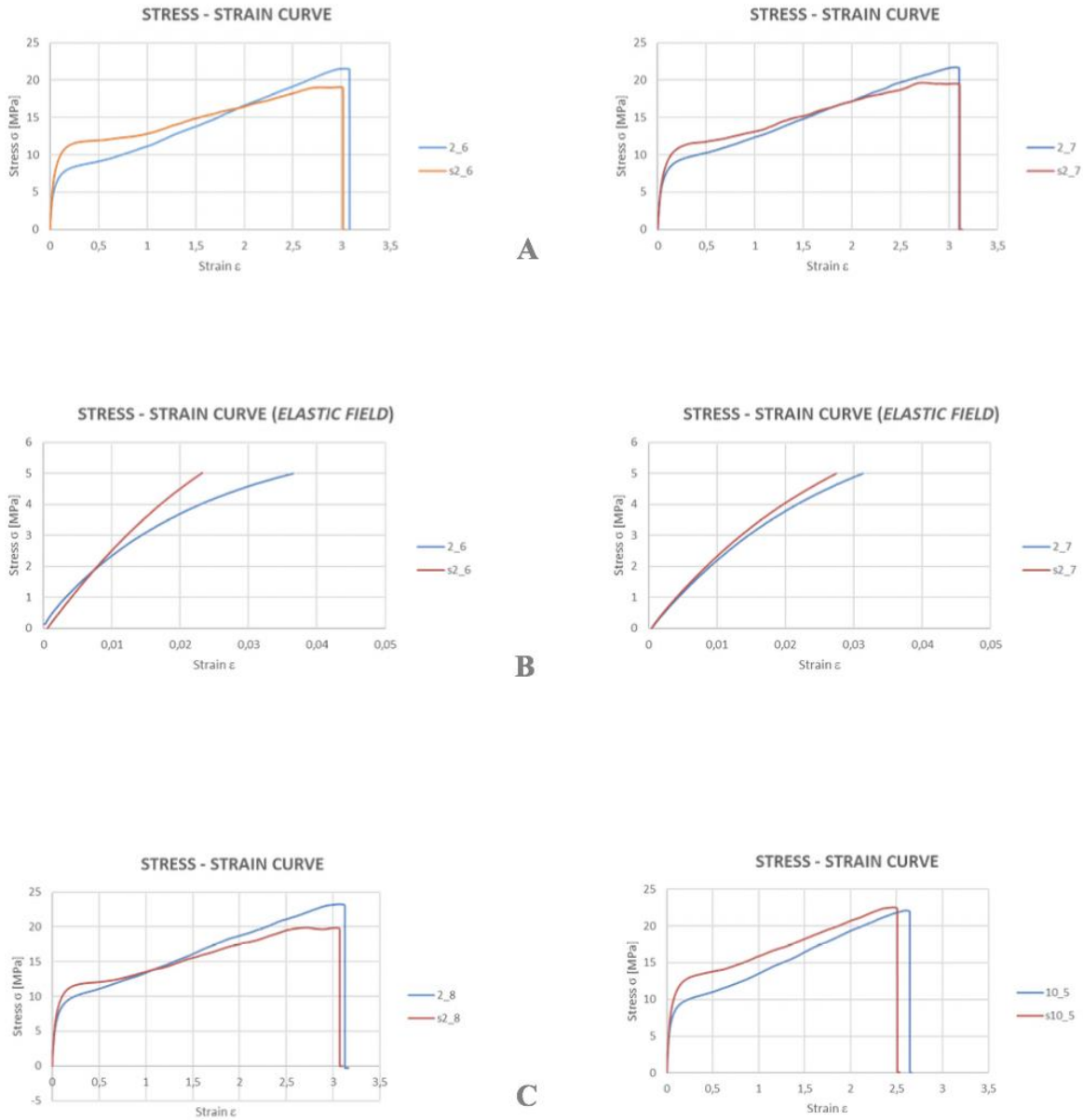

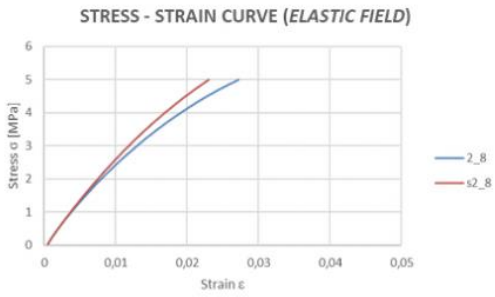
STRESS - STRAIN CURVE (*ELASTIC FIELD*)
Stress σ [MPa]
Strain ε
2_8
s2_8

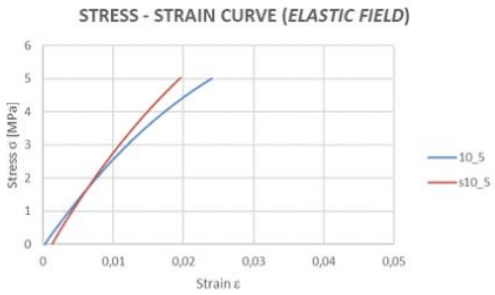
STRESS - STRAIN CURVE (*ELASTIC FIELD*)
Stress σ [MPa]
Strain ε
10_5
s10_5

D

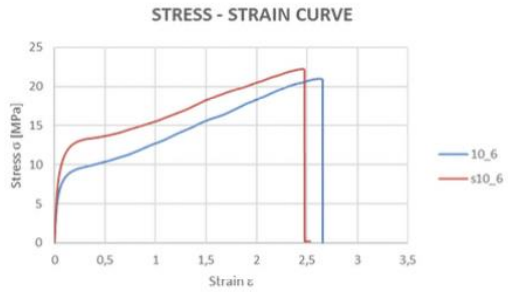
STRESS - STRAIN CURVE
Stress σ [MPa]
Strain ε
10_6
s10_6

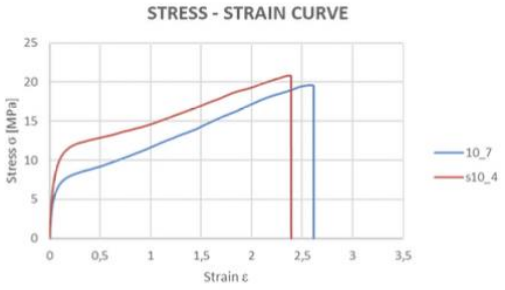
STRESS - STRAIN CURVE
Stress σ [MPa]
Strain ε
10_7
s10_4

E

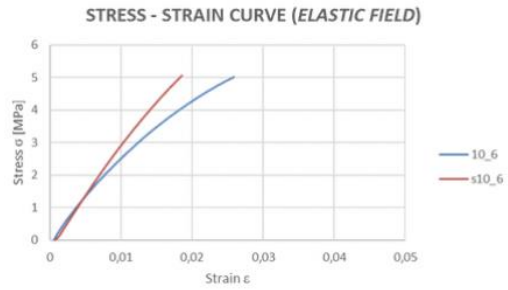
STRESS - STRAIN CURVE (*ELASTIC FIELD*)
Stress σ [MPa]
Strain ε
10_6
s10_6

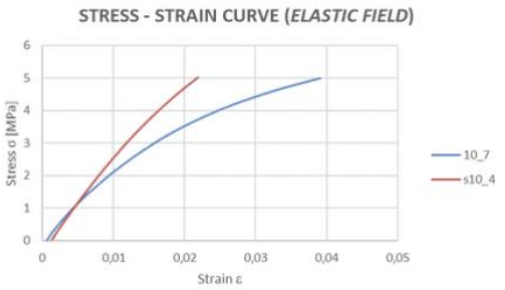
STRESS - STRAIN CURVE (*ELASTIC FIELD*)
Stress σ [MPa]
Strain ε
10_7
s10_4

F

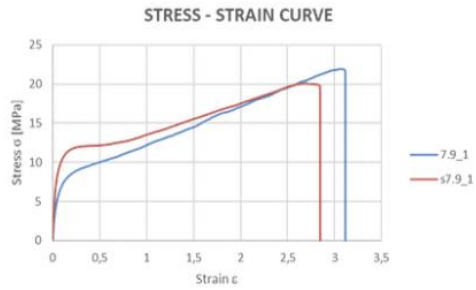
STRESS - STRAIN CURVE
Stress σ [MPa]
Strain ε
7.9_1
s7.9_1

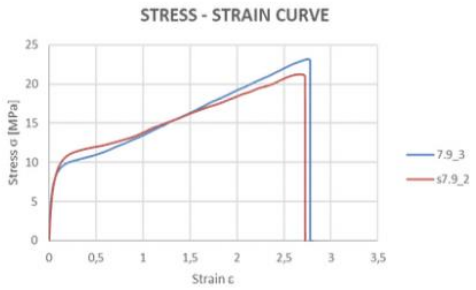
STRESS - STRAIN CURVE
Stress σ [MPa]
Strain ε
7.9_3
s7.9_2

G

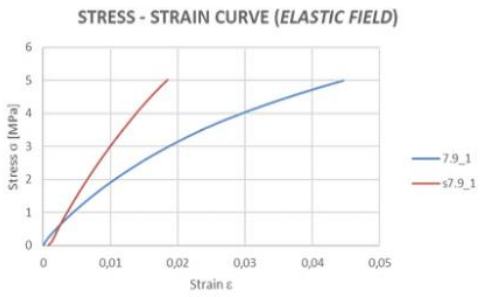
STRESS - STRAIN CURVE (*ELASTIC FIELD*)
Stress σ [MPa]
Strain ε
7.9_1
s7.9_1

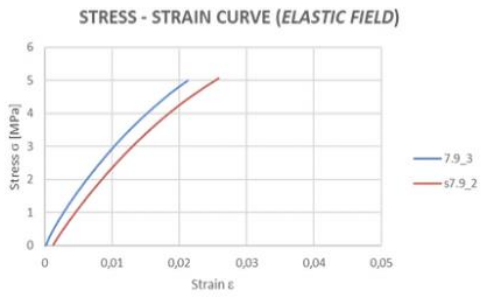
STRESS - STRAIN CURVE (*ELASTIC FIELD*)
Stress σ [MPa]
Strain ε
7.9_3
s7.9_2

H

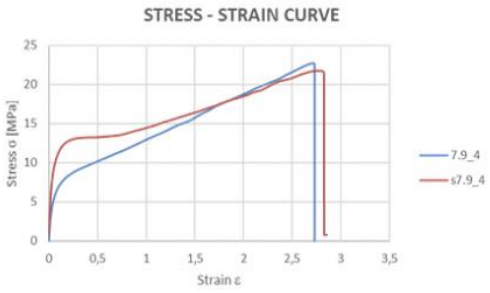
STRESS - STRAIN CURVE
Stress σ [MPa]
Strain ε
7.9_4
s7.9_4

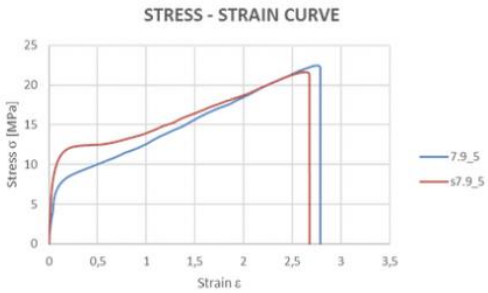
STRESS - STRAIN CURVE
Stress σ [MPa]
Strain ε
7.9_5
s7.9_5

I

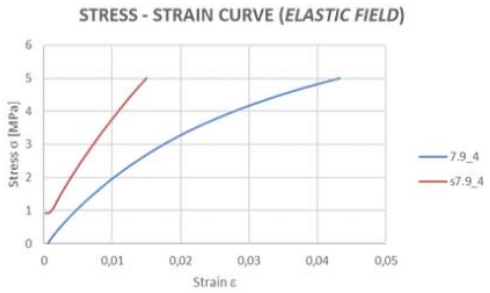
STRESS - STRAIN CURVE (*ELASTIC FIELD*)
Stress σ [MPa]
Strain ε
7.9_4
s7.9_4

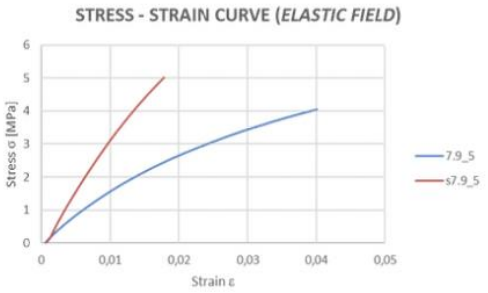
STRESS - STRAIN CURVE (*ELASTIC FIELD*)
Stress σ [MPa]
Strain ε
7.9_5
s7.9_5

L

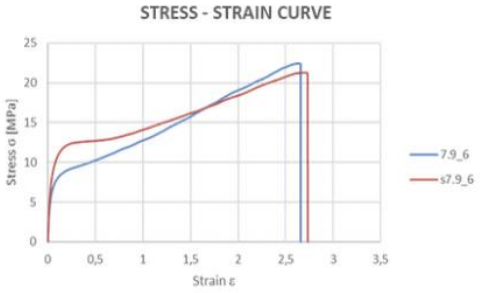
STRESS - STRAIN CURVE
Stress σ [MPa]
Strain ε
7.9_6
s7.9_6

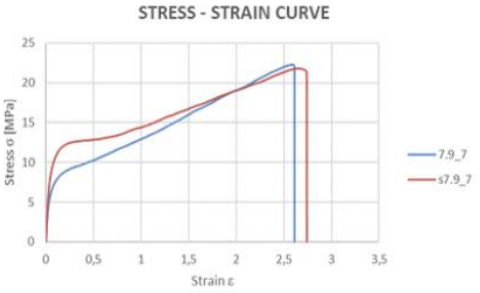
STRESS - STRAIN CURVE
Stress σ [MPa]
Strain ε
7.9_7
s7.9_7

M

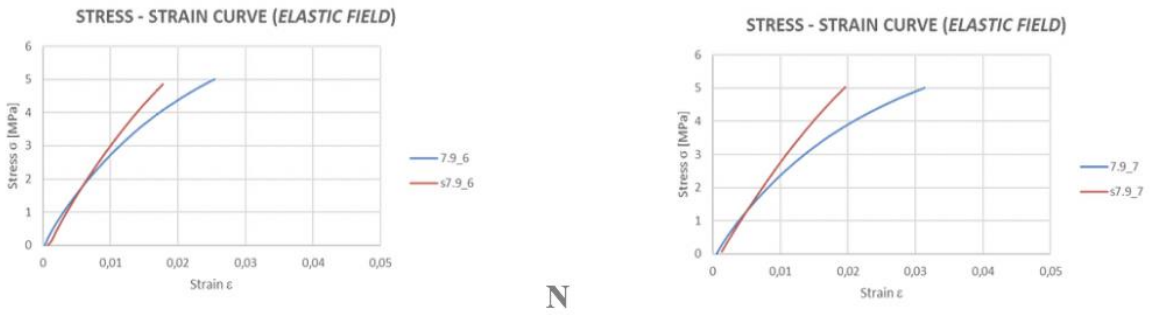

Figure D. 7: Comparison (from A to N) between pre and post-sterilization conditions of both tensile test results and linear regressions

In *Table D. 4* and *D. 5*, the average values of Young's modules in pre and post- sterilization conditions, respectively, by considering all the batches of the tested injected samples are reported:

Injected Sample	**Young's Modulus [MPa]**
2_6	198.59
2_7	210.06
2_8	234.45
10_5	253.23
10_6	246.12
10_7	191.91
7.9_1	154.8
7.9_3	288.53
7.9_4	171.81
7.9_5	123.47
7.9_6	260.98
7.9_7	223.76
Average	**213.14 ± 47.73**

Table D. 4: Average Young's modulus in pre-sterilization conditions

Injected and Sterilized Sample	**Young's Modulus [MPa]**
s2_1	225.14
s2_2	272.1
s2_3	269.21
s2_4	276.58
s2_5	276.8
s2_6	258.18
s2_7	226
s2_8	260.7
s10_2	253.24
s10_3	301.77
s10_4	274.93
s10_5	294.87
s10_6	311.87
s7.9_1	309.4
s7.9_2	250.87
s7.9_4	307.03
s7.9_5	311.66
s7.9_6	317.25
s7.9_7	306.46
s7.9_8	294.83
Average	**279.94 ± 28.27**

Table D. 5: Average Young's modulus in post-sterilization conditions

In *Table D. 6* and *D. 7*, the average values of both maximum stress and strain at break are reported, in pre and post-sterilization conditions respectively:

Injected Sample	Max Strain [-]	Max Stress [MPa]
2_6	3.11	21.54
2_7	3.13	21.72
2_8	3.16	23.25
7.9_1	3.13	21.90
7.9_3	2.81	23.18
7.9_4	2.75	22.70
7.9_5	2.82	22.45
7.9_6	2.68	22.42
7.9_7	2.64	22.26
10_5	2.66	22.10
10_6	2.70	20.98
10_7	2.65	19.62
Average	**2.85 ± 0.21**	**22.01 ± 0.09**

Table D. 6: Average of the maximum strain and stress at break in pre-sterilization conditions

Injected and Sterilized sample	Max Strain [-]	Max stress [MPa]
s2_1	3.10	18.67
s2_2	3.10	20.14
s2_3	3.20	18.77
s2_4	3.25	19.03
s2_5	3.16	19.91
s2_6	3.05	19.06
s2_7	3.13	19.65
s2_8	3.10	19.89
s7.9_1	2.94	20.05
s7.9_2	2.97	21.24
s7.9_4	2.85	21.75
s7.9_5	2.72	21.63
s7.9_6	2.81	21.27
s7.9_7	2.79	21.78
s7.9_8	2.76	21.32
s10_2	2.55	21.78
s10_3	2.53	21.60
s10_4	2.42	20.82
s10_5	2.53	22.53
s10_6	2.53	22.23
Average	**2.86 ± 0.26**	**20.65 ± 1.22**

Table D. 7: Average of the maximum strain and stress at break in post-sterilization conditions

2. *Polymer 4*

2.1 Tensile Test Results

2.1.1 Injected Samples

In *Figure D. 8*, the plots of the strain-stress curves and of the linear regressions for the evaluation of Young's modules for all the tested injected pins, in pre-sterilization conditions, are reported:

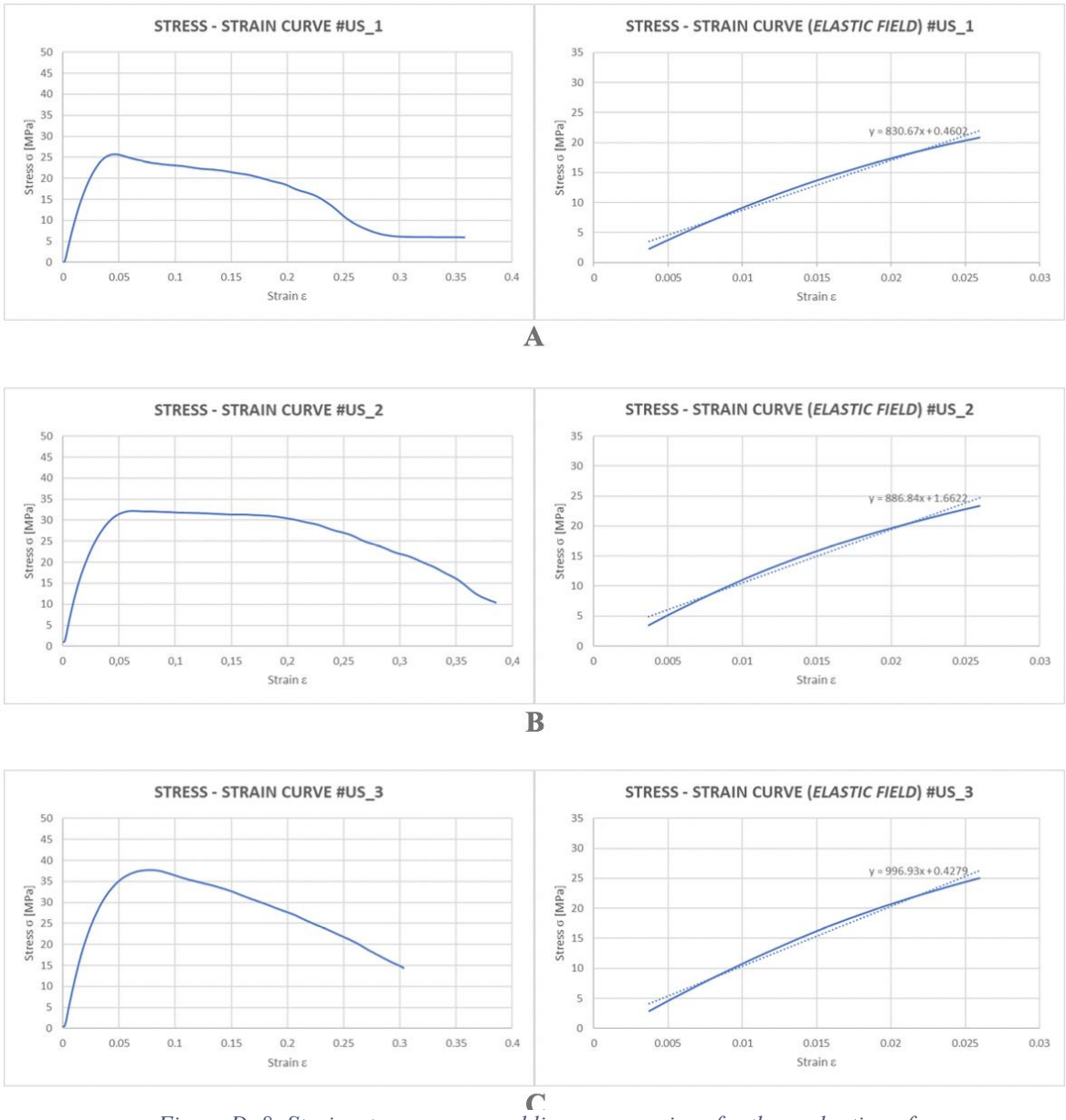

Figure D. 8: Strain–stress curves and linear regressions for the evaluation of Young's modules for all the tested injected pins (A, B and C), in pre-sterilization conditions

2.1.2 Post-Sterilization Injected Samples

In *Figure D. 9*, the plots of the strain-stress curves and of the linear regressions for the evaluation of Young's modules for all the tested injected pins, in post-sterilization conditions, are reported:

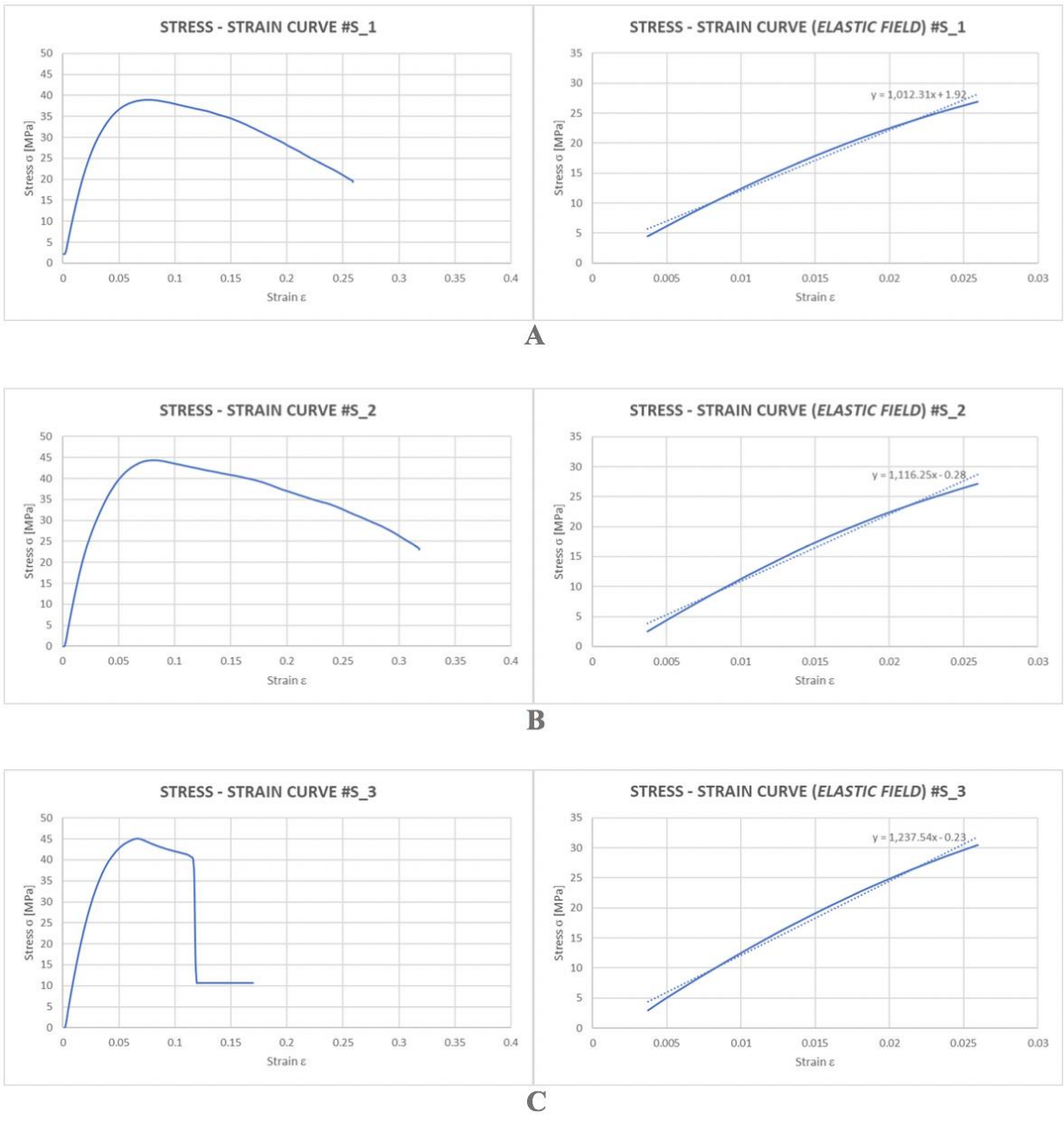

Figure D. 9: Strain–stress curves and linear regressions for the evaluation of Young's modules for all the tested injected pins (A, B and C), in post-sterilization conditions

2.1.3 Comparison Between Tensile Test Results Related to Injected Samples and Post-Sterilization Injected Samples

In *Figure D. 10*, the comparison between pre and post-sterilization conditions of both tensile test results and linear regressions is reported:

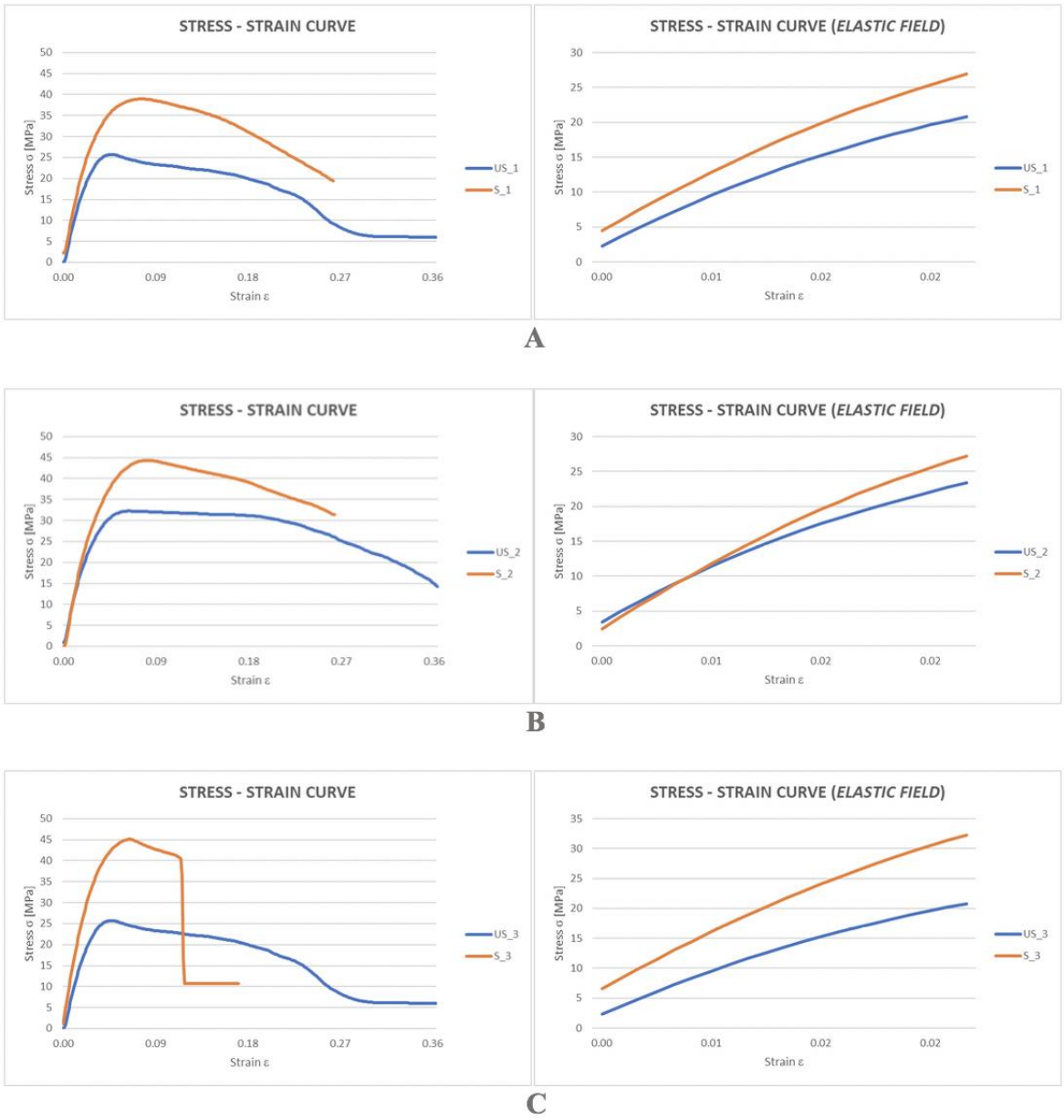

Figure D. 10: Comparison (from A to C) between pre and post-sterilization conditions of both tensile test results and linear regressions

In *Table D. 8* and *D. 9*, the average values of Young's modulus in pre and post- sterilization conditions, respectively, by considering all the tested injected samples are reported:

Injected Sample	**Young's Modulus [MPa]**
US_1	830.67
US_2	886.84
US_3	996.93
Average	**904.81± 84.57**

Table D. 8: Average value of Young's modulus of the injected samples in pre-sterilization conditions

Injected and Sterilized Sample	**Young's Modulus [MPa]**
S_1	1021.31
S_2	1116.25
S_3	1237.03
Average	**1125.03 ± 108.38**

Table D. 9: Average value of Young's modulus of the injected samples in post-sterilization conditions

2.2 Torsion Test Results

In *Figure D. 11, D. 12, D. 13* and *D. 14*, the stress-strain curves obtained from torque test data analysis for the four tested injected and sterilized pin are reported:

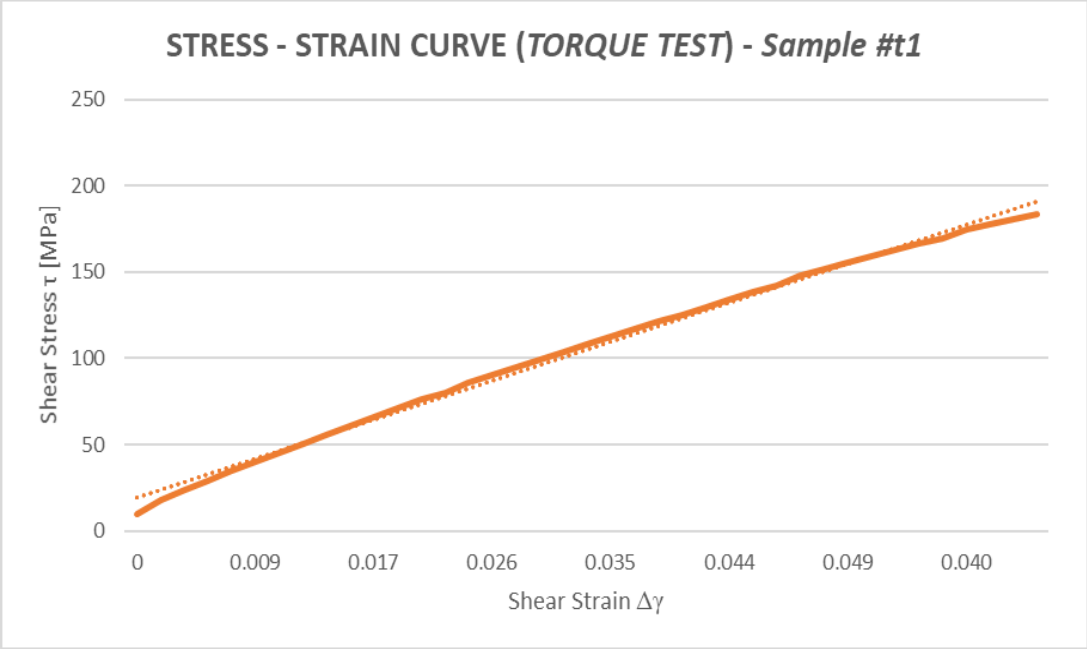

Figure D. 11: Stress-strain curve for sample #t1

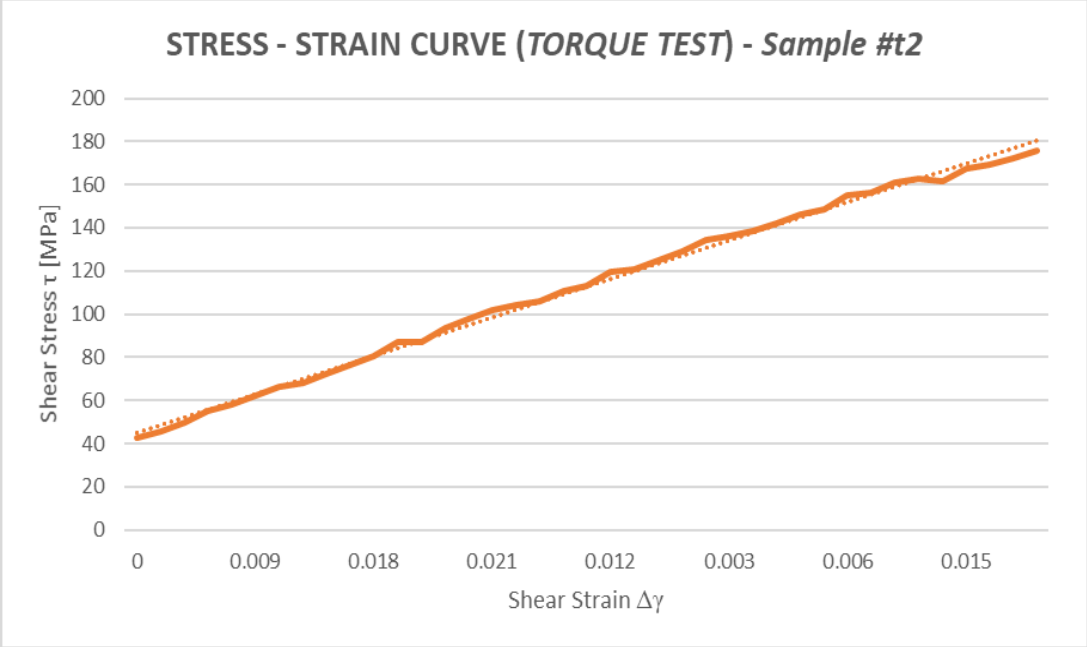

Figure D. 12: Stress-strain curve for sample #t2

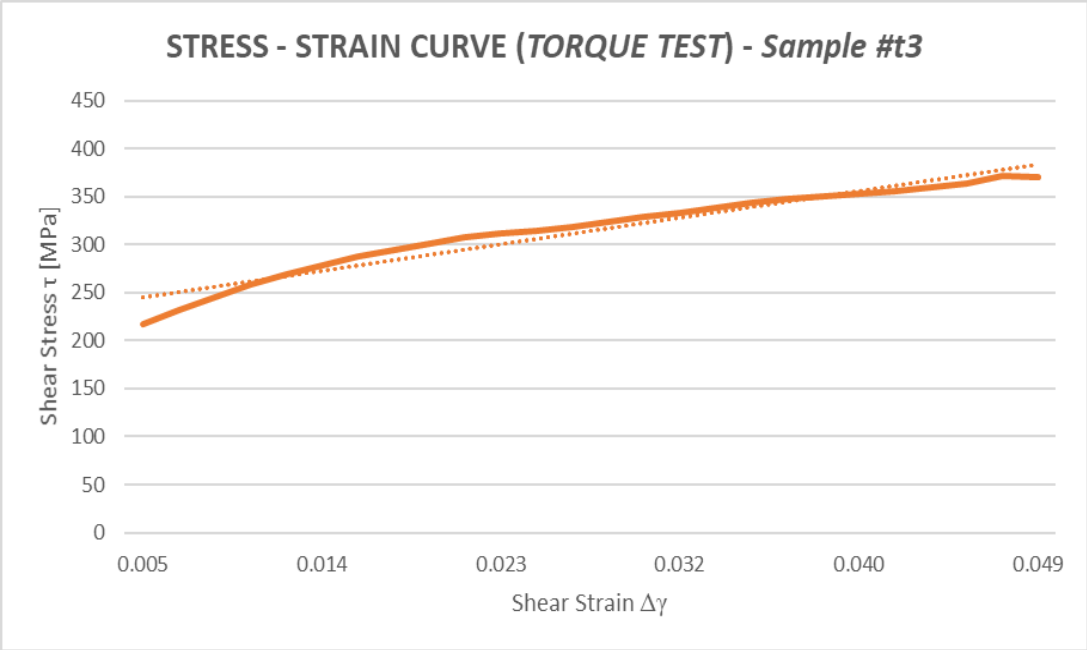

Figure D. 13: Stress-strain curve for sample #t3

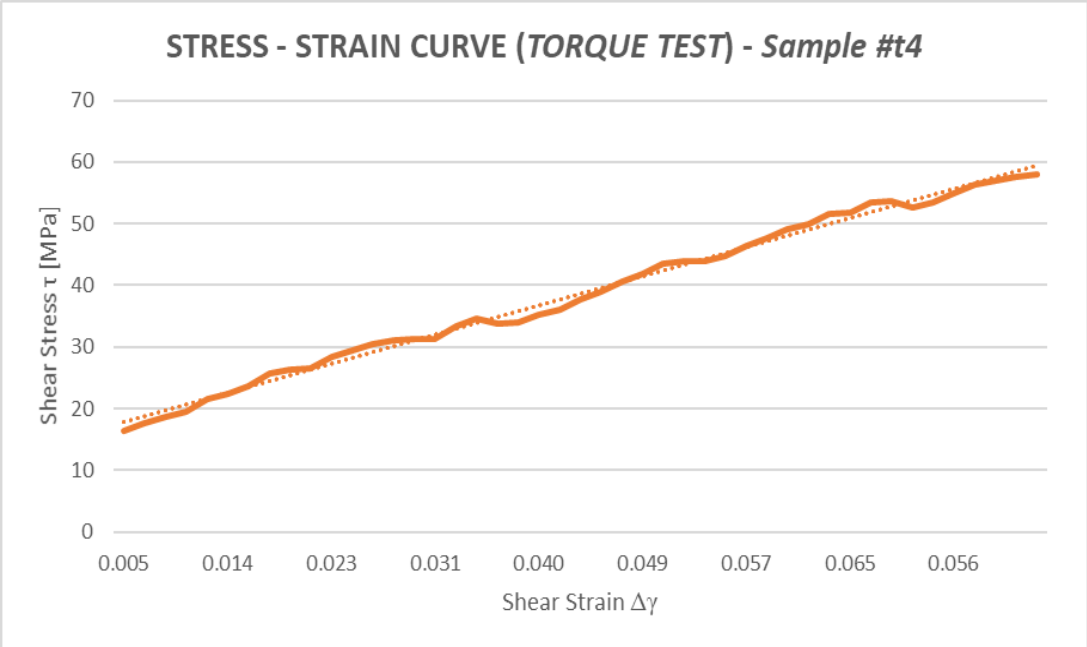

Figure D. 14: Stress-strain curve for sample #t4

In Table D. 10, the average of the shear module and of the maximum value of both shear stress and strain obtained from torsion test data analysis for the four tested sterilized pin samples are reported:

Injected and Sterilized Sample	Max Shear Strain [-]	Max Shear Stress [MPa]	Shear Modulus [MPa]
#t1	0.050	183.406	3125.870
#t2	0.023	175.750	2115.440
#t3	0.049	372.000	3168.052
#t4	0.049	58.080	1972.516
Average	**0.043 ± 0.013**	**197.309 ± 129.82**	**2595.47 ± 639.71**

Table D. 10: Average of the shear modulus and of the maximum value of both shear stress and strain

2.3 Three-Points Bending Test Results

In *Figure D. 15, D. 16* and *D. 17*, the stress-strain curves obtained from three-points bending test data analysis for the three tested injected pins are reported:

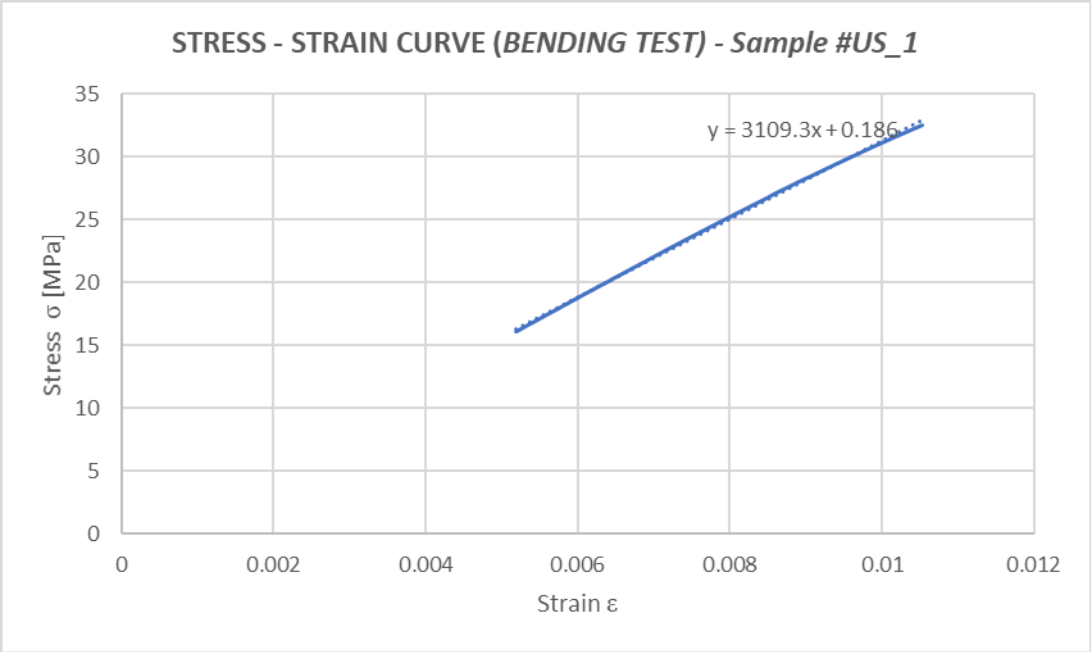

Figure D. 15: Stress-strain curves obtained from three-points bending test data analysis for sample #US_1

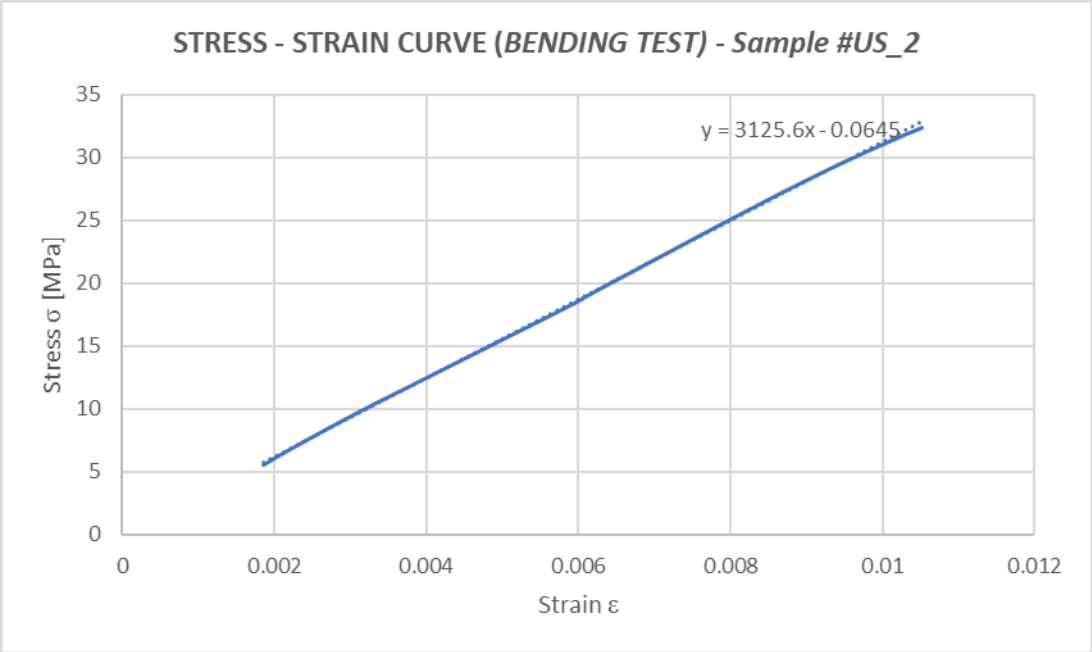

Figure D. 16: Stress-strain curves obtained from three-points bending test data analysis for sample #US_2

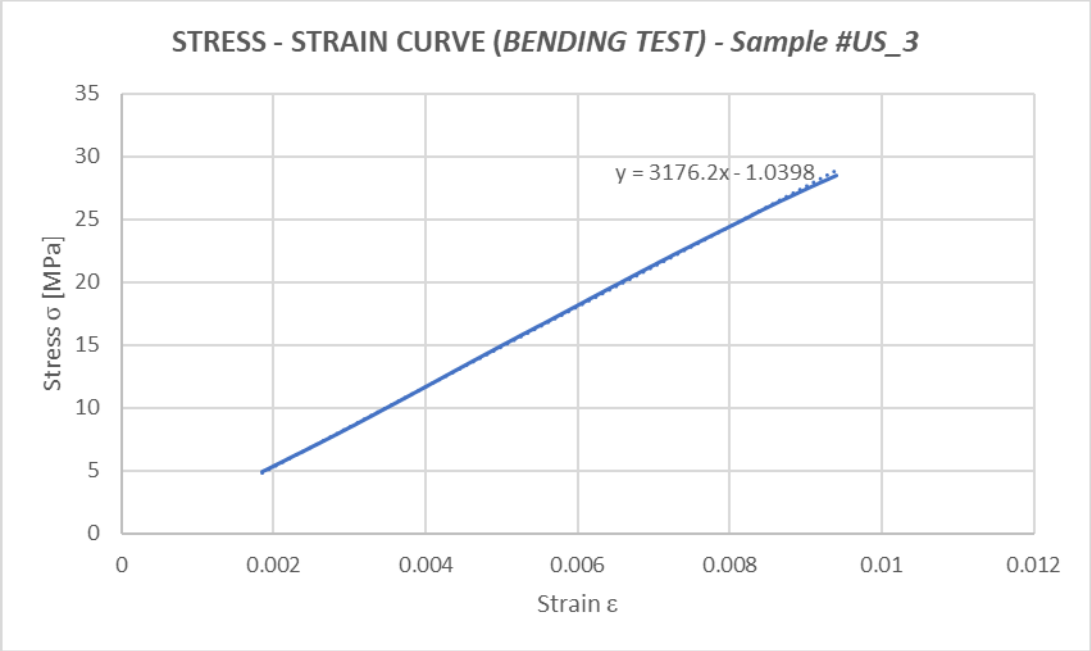

Figure D. 17: Stress-strain curves obtained from three-points bending test data analysis for sample #US_3

In *Figure D. 18, D. 19* and *D. 20*, the stress-strain curves obtained from three-points bending test data analysis for the three tested injected and sterilized pins are reported:

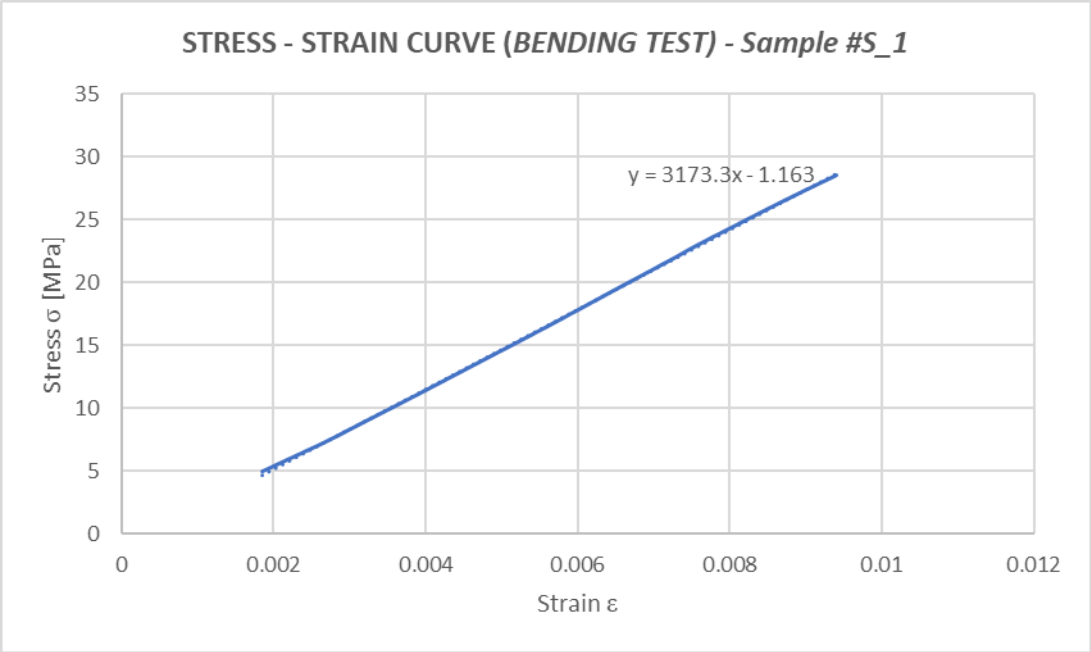

Figure D. 18: Stress-strain curves obtained from three-points bending test data analysis for sample #S_1

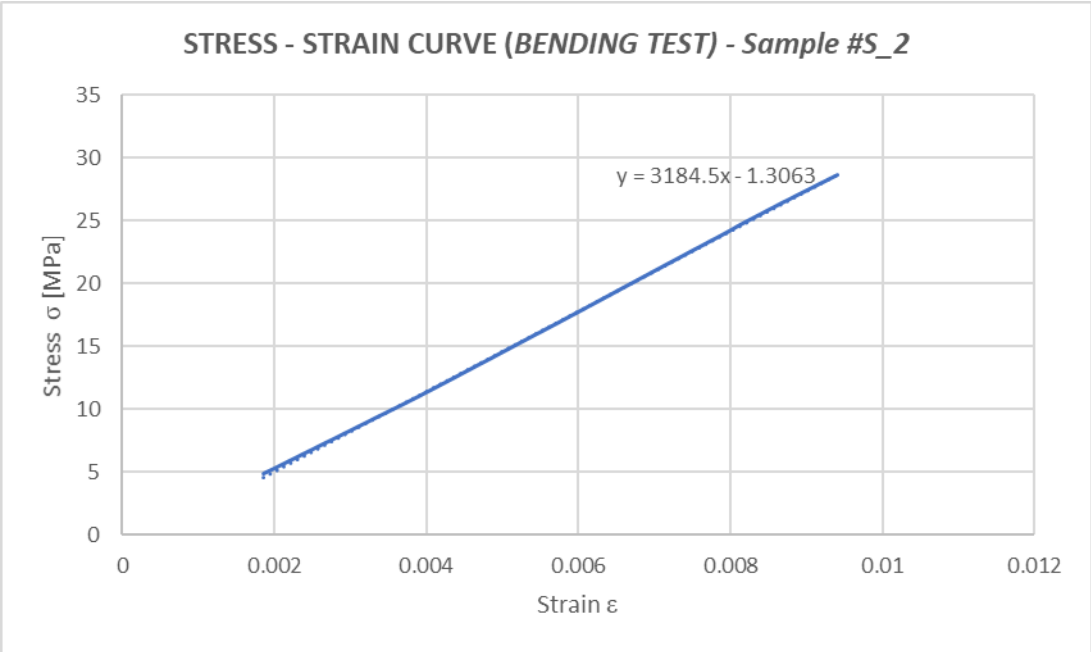

Figure D. 19: Stress-strain curves obtained from three-points bending test data analysis for sample #S_2

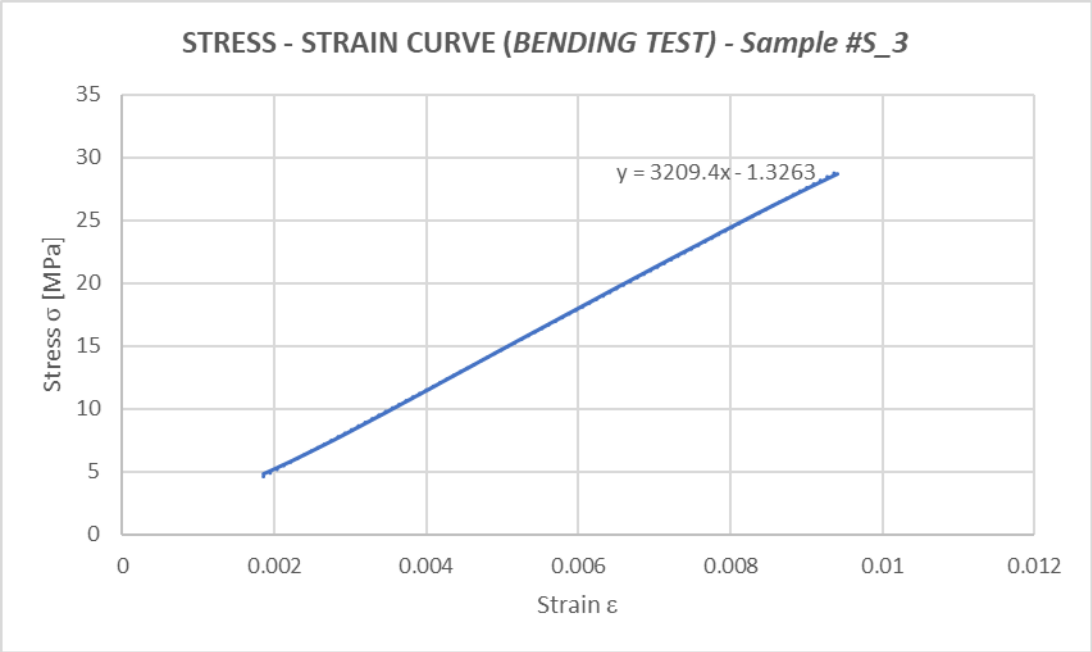

Figure D. 20: Stress-strain curves obtained from three-points bending test data analysis for sample #S_3

In *Table D. 11*, the average of Young's modulus and of the maximum value of both stress and strain obtained from three-points bending test output data analysis for the three tested injected pins are reported:

Injected Sample	Max Strain [-]	Max Stress [MPa]	Young's Modulus [MPa]
#US_1	0.001	32.51	3109.3
#US_2	0.001	32.38	3125.6
#US_3	0.009	28.48	3176.2
Average	**0.01 ± 0.0006**	**31.13 ± 2.29**	**3137.03 ± 34.88**

Table D. 11: Average of Young's modulus and of the maximum value of both stress and strain obtained from three-points bending test of the three injected tested samples

In *Table D. 12*, the average of Young's modulus and of the maximum value of both stress and strain obtained from three-points bending test output data analysis for the three tested injected and sterilized pins are reported:

Injected and Sterilized Sample	Max Strain [-]	Max Stress [MPa]	Young's Modulus [MPa]
#S_1	0.0094	28.57	3173.3
#S_2	0.0094	28.64	3184.5
#S_3	0.009	28.65	3209.4
Average	**0.009 ± 6.4E -07**	**28.62 ± 0.05**	**3189.06 ± 18.47**

Table D. 12: Average of Young's modulus and of the maximum value of both stress and strain obtained from three-points bending test of the three injected and sterilized tested samples

2.4 Four-Points Bending Test Results

In *Figure D. 21, D. 22* and *D. 23*, the stress-strain curves obtained from four-points bending test data analysis for the three tested injected and sterilized pins are reported:

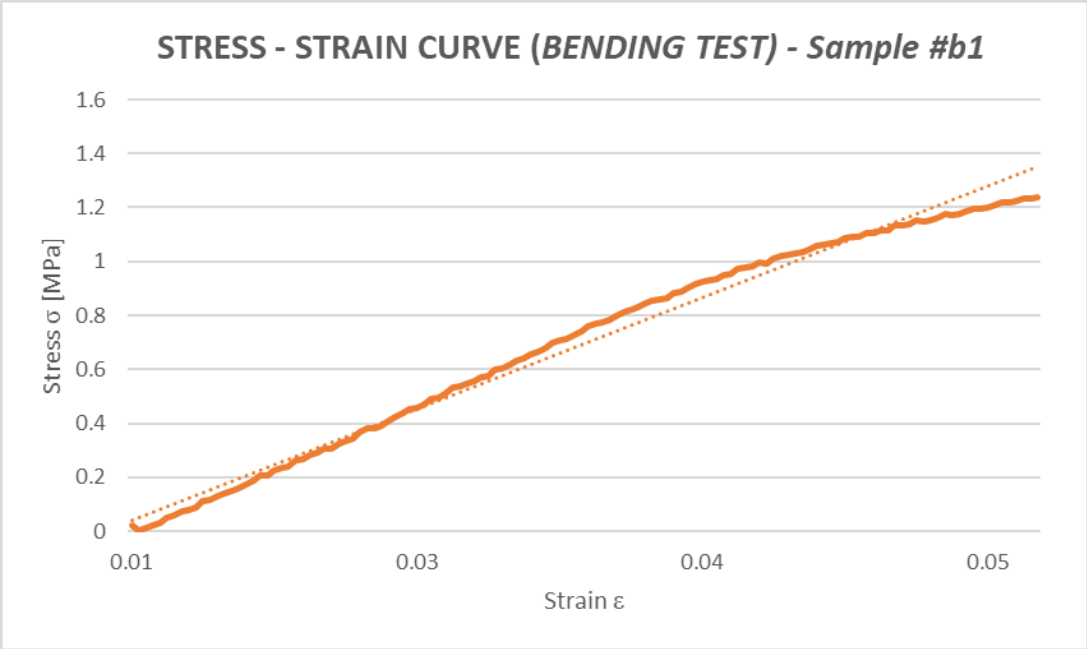

Figure D. 21: Stress-strain curve for sample #b1

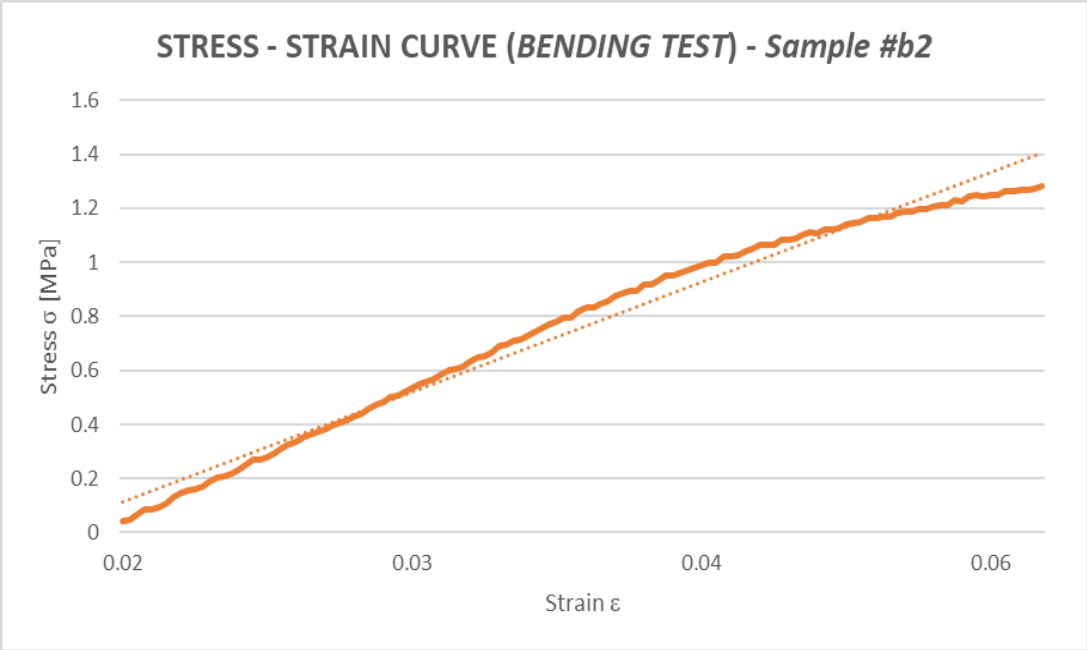

Figure D. 22: Stress-strain curve for sample #b2

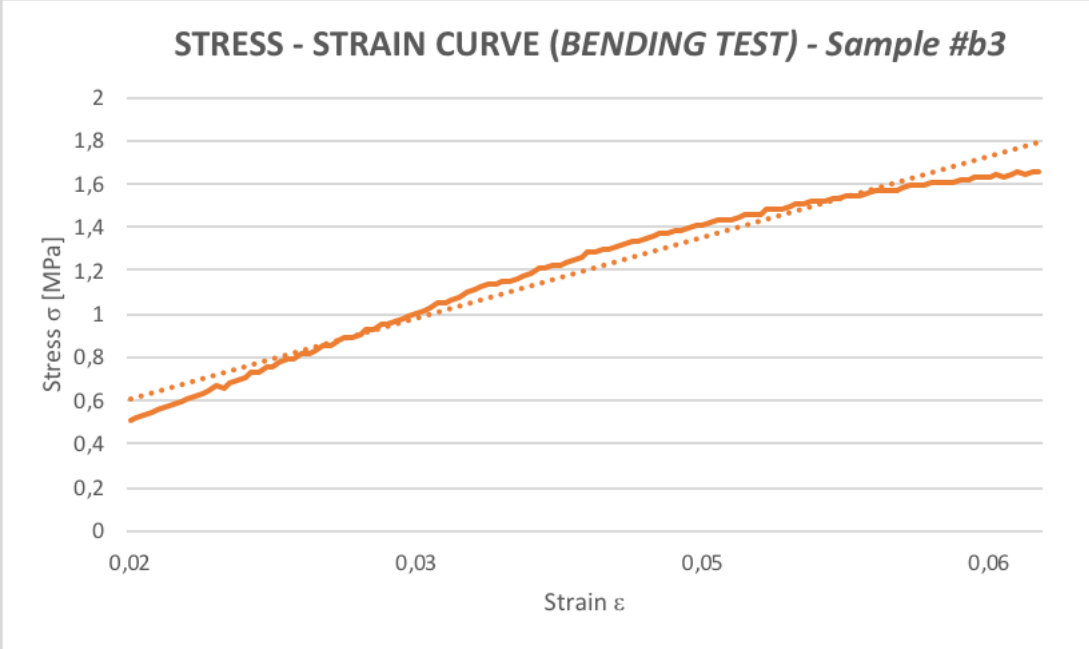

Figure D. 23: Stress-strain curve for sample #b3

In *Table D. 13*, the average of Young's modulus and of the maximum value of both stress and strain obtained from four-points bending test output data analysis for the three tested injected and sterilized pins are reported:

Sample	Max Strain [-]	Max Stress [MPa]	Young's modulus [MPa]
#b1	0.036	0.831	35.812
#b2	0.040	0.897	36.790
#b3	0.043	1.340	35.689
Average	**0.040 ± 0.003**	**1.023 ± 0.277**	**36.097 ± 0.603**

Table D. 13: Average of Young's modulus and of the maximum value of both stress and strain